THE SUSPENSION OF CARBON NANOTUBES IN BULK POLYMER

POLYMER FUNCTIONALIZATION FOR THE SUSPENSION OF CARBON NANOTUBES IN BULK POLYMER

By RYAN CHADWICK

B.Sc (University of Northern British Columbia, Canada) 2008

A Thesis Submitted to the School of Graduate Studies In Partial Fulfillment of the Requirements for the Degree of Doctor of Philosophy in Chemistry

McMaster University

DOCTOR OF PHILOSOPHY (2014) McMASTER UNIVERSITY

(Chemistry) Hamilton, Ontario

TITLE: Polymer Functionalization Strategies for the Suspension of Carbon Nanotubes in Bulk Polymers

AUTHOR: Ryan Chadwick, B.Sc.

(University of Northern British Columbia, Canada)

SUPERVISOR: Professor Alex Adronov

NUMBER OF PAGES: xxvii, 247

Abstract

Carbon nanotubes have great strength, high conductivities, and very large aspect ratios. Their physical, mechanical, and electrical properties are unique and ideally suited for use in structural materials, nano-electronic devices, and as a conductive filler.[1,2] The homogeneous incorporation of carbon nanotubes in bulk materials such as polymers is difficult to achieve. This is further complicated by the inhomogeneity of carbon nanotube samples. The desire to incorporate carbon nanotubes in a wide variety of devices has been the impetus for carbon nanotube chemistry over the last decade. This requires techniques for dispersal and processing, as well as methodologies for producing monodisperse samples.

In Chapter 1, this thesis discusses the fundamental properties of carbon nanotubes and gives a brief overview of the state-of-the-art in carbon nanotube separation, dispersion, and the incorporation of carbon nanotubes in bulk polymers. Chapters 2, 3, and 4 outline our efforts in the area of bulk polymer suspensions; in polystyrene (Ch. 2) and in crosslinked polydimethylsiloxane elastomers (Ch. 3 and 4). Chapter 2 describes our efforts to gain an understanding of the factors limiting the graft density of polymers on the surface of carbon nanotubes, and our insights on the ability of polymer grafts to compatibilize carbon nanotubes with a host polymer. Chapter 3 discusses the application of the Piers-Rubinsztajn reaction as a method of functionalizing the surface of nanotubes with silanes, and crosslinking them within silicone rubbers. Chapter 4 outlines the development of a supramolecular strategy for the dispersion of carbon nanotubes

within silicone elastomers using conjugated and di-block co-polymers. Lastly, Chapters 5 through 6 explore the initial stages of development of a “universal” polymer for the dispersion of carbon nanotubes based on highly reactive cyclooctyne monomer units (Ch. 5) and the precursor chemistry required to make this unit on sufficient scale (Ch. 6).

Acknowledgements

There are so many people involved in undertaking a Ph.D. I have had the great pleasure of working and spending time with many wonderful people during my studies at McMaster. I have so many people to thank at McMaster, in Hamilton, and further abroad. The people named below are just some of the people whom I have had the great pleasure to meet, work with, and learn from during the last decade. Without them, my work and my life in Hamilton in these last 6 years would have been greatly diminished.

Foremost, my doctoral supervisor, Professor Alex Adronov, deserves my sincerest thanks. For providing the advice and support I needed throughout my time in the Adronov Lab, for providing the model to learn from – in research and in teaching – and above all, for always having confidence in me – thank you.

I would like to thank Professor Mike Brook and Professor Kalai Saravanamuttu for all of the discussion, helpful advice, and opportunities to learn. I couldn't have asked for more from a supervisory committee! I was also lucky enough to participate in a productive collaboration with Professor Jonathan Coleman and Dr. Umar Khan at Trinity College in Dublin. While we have never met in person, I enjoyed and learned much from our collaboration.

I am thankful for the chance to work with a large number of talented individuals who deserve my sincerest thanks. Thanks to Dr. Ferdinand Gonzaga for his limitless help during the early days of my Ph.D. If I ever needed a sounding board, advice, or help, you were there. Thanks to Dominica Wong,

Callisto MacIssac, Sophie Liogier, Vlad Kardelis, Darryl Fong, and Phil Lim. I have been exceedingly lucky to collaborate with and learn alongside such a talented group of young chemists. Thanks to John Grande, Nicole Rice, and Sabrina Van Gyzen for the great ideas and fruitful collaborations!

I would also like to extend my thanks to the members of the Adronov group. From late night lab conversations, to beers at the Phoenix, to the vigorous debates during group meeting – you are the people that made graduate school the experience it was! I especially want to thank Greg, Gregor, Lukas, Stu, and Vlad for sharing fumehoods, countless conversations over lunch, and all of your ideas!

I would be remiss if I did not thank all of my colleagues who shared in the experience of developing and TAing 3LA3, most notably Phil Elder and Leigh Spencer. It certainly was an experience…

Additionally, I would like to thank the Ontario Graduate Scholarship program and the McMaster Department of Chemistry for providing me with funding, teaching assistantships, and the institutional support required for this endeavor. Briefly, I would like to remember Professor Brian McCarry, who welcomed us to the program, and who is deeply missed.

On a more personal note, I have had the pleasure of making a number of close friends while at McMaster. Many of these friends are people I worked with closely and are mentioned in the paragraphs above. But, I also want to thank Lisa, Janice, Chris, Brad, Vinodh, Antonio and all the members of the Backside Attacks, and the many other people with whom I have shared the last six years.

The long hours of graduate school would have been a quite a slog were it not for your company.

I could not have done this without my family and friends back home. I cannot thank them enough. To my parents, for always understanding, for supporting me unconditionally, for allowing me to build the confidence I needed, and for always being there for me! I've learned more from you than any schooling could ever provide! To Mike and Jocelyn for first providing a home away from home, then a home in truth. To the Angus sistren, for all of the fun times across the country. I can't wait for the future! Kayla & Chris, Nan & Papa, and the rest of my extended family back home – thank you for all of your love, support and news from home. Thank you to Chris Gall, for always being a friend and for always being up for a trip – even if they don't serve meat on a stick.

Finally, to Sarah. I will never be able to express the depths of the gratitude I feel for your company, your love, and your support. Not to mention the proofreading. I have loved every minute of our adventures over the last decade, and there is nothing I look forward to more than the next adventure with you. Thank you. For everything.

Table of Contents **Page**

Chapter 1: Introduction to the Physical Properties of Carbon Nanotubes and Strategies for their Dispersion 1

1.1. Introduction to Carbon Nanotubes and Other Graphitic Materials 1

1.1.1. Structure and Physical Properties of Graphene 2

1.1.2. Structure and Physical Properties of Fullerenes 6

1.1.3. Basic Structure and Properties of Carbon Nanotubes 7

1.2. Electrical Properties of Carbon Nanotubes 12

1.3. Chemical Reactivity of Carbon Nanotubes 16

1.4. π-π Stacking and Other Non-covalent Interactions in Nanotubes 19

1.5. Processing and Suspension of Carbon Nanotubes 21

1.6. Separation of Carbon Nanotube by Type/Diameter/Chirality 24

1.6.1. DNA Wrapping and Ion Exchange Chromatography 25

1.6.2. Density Gradient Ultracentrifugation 28

1.6.3. Selective Dispersion/Interaction and Other Separation Methods 29

1.6.4. Gel Filtration/Electrophoresis 31

1.7. Suspension of Carbon Nanotubes within Polymeric Matrices 32

1.7.1. Mechanical Reinforcement of Materials 33

1.7.2. Enhancement of Electrical Properties in Materials 38

1.7.3. Enhancement of Thermal Properties in Materials 45

1.7.4. Discrete SWNT/Polymer Complexes in Bulk Materials 46

1.8. Characterization of Carbon Nanotubes and their Composites 49

1.9. Conclusion and Summary of Objectives 54

1.10. References 56

Chapter 2: Polymer Grafting to Single-Walled Carbon Nanotubes: Effect of Chain Length on Solubility, Graft Density and Mechanical Properties of Macroscopic Structures 69

2.1. Introduction 71

2.2. Results and Discussion 74

2.2.1. Synthesis 74

2.2.2. Graft Density 79

2.2.3. Solubility 83

2.2.4. Mechanical Properties of Solids 85

2.3. Conclusion 90

2.4. Experimental 91

2.4.1. General Experimental 91

2.4.2. Synthesis 92

2.4.3. Polymerization of Styrene 94

2.4.4. Polystyrene/SWNT Coupling 95

2.4.5. SWNT Film Preparation and Characterization 96

2.5. References 97

Chapter 3: Functionalization of Single-Walled Carbon Nanotubes via the Piers-Rubinsztajn Reaction 100

3.1. Introduction 102

3.2. Results and Discussion 104

3.3. Conclusion 112

3.4. Experimental 113

3.4.1. General Experimental 113

3.4.2. Synthesis 114

3.4.3. Production of Composite Materials 115

3.5. References 117

Chapter 4: Bulk Suspension of Single-Walled Carbon Nanotubes in Silicone Rubbers Using Diblock Copolymers 120

4.1. Introduction 122

4.2. Results and Discussion 125

4.3. Conclusion 138

4.4. Experimental 139

4.4.1. General Experimental 139

4.4.2. Synthesis 140

4.4.3. Nanotube Dispersions 142

4.4.4. Electrical Measurements 144

4.5. References 145

Chapter 5: Synthesis of Conjugated Polymers Containing DIBAC-Derived Triazole Monomers..... 148

5.1. Introduction..... 150

5.2. Results and Discussion..... 153

5.3. Conclusion..... 163

5.4. Experimental..... 164

5.4.1. General Experimental..... 164

5.4.2. Coumarin Crosslinking Experiments..... 166

5.4.3. Synthesis..... 166

5.4.4. Polymerization Procedure (Compounds P1-P6)..... 182

5.4.5. Computational Methods..... 184

5.5. References..... 187

Chapter 6: Metal-Free Reduction of Secondary and Tertiary N-Phenyl Amides by Tris(pentafluorophenyl)boron Catalyzed Hydrosilylation..... 191

6.1. Introduction..... 193

6.2. Results and Discussion..... 197

6.3. Conclusion..... 202

6.4. Experimental..... 203

6.4.1. General Experimental..... 203

6.4.2. Synthesis..... 203

6.4.3. Synthesis of 3,8-Difluorodibenzo[b,f]azocin-6(5H)-one..... 204

6.4.3. Characterization of Amines 207

6.5. References 211

Chapter 7: Thesis Conclusions and Recommendations for Future Work .. 213

7.1. Summary and General Conclusions 213

7.2. Recommendations for Future Work 216

Appendix I: Supporting Information for: Polymer Grafting to Single-Walled Carbon Nanotubes: Effect of Chain Length on Solubility, Graft Density and Mechanical Properties of Macroscopic Structures 218

Appendix II: Supporting Information for: Functionalization of Single-Walled Carbon Nanotubes via the Piers-Rubinsztajn Reaction 221

Appendix III: Supporting Information for Synthesis of Conjugated Polymers Containing DIBAC-Derived Triazole Monomers 226

List of Figures **Page**

Chapter 1: Introduction to the Physical Properties of Carbon Nanotubes and Strategies for their Dispersion 1

Figure 1.1: a) Reduced graphene oxide dispersion, b) Atomic force micrograph image of single-layer graphene, c) Scanning tunneling micrograph image of single-layer graphene. Reproduced with permission from Ref. 29. Copyright American Chemical Society, 2009. 3

Figure 1.2: Further reactions of graphene oxide to produce graphene derivatives. Reproduced with permission from Ref. 40. Copyright Royal Society of Chemistry, 2009 4

Figure 1.3: C60 - Buckminsterfullerene - the most common and easily produced fullerene 7

Figure 1.4: Electron micrographs of a a) single-walled, b) double-walled, and c) multi-walled carbon nanotube. a) Reproduced with permission from Ref. 76. Copyright Nature Publishing Group, 1993. b,c) Reproduced with permission from Ref. 77. Copyright Elsevier, 2002 8

Figure 1.5: Carbon nanotube vector map 10

Figure 1.6: Representative armchair, zigzag and chiral carbon nanotubes. Reproduced with permission from Ref. 77. Copyright Elsevier, 2002 11

Figure 1.7: Schematic representation of electronic density of states for an individual semiconducting nanotube. E_{11} and E_{22} represent transitions in the

UV-Vis-NIR portion of the spectrum. Reproduced with permission from Ref. 96. Copyright American Association for the Advancement of Science, 2002..12

Figure 1.8: UV-Vis-NIR absorbance spectra for a series of carbon nanotube chiralities purified by DNA-wrapping and ion exchange chromatography. The spectrum of the starting HiPCO SWNT sample appears in black (top). The chiralties of the individual species are indicated to the right. Reproduced with permission from Ref. 187. Copyright Nature Publishing Group, 2009..... 27

Figure 1.9: a) Modulus enhancement and b) strength reinforcement as a function of fiber aspect ratio for aligned fibers by the rule of mixtures. Reproduced with permission from Ref. 81. Copyright Elsevier, 2006..... 35

Figure 1.10: Graphical representation of a "two-generation" functionalization scheme. Reproduced with permission from Ref. 171. Copyright Elsevier, 2012. 37

Figure 1.11: Plot of thin film conductivity vs. the inverse of the junction resistance for pristine and chemically modified SWNTs. Acid annealed SWNTs are more conductive. Reproduced with permission from Ref. 234. Copyright American Chemical Society, 2009.. 41

Figure 1.12: Large and well-defined percolation threshold produced by using PEDOT:PSS latex particles to bridge SWNT junctions. Reproduced from Ref. 247. Copyright Nature Publishing Group, 2011. 44

Figure 1.13: Schematic representations of the "grafting-to" vs. "grafting-from" approaches to carbon nanotube functionalization. Reproduced with permission from Ref. 221. Copyright Taylor and Francis, 2007..... 48

Figure 1.14: Raman spectra from a variety of sp^2-hybridized (graphitic) structures. Reproduced with permission from Ref. 265. Copyright American Chemical Society, 2010..... 50

Figure 1.15: HiPCO SWNT optical and Raman spectra after being suspended with a set of common surfactants. Suspensions of SWNT in SDBS show sharper transitions in both optical and Raman spectroscopy, indicating a greater degree of debundling. Reproduced with permission from Ref. 174. Copyright American Chemical Society, 2003..... 52

Chapter 2: Polymer Grafting to Single-Walled Carbon Nanotubes: Effect of Chain Length on Solubility, Graft Density and Mechanical Properties of Macroscopic Structures 69

Figure 2.1: A) Solubility of PS-SWNTs in THF as a function of the weight average molecular weight (Mw) of the PS graft polymer. B) Graft density and inset: mass percentage of PS within the PS-SWNT conjugates as a function of the weight average (Mw) molecular weight of the PS graft polymer..... 78

Figure 2.2: A) Plot of chain separation distance, R, as a function of grafted polymer M_w. B) Calculated chain separation versus molecular weight for

published data on PS functionalized SWNTs (refs. 21 and 23). In these papers the functionalization was performed in two distinct ways, by radical coupling and "click" coupling. 82

Figure 2.3: Dispersed concentration of PS-SWNTs plotted as a function of $M_W^{-1.176}$. This quantity is approximately proportional to the steric barrier height. The dashed line illustrates linearity. 85

Figure 2.4: A) Representative stress strain curves for some of the buckypapers studied in this work. B), C) and D) Young's modulus, strength, and strain at break for the Buckypapers plotted as a function of grafted chain density, N/A, respectively. Insets: Mechanical parameters plotted as a function of molecular weight. 87

Chapter 3: Functionalization of Single-Walled Carbon Nanotubes via the Piers-Rubinsztajn Reaction 100

Figure 3.1: Raman spectra of functionalized HiPCO SWNTs with excitation at a) 514 nm, b) 785 nm. 106

Figure 3.2: Photographs of SWNT/PDMS composites at a) 1× magnification (3 mm thick slice), and b) 10× magnification (1 mm thick slice). The different samples in each photograph correspond to the following: i) 1% SWNT foam (PR crosslinking); ii) 1% SWNT elastomer (PR crosslinking), iii) 0.030% SWNT elastomer (Dow Sylgard 184); iv) PDMS elastomer (Dow Sylgard 184). 112

Chapter 4: Bulk Suspension of Single-Walled Carbon Nanotubes in Silicone Rubbers Using Diblock Copolymers 120

Figure 4.1: ^{1}H NMR spectrum of P4 in $CDCl_3$ 127

Figure 4.2: TGA data showing mass loss upon heating under an argon atmosphere for P3DT-9.8k (4b), PDMS-2k, P3DT-*b*-PDMS (P5), P3DT-SWNT and P3DT-*b*-PDMS-SWNT samples. 128

Figure 4.3: UV-Vis-NIR absorption data for polymer-SWNT dispersions (**P1**-**P6**) in THF (a); absorption spectra for **P6**-SWNT in THF, toluene, xylenes, and $CHCl_3$ (b) 130

Figure 4.4: Photoluminescence maps of **P4**-SWNT samples in (a) THF (b) toluene and (c) xylenes 131

Figure 4.5: Conductivity, σ, as a function of SWNT wt %, when using (a) P3DT-*b*-PDMS (**P5**) or (b) P3DT (**4b**) to disperse SWNTs in crosslinked silicone. The error bars represent logarithmic relative error of triplicate measurements for each concentration. 134

Figure 4.6: Conductivity as a function of strain for: a) P3DT coated SWNTs within bulk PDMS (0.13 wt % SWNT), b) Pristine and pre-stretched (ca. 75% elongation) P3DT coated SWNTs within bulk PDMS (0.17 wt % SWNT). c) P3DT-*b*-PDMS coated SWNTs within bulk PDMS (0.077 wt % SWNT). Error bars (a, c) represent relative standard error calculated from the full series of duplicate measurements; b) is a series of single measurements 137

Chapter 5: Synthesis of Conjugated Polymers Containing DIBAC-Derived Triazole Monomers..... 148

Figure 5.1: (a) Simplest conceptual strain promoted azide-alkyne cycloaddition (SPAAC) using cyclooctyne. (b) Previously reported conjugated dibenzocyclooctynes and their second-order rate constants in the reaction with benzyl azide. 152

Figure 5.2: Normalized absorption (a) and emission (b) data for polymers **P1–P5**..... 158

Figure 5.3: (a) Structure of coumarin-containing **P6**. (b) The coumarin photo-cross-linking reaction 161

Figure 5.4: (c) UV–vis absorbance and emission spectra of **P6** in THF solution. (d) GPC data for the soluble fraction of **P6** before and after photo-cross-linking. (e) Time-resolved UV–vis absorbance study of cross-linking in a thin film of **P6**. 162

List of Appendix Figures **Page**

Appendix I: Supporting Information for: ***Polymer Grafting to Single-Walled Carbon Nanotubes: Effect of Chain Length on Solubility, Graft Density and Mechanical Properties of Macroscopic Structures*** ***218***

Figure A1.1. GPC Overlay plotted from raw data of ten runs. There are no peaks with retention times <14 min. Solvent front is at 28 min 218

Figure A1.2. Thermogravimetric analysis of pristine SWNTs and SWNT conjugates, before and after reaction with N_3-PS. 218

Figure A1.3: Raman spectra of pristine and functionalized SWNTs. The sharp increase in the D-band (~1300 cm^{-1}) indicates successful covalent functionalization 219

Figure A1.4: Overlay of Raman spectra of PS-SWNTs. No appreciable difference is noted between grafts 219

Figure A1.5: IR spectra for SWNTs, SWNT derivatives, and precursor molecules. (A) full spectra; (B) Upper region of the IR spectra; (C) Fingerprint region of the IR spectra 220

Appendix II: Supporting Information for: ***Functionalization of Single-Walled Carbon Nanotubes via the Piers-Rubinsztajn Reaction*** ***221***

Figure A2.1: TGA of Raw HiPCO SWNT 221

Figure A2.2: TGA of a-SWNT 221

Figure A2.3: TGA of TMDS-SWNT 222

Figure A2.4: TGA of PDMS-SWNT-1k 222

Figure A2.5: TGA of PDMS-SWNT-6k 223

Figure A2.6: TGA of PDMS-SWNT-17k 223

Figure A2.7: TGA of PDMS-SWNT-28k 224

Figure A2.8: TGA of PDMS+SWNT Control 224

Figure A2.9: Representative UV-Vis-NIR Spectra 225

Appendix III: ***Supporting Information for Synthesis of Conjugated Polymers Containing DIBAC-Derived Triazole Monomers..... 226***

Figure A3.1: Full polymer synthetic scheme for reference 226

Figure A3.2: Synthesis Scheme for coumarin polymer **P6** 227

Figure A3.3: Cyclic Voltammograms **P1-P5** 228

Figure A3.4: Emission spectra during the quenching of **P3** (0.004 mg/mL in THF) with nitrobenzene (1.0 M in THF) 229

Figure A3.5: ^{1}H-NMR spectrum of **2** in $CDCl_3$ 230

Figure A3.6: ^{1}H-NMR spectrum of **4** in $CDCl_3$ 230

Figure A3.7: ^{1}H-NMR spectrum of **5** in $CDCl_3$ 231

Figure A3.8. ^{1}H-NMR spectrum of **6** in DMSO-d6 231

Figure A3.9: ^{1}H-NMR spectrum of **6** in DMSO-d6 232

Figure A3.10: ^{1}H-NMR spectrum of **9** in $CDCl_3$ 232

Figure A3.11: ^{1}H-NMR spectrum of fluorene boronic ester in $CDCl_3$ 233

Figure A3.12: ^{1}H-NMR spectra of **10a** and **P1** (anisole derivative) 234

Figure A3.13: ^{1}H-NMR spectra of **10b** and **P2** (t-Bu derivative) 234

Figure A3.14: ^{1}H-NMR spectra of **10c** and **P3** (phenyl derivative)..... 235

Figure A3.15: ^{1}H-NMR spectra of **10d** and **P4** (Nitro derivative)..... 235

Figure A3.16: ^{1}H-NMR spectra of **10e** and **P5** (Pyrene derivative)..... 236

Figure A3.17: ^{1}H-NMR spectra of **10f** and **P6** (Coumarin derivative) 236

Figure A3.18: Tetramer of Model DIBAC Polymer (PM3)..... 237

Figure A3.19: Optimized Structures, a) Model Monomer, b) Model Dimer, c) Model Tetramer 237

Figure A3.20 a) Calculated dimer stationary point (B3LYP), b) Calculated dimer stationary point (PM3), c) Simplified DIBAC geometry, d) Crystal structure of known analog,[17] e) Crystal structure of (c), with extraneous structure removed (from CCDC database – YIKGOQ00). f) 2D-structure of DIBAC containing analog..... 238

List of Schemes **Page**

Scheme 2.1: General synthesis of PS-SWNTs. 75

Scheme 3.1: Functionalization of single-walled carbon nanotubes via Tour reaction, followed by Piers-Rubinsztajn reaction. 105

Scheme 4.1: Synthesis of 3-decyl-2,5-dibromothiophene 126

Scheme 4.2: Grignard metathesis polymerization of P3HT 126

Scheme 5.1: Synthesis of the 2,7-Dibromobiarylazacyclooctynone pro-monomer 153

Scheme 5.2: (a) Synthesis of Monomers **10a**–**e**; (b) Synthesis of Conjugated Copolymers **P1–P5** via Suzuki Polycondensation with 9,9-Didodecylfluorene-2,7-diboronic Acid Bis(1,3-propanediol) Ester as the Comonomer 155

Scheme 6.1: The reduction of model amides **1**, and **2** 197

List of Tables **Page**

Table 1.1: Physical properties of SWNT and MWNT. 9

Table 2.1: PS-SWNT Properties. 76

Table 3.1: Solubility and graft weights for silicone carbon nanotube composites. 105

Table 3.2: Solubility of TMDS-SWNT in a variety of solvents 109

Table 4.1: P3DT-*b*-PDMS properties: % mass of each block determined by TGA. 126

Table 5.1: The physical and electronic properties of the series of polymers 160

Table 6.1: Amines from the hydrosilylation of amides 199

Table 6.2: Product yield from hydrosilylative reduction using different silanes 202

List of Abbreviations

ARGET	Activator Regenerated by Electron Transfer
ATRP	Atom Transfer Radical Polymerization
B3LYP	Becke, 3-parameter, Lee-Yang-Parr
BARAC	Biarylazacyclooctynone
CNT	Carbon Nanotube
CP	Conjugated Polymer
CuAAC	Copper(I)-catalyzed Azide-Alkyne Cycloaddition
DIBAC	2,7-Dibromoazadibenzocyclooctyne
DDQ	2,3-Dichloro-5,6-dicyano-1,4-benzoquinone
DFT	Density Functional Theory
DMF	Dimethyl Formamide
DNA	Deoxyribonucleic Acid
DPMS	Diphenylmethylsilane
DPS	Diphenylsilane
DSC	Dynamic Scanning Calorimetry
DWNT	Double-walled Carbon Nanotube
GAMESS	General Atomic and Molecular Electronic Structure System
GO	Graphene Oxide
GRIM	Grignard Metathesis
GPC	Gel Permeation Chromatography
HiPCO	High Pressure Carbon Monoxide

HOMO	Highest Occupied Molecular Orbital
IR	Infrared
KHMDS	Potassium Hexamethyldisilazide
LUMO	Lowest Unoccupied Molecular Orbital
MS	Mass Spectrometry
MWNT	Multi-walled Carbon Nanotube
NIR	Near Infrared
P3DT	Poly(3-decylthiophene)
PC	Polycarbonate
PDI	Polydispersity Index
PDMS	Polydimethylsiloxane
PEDOT	Poly(3,4-ethylenedioxythiophene)
PET	Poly(ethylene terephthalate)
PL	Photoluminescence
PMHS	Polymethylhydrosilane
PMMA	Poly(methyl methacrylate)
PPF	Poly(phenylene-*co*-fluorene
PR	Piers-Rubinsztajn
PS	Polystyrene
PSS	Polystyrene Sulfonate
PTFE	Polytetrafluoroethylene
PVC	Poly(vinyl chloride)

RBM	Radial Breathing Mode
SCE	Saturated Calomel Electrode
SDBS	Sodium Dodecyl Benzyl Sulfonate
SPAAC	Strain-promoted Azide–alkyne Cycloaddition
SWNT	Single-walled Carbon Nanotube
m-SWNT	Metallic Single-walled Carbon Nanotube
sc-SWNT	Semiconducting Single-walled Carbon Nanotube
TCNQ	7,7,8,8-Tetracyanoquinodimethane
TEOS	Tetraethyl Orthosilicate
THP	Tetrahydropyranyl
TLC	Thin-layer Chromatography
TIPS	Triisopropylsilyl
TMDS	Tetramethyldisiloxoane
TGA	Thermogravimetric Analysis
THF	Tetrahydrofuran
THPTA	Tris(3-hydroxypropyltriazolylmethyl)amine
TMS	Trimethylsilyl
UV	Ultraviolet
Vis	Visible
XPS	X-ray Photoelectron Spectroscopy
XRD	X-ray Diffraction

Chapter 1: Introduction to the Physical Properties of Carbon Nanotubes and Strategies for their Dispersion

1.1. Introduction to Carbon Nanotubes and Other Graphitic Materials

Graphite, diamond, and "amorphous" carbon are allotropes of carbon that have been known since antiquity. Modern analytical methods have greatly expanded our understanding of the diversity in carbonaceous materials and several additional allotropes have been identified including glassy carbon (1950's),[3] lonsdaleite (1967),[4] carbon nanotubes (first observed in 1952, characterized in 1991),[5,6] fullerenes (1985),[7,8] carbon nanofoam (1997), [9,10] and the long-theorized monolayer of graphite: Graphene (2004).[11,12] Other exotic allotropes of carbon have also been theorized and investigated.[13-15]

The various glassy, amorphous, and crystalline carbonaceous materials all represent active fields of study, but recent research has focused on graphitic carbon. Fullerenes, graphene, and carbon nanotubes (CNTs) represent a very active area of chemical and materials research. Over the last two decades researchers have explored their exceptional electrical and mechanical properties, and their potential for medical applications.[16] Graphene and carbon nanotubes have been considered for uses in composite materials, coatings, microelectronics, energy storage, sensors, and medical devices.[1,17] Over the last decade, both nanotube and graphene research has accelerated each year.[1] Already, CNT materials have begun to find their way into commercial and specialty applications,

and the rate of growth in graphene patents suggests graphene applications are not far behind.[1,18]

The study of carbon nanotubes involves an understanding of the nature of graphitic materials including their drawbacks and the steps needed to overcome them. As such, a brief introduction to the various types of graphitic carbon is warranted.

1.1.1. Structure and Physical Properties of Graphene

While theorized and initially explored long before carbon nanotubes, single layer graphene was only first isolated in 2004 by Nobel laureates Andre Geim and Kostya Novoselov using the Scotch Tape method.[12,19] Since its discovery, graphene has become an area of intense research rivaling that of carbon nanotubes.

Graphene is an extensive sheet of sp^2-hybridized carbon. It is often referred to as a pseudo 2-dimensional material or crystal[20,21] due to its incredibly large aspect ratio and single atomic thickness.[20,22] Defect-free graphene has no band-gap, excellent conductivity, and extremely high carrier mobility – ideal properties for an electronic material.[22-24] Unfortunately, graphene's electrical properties require very low defect concentrations. The presence of sp^3 carbons or non-carbon dopants has a substantial electronic effect.[23,25] These defects are a major limitation in the development of graphene-based devices.[26,27] Nonetheless, a great deal of progress has been made and the production of large sheets of relatively high quality graphene is routine.[20,28]

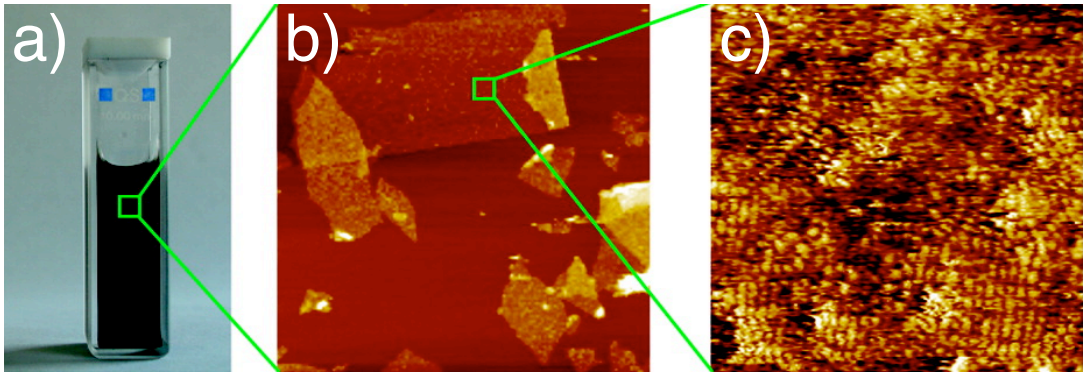

Figure 1.1: a) Reduced graphene oxide dispersion, b) Atomic force micrograph image of single-layer graphene, c) Scanning tunneling micrograph image of single-layer graphene. Reproduced with permission from Ref. 29. Copyright American Chemical Society, 2009.

Graphene and carbon nanotubes share similar synthesis and processing difficulties, such as strong π-stacking,[11,13,17,30,31] generally low solubility,[11,32] and the presence of defect sites.[33-35] In contrast to CNTs, however, graphene is planar and does not contain the rich blend of chirality and diameter-based properties, or their associated complications.

On a bulk scale, graphene and carbon nanotubes are exfoliated by sonication or shear-mixing,[32,36,37] and are solution-processed in very similar ways, including chemical functionalization, and the use of surfactants or polymers to produce supramolecular complexes.[38-40] The sp^2 carbons of graphene are generally unreactive and harsh conditions are typically required for their modification; the reactions are generally applicable to carbon nanotubes as well.

Graphene has been shown to be most reactive as a single-layer.[38,41] It has also been suggested that graphene reacts at strained regions: Defect sites and in chain reactions from an initial reaction site. The increased susceptibility to "rippling" via thermal or mechanical strain explains the enhanced reactivity of exfoliated graphene.[38,40,42]

Oxidations of graphene with oxidizing agents are, by far, the most common functionalization method. This process generates exfoliated graphene oxide (GO) with hydroxy, carboxyl, and epoxide functionalities which can be used for further functionalization.[43,44]

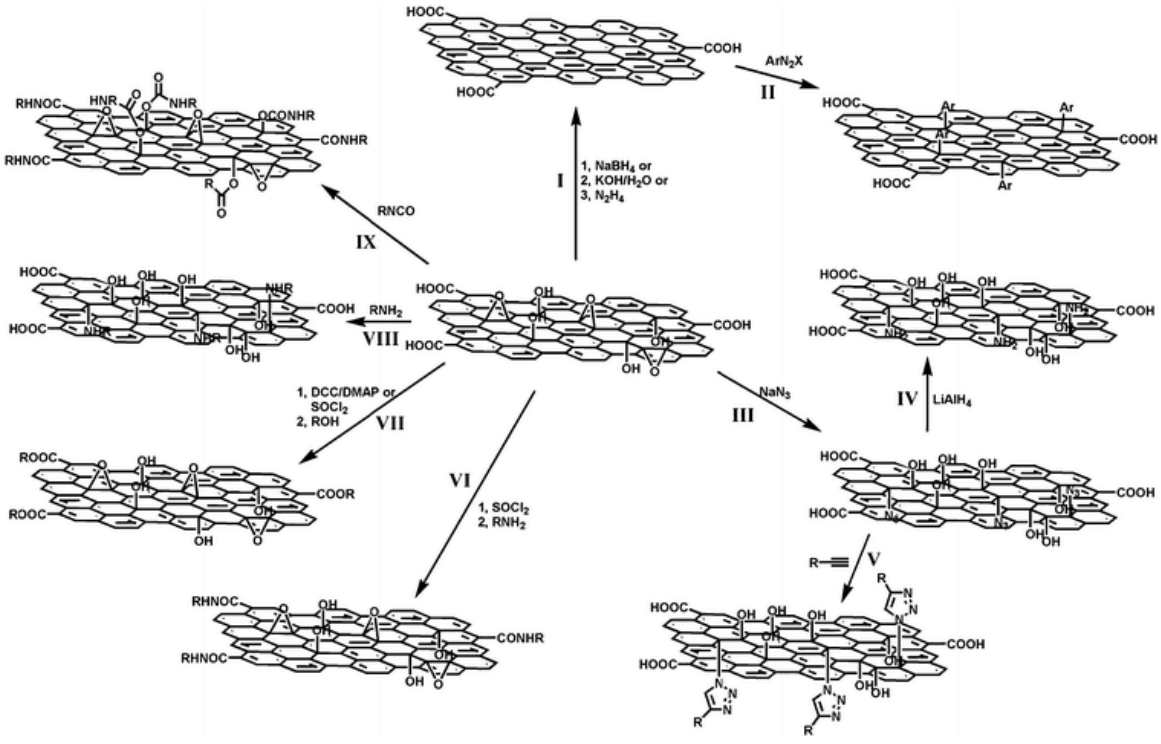

Figure 1.2: Further reactions of graphene oxide to produce graphene derivatives. Reproduced with permission from Ref. 40. Copyright Royal Society of Chemistry, 2009.

Samples of GO can also be reduced back to, now exfoliated, graphene. Additionally, free-radicals such as the aryl radicals produced via diazonium chemistry,[45,46] and powerful dienophiles like azomethine ylides,[47,48] nitrenes,[49,50] and benzynes,[51-56] are capable of functionalizing graphene surfaces.[39,45] Lastly, fluorographene and graphane[57-59] (hydrogenated graphene) can be produced using XeF_2[60,61] or cold hydrogen plasma, respectively.[39]

Covalent modification is used to improve processablility and to introduce band gaps, but generally it is desirable to leave graphene's electronic structure intact. Accordingly, the strong π-stacking characteristic is leveraged to suspend the graphene using conjugated molecules for organic solubility,[39,62-64] or surfactants for water solubility.[62,65] In this fashion, graphene can be manipulated without chemical modification. In general, the molecules used are also applicable to carbon nanotube processing, and vice versa.[49,66]

Finally, in an analogous fashion to chemical modification, graphene shares similar electronic, chemical, and mechanical properties to carbon nanotubes. As a single sheet, graphene is incredibly strong (tensile modulus of up to 1 TPa) and very conductive (>300 S cm^{-1}).[34,67] However, as a pseudo-2-dimensional object, it is most suited for applications where coatings or sheets are required, and is therefore complementary to CNTs in its potential applications. Finally, it is worth noting that it is reasonable to expect that many of the strategies employed in the following chapters could be equally relevant to the processing of graphene.

1.1.2. Structure and Physical Properties of Fullerenes

In the same way that carbon nanotubes can be conceptualized as rolled sheets of graphene, buckminsterfullerenes can be visualized as discrete, hollow "balls" of graphene or small, spherical pieces of carbon nanotubes. Fullerenes' physical properties are somewhat similar to other graphitic materials, but more reminiscent of their small molecule character. The increased bond strain and discreet molecular nature of fullerenes distinguishes their chemistry from graphene and carbon nanotubes. Likewise, their small size and considerably weaker π-stacking substantially decreases the difficulties in purification and production. Fullerenes are more reactive than their other graphitic counterparts due to the presence of low-lying LUMO levels.[68] This electron affinity arises from orbital rehybridization due to pyramidalization. The resulting increased *s* character of fullerene π-orbitals minimizes the electron delocalization and enhances the electrophilicity of fullerene, often even when compared to simple alkenes.[68] As such their chemical reactivity is more closely related to electron-deficient alkenes, rather than the more stable graphitic structures of graphene or carbon nanotubes.[69]

Fullerenes are produced as many different isomers,[70] including the eight most common: C_{60}, C_{70}, C_{76}, C_{78} (three common isomers), and C_{84} (two common isomers).[69] Their colours, and to some extent, their chemical and physical properties, vary according to their molecular weight and symmetry (isomerism).[69]

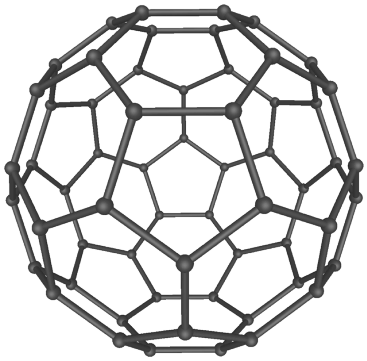

Figure 1.3: C_{60} - Buckminsterfullerene - the most common and easily produced fullerene. Wikimedia Commons, 2006.

Unsurprisingly, considering their simpler structure and early discovery, fullerene research is the most mature of the graphitic materials, and fullerene chemistry has been extensively explored.[71] Fullerenes have seen commercial use in polymer solar cells and have been utilized in various experimental organic electronics, experimental lubricants, and medical research.[72]

1.1.3. Basic Structure and Properties of Carbon Nanotubes

As discussed, fullerenes, graphene, and carbon nanotubes share many chemical and physical properties. In general, carbon nanotubes show electronic properties derived from their graphitic structure and they share their processing difficulties and purity concerns with their sheet-like counterparts. Moreover, like graphene, carbon nanotubes share many potential applications in materials and electronic devices.[2] In an analogous fashion to "2-dimensional" graphene, carbon nanotubes can be conceptualized as a "1- dimensional" graphitic wire; as cylindrical fullerenes, or as a rolled graphene sheet – though none of these

characterizations are completely satisfactory. CNTs can be open- or closed-ended;[73] have a wide range of diameters and lengths; and can have 1, 2, or many concentric shells.[74] These tube configurations are referred to as single-, double- or multi-walled carbon nanotubes – typically abbreviated SWNT, DWNT, and MWNT, respectively (Figure 1.4). These basic properties are typically controlled by the various synthetic methods used to produce them, however, no method produces a monodisperse sample of carbon nanotube, and commercial samples contain a wide variety of similar structures.[75]

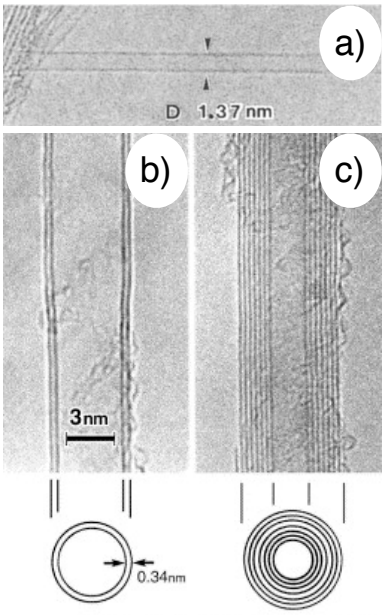

Figure 1.4: Electron micrographs of a a) single-walled, b) double-walled, and c) multi-walled carbon nanotube. a) Reproduced with permission from Ref. 76. Copyright Nature Publishing Group, 1993. b,c) Reproduced with permission from Ref. 77. Copyright Elsevier, 2002

In general, individual carbon nanotubes have exceptionally large moduli, strengths, conductivities, and current carrying capacities (Table 1.1).

Table 1.1: Physical properties of SWNT and MWNT:[78-85]

Property	**SWNT**	**MWNT**
Diameter	0.4-10 nm	2-100 nm
Young's Modulus	ca. 1 TPa	ca. 1 TPa
Tensile Strength	13-52 GPa	11-63 GPa
Thermal Conductivity [a]	> 200 W m^{-1} K^{-1}	> 200 W m^{-1} K^{-1}
Current Carrying Capacity	ca. $4x10^9$ A/cm^2 [b]	> 10^9 A/cm^2

[a] Thermal conductivity of individual nanotubes could be as high as 6600 W m^{-1} K^{-1}, and for bulk samples as low as 15 W m^{-1} K^{-1}. The quoted value is a best estimate of the maximum value for bulk materials.
[b] Metallic SWNTs

Single- and multiwalled carbon nanotubes have very similar mechanical properties. CNTs have a Young's modulus (stiffness) comparable to diamond and a tensile strength that is unparalleled.[81] Their current carrying capacities are *ca.* 3 orders of magnitude larger than an equivalent diameter of metallic wire, particularly in the absence of air;[86] some of the highest current carrying capacities known.[84] Their electron mobilities are unprecedented among known semiconductors.[87] Likewise, their thermal conductivities are exceptional – individual nanotubes may have thermal conductivities up to 37 000 W m^{-1} K^{-1} at 100 K, and 6 600 W m^{-1} K^{-1}.[88] CNT arrays or sheets have bulk thermal conductivities in excess of 200 W m^{-1} K^{-1}.[88] However, their bulk thermal and electrical properties are also highly dependent on tube type and inter-tube junctions. These effects are discussed in greater detail in Section 1.3.1.

While not synthesized in such a fashion, the conceptualization of single-walled carbon nanotubes as "rolled" graphene sheets is particularly valuable. For

single-walled carbon nanotubes, this conceptualization helps establish important concepts of carbon nanotube "chirality" as defined by a "roll-up vector". In a similar fashion to fullerene isomers, these vectors dictate the specific properties of carbon nanotubes, including their diameter, band-gap, colour, density, etc.[89-91]

The lattice vectors of carbon nanotubes can be defined as: $C = na_1 + ma_2$ and are typically expressed in the format of (*n, m*) where the integers *m* and *n* are the two component vectors defined by the graphene unit cell (see Figure 1.5). The angle between these vectors is referred to as the "chiral angle," and these vectors determine the diameter and many physical properties of the carbon nanotube. This characterization is the most straightforward and most valuable for single-walled carbon nanotubes.[92]

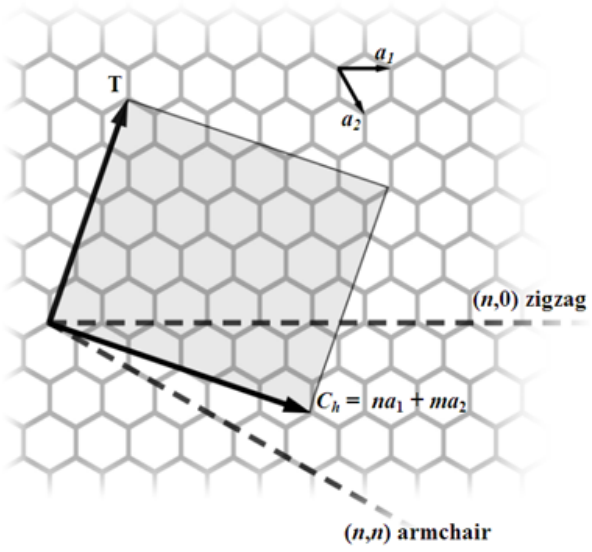

Figure 1.5: Carbon nanotube vector map. Public Domain. Wikimedia Commons, 2005.

A close inspection of the potential nanotube "chiralities" defined by their roll-up vector shows three fundamental groupings referred to as "armchair," "ziz-zag," and "chiral" carbon-nanotubes. SWNTs with a chiral index $m = n$ have a chiral angle of 0° are referred to as armchair SWNTs, those with a chiral index ($m,0$) or ($0,n$) are referred to as zig-zag, the remainder are "chiral", as their non-symmetrcial wrapping vectors lend a degree of handedness.

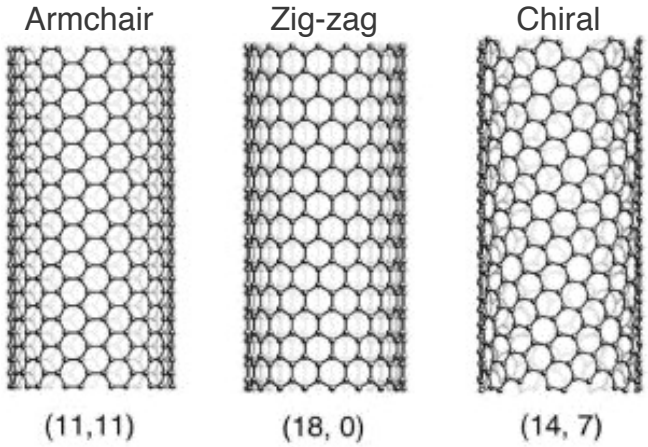

Figure 1.6: Representative armchair, zigzag and chiral carbon nanotubes. Reproduced with permission from Ref. 77. Copyright Elsevier, 2002

As mentioned previously, single-walled carbon nanotubes are typically divided into two categories based on their electronic properties: Metallic (m-SWNT) and semiconducting (sc-SWNT). While synthetic conditions can provide some control over the m-SWNT and sc-SWNT ratios, a selective synthesis has yet to be achieved. Most common production methods produce a roughly 1:2 ratio in favour of sc-SWNTs as is predicted by a simple statistical synthesis. In a similar

fashion, double-walled carbon nanotubes are metallic (if one or both tubes are metallic), or semi-conducting (if both are semi-conducting) in a roughly 2:1 ratio. As a single metallic shell renders an entire MWNT conductive, virtually all MWNTs exhibit metallic behavior.

1.2. Electrical Properties of Carbon Nanotubes

SWNT electrical properties are based on their chiralities and diameters. Armchair SWNTs ($m = n$) are metallic.[93,94] They do, however, exhibit a "pseudo bandgap," reducing the density of states near the Fermi level.[95]

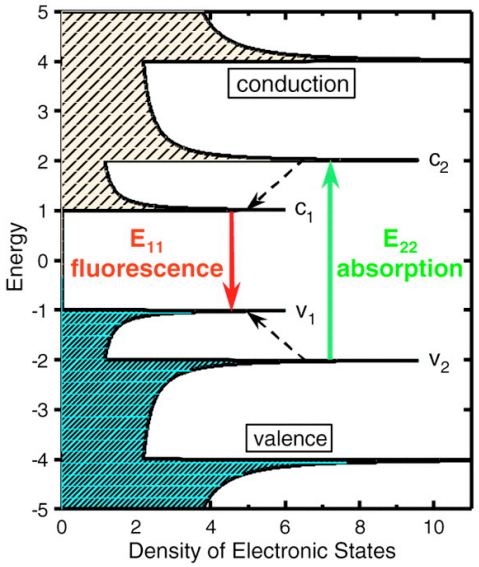

Figure 1.7: Schematic representation of electronic density of states for an individual semiconducting nanotube. E_{11} and E_{22} represent transitions in the UV-Vis-NIR portion of the spectrum. Reproduced with permission from Ref. 96. Copyright American Association for the Advancement of Science, 2002.

The presence of a pseudo bandgap is predicted to make armchair SWNTs susceptible to charge localization and doping, potentially allowing some tailoring of their conductivity or their use in sensors.[95] The pseudo bandgap in armchair SWNTs is inversely related to their diameter and is more pronounced in bundled SWNTs; isolated SWNTs are closer to "truly metallic".[97]

Zig-zag or chiral SWNTs, where $(m\text{-}n)/3$ is an integer, have a very small bandgap. This bandgap ranges from about 2 to 50 meV, over a diameter range of 3.0 to 0.7 nm; it scales with the square of the diameter.[98] The bandgap is induced by tube "twist" or curvature,[99,100] but due to its small size, these nanotubes are also often considered metallic.[2,93] However, it has been suggested that non-armchair nanotubes are much more susceptible to strain-induced conductivity changes than their armchair counterparts.[101,102]

The remaining two thirds of SWNT species are semi-conducting. They have a defined bandgap, inversely related to their diameter, ranging from about 2.2 eV (diameter = 0.4 nm) to <0.4 eV (diameter > 3.0 nm).[103]

The model of SWNT conductivity breaks down to some degree for very small diameter armchair and metallic zig-zag SWNTs whose metallicity is somewhat unpredictable.[104,105] However, this effect is only present for very small diameter carbon nanotubes, and can be explained by the rehybridization of the sidewall orbitals to account for high degrees of curvature.[94,106]

The precise nature of carbon nanotube conductivity has been well explored over the last two decades.[107] Bulk samples of MWNT or SWNTs are

highly conductive, individual m-SWNTs are ballistic conductors;[108] their conductance is quantized and is independent of diameter and nearly independent of voltage.[109] sc-SWNTs are good hole conductors and typically mimic *p*-type semiconductors.[110] Conductivity in both individual and bulk samples is improved by doping with an electron-withdrawing moiety,[111] and degraded by an electron-donating dopant.[112] Like bandgap, conductivity within individual semi-conducting nanotubes is dominated by diameter and chirality.[113] Defects reduce the conductivity of carbon nanotubes; large diameter tubes are less affected than their small diameter counterparts.[114] Covalent functionalization typically degrades conductivity, but this effect is greatly lessened by the use of "divalent" cycloaddition chemistry, such as carbene or nitrene reactions.[115,116]

The conductivity of individual CNTs is well understood, and this knowledge has been utilized in the production of devices that rely on individual carbon nanotubes. However, in bulk devices the electrical properties of carbon nanotubes are dominated by the nature of nanotube-nanotube junctions, *i.e.* nanotube percolation networks rather than the properties of the individual tubes themselves.[117]

The most significant source of resistance in a bulk CNT sample is junction resistance. Conductivity at junctions is dependent on quantum tunneling. Moreover, the probability of tunneling, and thereby the resistance, is dependent on the nature of the nanotubes involved, with semiconducting (sc-sc), metallic (m-m), and semiconducting/metallic (sc-m) junctions exhibiting substantial

differences in their conductivities.[118] Metallic/metallic junctions show very high transmission probabilities (low resistances) and semiconducting junctions are nearly as conducting, though more difficult to measure due to the challenge of obtaining good contact with semi-conducting tubes.[109] In contrast, the transmission probabilities are at least 2 orders of magnitude lower for metallic/semiconducting junctions[109] due to the formation of Schottky barriers with resistances much larger than those observed across the metallic tube itself.[118] Moreover, the m-sc junction is "rectifying", *i.e.* the conductivity is substantially higher in one direction (positive at sc).[109] Finally, the nature of this junction depletes the charge carrier density in the sc-SWNT near the junction, further reducing the conductivity within the sc-SWNT.[109,119] These effects are so prominent that the majority of the current in bulk samples is carried though entirely metallic/metallic connection networks, and the rest through all semiconducting junctions, even though these make up respectively small minorities of the total pathways.[118] This represents a major incentive for the purification of carbon nanotubes by type (discussed in Section 1.7).

Due to the potential control over electronic properties through chirality selection, SWNTs are the most useful for producing a wide variety of electronic devices. Multi-walled and double-walled carbon nanotubes are metallic as long as one shell is metallic. This means that more than half of the DWNT and virtually all MWNT show metallic character, and typically show a relatively consistent

work function across a given sample. Again, this can be modified by absorption of dopants,[120] or covalent modification.[121]

The rich, chirality-dependent, electronic structure of carbon nanotubes explains the interest for their use in electronics. However, it also leads to a particularly thorny problem. For SWNT-based electronic devices to be practical, single chirality SWNTs must be selectively produced, or the separation of a mixed chirality sample must be achieved. At the very least, SWNTs must be separated by conductivity and into groups of similar diameter. Separations on a small scale have been demonstrated, but these technologies are very labour-intensive. A satisfactory, scaleable method remains to be developed.[7] These challenges and methods are discussed in detail in Section 1.6.

1.3. Chemical Reactivity of Carbon Nanotubes

Carbon nanotubes show chemical reactivity intermediate to fullerenes and graphene. Like fullerenes, carbon nanotubes have a diverse range of structures, and their chemistry varies by type, diameter, and configuration. The most significant division in carbon nanotube structure is the difference between multi-walled and single-walled carbon nanotubes. In most cases, SWNTs are more chemically reactive than their less-strained MWNT counterparts. Reactivity generally increases with increased sidewall curvature (strain), but is also dependent on chiral angle and metallicity.[122]

Like graphene, the initial approaches to chemically functionalizing carbon nanotubes targeted defect sites produced in their synthesis.[123] However, as

the quality of carbon nanotubes improved, the concentration of defect sites decreased. Also as higher degrees, or more evenly distributed functionality was desired, strategies for the direct reaction of pristine carbon nanotube sidewalls developed. The scope of the available chemistry is broad,[122] much of it is outside the scope of this review, however, a brief summary is presented in the following pages.

Some of the less sophisticated methods of chemically modifying carbon nanotubes involve directly oxidizing the sidewalls using the same powerful oxidizing conditions used for graphene,[124] *e.g.* Piranha solution, nitric acid, $KMnO_4$, F_2,[125] O_3,[126] or by electrochemical means.[127] However, these conditions tend to introduce an excessive number of defects, and are capable of introducing a very limited variety of functionalities.

Fortunately, carbon nanotubes have reactivity intermediate to that of graphene and fullerenes, and less extreme conditions can also be effective. Most carbon nanotube reactions rely on a radical- or cycloaddition-type mechanism. In general, carbon nanotubes react as nucleophiles (in contrast to fullerenes), and most functionalization strategies rely on electron-deficient or electrophilic reagents. As mentioned previously, narrow diameter, metallic SWNTs exhibit the greatest intrinsic reactivity, at least toward electrophilic and radical chemistry, as they have the highest electron density.[128-133] For example, even moderate electrophiles, such as silanes can react with small, metallic SWNTs.[134] Highly

electrophilic diazonium, pyrylium, dithiolyium, and nitronium compounds react readily with the surface of all carbon nanotubes in radical-type reactions.[134]

In fact, most *in situ* generated radicals will react with carbon nanotubes – for example, reactions with polymeric radicals generated via nitroxide-mediated polymerization,[135] or radicals generated in Billups and Billups/Birch type reactions.[136-140] Generally, radical reactions lead to a high functional group density.

Unfortunately, radical reactions also tend to disrupt the carbon nanotube electrical/mechanical properties to the greatest degree,[116] therefore, the use of cycloaddition reactions is often preferred.[141] The simplest of these reactions is arguably the use of carbenes or nitrenes in a 1+2 cycloaddition reaction with the CNT surface to form cyclopropane or aziridine rings.[142] The difficulty in generating carbenes with useful functionality has restricted their practical application in materials chemistry, but dichlorocarbene has been extensively used to explore the properties of carbon nanotubes.[115,143,144] The Bingle reaction is a more versatile method of introducing cyclopropanyl groups – allowing further chemical modification in a second step.[145] Likewise, nitrene functionalization has allowed especially easy access to a wide variety of surface functionalities due to the facile synthesis of azides.[146-148]

In addition to the preceding 1+2 cycloadditions, other reaction schemes have been developed. The reaction of CNTs with azomethine ylides to generate N-methylpyrrolidone moieties (Prato reaction) has been used extensively.[149,150]

Electron-rich nitrile imines react to generate pyrazoline-type structures.[151] Swager and colleagues have developed cycloadditions using dialkyldicarboxyacetylenes that allow the introduction of a number of useful functional groups under mild conditions.[152,153] Lastly, Diels-Alder chemistry has also been developed, however this reaction is generally not favorable on carbon nanotube surfaces: Nanotubes have too little strain energy.[141] As such, uniquely reactive dienes, such as *in situ* generated quinodimethanes[154] or benzocyclobutanes,[155] are required to achieve high functional group densities. Additionally, there are reports of modest functional group densities achieved by using maleimides and furans,[156,157] or through the use of electron-rich dienes in the presence of a $Cr(CO)_6$ catalyst at high-pressures.[158]

At this point in the development of CNT chemistry, there are typically several possible methods of obtaining any given functionality. Consequently, the pace of development of new covalent functionalization methodologies has slowed. Regardless of the method of covalent functionalization, defects are introduced, and at least some disruption of the electronic and mechanical properties is expected. As such, a great deal of current research has focused on non-covalent methods of modifying nanotubes.[159]

1.4. π-π Stacking and Other Non-covalent Interactions in Nanotubes

Carbon nanotube use and processing is dominated by the strong tube-tube interactions.[160] The nature and strength of the interaction within carbon nanotube bundles has been heavily explored. For single-walled carbon nanotubes this

interaction strength has been calculated at approximately 1.12 eV/nm^{-1} for a (*10,10)* SWNT. [161] Similar values have been determined for other SWNT chiralities and other graphitic van der Waals interactions.[162,163] Carbon nanotube suspension strategies are governed by the need to overcome or control these interactions. Interactions between carbon nanotubes and other π-systems are rapidly becoming the dominant method of nanotube modification.

An understanding of π-interactions is especially important for the use of nanotubes in bulk reinforcement. It has been well-demonstrated that the bundle bending modulus and tensile strength decreases with bundle size.[164] While nanotubes are difficult to completely pull apart, they have little barrier to sliding within bundles and relatively small shear forces are required.[165] Likewise, there is often little barrier to sliding within bulk materials.[81] Cross-linking within small bundles and covalent anchoring is often required.[166,167] In their pristine form MWNTs are often better suited to polymer reinforcement than the theoretically superior SWNTs[165] due to their reduced propensity to bundle.[168] This reduced bundling propensity is due to the decrease in binding energy associated with additional MWNT shells.[163]

The nanotube van der Waals interactions arise from the delocalized p_z orbitals on the surface of the carbon nanotube, and are, unsurprisingly, dependent on the degree of delocalization, which arises from the chirality and the diameter of the SWNT.[169] In general, there are several different modes of π-stacking available to graphitic materials. The simplest system is the stacking of benzene on

a carbon nanotube surface. There are three possible configurations: 1) stacking, such that the benzene molecule is directly above a tube hexagon, 2) staggered, where the benzene is centered on a nanotube C=C bond, and 3) CH-π where the electron-poor "edges" of the benzene ring allow for the formation of a quadrupolar interaction or CH-π "hydrogen bond."[170] Depending on the method of calculation, the interaction strength of a single benzene-nanotube interaction ranges from about 8-40 kJ/mol.[170] For systems where the π-systems are at similar energy levels, the staggered configuration is preferred by virtually all calculations, though the hexagon-hexagon stacking is nearly as strong. In contrast, the CH-π bonds are quite weak.[170] In general, the interactions are additive, and their strength depends on both the chirality of the nanotube and the size/shape of the aromatic system.[170] As expected from their relative electron richness, charge transfer can occur when nanotubes are stacked with a molecule that is a strong π-electron acceptor such as 2,3-dichloro-5,6-dicyano-1,4-benzoquinone (DDQ), or 7,7,8,8-tetracyanoquinodimethane (TCNQ) resulting in an even stronger interaction.[9]

1.5. Processing and Suspension of Carbon Nanotubes

Due to the strong inter-tube interactions, the uniform dispersion of CNTs in solvents or bulk solids is difficult to achieve. Processing options used to circumvent the formation of bundled nanotubes can be broken down into two categories: Covalent modification and supramolecular functionalization.[159] In each case, the carbon nanotube's surface is modified or coated in a material to

provide steric bulk and/or charge in order to prevent the formation of strongly-interacting CNT aggregates.[171,172] There are a vast number of modification strategies using most of the chemistries discussed in Section 1.4. Generally the graft material is chosen so as to maximize interaction with the host solvent or material.[171] For example, Chapter 2 outlines the use of polystyrene to suspend SWNTs within organic solvents and intercalate with polystyrene itself. Chapter 3 outlines a similar strategy for silicones. However, as discussed previously, the greatest disadvantage in covalently modifying carbon nanotubes is the effect on the electrical properties of the nanotube through the introduction of defects into the graphitic sidewalls. Accordingly, a large proportion of recent studies have focused on the use of non-covalent modification strategies.[171,172]

Non-covalent methods are conceptually similar to their covalent counterparts: The objective is still the addition of charge or steric bulk to prevent re-aggregation, however, instead of relying on covalent bonds, the nanotube is coated or wrapped with a material via many, weaker interactions.[173] For example, the use of charged or uncharged surfactants, such as sodium dodecyl benzyl sulfonate, sodium cholate, or Pluronics™ diblock-co-polymers, allows the suspension of carbon nanotubes in water, where the surfactants are retained on the CNT surface due to hydrophobic interactions.[174] Likewise, amines,[175] and a variety of other small molecules that have electronic interactions with the CNT surfaces can be employed for suspending carbon nanotubes.[176] Furthermore,

surfactants have shown some success at assisting in the suspension of carbon nanotubes within bulk materials to improve mechanical properties.[54]

The use of conjugated polymers for the suspension of SWNTs is particularly effective.[177] The strong π-π interactions between the polymer and the CNT prevent re-aggregation into tight bundles; the distribution of steric bulk contributed by the polymer side-chains helps stabilize the SWNT/polymer suspensions in solvent. Control over the polymer side-chain chemistry allows compatibilization with a variety of solvents ranging from non-polar organic solvents to water.[177]

Most conjugated polymers interact strongly with carbon nanotubes. For example, poly(phenylenevinylene),[178,179] poly(phenyleneethynylene),[180,181] poly(thiophene),[182] poly(fluorene),[13,15] and poly(carbazole)[183] derivatives have all been used to suspend carbon nanotubes, along with a variety of more exotic conjugated polymer structures.[177] In general, increasing steric bulk though more numerous or larger side-chains increases the solubility of the polymer-SWNT complex. Likewise, solutions of SWNTs wrapped in charged or polar side chains have shown exceptional stability.[18] These factors are unsurprising considering the colloidal nature of nanotube suspensions.

Finally, several biopolymers have also been effective at suspending carbon nanotubes,[171] most notably DNA.[19] While not conjugated, DNA contains many nitrogenous bases that undergo electrostatic interactions with the carbon nanotubes.[184]

1.6. Separation of Carbon Nanotube by Type/Diameter/Chirality

Solubilization is only one facet of CNT usage in composite materials and devices. As discussed above, carbon nanotubes are produced as a complex mixture of diameters, lengths, types, and chirality. This is primarily a concern for SWNTs whose properties vary greatly by chirality. Accordingly, the production or separation of carbon nanotubes by these properties is a very active field,[7,20] though the separation metric is dependent on intended use. For structural materials, nanotube type (MWNT vs. SWNT), length, diameter, and defect concentration are the important variables. Moreover, cost is a key consideration in these fields, so control over these variables is typically asserted at production.[185] Fortunately, structural reinforcement does not require monodisperse nanotubes samples – greatly simplifying the separation considerations.

In contrast, the separation of carbon nanotubes into highly monodisperse samples is of utmost importance for use in electronic devices, and has been one of the most active areas of research in carbon nanotubes in the last decade. It has been stated that a chiral purification level of 99.999% is desirable for devices such as sensors, transistors, and photovoltaics.[186] It is likely that a much lower level of purification is required for bulk electrical modification, but even here, the deleterious effects of metallic to semiconducting junctions demand a high level of purification by nanotube type. Many methods have been attempted to accomplish diameter-, electronics-, or chirality-based separations of SWNTs; a thorough review of the field is available.[20] The following sections discuss some of the

better-researched or more effective methods. Currently no method comes close to producing 99.999% chiral purity, and, while there are a number of methods that produce significant enrichments of semi-conducting or metallic tubes, 95% enrichment is still considered a state-of-the-art result, especially for scalable methods.[7]

1.6.1. DNA Wrapping and Ion Exchange Chromatography

In terms of separation efficiency, the combined approach of DNA wrapping and ion exchange chromatography has been the most successful. In a series of papers Zheng and colleagues were able to develop a series of short DNA strands comprised of different repeating patterns.[19,187] These strands exhibited different wrapping morphologies on the surface of SWNTs of different diameter/chirality, and certain strands displayed a favorable fit for a specific chirality. DNA is a charged molecule, thus allowing the separation of the differentially-wrapped carbon nanotubes by high-performance ion exchange chromatography. Notably, the authors were able to separate two chiralities of SWNT with the same diameter (Figure 1.8).[188]

Though very effective, this technique is not particularly scalable. A major drawback of DNA mediated separations is the cost of DNA sequences and the waste inherent in both centrifugation and ion exchange chromatography. While this work is of seminal importance to the field of nanotube characterization and the development of prototype electronic devices,[189] the microgram quantities of carbon nanotubes produced by Zheng *et al.* are insufficient to appeal to

researchers investigating bulk materials. However, there are no fundamental impedances, aside from cost, to the scaling of this work.

In response to these economic hurdles, researchers have explored the use of natural-sourced DNA for the suspension, separation, use, and purification of carbon nanotubes.[190] Naik and co-workers were able to obtain substantial enrichment, ~86% of single chirality (*6,5*) SWNTs, and the elimination of metallic components using genomic DNA.[186] The typical source for the DNA is salmon sperm, harvested as a waste product of the fish farming industry. Nonetheless, the relative difficulty of these procedures likely precludes any products from use in bulk materials.

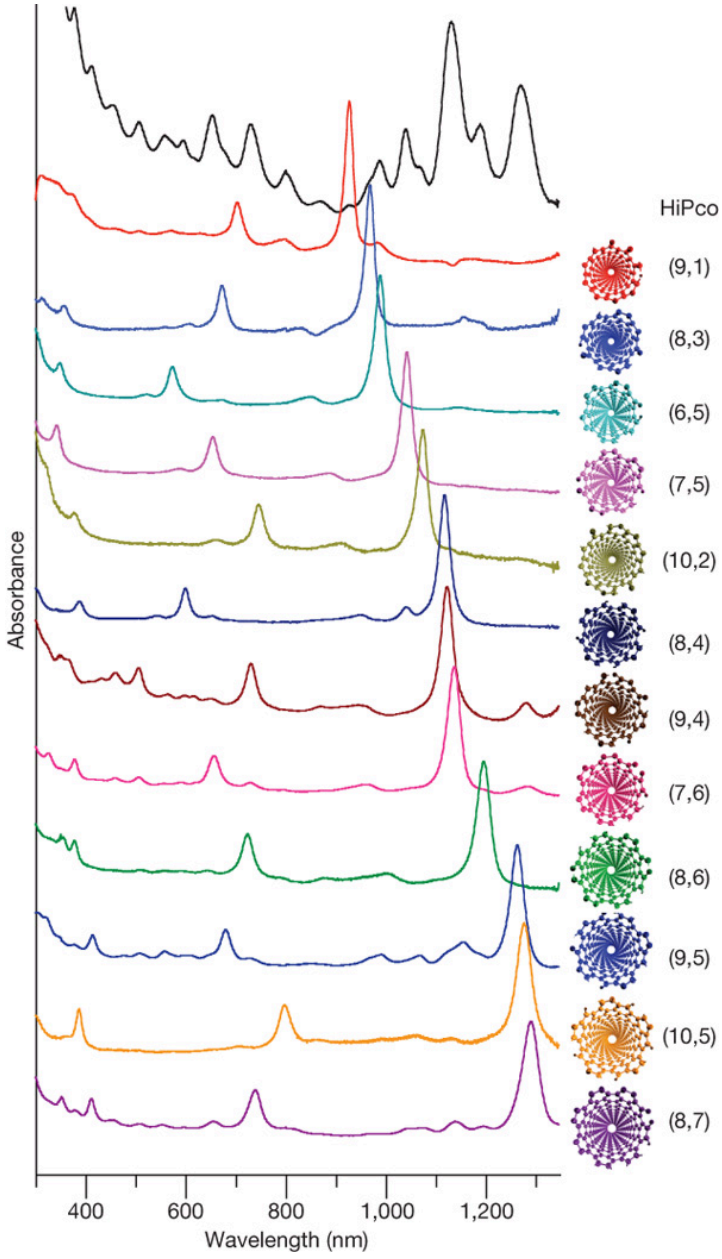

Figure 1.8: UV-Vis-NIR absorbance spectra for a series of carbon nanotube chiralities purified by DNA-wrapping and ion exchange chromatography. The spectrum of the starting HiPCO SWNT sample appears in black (top). The chiralties of the individual species are indicated to the right. Reproduced with permission from Ref. 187. Copyright Nature Publishing Group, 2009.

1.6.2. Density Gradient Ultracentrifugation

The separation of surfactant-wrapped carbon nanotubes by density is also a viable method of chiral purification and is the state-of-the-art method for separating metallic and semiconducting nanotubes with high (>99%) purity.[191] This technique has been commercialized, but the iterative process required for high purities results in prices ranging from $200-$900/mg.

The separation relies on the difference in packing of surfactants, such as sodium dodecylbenzene sulfonate or sodium cholate, on the surface of carbon nanotubes of different diameters. Different surface packing results in nanotube complexes with slightly different densities. Diameter-based separations are then afforded by static or dynamic separations on a density gradient, using ultracentrifugation. By changing or blending the surfactants, or by changing the gradient protocol, the relative separation and order of the species can be altered.[192] However, unlike DNA-based separations, density gradient ultracentrifugation is based first on type of nanotube (sc vs. m), then almost completely on diameter, and is typically not able to select for a wide variety of chiralities in high purity. Nonetheless, carefully tailored, non-linear gradients have allowed the separation of nanotube fractions enriched in each of the (*6,4*), (*7,3*), (*6,5*), (*9,1*), (*8,3*), (*9,2*), (*7,5*), (*8,4*), (*10,2*) and (*7,6*) chiral vectors. First-run purities range from 88% (*6,4*) to 34% (*8,4*).[23] Notably, density gradient separations using chirally-pure bile salt (cholate) surfactants have been able to enantiomerically enrich SWNTs.[193]

There is a great deal of precedence for density-based separations in biological materials and the techniques are mature and scaleable. Multiple types and chiralities of SWNT can be obtained from the same sample, though some drawbacks exist. The techniques require high-power centrifuges, and are accordingly expensive; multiple sequential runs are required to achieve high levels of purity, and certain diameters and chiralities are much more easily purified than others.[23] Nonetheless, density gradient ultracentrifugation remains the state-of-the-art technique for separating semiconducting and metallic nanotubes, and is currently the only way of obtaining bulk samples of chirally enriched carbon nanotubes.

1.6.3. Selective Dispersion/Interaction and Other Separation Methods

The concept behind selective dispersion of carbon nanotubes is very simple – find a molecule, or molecules, capable of selectively suspending or precipitating only a single type, diameter, or chirality of carbon nanotube. Small molecules demonstrating selectivity have ranged from simple amines to complicated molecular tweezers. Synthetic and biological macromolecules have also been explored.

Amines have been demonstrated to selectively coordinate either metallic or semi-conducting SWNTs, depending on their degree of acid-functionalization.[194,195] By optimizing conditions and performing multiple rounds of purification, researchers have been able to produce ~90% enrichment in either type.[196,197] Strongly electron-withdrawing molecules such as DDQ have been

explored as a method of selecting for nanotubes that are more electron-rich (small, metallic), however, at this point the results remain mostly theoretical.[26]

Molecular- or nano-tweezers, conjugated molecules with a specific bite angle, have also been shown to select for specific diameters of nanotubes, albeit with lower efficiency than DNA or density gradient centrifugation.[20,198,199] There is strong evidence that these molecules can also select carbon nanotubes in an enantioselective fashion, but the degree to which this is true is difficult to evaluate. Unfortunately, these bridged molecules are generally difficult to synthesize, hindering their investigation.

Bio- and conjugated polymer-based separations represent fields that are currently very active. Inspired by the degree to which DNA-based separations are able to differentiate by diameter and chirality, it seems logical to focus efforts on other molecules that can wrap carbon nanotubes. To date, efforts with conjugated polymers have exhibited mixed success. Various conjugated polymers have shown affinity for specific chiralities of carbon nanotube,[13,31,182,183,200-202] however, researchers have yet to demonstrate success in achieving bulk-scale separations. Encouragingly, many conjugated polymers have been used to effectively purify semiconducting carbon nanotubes, *e.g.* Lee *et al.* were able to remove ~98% of the metallic tubes in a sample of HiPCO SWNTs using regioregular polythiophene.[182] Similar results have been demonstrated with polyfluorene,[203,204] and polycarbazole derivatives.[201] Work in this field has just

begun and the synthetic space is large. It seems likely that these methods will turn out to be successful, but more development is needed.

The use of biopolymers (outside of DNA-based separations) has been less successful. In fact, small biomolecules such as heparin,[205] or flavin mononucleotide,[206] have exhibited greater success. However, when coupled with density gradient ultracentrifugation, biopolymer,[207] or conjugated polymer wrapped SWNTs,[33,35] can be separated in much the same way as surfactant-coated SWNTs. Any advantage over the use of simple surfactants has yet to be established.

Selective extraction appears to be plagued by the ability of most conjugated or biopolymers to suspend all SWNTs of a given type (or even all types). As such, a secondary method of separation may continue to be required for most cases; hopefully methods that rely on simple filtration or low-speed centrifugation can be developed. Regardless of the mixed success to date, the field of selective extraction remains the most active in nanotube separation, because of the potential for a simple, inexpensive, and scalable method of separation, and because of the extraordinarily large chemical space in which to explore.

1.6.4. Gel Filtration/Electrophoresis

SWNT separation using electrophoresis achieves high degrees of metallicity-based separation and moderate levels of diameter-based separation.[36,208-210] However, the purity levels are arguably not commensurate with the drawbacks of electrophoresis, *i.e.* relative difficulty and small scale.

Demonstration by Tanaka and colleagues of the ability of agarose gels to separate SWNTs in an entirely chromatographic fashion is more relevant to materials scientists. The researchers explored different chromatographic methodologies – eventually settling on a system analogous to flash column chromatography.[211,212] The purities achieved are excellent – greater than 90% metallic purity and 95% semiconducting purity.[38] Like silica gel chromatography, the use of flash-style columns, or gel centrifugation methods, allows for small matrix particle sizes and high resolution, and is also highly scalable and easily automated.[42] Moreover, with recent improvements in methodologies using successively more concentrated solutions of sodium dodecyl sulfate and sodium deoxycholate as eluents, Tanaka and colleagues were able to fractionate both the semiconducting and metallic SWNTs by diameter.[43,213,214]

While gel filtration will likely never reach the desired 99.999% chiral purity levels needed by device manufacturers, its inherent advantages render it ideal for materials usages, and potentially useful as a pre-purification method for other separation methodologies.

1.7. Suspension of Carbon Nanotubes within Polymeric Matrices

There are two primary uses for CNTs in composites: Structural reinforcement or conductivity enhancement. Nanomaterials must be well dispersed and evenly distributed within polymer composites to be useful for either task,[215] however, there are more specific requirements depending on intended use.

1.7.1. Mechanical Reinforcement of Materials

Graphene and diamond both show exceptional mechanical properties, and both are widely exploited for their strength. Their 2-and 3-dimensional structures, however, make them ill-suited for use as mechanical reinforcing agents. Instead, carbon or glass fibers are typically used, despite their inferior mechanical properties. As mentioned in Section 1.3, carbon nanotubes combine many of the mechanical characteristics of diamond or graphene, with a high aspect ratio and favourable geometry for mechanical reinforcement. As such, they should be ideal for fillers in a variety of materials.[51,53-56]

The real-world scenario is more complicated; the properties of individual carbon nanotubes are often controlled not by their theoretical properties, but rather, by the presence of defects. Even single atom vacancy defects reduce the strength of an individual carbon nanotube by ~26%, and larger defects have even greater effects – potentially reducing nanotube tensile strengths by as much as 50%.[216,217] Moreover, the presence of bundling among carbon nanotube complicates the evaluation of their strengths. CNT bundles behave very differently than individual tubes, and their mechanical properties are substantially inferior.

Currently, the most successful results in harnessing the strength of carbon nanotubes have been obtained using MWNTs. While inferior in strength and strength-to-weight ratio, and plagued by an additional "sword-and-sheath" mechanism of failure,[81] MWNTs bundle more weakly than their single-walled

counterparts.[163] MWNT properties reduce the complications involved in CNT processing and have, to date, allowed for the production of higher quality suspensions within composites. Nonetheless, if the mechanical properties of carbon nanotubes are to be realized, especially for such exotic applications as a space elevator, methods for the integration of SWNT must be developed.

Coleman *et al.* define four main "system requirements" for carbon nanotube reinforced polymer systems:[81]

i. Large aspect ratios

ii. Appropriate alignment

iii. Good dispersion

iv. Good interfacial stress transfer

Alignment and aspect ratio are typically controlled by composite engineering and nanotube synthesis practices. Alignment is also a factor governed by compromise. A material with a perfectly aligned fiber receives about five times as much reinforcement compared to a material with randomly aligned fibers – but only in the parallel direction. It receives very little strength enhancement in the perpendicular direction. Accordingly, alignment is a factor that must be evaluated case by case. Generally, alignment is desired in fibers and avoided in bulk materials.[81]

Nanotubes can be produced with enormous length-to-diameter ratios, however, theory predicts diminishing returns beyond certain aspect ratios: ~1000:1.[81] As most commercial nanotube samples (SWNT and MWNT) are

produced with greater aspect ratios – this is not typically a concern for nanotube composites (Figure 1.9).

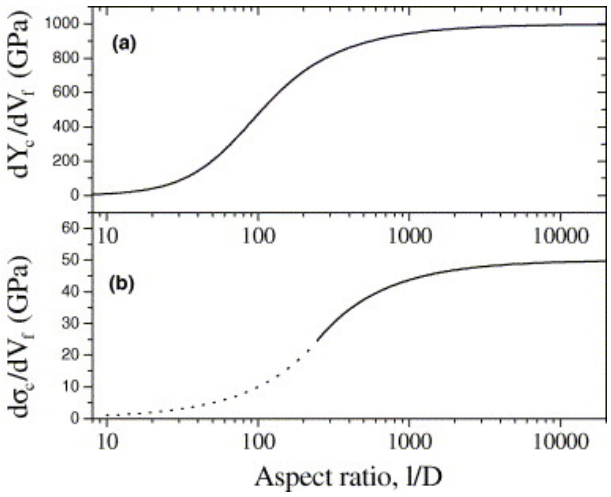

Figure 1.9: a) Modulus enhancement and b) strength reinforcement as a function of fiber aspect ratio for aligned fibers by the rule of mixtures. Reproduced with permission from Ref. 81. Copyright Elsevier, 2006.

Interfacial shear strength is a more significant factor for carbon nanotube composites. The interfacial strength is generally quite poor for unmodified carbon nanotubes (50-100 MPa),[81] and even when carbon nanotubes have relatively strong interactions with the host polymer, such as polystyrene or epoxy, the interfacial shear stress is below 200 MPa.[218] While this is true for pristine carbon nanotubes in most common structural polymers, it is not the case when stronger interactions between carbon nanotubes and their matrices are introduced, for example, the use of conjugated polymers or covalently bound functional groups enhance these interactions. Both strategies have been utilized; covalent bonding

extensively, and some examples show reinforcement capacity near the theoretical maximum.[219]

The final factor addressed by Coleman *et al.* is that of dispersion.[81] The authors identify dispersion as the "most fundamental" issue. It is clear that both high quality dispersions and good interfacial strength are required for optimal reinforcement. Some very promising results have been achieved using small molecule, covalent, modification of the CNT surfaces, *e.g.* the multistep surface addition of poly(p-phenylene terephthalamide) (Kevlar™) oligomers by Fréchet and colleagues for use in Kevlar™ nanocomposites.[219] However, small molecules often have a limited ability to stabilize carbon nanotube suspensions. They are most successful when charged or polar, as predicted by colloid properties, but this drastically limits the range of polymers with which they have compatibility. Small molecules must have a chemical interaction with the host polymer of some form *i.e.* hydrogen bonding, π –stacking, or covalent bonds. The reliance on covalent bonds in particular further limits the selection of polymer materials to those that can be polymerized or cross-linked *in situ*. This explains the prevalence of epoxy resins as host materials for carbon nanotubes. The introduction of more elaborate compatibilization schemes shows greater promise. Park and colleagues refer to these schemes as "second generation" carbon nanotube coatings, as they generally require a two-step procedure.[171]

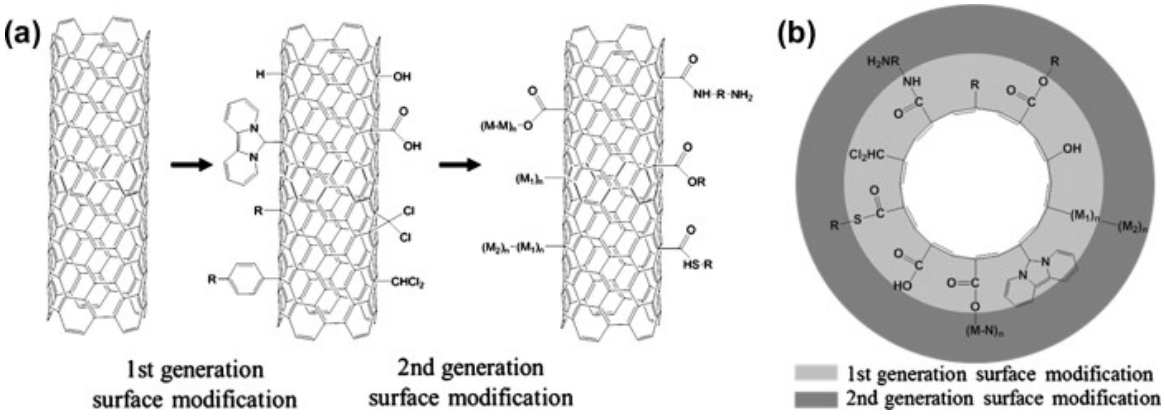

Figure 1.10: Graphical representation of a "two-generation" functionalization scheme. Reproduced with permission from Ref. 171. Copyright Elsevier, 2012.

In these "two-generation" reaction schemes the CNT surfaces are initially functionalized with small molecule functional groups, after which these groups are grafted with a larger, more elaborate, often polymeric graft. In some cases it is possible to graft the polymer directly to the carbon nanotube surface (by radical coupling),[220] and while technically not "second generation" by Park's definition, the products are conceptually the same. Due to the effectiveness of covalent grafting, a large number of grafting schemes have been developed.[221]

The grafts used for mechanical reinforcement are typically covalent, as the electrical properties are usually not the primary consideration, and because covalent modification schemes are straightforward to perform. However, non-covalent (π-stacking) arrangements are much stronger than simple wrapping or hydrophobic interactions, and are also capable of providing equivalent interfacial strength.[222,223] The non-covalent modification avoids introducing defects that

weaken the nanotubes and also allows the full synthesis of the graft material prior to nanotube grafting – potentially invaluable for complicated graft structures.

In short, grafted macromolecules, such as synthetic- or biopolymers, allow exceptionally stable colloidal suspensions of carbon nanotubes, and they provide a high degree of compatibilization. Moreover, these schemes are potentially compatible with the crosslinking of the CNT materials within their polymeric hosts, further improving the interfacial strength. Many of the most impressive results in the field of nanotube reinforcement have been achieved using these methods and this is one of the central strategies of carbon nanotube suspension explored in this thesis.

1.7.2. Enhancement of Electrical Properties in Materials

The same factors that govern the use of carbon nanotubes for mechanical reinforcement also govern their use for the modification of electrical or thermal properties in bulk polymers. However, they differ in importance and degree of complexity.

Alignment of the nanotubes is critical to controlling the degree of anisotropy of the material. In general, wires, films, and similar structures demand the use of aligned (1-D or 2-D) nanotubes, whereas bulk materials do not. However, this is application-dependent as, for example, a heat sink may demand anisotropic design.

Large aspect ratios are of key importance to nanotube conductivity. For short nanotubes, junction resistance is much more significant than nanotube

resistance. Thus, the relationship between conductivity and nanotube (or bundle) length can be fit to a power law whose exponent depends on the exact properties of the nanotubes/bundles in question.[224] Like mechanical reinforcement, this effect is limited, and at a certain point the nanotube resistance approaches that of the junction resistance.[224] At this point, increasing the length will have little additional effect on the network conductivity. In the case of studies by Hecht *et al.,* this point was calculated to be greater than 20 μm for SWNTs, considerably longer than most available samples.[224] Increasing the length of carbon nanotubes may have major implications on conductive composites, much more so than their counterparts in mechanical reinforcement. Likewise, these variables depend considerably on the diameter and type of nanotube as well as the defect concentration within the nanotube sample.

Chemical functionalization complicates the issue further. Many studies attribute a severe detrimental effect to covalent functionalization,[133,225] but some note little change,[226] or even an increase in conductivity.[227] A study by Park *et al.* reconciles these observations by suggesting that the type of defect site is an important consideration. In particular, the authors suggest that "divalent" functionalization has much less impact on the conductivity of the SWNTs when compared to "monovalent" modification.[116] While studies are performed in an effort to develop methodologies for the usage of covalent grafting in electronic property modification,[228] it seems prudent to avoid covalent modification when conductivity is the main concern, unless absolutely necessary.

As in mechanical reinforcement, dispersion quality and quality of interfacial interaction are more complex factors. Interfacial strength tends to be an application-specific property; if the filled material is being used in mechanical fashion, such as a sensor, flexible/stretchable device, or electrode, the interface properties may be the most important consideration. Interfacial interaction is further complicated by the challenge of defining what is meant by "quality" of interfacial interaction. In the case of carbon nanotube electronics, it is not simply a matter of interfacial shear strength. Other possible considerations may include, for instance, elasticity, and contact resistance. In many cases, these properties are harder to define, and/or must be considered holistically.

Arriving at a useful definition of dispersion quality is hindered by the nature of nanotube conductivity. Ideally, metallic nanotubes are ballistic conductors within individual tubes and experiment confirms this for individual metallic SWNTs[109] and MWNTs.[229] This means conductance within a given nanotube is quantized,[230] and resistance is generally low. However, within a bulk material, nanotubes are dependent on a percolation-based model of conductivity.[47] The problem of defining dispersion quality is compounded by variations in nanotube conductance and junction,[107] nanotube alignment (*i.e.* bulk sample morphology),[231,232] and nanotube sample composition.

The majority of the resistance in percolating carbon nanotubes arises from tube-tube or bundle-bundle resistance and the overall network can be thought of as "conducting islands" separated by small barriers.[117] As such, the overall

conductivity is primarily dependent on the inter-tube contacts.[117] In pristine carbon nanotubes, conductance and charge mobility are approximately four orders of magnitude lower in sheet or bulk form, as compared to individual carbon nanotubes.[233] Decreased temperature or the addition of tube-end organic functionalization, which increases tube-tube distance, was found to reduce the conductivity by two or more orders of magnitude.[117] The junction resistance also increases proportionally with the diameter of carbon nanotube bundles; this necessitates the maximal possible dispersion quality for the lowest sheet or bulk resistances.[234]

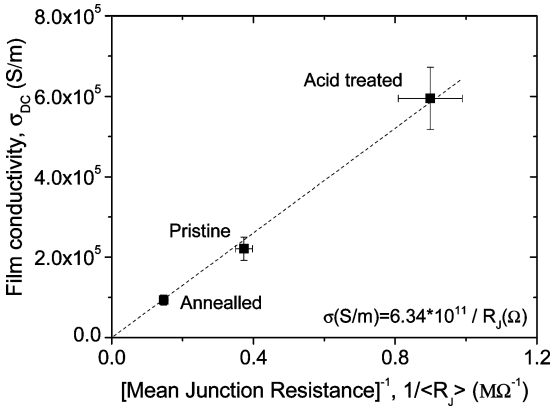

Figure 1.11: Plot of thin film conductivity vs. the inverse of the junction resistance for pristine and chemically modified SWNTs. Acid annealed SWNTs are more conductive. Reproduced with permission from Ref. 234. Copyright American Chemical Society, 2009.

In general, it has been demonstrated that bulk or sheet conductivity is entirely proportional to the junction resistance, at least for most nanotube lengths.[234] Unsurprisingly, reducing the intratube resistance has been identified as the "primary avenue" for improving device performance.[233] This has been achieved primarily by doping, for example by acid treatment, a one-electron oxidant, silver salt, π-accepting metal complex, or electron withdrawing organic molecule, such as tetrafluoro- tetracyano-p-quinodimethane or 2,3-Dichloro-5,6-dicyano-1,4-benzoquinone.[235,236] Tetrafluorotetracyano-p-quinodimethane is particularly effective; its electron-withdrawing effects reduce the contact resistance by a factor of ten.[235] Another approach to reducing contact resistance is to enhance the attractive forces between carbon nanotubes at the junctions (so-called "sticky nanotubes"). This reduces the inter-tube distances and increases the transmittance probability and conductance.[237-240] Likewise, the addition of small graphene fragments has been shown to greatly improve the conductivity of thin films, most likely by bridging the CNT junctions.[241,242]

The dependence on percolation implies the conductivity of nanotubes and their composites are dependent on both the quality and the "type" of percolation network. Better dispersions result in lower percolation thresholds because there are a greater number of "wires" and therefore a greater number of possible interconnects. However, a completely random distribution will not be the most efficient way to maximize the conductivity, or minimize the percolation threshold within a percolating network. Instead, some carbon nanotube re-agglomeration

(but not full re-bundling) results in a greater than expected number of interconnects and thereby a lower than expected percolation threshold.[47] These reaggregated networks are referred to as kinetic percolation networks.

Finally, the conductivity of the composite also appears to be affected by the nature of the polymer in which the carbon nanotubes are distributed.[243,244] It has been argued that the conductivity of the nanotubes and their junctions is relatively unimportant compared to the inter-tube distance and the resistivity of the polymer between them.[245] This phenomenon has been manipulated by the addition of a conducting poly(3,4-ethylenedioxythiophene):Polystyrene sulfonate (PEDOT:PSS) polymer latex to a suspension of SWNTs in polystyrene. The addition of the conducting "spheres" caused a very sharp percolation transition, increasing conductivity by nearly fourteen orders of magnitude.[246]

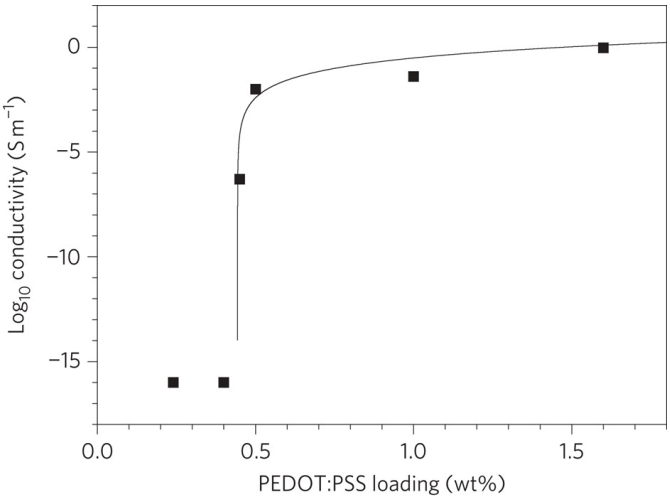

Figure 1.12: Large and well-defined percolation threshold produced by using PEDOT:PSS latex particles to bridge SWNT junctions. Reproduced from Ref. 247. Copyright Nature Publishing Group, 2011.

Given the complexity of tube-polymer and tube-tube interactions, it seems that this is an overly simplistic view, especially in light of the demonstrated effects of modifying carbon nanotubes outlined previously.

The strategies used in modifying carbon nanotubes for electrical uses are generally different than those employed for mechanical reinforcement. Covalent modification is often precluded by the imperative to not introduce defect sites on the nanotube sidewalls and thereby decrease the conductivity. Instead, the most successful strategies for compatiblizing CNTs within electronic materials rely on π-stacking methodologies.[49,244]

1.7.3. Enhancement of Thermal Properties in Materials

Despite being one of the best-known thermal conductors, this aspect of carbon nanotube modification is less explored. A recent review highlights only a few dozen experimental and theoretical studies.[248] Research indicates that while carbon nanotubes are excellent thermal modifiers in a relative sense, the absolute improvements in thermal conductivity remain quite modest. B.P. Grady goes so far as to claim that, "the thermal conductivity of a composite filled with nanotubes does not in general increase anywhere near to the point where such materials would be useful as thermal conductors."[249]

When used to enhance the thermal properties of bulk materials, carbon nanotubes are effective at much lower concentrations than most conventional materials, however, the effects are modest even when loadings are high.[248] The improvements observed are much smaller than predicted by a percolation-governed phenomenon.[250] This stems from the nature of carbon nanotube conductivity in bulk. Unlike electrical conductivity, thermal transport by carbon nanotubes is not percolation-governed; enhancement is typically linear.[249] Moreover, the thermal conductivities at the polymer/nanotube interfaces dominate the heat transport and are very inefficient.[250] As such the ballistic heat transport within the carbon nanotubes is irrelevant to their use as polymer fill materials.[249]

While it may be somewhat less important for thermal enhancement – due to the large loading levels required – modification of carbon nanotubes to improve suspension is still an important consideration. The covalent modification of

nanotubes is predicted to have a deleterious effect on their individual thermal conductivity.[251] However, unsurprisingly, in bulk, covalent functionalization has been shown to have little effect,[252] or even a small improvement due to enhanced dispersion.[253] Finally, some predictions suggest that covalent modification at the interfaces should partially ameliorate the high interface resistance, improving the bulk heat transfer.[254] In fact, in cases where the interfaces were tightly controlled (by plasma etching followed by gold coating the MWNT ends), and the aligned nanotubes directly and entirely bridged the thermal gap, thermal conductivity improved by several orders of magnitude.[255]

To summarize, the use of carbon nanotubes for the improvement of heat transfer in bulk materials has not been successful. However, as B.P. Grady opines, there is hope that "the right interfacial modification" will allow for much greater degrees of thermal enhancement.[249]

1.7.4. Discrete SWNT/Polymer Complexes in Bulk Materials

The use of carbon nanotubes in polymer and other structural material reinforcement (including metals,[256] concrete,[257] and textiles[258,259]) is a large field that transcends chemistry into engineering, materials science, and other fields. A wide variety of polymers have been used as a matrix; it seems that most polymers have been evaluated. The scope of the literature is large, and a thorough review untenable. Fortunately, the field has been extensively reviewed from a chemical and materials standpoint.[51,53-56,223] Much of the literature conveys studies where the authors simply suspend unmodified carbon nanotubes within a bulk matrix.

For reasons discussed previously, the use of unmodified SWNTs and MWNTs in bulk materials has generally demonstrated only modest success. Effective dispersion requires surface modification.[171] The slightly more elaborate approach using a covalently-bound, small-molecule compatibilizer, is limited to cases where the polymer can crosslink with the CNT surface functionality and often results in reaggregation.[223] Surfactants and the π-stacking of small molecules provide excellent dispersion, but rarely provide the necessary level of interaction with the host polymer – particularly for usage in mechanical reinforcement.[223] The most general method, for both mechanical and electrical reinforcement is the coating of SWNT surfaces with grafted polymer chains,[81] and several examples have been given previously for mechanical and electrical modification (Sections 1.7.1 and 1.7.2).

The conceptually simplest method of covalent modification is the "grafting-to" of pre-polymerized polymers directly to the carbon nanotube surface (Figure 1.13a). This is relatively straightforward for polymers generated by living free-radical polymerization, which can be directly reacted with carbon nanotube surfaces by radical coupling, or for polymers whose end-groups have been modified with a functional group known to undergo addition to carbon nanotube surfaces. Reactions at the surface of carbon nanotubes tend to be inefficient on a molar basis, often requiring a large excess of polymer.[221] More efficient is the pre-modification of the carbon nanotube surface with a functional small molecule, followed by coupling using efficient reaction chemistry, *e.g.* 1,3-Huisgen

cycloaddition,[57] or condensation with an acyl chloride.[60] This modular philosophy allows the facile attachment of a variety of macromolecules. If higher densities of polymer are desired, *i.e.* carbon nanotube/polymer brushes, then the nanotube can be grafted with initiator groups,[260] and the polymer grown from the surface of the nanotube in a "grafting-from" approach (Figure 1.13b). This technique has yielded the highest polymer densities and has been notably successful for bulk reinforcement.[81]

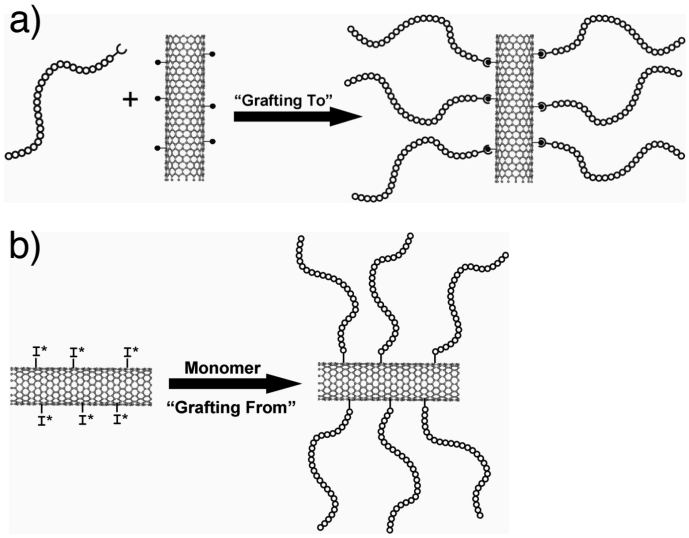

Figure 1.13: Schematic representations of the "grafting-to" vs. "grafting-from" approaches to carbon nanotube functionalization. Reproduced with permission from Ref. 221. Copyright Taylor and Francis, 2007.

Unfortunately, the covalent attachment of polymers is only suitable for the mechanical reinforcement of bulk materials; they suffer from the same disadvantages as any covalent modification where electronic properties are

concerned. Moreover, even though polymer modified carbon nanotubes show strong interfacial adhesion within their matrices, re-aggregation can still be a significant problem.[62] As such, where nanotubes are being used to modify the electrical properties of a bulk material, it is highly advantageous to use supramolecular interactions. Simply wrapping the carbon nanotube with a conjugated polymer is not always effective; the quality of the nanotube suspension and the interaction adhesion are both dependent on the affinity of the wrapped polymer with the matrix polymer.[62] In many cases, the conjugated polymers show greater affinity for themselves than their matrix.[261] The use of block-co-polymers has been more successful. Zou and colleagues were able to demonstrate that block-co-polymers of a conjugated and non-conjugated polymer are able to produce high quality suspensions in a matrix that matches the non-conjugated block.[261,262] Furthermore, they were able to demonstrate that block-co-polymer coated CNTs showed enhanced affinity for polymers that matched the non-conjugated block, and lessened affinity for mismatched polymers.[49] A study has been performed using covalently bound polymers by Mayo *et al.*[67]

Chapter 4 outlines the use of a similar strategy, using a silicone-P3HT block-co-polymer to achieve this objective for silicone elastomers.

1.8. Characterization of Carbon Nanotubes and their Composites

There are a wide variety of methods for characterizing carbon nanotubes and their composites, both in terms of composition and purity.[263] Raman spectroscopy is arguably the most widely applicable method.[264] At its simplest,

Raman allows the differentiation of various forms of graphitic and sp^3 carbon.[265] This allows for the identification of carbon nanotubes, as well as the assessment of defect concentration (sp^3 sites). This information is typically garnered from the radial breathing modes (RBM), tangential mode (G-band), and disorder-induced mode (D-band) of the Raman spectrum. [266]

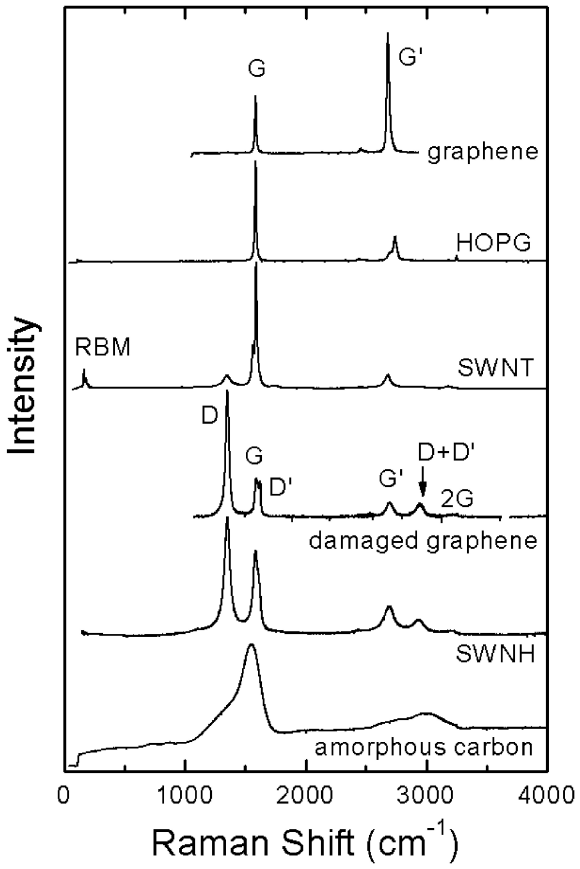

Figure 1.14: Raman spectra from a variety of sp^2-hybridized (graphitic) structures. Reproduced with permission from Ref. 265. Copyright American Chemical Society, 2010.

Upon deeper analysis, it is also possible to identify and quantify the species of nanotube present[267-269] and their bundling,[270] by observing resonances in the radial breathing mode (RBM),[271,272] and C-C region.[273] While each diameter of carbon nanotube yields a difference resonance wavelength, not all SWNTs are excited at each laser wavelength.[272,273] As such, multiple lasers and in-depth analysis are required to interpret these results.[264,273]

The UV-Vis and near IR absorption spectra can be used in a complementary fashion to Raman spectra in the characterization of carbon nanotube samples. Optical spectra do not yield information about the degree of defects in the carbon nanotubes, but they provide a great deal of information about the composition of the sample. Carbon nanotubes are very strongly absorbing in the visible and near IR region. Each semiconducting carbon nanotube chirality has a characteristic sharp and intense peak corresponding to optical excitation. Optical spectroscopy can be used to provide a survey of the types of nanotubes present.[274] Both semi-conducting and metallic nanotubes adsorb.[275] Metallic SWNTs absorb at short wavelengths corresponding to the metallic "pseudo bandgap." In general, the bundling of carbon nanotubes broadens their transitions – as such, the UV-Vis and near IR spectra can also be used to obtain a rough assessment of the degree of bundling in a SWNT sample (Figure 1.15.)[174]

In addition to being strong absorbers in the optical and near IR ranges, SWNTs are also fluorescent, emitting in the near IR portion of the

electromagnetic spectrum.[276] This allows the construction of 2-dimensional photoluminescence maps, and in theory allows researchers to assess the distribution of carbon nanotube chiralities within a sample.[13,277]

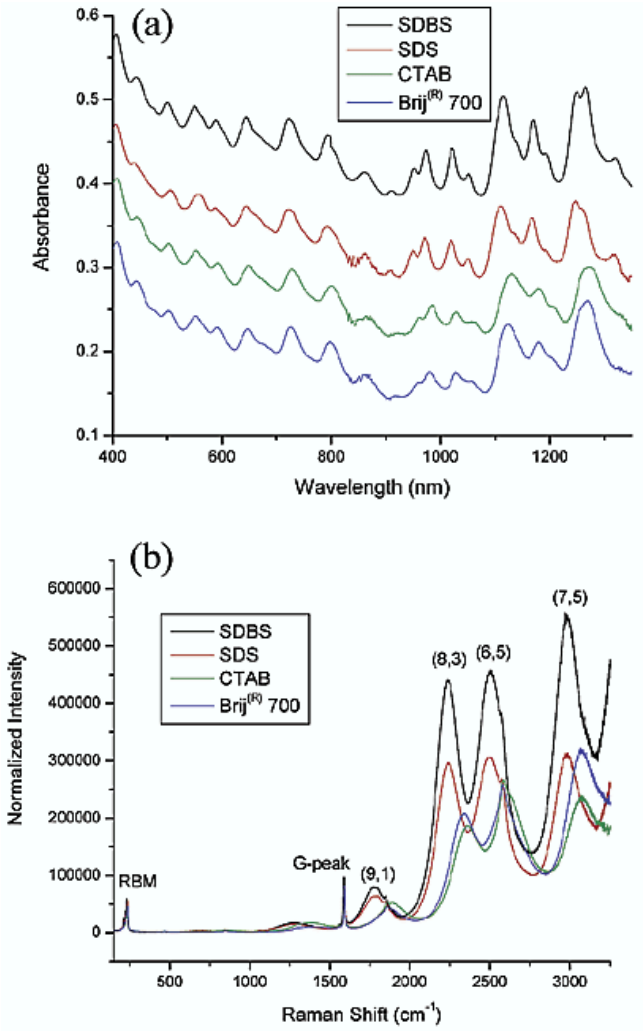

Figure 1.15: HiPCO SWNT optical and Raman spectra after being suspended with a set of common surfactants. Suspensions of SWNT in SDBS show sharper transitions in both optical and Raman spectroscopy, indicating a greater degree of debundling. Reproduced with permission from Ref. 174. Copyright American Chemical Society, 2003.

Unfortunately, bundling, particularly with metallic carbon nanotubes, quenches this fluorescence.[278,279] In practice, this restricts photoluminescence spectroscopy to a secondary technique. It is very valuable for determining if a specific chirality or multiple chiralities are being preferentially suspended, for example. However, results are easily conflated by bundling and agreement with Raman or UV-Vis spectra can be poor.

In addition to spectroscopy, microscopic techniques are in heavy use in the characterization of carbon nanotubes, especially in materials or device application. Atomic force microscopy,[280] scanning electron microscopy, [281] and transmission electron microscopy[282] are all useful techniques.[283] Atomic force microscopy allows researchers to determine the length distribution of nanotube samples, probe the quality of dispersions by evaluating the presence of bundles after casting, or to explore the morphology of carbon nanotubes on a surface or in thin films. It can also be used to demonstrate wrapping or functionalization, especially with polymers. In a similar fashion, electron microscopy can be used to probe the morphologies of carbon nanotubes on surfaces or within materials.

Carbon nanotube composites are also analyzed with a suite of analytical techniques used in polymer and materials chemistry. Thermogravimetric analysis (TGA), or TGA-MS are useful tools to determine the degree and nature of CNT functionalization.[284] Differential scanning calorimetry (DSC), and bulk-mechanical testing (*e.g.* Instron, Nanoindentor, *etc.*) are essential for exploring the mechanical properties of polymer/nanotube composites.[81] Infrared spectroscopy

has been useful for assessing CNT functionalization.[223] Finally, x-ray-based techniques (XPS, XRD) have been heavily used to explore functionalization and defects.[223]

1.9. Conclusion and Summary of Objectives

We can define two objectives for this work:

1) The development of robust or universal systems for the suspension of individualized carbon nanotubes in solid polymer, gels, and solutions.
2) The development of strategies for the anchoring of individualized carbon nanotubes within bulk materials.

While much of the early work described in this introduction focuses on the suspension of pristine carbon nanotubes within solid polymer, studies suggest that this, in itself, is impractical. To successfully incorporate individualized carbon nanotubes, the tubes must first be exfoliated, generally by a solution processing method, then a stable colloidal suspension formed with the bulk material, or its precursors (monomeric or polymeric). Then the colloid must remain stable throughout the processing or curing period. To achieve these objectives we have focused on two main areas:

1) The colloidal stabilization of carbon nanotubes within solvent and polymer solutions using polymer modification.
2) The development of practical and rapid crosslinking or anchoring methods compatible with common silicon elastomer chemistries.

The suspension of carbon nanotubes is discussed in Chapters 2, 3, 4 and 5; and the development of crosslinking strategies in Chapters 3 and 5. Chapters 6 and 7 are devoted to chemistry performed as groundwork for the development of the strategy discussed in Chapter 5.

1.10. References

(1) De Volder, M. F. L.; Tawfick, S. H.; Baughman, R. H.; Hart, A. J. *Science* **2013**, *339*, 535–539.
(2) Baughman, R. H.; Zakhidov, A. A.; de Heer, W. A. *Science* **2002**, *297*, 787–792.
(3) Lewis, J. C.; Redfern, B.; Cowlard, F. C. *Solid State Electron.* **1963**, *6*, 251–2544.
(4) Bundy, F. P.; Kasper, J. S. *J. Chem. Phys.* **2004**, *46*, 3437–3446.
(5) Iijima, S. *Nature* **1991**, *354*, 56–58.
(6) Monthioux, M.; Kuznetsov, V. L. *Carbon* **2006**, *44*, 1621–1623.
(7) Hersam, M. *Nat. Nanotechnol.* **2008**, *3*, 387–394.
(8) Kroto, H. W.; Heath, J. R.; O'Brien, S. C.; Curl, R. F.; Smalley, R. E. *Nature* **1985**, *318*, 162–163.
(9) Tournus, F.; Latil, S.; Heggie, M. I.; Charlier, J. C. *Phys. Rev. B* **2005**, *72*, 075431.
(10) Rode, A. V.; Hyde, S. T.; Gamaly, E. G.; Elliman, R. G.; McKenzie, D. R.; Bulcock, S. *Appl. Phys. A Mater. Sci. Process.* **1999**, *69*, S755–S758.
(11) Lee, H. W.; Yoon, Y.; Park, S.; Oh, J. H.; Hong, S.; Liyanage, L. S.; Wang, H.; Morishita, S.; Patil, N.; Park, Y. J.; Park, J. J.; Spakowitz, A.; Galli, G.; Gygi, F.; Wong, P. H. S.; Tok, J. B.-H.; Kim, J. M.; Bao, Z. *Nat. Comm.* **2011**, *2*, 541–548.
(12) Novoselov, K. S.; Geim, A. K.; Morozov, S. V.; Jiang, D.; ZHANG, Y.; Dubonos, S. V.; Grigorieva, I. V.; Firsov, A. A. *Science* **2004**, *306*, 666–669.
(13) Nish, A.; Hwang, J.-Y.; Doig, J.; Nicholas, R. J. *Nat. Nanotechnol.* **2007**, *2*, 640–646.
(14) Falcao, E. H.; Wudl, F. *J. Chem.Technol. Biotechnol.* **2007**, *82*, 524–531.
(15) Cheng, F.; Imin, P.; Maunders, C.; Botton, G.; Adronov, A. *Macromolecules* **2008**, *41*, 2304–2308.
(16) Bianco, A.; Kostarelos, K.; Partidos, C. D.; Prato, M. *Chem. Commun.* **2005**, *0*, 571–577.
(17) Lemasson, F. A.; Strunk, T.; Gerstel, P.; Hennrich, F.; Lebedkin, S.; Barner-Kowollik, C.; Wenzel, W.; Kappes, M. M.; Mayor, M. *J. Am. Chem. Soc.* **2010**, *133*, 652–655.
(18) Cheng, F.; Imin, P.; Lazar, S.; Botton, G. A.; de Silveira, G.; Marinov, O.; Deen, J.; Adronov, A. *Macromolecules* **2008**, *41*, 9869–9874.
(19) Zheng, M.; Jagota, A.; Strano, M.; Santos, A.; Barone, P.; Chou, S.; Diner, B.; Dresselhaus, M.; Mclean, R.; Onoa, G.; Samsonidze, G.; Semke, E.; Usrey, M.; Walls, D. *Science* **2003**, *302*, 1545.
(20) Komatsu, N.; Wang, F. *Materials* **2010**, *3*, 3818–3844.
(21) Geim, A. K.; Novoselov, K. S. *Nat. Mater.* **2007**, *6*, 183–191.

(22) Geim, A. K. *Science* **2009**, *324*, 1530–1534.
(23) Ghosh, S.; Bachilo, S. M.; Weisman, R. B. *Nat. Nanotechnol.* **2010**, *5*, 443–450.
(24) Peplow, M. *Nature* **2013**, *503*, 327–329.
(25) Banhart, F.; Kotakoski, J.; Krasheninnikov, A. V. *ACS Nano* **2010**, *5*, 26–41.
(26) Lu, J.; Nagase, S.; Zhang, X.; Wang, D.; Ni, M.; Maeda, Y.; Wakahara, T.; Nakahodo, T.; Tsuchiya, T.; Akasaka, T.; Gao, Z.; Yu, D.; Ye, H.; Mei, W.; Zhou, Y. *J. Am. Chem. Soc.* **2006**, *128*, 5114–5118.
(27) Chen, J.-H.; Jang, C.; Xiao, S.; Ishigami, M.; Fuhrer, M. S. *Nat. Nanotechnol.* **2008**, *3*, 206–209.
(28) Bae, S.; Kim, H.; Lee, Y.; Xu, X.; Park, J.-S.; Zheng, Y.; Balakrishnan, J.; Lei, T.; Kim, H. R.; Song, Il, Y.; Kim, Y.-J.; Kim, K. S.; Ozyilmaz, B.; Ahn, J.-H.; Hong, B. H.; Iijima, S. *Nat. Nanotechnol.* **2010**, *5*, 574–578.
(29) Paredes, J. I.; Villar-Rodil, S.; Solís-Fernández, P.; Martínez-Alonso, A.; Tascón, J. M. D. *Langmuir* **2009**, *25*, 5957–5968.
(30) Björk, J.; Hanke, F.; Palma, C.-A.; Samori, P.; Cecchini, M.; Persson, M. *J. Phys. Chem. Lett.* **2010**, *1*, 3407–3412.
(31) Wang, H.; Mei, J.; Liu, P.; Schmidt, K.; Jiménez-Osés, G.; Osuna, S.; Fang, L.; Tassone, C. J.; Zoombelt, A. P.; Sokolov, A. N.; Houk, K. N.; Toney, M. F.; Bao, Z. *ACS Nano* **2013**, *7*, 2659–2668.
(32) Park, S.; An, J.; Jung, I.; Piner, R. D.; An, S. J.; Li, X.; Velamakanni, A.; Ruoff, R. S. *Nano Lett.* **2009**, *9*, 1593–1597.
(33) Yi, W.; Malkovskiy, A.; Chu, Q.; Sokolov, A. P.; Colon, M. L.; Meador, M.; Pang, Y. *J. Phys. Chem. B* **2008**, *112*, 12263–12269.
(34) Chen, H.; Müller, M. B.; Gilmore, K. J.; Wallace, G. G.; Li, D. *Adv. Mater.* **2008**, *20*, 3557–3561.
(35) Hennrich, F.; Lebedkin, S.; Kappes, M. M. *Phys. Stat. Sol. (b)* **2008**, *245*, 1951–1953.
(36) Lutz, T.; Donovan, K. *Carbon* **2005**, *43*, 2508–2513.
(37) Paton, K. R.; Varrla, E.; Backes, C.; Smith, R. J.; Khan, U.; O'Neill, A.; Boland, C.; Lotya, M.; Istrate, O. M.; King, P.; Higgins, T.; Barwich, S.; May, P.; Puczkarski, P.; Ahmed, I.; Moebius, M.; Pettersson, H.; Long, E.; Coelho, J.; O'Brien, S. E.; McGuire, E. K.; Sanchez, B. M.; Duesberg, G. S.; McEvoy, N.; Pennycook, T. J.; Downing, C.; Crossley, A.; Nicolosi, V.; Coleman, J. N. *Nat. Mater.* **2014**, ASAP.
(38) Tanaka, T.; Urabe, Y.; Nishide, D.; Kataura, H. *Appl. Phys. Express* **2009**, *2*, 125002.
(39) Georgakilas, V.; Otyepka, M.; Bourlinos, A. B.; Chandra, V.; Kim, N.; Kemp, K. C.; Hobza, P.; Zboril, R.; Kim, K. S. *Chem. Rev.* **2012**, *112*, 6156–6214.
(40) Loh, K. P.; Bao, Q.; Ang, P. K.; Yang, J. *J. Mater. Chem.* **2010**, *20*, 2277–2289.

(41) Liu, H.; Ryu, S.; Chen, Z.; Steigerwald, M. L.; Nuckolls, C.; Brus, L. E. *J. Am. Chem. Soc.* **2009**, *131*, 17099–17101.
(42) Tanaka, T.; Jin, H.; Miyata, Y.; Fujii, S.; Nishide, D.; Kataura, H. *Phys. Stat. Sol. (b)* **2009**, *246*, 2490–2493.
(43) Tanaka, T.; Urabe, Y.; Nishide, D.; Liu, H.; Asano, S.; Nishiyama, S.; Kataura, H. *Phys. Stat. Sol. (b)* **2010**, *247*, 2867–2870.
(44) Dreyer, D. R.; Park, S.; Bielawski, C. W.; Ruoff, R. S. *Chem. Soc. Rev.* **2010**, *39*, 228–240.
(45) Homenick, C. M.; Lawson, G.; Adronov, A. *Polym Rev* **2007**, *47*, 265–290.
(46) Paulus, G. L. C.; Wang, Q. H.; Strano, M. S. *Acc. Chem. Res.* **2013**, *46*, 160–170.
(47) Bauhofer, W.; Kovacs, J. *Compos. Sci. Technol.* **2009**, *69*, 1486–1498.
(48) Georgakilas, V.; Bourlinos, A. B.; Zboril, R.; Steriotis, T. A.; Dallas, P.; Stubos, A. K.; Trapalis, C. *Chem. Commun.* **2010**, *46*, 1766–1768.
(49) Zou, J.; Khondaker, S.; Huo, Q.; Zhai, L. *Adv. Funct. Mater.* **2009**, *19*, 479–483.
(50) Strom, T. A.; Dillon, E. P.; Hamilton, C. E.; Barron, A. R. *Chem. Commun.* **2010**, *46*, 4097–4099.
(51) Harris, P. J. F. *Inter. Mater. Rev.* **2004**, *49*, 31–43.
(52) Magedov, I. V.; Frolova, L. V.; Ovezmyradov, M.; Bethke, D.; Shaner, E. A.; Kalugin, N. G. *Carbon* **2013**, *54*, 192–200.
(53) Spitalsky, Z.; Tasis, D.; Papagelis, K.; Galiotis, C. *Prog. Polym. Sci.* **2010**, *35*, 357–401.
(54) Ma, P.-C.; Siddiqui, N. A.; Marom, G.; Kim, J.-K. *Compos. Part A: Appl. S.* **2010**, *41*, 1345–1367.
(55) Roy, N.; Sengupta, R.; Bhowmick, A. K. *Prog. Polym. Sci.* **2012**, *37*, 781–819.
(56) Byrne, M.; Gun'ko, Y. *Adv. Mater.* **2010**, *22*, 1672–1688.
(57) Li, H.; Cheng, F.; Duft, A. M.; Adronov, A. *J. Am. Chem. Soc.* **2005**, *127*, 14518–14524.
(58) Elias, D. C.; Nair, R. R.; Mohiuddin, T. M. G.; Morozov, S. V.; Blake, P.; Halsall, M. P.; Ferrari, A. C.; Boukhvalov, D. W.; Katsnelson, M. I.; Geim, A. K.; Novoselov, K. S. *Science* **2009**, *323*, 610–613.
(59) Ryu, S.; Han, M. Y.; Maultzsch, J.; Heinz, T. F.; Kim, P.; Steigerwald, M. L.; Brus, L. E. *Nano Lett.* **2008**, *8*, 4597–4602.
(60) Lawson, G.; Gonzaga, F.; Huang, J.; de Silveira, G.; Brook, M. A.; Adronov, A. *J. Mater. Chem.* **2008**, *18*, 1694–1702.
(61) Robinson, J. T.; Burgess, J. S.; Junkermeier, C. E.; Badescu, S. C.; Reinecke, T. L.; Perkins, F. K.; Zalalutdniov, M. K.; Baldwin, J. W.; Culbertson, J. C.; Sheehan, P. E.; Snow, E. S. *Nano Lett.* **2010**, *10*, 3001–3005.
(62) Ma, P.-C.; Siddiqui, N.; Marom, G.; Kim, J.-K. *Compos. Part A: Appl. S.* **2010**, *41*, 1345–1367.

(63) Yang, Z.; Shi, X.; Yuan, J.; Pu, H.; Liu, Y. *Appl. Surf. Sci.* **2010**, *257*, 138–142.
(64) Chunder, A.; Liu, J.; Zhai, L. *Macromol. Rapid Commun.* **2010**, *31*, 380–384.
(65) Lotya, M.; Hernandez, Y.; King, P. J.; Smith, R. J.; Nicolosi, V.; Karlsson, L. S.; Blighe, F. M.; De, S.; Wang, Z.; McGovern, I. T.; Duesberg, G. S.; Coleman, J. N. *J. Am. Chem. Soc.* **2009**, *131*, 3611–3620.
(66) Coleman, J. N. *Adv. Funct. Mater.* **2009**, *19*, 3680–3695.
(67) Mayo, J. D.; Behal, S.; Adronov, A. *J Polym Sci Pol Chem* **2009**, *47*, 0.
(68) Sola, M.; Mestres, J.; Duran, M. *J. Phys. Chem.* **1995**, *99*, 10752–10758.
(69) Langa, F.; Nierengarten, J. F. *Fullerenes: principles and applications*; Royal Society of Chemistry, 2007.
(70) Voytekhovsky, Y. L.; Stepenshchikov, D. G. *Acta Crystallogr. A* **2003**, *59*, 283–285.
(71) Hirsch, A. *The chemistry of the fullerenes*; Wiley-VCH Verlag GmbH: Weinheim, Germany, 1994.
(72) Hirsch, A. *Nat. Mater.* **2010**, *9*, 868–871.
(73) Liu, J.; Rinzler, A. G.; Dai, H.; Hafner, J. H.; Bradley, R. K.; Boul, P. J.; Lu, A.; Iverson, T.; Shelimov, K.; Huffman, C. B.; Rodriguez-Macias, F.; Shon, Y.-S.; Lee, T. R.; Colbert, D. T.; Smalley, R. E. *Science* **1998**, *280*, 1253–1256.
(74) Penev, E. S.; Artyukhov, V. I.; Yakobson, B. I. *ACS Nano* **2014**, *8*, 1899–1906.
(75) Rümmeli, M. H.; Ayala, P.; Pichler, T. *Carbon Nanotubes and Related Structures: Production and Formation*; WILEY-VCH Verlag GmbH & Co. : Weinheim, 2010; pp. 1–22.
(76) Iijima, S.; Ichihashi, T. *Nature* **1993**, *363*, 603–605.
(77) Iijima, S. *Phys. B* **2002**, *323*, 1–5.
(78) Guo, J.; Yang, C.; Li, Z.; Bai, M.; Liu, H.; Li, G.; Wang, E.; Chan, C.; Tang, Z.; Ge, W.; Xiao, X. *Phys. Rev. Lett.* **2004**, *93*, 017402.
(79) Ma, J.; Wang, J. N.; Wang, X. X. *J. Mater. Chem.* **2009**, *19*, 3033–3041.
(80) Dresselhaus, M. S.; Dresselhaus, G.; Eklund, P.C.; Rao, A. M. In *Physics and Chemistry of Materials with Low-Dimensional Structures*; Springer Netherlands, 2000; Vol. 23, pp. 331–379.
(81) Coleman, J.; Khan, U.; Blau, W.; Gunko, Y. Carbon. **2006**, *44*, 1624–1652.
(82) Pantano, A.; M Parks, D.; Boyce, M. C. *J. Mech. Phys. Solids* **2004**, *52*, 789–821.
(83) Hong, S.; Myung, S. *Nat. Nanotechnol.* **2007**, *2*, 207–208.
(84) Wei, B. Q.; Vajtai, R.; Ajayan, P. M. *Appl. Phys. Lett.* **2001**, *79*, 1172–1174.

(85) Zhang, Q.; Chen, G.; Yoon, S. F.; Ahn, J.; Wang, S. G.; Zhou, Q. *Phys. Rev. B* **2002**.
(86) Collins, P. G.; Hersam, M.; Arnold, M.; Martel, R.; Avouris, P. *Phys. Rev. Lett.* **2001**, *86*, 3128–3131.
(87) T Dürkop; S A Getty; Enrique Cobas, A.; Fuhrer, M. S. *Nano Lett.* **2003**, *4*, 35–39.
(88) Hone, J.; Llaguno, M. C.; Biercuk, M. J.; Johnson, A. T.; Batlogg, B.; Benes, Z.; Fischer, J. E. *Appl. Phys. A Mater. Sci. Process.* **2002**, *74*, 339–343.
(89) Yanagi, K.; Miyata, Y.; Tanaka, T.; Fujii, S.; Nishide, D.; Kataura, H. *Diam. Relat. Mater.* **2009**, *18*, 935–939.
(90) Yanagi, K.; Miyata, Y.; Kataura, H. *Appl. Phys. Express* **2008**, *1*, 034003.
(91) Hároz, E. H.; Duque, J. G.; Lu, B. Y.; Nikolaev, P.; Arepalli, S.; Hauge, R. H.; Doorn, S. K.; Kono, J. *J. Am. Chem. Soc.* **2012**, *134*, 4461–4464.
(92) Dresselhaus, M. S.; Dresselhaus, G.; Saito, R. *Carbon* **1995**, *33*, 883–891.
(93) Wilder, J. W. G.; Venema, L. C.; Rinzler, A. G.; Smalley, R. E.; Dekker, C. *Nature* **1998**, *391*, 59–62.
(94) Xin Lu, A.; Zhongfang Chen. *Chem. Rev.* **2005**, *105*, 3643–3696.
(95) Ouyang, M.; Huang, J. L.; Cheung, C. L.; Lieber, C. M. *Science* **2001**, *292*, 702–705.
(96) Bachilo, S. M.; Strano, M. S.; Kittrell, C.; Hauge, R. H.; Smalley, R. E.; Weisman, R. B. *Science* **2002**, *298*, 2361–2366.
(97) Min Ouyang; Jin-Lin Huang, A.; Charles M Lieber. *Acc. Chem. Res.* **2002**, *35*, 1018–1025.
(98) Zhou, C.; Kong, J.; Dai, H. *Phys. Rev. Lett.* **2000**, *84*, 5604–5607.
(99) Miyake, T.; Saito, S. *Phys. Rev. B* **2005**, *72*, 073404.
(100) Kleiner, A.; Eggert, S. *Phys. Rev. B* **2001**, *63*, 073408.
(101) Maiti, A.; Svizhenko, A.; Anantram, M. P. *Phys. Rev. Lett.* **2002**, *88*, 126805.
(102) Yang, L.; Han, J. *Phys. Rev. Lett.* **2000**, *85*, 154–157.
(103) Ahmed Jamal, G. R.; Shamsul Arefin, M.; Mominuzzaman, S. M. *Empirical prediction of bandgap in semiconducting single-wall carbon nanotubes*; IEEE, 2012; pp. 221–224.
(104) Kleiner, A.; Eggert, S. *Phys. Rev. B* **2001**, *64*, 113402.
(105) Cabria, I.; Mintmire, J.; White, C. *Phys. Rev. B* **2003**, *67*, 121406.
(106) Blase, X.; Benedict, L. X.; Shirley, E. L.; Louie, S. G. *Phys. Rev. Lett.* **1994**.
(107) Ebbesen, T. W.; Lezec, H. J.; Hiura, H.; Bennett, J. W.; Ghaemi, H. F.; Thio, T. *Nature* **1996**, *382*, 54–56.
(108) White, C. T.; Todorov, T. N. *Nature* **1998**, *393*, 240–242.
(109) Bachtold, A.; Fuhrer, M. S.; Plyasunov, S.; Forero, M.; Anderson, E. H.; Zettl, A.; McEuen, P. L. *Phys. Rev. Lett.* **2000**, *84*, 6082–6085.

(110) Zhou, C.; Kong, J.; Dai, H. *Appl. Phys. Lett.* **2000**, *76*, 1597.
(111) Zhao, J.; Lu, J. P.; Han, J.; Yang, C. K. *Appl. Phys. Lett.* **2003**, *82*, 3746.
(112) Takenobu, T.; Takano, T.; Shiraishi, M.; Murakami, Y.; Ata, M.; Kataura, H.; Achiba, Y.; Iwasa, Y. *Nat. Mater.* **2003**, *2*, 683–688.
(113) Ding, J. W.; Yan, X. H.; Cao, J. X. *Phys. Rev. B* **2002**.
(114) Chico, L.; Benedict, L.; Louie, S.; Cohen, M. *Phys. Rev. B* **1996**, *54*, 2600–2606.
(115) Bouilly, D.; Cabana, J.; Martel, R. *Appl. Phys. Lett.* **2012**, *101*, 053116.
(116) Park, H.; Zhao, J.; Lu, J. P. *Nano Lett.* **2006**, *6*, 916–919.
(117) Bekyarova, E.; Itkis, M. E.; Cabrera, N.; Zhao, B.; Yu, A.; Gao, J.; Haddon, R. C. *J. Am. Chem. Soc.* **2005**, *127*, 5990–5995.
(118) Stadermann, M.; Papadakis, S.; Falvo, M.; Novak, J.; Snow, E.; Fu, Q.; Liu, J.; Fridman, Y.; Boland, J.; Superfine, R.; Washburn, S. *Phys. Rev. B: Condens. Matter Mater. Phys.* **2004**, *69*, 201402.
(119) He, Y.; Zhang, J.; Li, D.; Wang, J.; Wu, Q.; Wei, Y.; Zhang, L.; Wang, J.; Liu, P.; Li, Q.; Fan, S.; Jiang, K. *Nano Lett.* **2013**, *13*, 5556–5562.
(120) Kanbara, T.; Takenobu, T.; Takahashi, T.; Iwasa, Y.; Tsukagoshi, K.; Aoyagi, Y.; Kataura, H. *Appl. Phys. Lett.* **2006**, *88*, 053118.
(121) Ago, H.; Kugler, T.; Cacialli, F.; Salaneck, W. R.; Shaffer, M. S. P.; Windle, A. H.; Friend, R. H. *J. Phys. Chem. B* **1999**, *103*, 8116–8121.
(122) Tasis, D.; Tagmatarchis, N.; Bianco, A.; Prato, M. *Chem. Rev.* **2006**, *106*, 1105–1136.
(123) Srivastava, D.; Brenner, D. W.; Schall, J. D.; Kevin D Ausman; Yu, M.-F.; Ruoff, R. S. *J. Phys. Chem. B* **1999**, *103*, 4330–4337.
(124) Banerjee, S.; Hemraj-Benny, T.; Wong, S. S. *Adv. Mater.* **2005**, *17*, 17–29.
(125) Mickelson, E.; Huffman, C.; Rinzler, A.; Smalley, R.; Hauge, R.; Margrave, J. *Chem. Phys. Lett.* **1998**, *296*, 188–194.
(126) Douglas B Mawhinney; Viktor Naumenko; Anya Kuznetsova, A.; John T Yates, J.; and, J. L.; Smalley, R. E. *J. Am. Chem. Soc.* **2000**, *122*, 2383–2384.
(127) Unger, E.; Graham, A.; Kreupl, F.; Liebau, M.; Hoenlein, W. *Curr. Appl. Phys.* **2002**, *2*, 107–111.
(128) Banerjee, S.; Wong, S. S. *Nano Lett.* **2004**, *4*, 1445–1450.
(129) Liu, B.; Jiang, H.; Krasheninnikov, A. V.; Nasibulin, A. G.; Ren, W.; Liu, C.; Kauppinen, E. I.; Cheng, H.-M. *Small* **2013**, *9*, 1379–1386.
(130) Hye-Mi So; Byoung-Kye Kim; Dong-Won Park; Beom Soo Kim; Ju-Jin Kim; Ki-jeong Kong; Hyunju Chang, A.; Jeong-O Lee. *J. Am. Chem. Soc.* **2007**, *129*, 4866–4867.
(131) Kay Hyeok An; Jin Sung Park; Cheol-Min Yang; Seung Yol Jeong; Seong Chu Lim; Chul Kang; Joo-Hiuk Son; Mun Seok Jeong, A.; Young Hee Lee. *J. Am. Chem. Soc.* **2005**, *127*, 5196–5203.
(132) Wang, C.; Cao, Q.; Ozel, T.; Gaur, A.; Rogers, J.; Shim, M. **2005**, *127*,

11460–11468.
(133) Strano, M. S.; Dyke, C. A.; Usrey, M. L.; Barone, P. W.; Allen, M. J.; Shan, H.; Kittrell, C.; Hauge, R. H.; Tour, J. M.; Smalley, R. E. *Science* **2003**, *301*, 1519–1522.
(134) Lee, Y.; Jeon, K.-S.; Lim, H.; Shin, H. S.; Jin, S. M.; Byon, H. R.; Suh, Y. D.; Choi, H. C. *Small* **2009**, *5*, 1398–1402.
(135) Liu, Y.; Yao, Z.; Adronov, A. *Macromolecules* **2005**, *38*, 1172–1179.
(136) Ying, Y.; Saini, R.; Liang, F.; Sadana, A.; Billups, W. *Org. Lett.* **2003**, *5*, 1471–1473.
(137) Stephenson, J. J.; Sadana, A. K. *Chem. Mater.* **2006**, *18*, 4658–4661.
(138) Martínez-Rubí, Y.; Guan, J.; Lin, S.; Scriver, C.; Sturgeon, R.; Simard, B. *Chem. Commun.* **2007**, *2007*, 5146–5148.
(139) Deng, S.; Brozena, A. H.; Zhang, Y.; Piao, Y.; Wang, Y. *Chem. Commun.* **2011**, *47*, 758–760.
(140) Deng, S.; Zhang, Y.; Brozena, A. H.; Mayes, M. L.; Banerjee, P.; Chiou, W.-A.; Rubloff, G. W.; Schatz, G. C.; Wang, Y. *Nat. Comm.* **2011**, *2*, 382.
(141) Kumar, I.; Rana, S.; Cho, J.-W. *Chem. Eur. J.* **2011**, *17*, 11092–11101.
(142) Holzinger, M.; Vostrowsky, O.; Hirsch, A.; Hennrich, F.; Kappes, M.; Weiss, R.; Jellen, F. *Angew. Chem. Int. Ed.* **2001**, *40*, 4002–4005.
(143) Hu, H.; Zhao, B.; Hamon, M. A.; Kamaras, K.; Itkis, M. E.; Haddon, R. C. *J. Am. Chem. Soc.* **2003**, *125*, 14893–14900.
(144) Zhang, K.; Zhang, Q.; Liu, C.; Marzari, N.; Stellacci, F. *Adv. Funct. Mater.* **2012**, *22*, 5216–5223.
(145) Coleman, K. S.; Bailey, S. R.; Fogden, S.; Green, M. L. H. *J. Am. Chem. Soc.* **2003**, *125*, 8722–8723.
(146) Gao, C.; He, H.; Zhou, L.; Zheng, X.; Zhang, Y. *Chem. Mater.* **2009**, *21*, 360–370.
(147) Holzinger, M.; Abraham, J.; Whelan, P.; Graupner, R.; Ley, L.; Hennrich, F.; Kappes, M.; Hirsch, A. *J. Am. Chem. Soc.* **2003**, *125*, 8566–8580.
(148) Holzinger, M.; Steinmetz, J.; Samaille, D.; Glerup, M.; Paillet, M.; Bernier, P.; Ley, L.; Graupner, R. *Carbon* **2004**, *42*, 941–947.
(149) Georgakilas, V.; Kordatos, K.; Prato, M.; Guldi, D.; Holzinger, M.; Hirsch, A. **2002**, *124*, 760–761.
(150) Vázquez, E.; Prato, M. *Pure Appl. Chem.* **2010**, *82*.
(151) Alvaro, M.; Atienzar, P.; la Cruz, de, P. *J. Phys. Chem. B* **2004**, *108*, 12691–12697.
(152) Zhang, W.; Swager, T. M. *J. Am. Chem. Soc.* **2007**, *129*, 7714–7715.
(153) Zhang, W.; Sprafke, J. K.; Ma, M.; Tsui, E. Y.; Sydlik, S. A.; Rutledge, G. C.; Swager, T. M. *J. Am. Chem. Soc.* **2009**, *131*, 8446–8454.
(154) Delgado, J. L.; la Cruz, de, P.; Langa, F.; Urbina, A.; Casado, J.; Navarrete, J. T. L. *Chem. Commun.* **2004**, 1734–1735.
(155) Sakellariou, G.; Ji, H.; Mays, J. W. *Chem. Mater.* **2007**, *19*, 6370–6372.

(156) Munirasu, S.; Albuerne, J.; Boschetti-de-Fierro, A.; Abetz, V. *Macromol. Rapid Commun.* **2010**, *31*, 574–579.
(157) Chang, C.-M.; Liu, Y.-L. *Carbon* **2009**, *47*, 3041–3049.
(158) Ménard-Moyon, C.; Dumas, F.; Doris, E.; Mioskowski, C. *J. Am. Chem. Soc.* **2006**, *128*, 14764–14765.
(159) Zhao, Y.-L.; Stoddart, J. *Acc. Chem. Res.* **2009**, *42*, 1161–1171.
(160) Qian, D. *Compos. Sci. Technol.* **2003**, *63*, 1561–1569.
(161) Zheng, M.; Jagota, A.; Semke, E. D.; Diner, B. A.; Mclean, R. S.; Lustig, S. R.; Richardson, R. E.; Tassi, N. G. *Nat. Mater.* **2003**, *2*, 338–342.
(162) Girifalco, L. A.; Hodak, M.; Lee, R. S. *Phys. Rev. B* **2000**, *62*, 13104–13110.
(163) Hertel, T.; Walkup, R. E.; Avouris, P. *Phys. Rev. B* **1998**, *58*, 13870–13873.
(164) Ajayan, P. M.; Banhart, F. *Nat. Mater.* **2004**, *3*, 135–136.
(165) Salvetat, J.-P.; Briggs, G.; Bonard, J.-M.; Bacsa, R.; Kulik, A.; Stöckli, T.; Burnham, N.; Forró, L. *Phys. Rev. Lett.* **1999**, *82*, 944–947.
(166) Kis, A.; nyi, G. C. A.; Salvetat, J. P.; Lee, T.-N.; Couteau, E.; Kulik, A. J.; Benoit, W.; Brugger, J.; oacute, L. F. *Nat. Mater.* **2004**, *3*, 153–157.
(167) Filleter, T.; Bernal, R.; Li, S.; Espinosa, H. D. *Adv. Mater.* **2011**, *23*, 2855–2860.
(168) Coleman, J. N.; Cadek, M.; Blake, R.; Nicolosi, V.; Ryan, K. P.; Belton, C.; Fonseca, A.; Nagy, J. B.; Gun'ko, Y. K.; Blau, W. J. *Adv. Funct. Mater.* **2004**, *14*, 791–798.
(169) Vaisman, L.; Wagner, H. D.; Marom, G. *Adv. Colloid Interface Sci.* **2006**, *128-130*, 37–46.
(170) Kar, T.; Bettinger, H. F.; Scheiner, S.; Roy, A. K. *J. Phys. Chem. C* **2008**, *112*, 20070–20075.
(171) Kim, S. W.; Kim, T.; Kim, Y. S.; Choi, H. S.; Lim, H. J.; Yang, S. J.; Park, C. R. *Carbon* **2012**, *50*, 3–33.
(172) Mittal, V. *Surface Modification of Nanotube Fillers*; Wiley, 2011.
(173) Britz, D. A.; Khlobystov, A. N. *Chem. Soc. Rev.* **2006**, *35*, 637–659.
(174) Moore, V. C.; Strano, M. S.; Haroz, E. H.; Hauge, R. H. *Nano Lett.* **2003**, *3*, 1379–1382.
(175) Chattopadhyay, D.; Galeska, I.; Papadimitrakopoulos, F. *J. Am. Chem. Soc.* **2003**, *125*, 3370–3375.
(176) Bergin, S. D.; Sun, Z.; Rickard, D.; Streich, P. V.; Hamilton, J. P.; Coleman, J. N. *ACS Nano* **2009**, *3*, 2340–2350.
(177) Tuncel, D. *Nanoscale* **2011**, *3*, 3545–3554.
(178) A B Dalton; C Stephan; J N Coleman; B McCarthy; P M Ajayan; S Lefrant; P Bernier; W J Blau, A.; Byrne, H. J. *J. Phys. Chem. B* **2000**, *104*, 10012–10016.
(179) S M Keogh; T G Hedderman; P Lynch; G F Farrell, A.; Byrne, H. J. *J. Phys. Chem. B* **2006**, *110*, 19369–19374.

(180) Chen, J.; Liu, H.; Weimer, W. A.; Halls, M. D.; Waldeck, D. H.; Walker, G. C. *J. Am. Chem. Soc.* **2002**, *124*, 9034–9035.
(181) Rice, N. A.; Soper, K.; Zhou, N.; Merschrod, E.; Zhao, Y. *Chem. Commun.* **2006**, 4937–4939.
(182) Lee, H. W.; Yoon, Y.; Park, S.; Oh, J. H.; Hong, S.; Liyanage, L. S.; Wang, H.; Morishita, S.; Patil, N.; Park, Y. J.; Park, J. J.; Spakowitz, A.; Galli, G.; Gygi, F.; Wong, P. H. S.; Tok, J. B.-H.; Kim, J. M.; Bao, Z. *Nat. Comm.* **2011**, *2*, 541.
(183) Lemasson, F. A.; Strunk, T.; Gerstel, P.; Hennrich, F.; Lebedkin, S.; Barner-Kowollik, C.; Wenzel, W.; Kappes, M. M.; Mayor, M. *J. Am. Chem. Soc.* **2011**, *133*, 652–655.
(184) Qiu, X.; Khripin, C. Y.; Ke, F.; Howell, S. C.; Zheng, M. *Phys. Rev. Lett.* **2013**, *111*, 048301.
(185) Prasek, J.; Drbohlavova, J.; Chomoucka, J.; Hubalek, J.; Jasek, O.; Adam, V.; Kizek, R. *J. Mater. Chem.* **2011**, *21*, 15872–15884.
(186) Kim, S. N.; Kuang, Z.; Grote, J. G.; Farmer, B. L.; Naik, R. R. *Nano Lett.* **2008**, *8*, 4415–4420.
(187) Tu, X.; Manohar, S.; Jagota, A.; Zheng, M. *Nature* **2009**, *460*, 250.
(188) Zheng, M.; Semke, E. *J. Am. Chem. Soc.* **2007**, *129*, 6084–6085.
(189) Zhang, L.; Tu, X.; Welsher, K.; Wang, X.; Zheng, M.; Dai, H. *J. Am. Chem. Soc.* **2009**, *131*, 2454–2455.
(190) Cathcart, H.; Quinn, S.; Nicolosi, V.; Kelly, J. M.; Werner J Blau; Coleman, J. N. *J. Phys. Chem. C* **2006**, *111*, 66–74.
(191) Hersam, M.; Stupp, S. I.; Arnold, M. S. Separation of carbon nanotubes in density gradients. WO2006096613 A3, 2007.
(192) Arnold, M.; Green, A.; Hulvat, J.; Stupp, S.; Hersam, M. *Nat. Nanotechnol.* **2006**, *1*, 60–65.
(193) Green, A.; Duch, M.; Hersam, M. *Nano Res.* **2009**, *2*, 69–77.
(194) Kim, S. N.; Luo, Z.; Papadimitrakopoulos, F. *Nano Lett.* **2005**, *5*, 2500–2504.
(195) Chattopadhyay, D.; Galeska, I.; Papadimitrakopoulos, F. *J. Am. Chem. Soc.* **2003**, *125*, 3370–3375.
(196) Samsonidze, G. G.; Chou, S. G.; Santos, A. P.; Brar, V. W.; Dresselhaus, G.; Dresselhaus, M. S.; Selbst, A.; Swan, A. K.; Ünlü, M. S.; Goldberg, B. B.; Chattopadhyay, D.; Kim, S. N.; Papadimitrakopoulos, F. *Appl. Phys. Lett.* **2004**, *85*, 1006–1008.
(197) Maeda, Y.; Kimura, S.-I.; Kanda, M.; Hirashima, Y.; Hasegawa, T.; Wakahara, T.; Lian, Y.; Nakahodo, T.; Tsuchiya, T.; Akasaka, T.; Lu, J.; Zhang, X.; Yu, Y.; Nagase, S.; Kazaoui, S.; Minami, N.; Shimizu, T.; Tokumoto, H.; Saito, R. *J. Am. Chem. Soc.* **2005**, *127*, 10287–10290.
(198) Marquis, R.; Kulikiewicz, K.; Lebedkin, S.; Kappes, M. M.; Mioskowski, C.; Meunier, S.; Wagner, A. *Chem. Eur. J.* **2009**, *15*, 11187–11196.
(199) Peng, X.; Komatsu, N.; Kimura, T.; Osuka, A. *J. Am. Chem. Soc.* **2007**,

129, 15947–15953.
(200) Lemasson, F.; Berton, N.; Tittmann, J.; Hennrich, F.; Kappes, M. M.; Mayor, M. *Macromolecules* **2011**, *45*, 713–722.
(201) Fukumaru, T.; Toshimitsu, F.; Fujigaya, T.; Nakashima, N. *Nanoscale* **2014**, *6*, 5879–5886.
(202) Tange, M.; Okazaki, T.; Iijima, S. *J. Am. Chem. Soc.* **2011**, *133*, 11908–11911.
(203) Ding, J.; Li, Z.; Lefebvre, J.; Cheng, F.; Dubey, G.; Zou, S.; Finnie, P.; Hrdina, A.; Scoles, L.; Lopinski, G. P.; Kingston, C. T.; Simard, B.; Malenfant, P. R. L. *Nanoscale* **2014**, *6*, 2328–2339.
(204) Rice, N. A.; Adronov, A. *Macromolecules* **2013**, *46*, 3850–3860.
(205) Yan, L. Y.; Li, W.; Fan, X. F.; Wei, L.; Chen, Y.; Kuo, J.-L.; Li, L.-J.; Kwak, S. K.; Mu, Y.; Chan-Park, M. B. *Small* **2010**, *6*, 110–118.
(206) Ju, S.-Y.; Doll, J.; Sharma, I.; Papadimitrakopoulos, F. *Nat. Nanotechnol.* **2008**, *3*, 356–362.
(207) Saito, K.; Troiani, V.; Qiu, H.; Solladié, N.; Sakata, T.; Mori, H.; Ohama, M.; Fukuzumi, S. *J. Phys. Chem. C* **2007**, *111*, 1194–1199.
(208) Heller, D. A.; Mayrhofer, R. M.; Baik, S.; Grinkova, Y. V.; Usrey, M. L.; Strano, M. S. *J. Am. Chem. Soc.* **2004**, *126*, 14567–14573.
(209) Kim, Y.; Hong, S.; Jung, S.; Strano, M. S.; Choi, J.; Baik, S. *J. Phys. Chem. B* **2006**, *110*, 1541–1545.
(210) Shin, D. H.; Kim, J.-E.; Shim, H. C.; Song, J.-W.; Yoon, J.-H.; Kim, J.; Jeong, S.; Kang, J.; Baik, S.; Han, C.-S. *Nano Lett.* **2008**, *8*, 4380–4385.
(211) Tanaka, T.; Jin, H.; Miyata, Y.; Fujii, S.; Suga, H.; Naitoh, Y.; Minari, T.; Miyadera, T.; Tsukagoshi, K.; Kataura, H. *Nano Lett.* **2009**, *9*, 1497–1500.
(212) Hirano, A.; Tanaka, T.; Urabe, Y.; Kataura, H. *J. Phys. Chem. C* **2012**, *116*, 9816–9823.
(213) Liu, H.; Feng, Y.; Tanaka, T.; Urabe, Y.; Kataura, H. *J. Phys. Chem. C* **2010**, *114*, 9270–9276.
(214) Tanaka, T.; Liu, H.; Fujii, S.; Kataura, H. *Phys. Status Solidi RRL* **2011**, *5*, 301–306.
(215) Al-Saleh, M. H.; Sundararaj, U. *Compos. Part A: Appl. S.* **2011**, *42*, 2126–2142.
(216) Mielke, S. L.; Troya, D.; Zhang, S.; Li, J.-L.; Xiao, S.; Car, R.; Ruoff, R. S.; Schatz, G. C.; Belytschko, T. *Chem. Phys. Lett.* **2004**, *390*, 413–420.
(217) Sammalkorpi, M.; Krasheninnikov, A.; Kuronen, A. *Phys. Rev. B* **2004**.
(218) Wong, M.; Paramsothy, M.; Xu, X. J.; Ren, Y.; Li, S.; Liao, K. *Polymer* **2003**, *44*, 7757–7764.
(219) Sainsbury, T.; Erickson, K.; Okawa, D.; Zonte, C.; Fréchet, J.; Zettl, A. *Chem. Mater.* **2010**, *22*, 2164–2171.
(220) Lou, X.; Detrembleur, C.; Sciannamea, V.; Pagnoulle, C.; Jerome, R. *Polymer* **2004**, *45*, 6097–6102.

(221) Homenick, C. M.; Lawson, G.; Adronov, A. *Polym. Rev.* **2007**, *47*, 265–290.
(222) Yuan, W.; Chan-Park, M. B. *ACS Appl. Mater. Interfaces* **2012**, *4*, 2065–2073.
(223) Ma, P. C.; Kim, J.-K. *Carbon Nanotubes for Polymer Reinforcement*; Taylor & Francis, 2011.
(224) Hecht, D.; Hu, L.; Gruner, G. *Appl. Phys. Lett.* **2006**.
(225) Kamaras, K.; Itkis, M. E.; Hu, H.; Zhao, B.; Haddon, R. C. *Science* **2003**, *301*, 1501.
(226) Manuel Melle-Franco; Massimo Marcaccio; Demis Paolucci; Francesco Paolucci; Vasilios Georgakilas; Dirk M Guldi; Maurizio Prato, A.; Francesco Zerbetto. *J. Am. Chem. Soc.* **2004**, *126*, 1646–1647.
(227) V Skákalová; A B Kaiser; U Dettlaff-Weglikowska; K Hrnčariková, A.; Roth, S. *J. Phys. Chem. B* **2005**, *109*, 7174–7181.
(228) Zhao, J.; Chen, Z.; Zhou, Z.; Park, H.; Schleyer, P. V. R.; Lu, J. P. *ChemPhysChem* **2005**, *6*, 598–601.
(229) Frank, S.; Poncharal, P.; Wang, Z.; Heer, W. *Science* **1998**, *280*, 1744–1746.
(230) Sanvito, S.; Kwon, Y.; Tomanek, D.; Lambert, C. *Phys. Rev. Lett.* **2000**, *84*, 1974–1977.
(231) Zeng, X.; Xu, X.; Shenai, P. M.; Kovalev, E.; Baudot, C.; Mathews, N.; Zhao, Y. *J. Phys. Chem. C* **2011**, *115*, 21685–21690.
(232) Shimizu, M.; Fujii, S.; Tanaka, T.; Kataura, H. *J. Phys. Chem. C* **2013**, *117*, 11744–11749.
(233) L Hu; D S Hecht, A.; Gruner, G. *Nano Lett.* **2004**, *4*, 2513–2517.
(234) Nirmalraj, P. N.; Lyons, P. E.; De, S.; Coleman, J. N.; Boland, J. J. *Nano Lett.* **2009**, *9*, 3890–3895.
(235) Nosho, Y.; Ohno, Y.; Kishimoto, S.; Mizutani, T. *Nanotechnology* **2007**, *18*, 415202.
(236) Afzali-Ardakani, A.; Avouris, P.; Chen, J.; Klinke, C. Method and apparatus for solution processed doping of carbon nanotube. US7253431 B2, 2007.
(237) Vigolo, B.; Coulon, C.; Maugey, M.; Zakri, C.; Poulin, P. *Science* **2005**, *309*, 920–923.
(238) Zakri, C.; Poulin, P. *J. Mater. Chem.* **2006**, *16*, 4095–4098.
(239) Lu, C.; Mai, Y.-W. *J. Mater. Sci.* **2008**, *43*, 6012–6015.
(240) Kyrylyuk, A. V.; van der Schoot, P. *Proc. Natl. Acad. Sci. U. S. A.* **2008**, *105*, 8221–8226.
(241) King, P. J.; Khan, U.; Lotya, M.; De, S.; Coleman, J. N. *ACS Nano* **2010**, *4*, 4238–4246.
(242) Khan, U.; O'Connor, I.; Gun'ko, Y. K.; Coleman, J. N. *Carbon* **2010**, *48*, 2825–2830.
(243) Kilbride, B. E.; Coleman, J. N.; Fraysse, J.; Fournet, P.; Cadek, M.; Drury, A.; Hutzler, S.; Roth, S.; Blau, W. J. *J. Appl. Phys.* **2002**, *92*,

4024–4030.
(244) Bilalis, P.; Katsigiannopoulos, D.; Avgeropoulos, A.; Sakellariou, G. *RSC Adv.* **2013**, *4*, 2911–2934.
(245) Gau, C.; Kuo, C.-Y.; Ko, H. *Nanotechnology* **2009**, *20*, 395705.
(246) Kyrylyuk, A. V.; Hermant, M.-C.; Schilling, T.; Klumperman, B.; Koning, C. E.; van der Schoot, P. *Nat. Nanotechnol.* **2011**, *6*, 364–369.
(247) Kyrylyuk, A. V.; Hermant, M.-C.; Schilling, T.; Klumperman, B.; Koning, C. E.; van der Schoot, P. *Nat. Nanotechnol.* **2011**, *6*, 364–369.
(248) Balandin, A. A. *Nat. Mater.* **2011**, *10*, 569–581.
(249) Grady, B. P. *Carbon nanotube-polymer composites: manufacture, properties, and applications*; Wiley: Hoboken, 2011.
(250) Huxtable, S. T.; Cahill, D. G.; Shenogin, S.; Xue, L.; Ozisik, R.; Barone, P.; Usrey, M.; Strano, M. S.; Siddons, G.; Shim, M.; Keblinski, P. *Nat. Mater.* **2003**, *2*, 731–734.
(251) Padgett, C. W.; Brenner, D. W. *Nano Lett.* **2004**, *4*, 1051–1053.
(252) Liu, C. H.; Fan, S. S. *Appl. Phys. Lett.* **2005**.
(253) Ji, P.; Sun, H.; Zhong, Y.; Feng, W. *Chem. Eng. Sci.* **2012**, *81*, 140–145.
(254) Clancy, T. C.; Gates, T. S. *Polymer* **2006**, *47*, 5990–5996.
(255) Sihn, S.; Ganguli, S.; Roy, A. K.; Qu, L.; Dai, L. *Compos. Sci. Technol.* **2008**, *68*, 658–665.
(256) Bakshi, S. R.; Lahiri, D.; Agarwal, A. *Inter. Mater. Rev.* **2013**, *55*, 41–64.
(257) Scrivener, K. L.; Kirkpatrick, R. J. *Cement Concrete Res.* **2008**, *38*, 128–136.
(258) Hu, L.; Pasta, M.; Mantia, F. L.; Cui, L.; Jeong, S.; Deshazer, H. D.; Choi, J. W.; Han, S. M.; Cui, Y. *Nano Lett.* **2010**, *10*, 708–714.
(259) Dalton, A. B.; Collins, S.; oz, E. M. N.; Razal, J. M.; Howard Ebron, Von; Ferraris, J. P.; Coleman, J. N.; Kim, B. G.; Baughman, R. H. *Nature* **2003**, *423*, 703–703.
(260) Qin, S.; Qin, D.; Ford, W. T.; Resasco, D. E.; Herrera, J. E. *Macromolecules* **2004**, *37*, 752–757.
(261) Zou, J.; Liu, L.; Chen, H.; Khondaker, S. I.; McCullough, R. D.; Huo, Q.; Zhai, L. *Adv. Mater.* **2008**, *20*, 2055–2060.
(262) Zou, J.; Chen, H.; Chunder, A.; Yu, Y.; Huo, Q.; Zhai, L. *Adv. Mater.* **2008**, *20*, 3337–3341.
(263) Itkis, M. E.; Perea, D. E.; Jung, R.; Niyogi, S.; Haddon, R. C. *J. Am. Chem. Soc.* **2005**, *127*, 3439–3448.
(264) Dresselhaus, M. S.; Dresselhaus, G.; Jorio, A. *J. Phys. Chem. C* **2007**, *111*, 17887–17893.
(265) Dresselhaus, M. S.; Jorio, A.; Hofmann, M.; Dresselhaus, G.; Saito, R. *Nano Lett.* **2010**, *10*, 751–758.
(266) Jorio, A.; Pimenta, M. A.; Filho, A. G. S.; Saito, R.; Dresselhaus, G.; Dresselhaus, M. S. *New J. Phys.* **2003**, *5*, 139–139.
(267) Dresselhaus, M. S.; Dresselhaus, G.; Jorio, A.; Souza Filho, A. G.;

Saito, R. *Carbon* **2002**, *40*, 2043–2061.
(268) Jorio, A.; Fantini, C.; Pimenta, M. A.; Capaz, R. B.; Samsonidze, G. G.; Dresselhaus, G.; Dresselhaus, M. S.; Jiang, J.; Kobayashi, N.; Grüneis, A.; Saito, R. *Phys. Rev. B* **2005**, *71*, 075401.
(269) Jorio, A.; Santos, A. P.; Ribeiro, H. B.; Fantini, C.; Souza, M.; Vieira, J. P. M.; Furtado, C. A.; Jiang, J.; Saito, R.; Balzano, L.; Resasco, D. E.; Pimenta, M. A. *Phys. Rev. B* **2005**, *72*, 075207.
(270) Heller, D. A.; Barone, P. W.; Swanson, J. P.; Mayrhofer, R. M.; Strano, M. S. *J. Phys. Chem. B* **2004**, *108*, 6905–6909.
(271) Jorio, A.; Saito, R.; Hafner, J. H.; Lieber, C. M.; Hunter, M.; McClure, T.; Dresselhaus, G.; Dresselhaus, M. S. *Phys. Rev. Lett.* **2001**, *86*, 1118–1121.
(272) Maultzsch, J.; Telg, H.; Reich, S.; Thomsen, C. *Phys. Rev. B* **2005**, *72*, 205438.
(273) Rao, A. M.; Richter, E.; Bandow, S.; Chase, B.; Eklund, P.C.; Williams, K. A.; Fang, S.; Subbaswamy, K. R.; Menon, M.; Thess, A.; Smalley, R. E.; Dresselhaus, G.; Dresselhaus, M. S. *Science* **1997**, *275*, 187–191.
(274) Weisman, R. B.; Bachilo, S. M. *Nano Lett.* **2003**, *3*, 1235–1238.
(275) Kataura, H.; Kumazawa, Y.; Maniwa, Y.; Umezu, I.; Suzuki, S.; Ohtsuka, Y.; Achiba, Y. *Synth. Met.* **1999**, *103*, 2555–2558.
(276) O'Connell, M. J.; Bachilo, S. M.; Huffman, C. B.; Moore, V. C.; Strano, M. S.; Hároz, E. H.; Rialon, K. L.; Boul, P. J.; Noon, W. H.; Kittrell, C.; Ma, J.; Hauge, R. H.; Weisman, R. B.; Smalley, R. E. *Science* **2002**, *297*, 593–596.
(277) Iakoubovskii, K.; Minami, N.; Kazaoui, S.; Ueno, T.; Miyata, Y.; Yanagi, K.; Kataura, H.; Ohshima, S.; Saito, T. *J. Phys. Chem. B* **2006**, *110*, 17420–17424.
(278) Crochet, J.; Clemens, M.; Hertel, T. *J. Am. Chem. Soc.* **2007**, *129*, 8058–8059.
(279) Gaufres, E.; Izard, N.; Vivien, L.; Kazaoui, S.; Marris-Morini, D.; Cassan, E. *Opt. Lett.* **2009**, *34*, 3845–3847.
(280) Bellucci, S.; Gaggiotti, G.; Marchetti, M.; Micciulla, F.; Mucciato, R.; Regi, M. *J. Phys.: Conf. Ser.* **2007**, *61*, 99–104.
(281) Odom, T. W.; Hafner, J. H.; Lieber, C. M. In *Carbon Nanotubes*; Springer, 2001; pp. 173–211.
(282) Branca, C.; Frusteri, F.; Magazù, V.; Mangione, A. *J. Phys. Chem. B* **2004**, *108*, 3469–3473.
(283) Safarova, K.; Drovak, A.; Kubinek, R.; Vujtek, M. In *Modern Research and Educational Topics in Microscopy*; Modern Research and Educational Topics in Microscopy, 2007.
(284) Saini, R. K.; Chiang, I. W.; Peng, H.; Smalley, R. E.; Billups, W. E.; Hauge, R. H.; Margrave, J. L. *J. Am. Chem. Soc.* **2003**, *125*, 3617–3621.

Chapter 2: Polymer Grafting to Single-Walled Carbon Nanotubes: Effect of Chain Length on Solubility, Graft Density and Mechanical Properties of Macroscopic Structures

Ryan C. Chadwick[1], Umar Khan[2], Jonathan N. Coleman*[2], and Alex Adronov*[1]

[1]*Department of Chemistry and Chemical Biology,*
McMaster University,
1280 Main St. W.,
Hamilton, Ontario, L8S 4M1 (Canada)

[2]*School of Physics and CRANN,*
Trinity College Dublin,
Dublin 2, (Ireland)

This chapter has been reproduced with permission from Small, 2013, 9, 552-560, DOI: 10.1002/smll.201201683.

The work detailed in this chapter was carried out in collaboration with Dr. Umar Khan and Professor Jonathan Coleman (School of Physics – Trinity College, Dublin). Ryan Chadwick performed the synthesis and characterization of the polymers and functionalized carbon nanotubes. Dr. Khan prepared the intercalated materials and performed the mechanical testing.

Graphical Abstract:

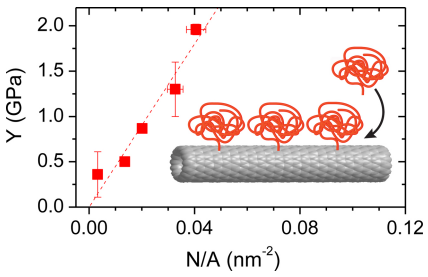

Abstract

Single-walled carbon nanotubes are grafted with polystyrene chains employing a graft-to protocol. Thermogravimetric analysis allows calculation of the grafted chain density and average interchain separation on the nanotube surface as a function of molecular weight. The separation scales with molecular weight as a power law with an exponent of ca. 0.588, showing the grafted chains to be in a swollen random walk conformation. This implies that chain packing is controlled by coil size in solution. In addition, the dispersed concentration of functionalized nanotubes scales with the size of the steric potential barrier that prevents aggregation of polymer functionalized nanotubes. It is also shown that the molecular weight of the grafted chains significantly affects the mechanical properties of nanotube films.

2.1. Introduction

As a result of their unique electronic, structural, and mechanical properties, carbon nanotubes have attracted significant research interest.[1-6] The combination of their high aspect ratio, extraordinary mechanical strength, and high electrical and thermal conductivity enables their application as key components in high-strength composites,[7] electronic devices,[8] sensors,[9] actuators,[10] and a variety of other constructs.[11,12] However, the structural properties that enable these advanced applications, namely the high aspect ratio and extended π-conjugation of the nanotube sidewall, are also responsible for the strong inter-nanotube van der Waals interactions that cause them to aggregate into large bundles and greatly diminish their solubility in both organic and aqueous solvents.[13] This lack of solubility has posed a significant obstacle to homogeneous dispersion within host materials, which is a necessary requirement for many of their potential applications. To improve nanotube solubility, covalent functionalization of their sidewalls has proven extremely effective and versatile.[13-16] A number of research groups have investigated functionalization reactions involving treatment of CNTs with highly reactive nitrenes, carbenes, radicals, azomethine ylides, and halogens under various conditions.[13,15,17] This chemistry has resulted in the introduction of small molecules on the nanotube surface and has proven effective in debundling and solubilizing carbon nanotubes. Additionally, for materials applications in which nanotubes must interface with polymers, recent attention has focused on the introduction of macromolecules on

the nanotube surface that can interact and entangle with the surrounding polymers to improve the homogeneity of blended materials.[18,19] Considering that modern polymerization methods allow exquisite control over polymer composition, size, architecture, and solubility, the conjugation of synthetic polymers to the nanotube surface enables not only the introduction of numerous desirable properties, but also optimization of the resulting materials to specific applications.

Covalent introduction of polymers on the nanotube surface can be accomplished by either the "grafting from" or "grafting to" methodologies.[18] Although both approaches have been extensively exploited for nanotube functionalization, the most successful methods of suspension have used "grafting from" or *in situ* polymerization approaches.[7] On the contrary, the ability to synthesize and characterize the polymer chains prior to coupling onto the nanotube surface, as in the "grafting to" approach, poses a distinct advantage. Unfortunately, this method limits graft densities as a result of steric hindrance between incoming polymer chains and those that are already on the surface, especially for high molecular weight polymers. This reactivity hindrance necessitates the use of highly efficient coupling chemistry between the SWNT surface and the polymer chain end. Consequently, highly efficient click coupling between azide-terminated polymer chains and alkyne-functionalized SWNTs, using the well-known Copper(I)-catalyzed Azide-Alkyne Cycloaddition (CuAAC)[20] has recently been employed in "graft to" approaches to covalent decoration of SWNTs with polymers.[21,22]

Several studies investigating the effect of polymer chain length on graft density have shown that graft density is reduced with increasing polymer molecular weight.[23] However, the exact morphology and conformation of polymers on the nanotube surface is still poorly understood. Nevertheless, it is reasonable to expect that polymer molecular weight and conformation will play an important role in dictating the organization and distribution of polymer chains on the nanotube surface. These parameters will directly impact both the graft density achievable under specific conditions, and the degree of interaction between grafted polymer chains and surrounding materials. To gain a better understanding of the role of molecular weight on grafted polymer conformation and mechanical strength of composites, we have utilized the CuAAC reaction to prepare a series of SWNTs grafted with well-defined, narrow polydispersity polystyrene chains of different molecular weight. We use polystyrene as our grafting polymer because synthetic methods to produce narrow polydispersity samples are readily available[24] and because polystyrene lacks appreciable affinity for carbon nanotubes (*i.e.* it is unable to non-covalently interact with the CNT sidewall and impart solubility).[21] We demonstrate the grafting of narrow PDI polystyrene samples to HiPco carbon nanotubes in a "good" solvent (warm DMF), with the intention of sterically limiting the graft density to levels that can be achieved by the polymer chains in a random coil conformation. By measuring the mass of grafted polymer for a range of well-defined molecular weights, we can calculate the graft density as a function of molecular weight. By estimating the average

interchain separation from the graft density, we show that the packing of grafted chains on the nanotube surface is consistent with the chains retaining the conformation they had adopted while in solution. Once the conformation of the grafted chains is known, we can show that the dispersed concentration is consistent with the steric stabilization mechanism. Finally, we show that the mechanical properties of vacuum-filtered nanotube films are directly sensitive to the graft density which is of course controlled by the molecular weight.

2.2. Results and Discussion

2.2.1. Synthesis

To produce the desired series of PS-SWNT samples, we took advantage of the CuAAC reaction, well documented for use in polymer "grafting to" CNTs.[25] Using as-purchased acid-purified HiPco SWNTs, we prepared the polystyrene-SWNT hybrids (PS-SWNTs) according to the procedure outlined in Scheme 2.1. First we carried out a Pschorr-type diazonium reaction to arylate the surface of the SWNTs with TMS-protected alkyne groups, as performed by Palacin *et al.*, to produce alkyne-funtionalized carbon nanotubes (af-SWNTs).[26,27] Here, the TMS groups appear to minimize the breakdown of the alkyne species. Previous studies with un-protected alkyne ethers required immediate use of the af-SWNTs to produce highly soluble materials.[21] The TMS protected version is stable at least on the order of weeks and can even be re-suspended in solvent after drying. The graft density of this reaction was relatively constant, amounting to a grafting mass percentage of ca. 8% to within the error of the TGA measurement. This

corresponds to a density of approximately 1 graft per 150 CNT carbons. When performed on carbon nanotubes, Pschorr-type chemistry has been previously demonstrated to produce relatively uniform grafting, albeit with a small amount of oligimerization.[15] For the purpose of our study, this chemistry results in a large excess of alkyne groups relative to the number polystyrene chains that can be introduced on the nanotube surface.

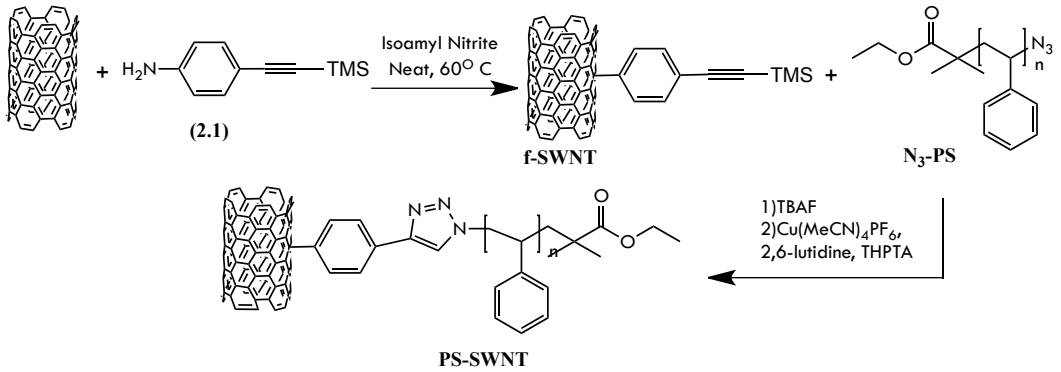

Scheme 2.1. General synthesis of PS-SWNTs.

Characterization of the af-SWNTs was carried out using both Raman and Infrared (IR) spectroscopy. A sharp increase in the Raman D-band after the diazonium decomposition reaction provides evidence for the high-degree of covalent sidewall functionalization that occurred at this step (Figures A1.3 and A1.4). In addition, the IR spectrum of the af-SWNTs shows a signal at *ca*. 2150 cm^{-1} that is characteristic of the alkyne C≡C triple bond stretch, which is also present in the 4-TMS-ethynylbenezne (Figure A1.5). Matching signals in the fingerprint region at ca. 950 cm^{-1} in the af-SWNT and TMS-ethynylbenzene also

provide additional evidence for the SWNT sidewall functionalization (Figure A1.5).

We then produced a series of nine low-polydispersity polystyrene samples via the ARGET variant of atom transfer radical polymerization (ATRP).[24] Ethyl-2-bromoisobutyrate was used as the initator, and the Me_6Tren/Cu complex was used as the catalyst. We chose to prepare nine different molecular weights with M_w ranging from 2 to 200 kDa (Table 2.1). All but the highest M_w sample had a low polydispersity index (PDI). The terminal bromide functionality in each of these samples was converted to an azide via substitution with sodium azide. Complete conversion in this reaction was determined by using previously developed ^{1}H-NMR methods, where a shift of the terminal methylene protons from 4.4 to 3.9 ppm was observed.[21]

Table 2.1: PS-SWNT Properties.

M_w (kDa)	M_n (kDa)	PDI	% Mass Polymer in PS-SWNTs[†]	Solubility[*] (mg/L)	Graft Density (per 1000 C)
2.0	1.7	1.16	31.9 ± 2.8	85 ± 66[a]	1.89
4.2	3.9	1.12	40.1 ± 3.6	152 ± 23	1.16
7.5	6.8	1.10	39.8 ± 3.6	203 ± 30	0.64
9.4	8.7	1.09	40.0 ± 3.6	241 ± 10	0.51
13.0	11.6	1.12	36.2 ± 3.2	29 ± 2	0.34
19.7	17.3	1.14	36.7 ± 3.3	13 ± 2	0.22
27.8	24.0	1.13	31.4 ± 2.8	27 ± 10	0.14
47.2	39.5	1.19	25.0 ± 2.2	4.3 ± 0.4	0.06
176.0	89.0	1.97	12.2 ± 1.1	1.6 ± 0.6	0.01

[†]Measured by TGA

[*]All +/- values are 1 standard deviation of triplicate measurements.

[a] The 2.0 kDa grafter preciptates over time, but resuspends with slight agitation. This makes precise determination of solubility difficult.

Having prepared this series of azide functionalized polystyrenes, we then coupled each polymer sample to the af-SWNTs, using a slight modification of previously reported methods.[27] THPTA/Cu(I) was used as the catalyst, and the reactions were carried out in DMF. This methodology, compared with our previous studies,[21] was found to be much less air sensitive, more reproducible, and proceeded more efficently at low temperature. A large excess of polymer was used to ensure that steric hindrance was the main limiting factor in the functionalization chemistry. Once the reactions were carried out for 48 h, excess polymer was removed by ultrafiltration through a PTFE membrane (200 nm pore diameter) and washing with THF. Excess copper was removed by washing the residue with aqueous ammonium hydroxide. IR spectroscopy provides evidence of polystyrene grafting (Figure A1.5). The spectra of the ps-SWNT and polystyrene show the same peaks in the regions of 600-800, and 1500-1600 cm^{-1}. In addition the ps-SWNTs show the peaks expected for the aromatic stretches and bends of polystyrene. These changes are generally consistent with those found in the literature for polystyrene grafts.[28]

The solubility of each PS-SWNT sample was measured by UV-Vis spectroscopy. Solutions were prepared by first stirring 10 mg of each PS-SWNT sample in approximately 3 mL of THF overnight, which produced a thick nanotube slurry. The PS-SWNT slurries were then diluted with THF to a volume of 40 mL, and sonicated for 40 min. The resulting suspensions were centrifuged (at 2,487 g) twice for 20 min, decanting between cycles. Solutions were also

passed through glass wool to remove any parts of the pellet that had not adhered to the centrifuge tube prior to measurement. Table 2.1 lists the solubility data for the various samples, and Figure 2.1A shows a plot of sample solubility as a function of molecular weight. Interestingly the solubility shows a peak at the relatively high value of ~300 mg/L for polymer chains with M_w of approximately 10 kDa.

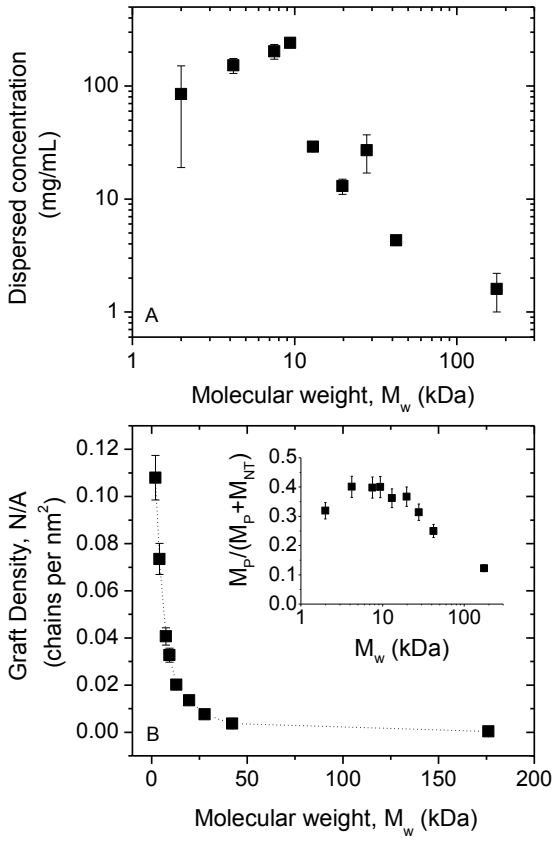

Figure 2.1: A) Solubility of PS-SWNTs in THF as a function of the weight average molecular weight (M_w) of the PS graft polymer. B) Graft density and inset: mass percentage of PS within the PS-SWNT conjugates as a function of the weight average (M_w) molecular weight of the PS graft polymer.

2.2.2. Graft Density

To determine the graft density, thermogravimetric analysis (TGA) was performed on the SWNTs, af-SWNTs, and PS-SWNTs of each batch. From the TGA data we could estimate the fractional mass of polymer in PS-SWNTs [$M_P/(M_P+ M_{NT})$], where M_P is the total mass of grafted polymer and M_{NT} is the total mass of nanotubes. This data is provided in Table 2.1 and plotted as a function of PS molecular weight in Figure 1B, inset (the raw TGA data is given in Figure A1.2 of Appendix 1). We can use this data to calculate the graft density as defined by the number of polymers per area of nanotube surface, N/A:

$$\frac{N}{A} = \frac{M}{A}\frac{M_P}{M_{NT}}\frac{1}{M_W} \qquad (1)$$

Where M/A is the mass per unit area of a graphene sheet (7.7×10^{-7} kg/m^2), M_P/M_{NT} is calculated from $M_P/(M_P + M_{NT})$ and M_w is converted to kg/molecule. The graft density, N/A, is plotted as a function of PS molecular weight in Figure 1B. This data shows that the graft density drops rapidly with increasing molecular weight of the polymer. Considering that steric hindrance surrounding the terminal azide functionality on the polymer chain end will increase with molecular weight, and the difficulty in packing larger polymer chains on the SWNT surface will also similarly increase, the observed drop in graft density at higher molecular weights is not surprising.

Once we know N/A, we can then estimate the average separation of grafted polymer chains, $R_{P\text{-}P}$, from

$$R_{P-P} = \left(\frac{N}{A}\right)^{-1/2} \quad (2)$$

A plot of R_{P-P} as a function of M_w is given in Figure 2.2A. It is clear from this data that the average chain separation increases with molecular weight approximately as a power law. With this in mind, we can consider the factors controlling the graft density. In solution, polymer chains tend to follow a random walk configuration. In this scenario we can approximately characterize the size of the chain by the typical distance between chain ends[29,30]

$$R_C = bN^{\nu} \quad (3)$$

where b is the length of a Kuhn monomer (i.e. a section of chain which approximates a link in a "freely jointed chain",[29,30] b~1.8 nm for PS[30]), N is number of Kuhn monomers per chain, and ν is an exponent that determines whether the coil is swollen.[29,30] Note that

$$N = M_w / M_{Kuhn} \quad (4)$$

where M_{Kuhn} is the mass of a Kuhn monomer (~720 g/mol for PS).[30] In a theta solvent, the chain follows ideal chain statistics resulting in $\nu = 1/2$. However, in a good solvent the chain swells, giving $\nu = 0.588$, while in a poor solvent the chain contracts, giving $\nu = 1/3$.[30] Assuming that the chain is in its preferred conformation at the time of the reaction between polymer and functionalized SWNT, it is reasonable to expect that the area occupied by the polymer chain on the nanotube is limited by chain size. Ultimately, this suggests that the spacing

between chains is closely related to the chain size in solution i.e. $R_C \sim R_{P-P}$. In reality we expect the spacing to be proportional to the chain size as R_C refers to the end-to-end distance, which is a rather arbitrary measure of the chain size. Thus, we expect the spacing to be given by

$$R_{P-P} = kbN^{\nu} \quad (5)$$

where *k* is a constant close to 1. We have fit this expression to the data in Figure 2.2A, finding very good agreement for ν=0.588 and *k*=0.75. The value of ν shows the chains to be in a swollen conformation while the value of *k* indicates that the average interchain separation after functionalization is 75% of the typical distance between chain ends in solution. Put another way, on average R_{P-P} is approximately twice the radius of gyration of the polymer chains. [30] Clearly, this shows that the graft density is indeed controlled by the size of the coil.

In addition, we have analyzed data from two literature reports using alternative chemistry to functionalize SWNTs with polystyrene (both in DMF).[21,23] These samples were prepared by two different functionalization chemistries; radical coupling[23] and "click" coupling.[21] As described above, we calculate the grafted density, *N/A*, from the published data. This is plotted as a function of molecular weight in Figure 2.2B. We have fitted equation 5 to this data, finding very good agreement for ν=1/2 and *k*=0.75.

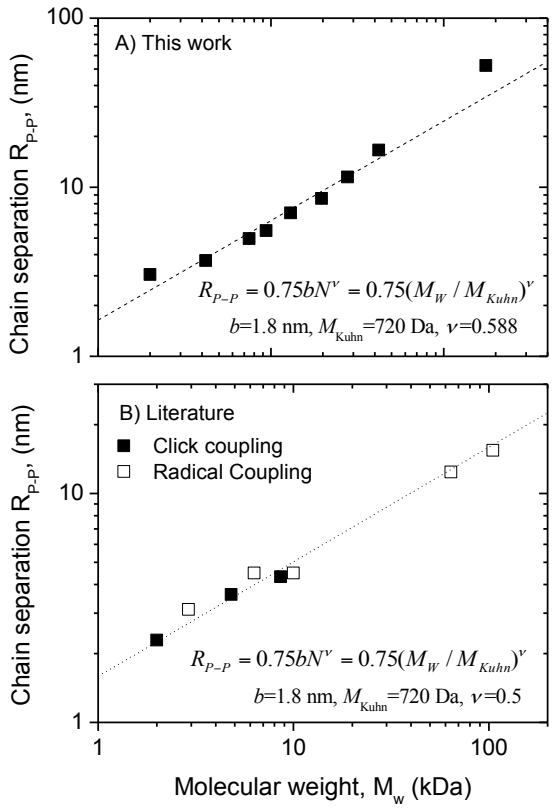

Figure 2.2: A) Plot of chain separation distance, R, as a function of grafted polymer M_w. B) Calculated chain separation versus molecular weight for published data on PS functionalized SWNTs (refs. 21 and 23). In these papers the functionalization was performed in two distinct ways, by radical coupling and "click" coupling.

The result of this analysis is very interesting. The fact that both the data presented here and two sets of literature data are all consistent with k=0.75 suggests that the steric hindrance between chains is such that the degree of interpenetration between chains (as described by k) is similar in all cases. It is also

interesting that the data presented in this work is consistent with ν=0.588, suggesting the coils to be swollen and indicating that DMF is a good solvent for PS. Interestingly, the prior literature data is consistent with ν=1/2, indicating that DMF is a theta solvent for PS under the reaction conditions used. This is puzzling as the reactions were carried out at different temperatures (125°C for radical coupling,[23] 60°C for prior "click" coupling,[21] and room temperature for the current work). In fact, it is worth noting that the Hildebrand solubility parameters[30] of DMF and polystyrene are far enough apart (δ_{DMF} = 24.7 $MPa^{1/2}$ and δ_{PS} = 18.5 $MPa^{1/2}$ respectively)[31] that, at first glance, DMF might be considered as a bad solvent for PS. This is supported by some theoretical work. [32] However, experimental work on the viscosity of PS/DMF solutions at a range of temperatures (close to room temperature) and molecular weights has given a Mark-Houwink[30] constant of 0.603.[33] This is consistent with a value of ν=0.534, suggesting that DMF is intermediate between a theta solvent and a good solvent for PS.

2.2.3. Solubility

It is clear from the data described above that the grafted polystyrene chains remain in a random walk conformation with spacing of $R_{P-P} = kbN^{\nu}$. These chains protrude out to a distance of approximately $R_C = bN^{\nu}$ from the surface of the nanotube. With this in mind we can consider the effects of molecular weight on solubility. Colloids coated with grafted polymer chains are stabilized against aggregation by the steric stabilization mechanism.[34] Here, when

chains attached to adjacent colloids begin to interact, the number of possible conformations is reduced, resulting in a repulsive force that is entropic in nature. This repulsive force is associated with a potential barrier, the height of which can be approximated as $V_{BS} \propto L/s^3$, where L is the spatial extent of the protruding chain and s is the average distance between grafted chains.[35] It has been suggested that the dispersed concentration scales with the height of this potential barrier.[35] In our case, $s = R_{P-P}$ and $L = R_C$. This means we can write $V_{BS} \propto M_W^{-2\nu} = M_W^{-1.176}$. We can test this hypothesis by plotting the dispersed concentration of PS-SWNT as a function of $M_W^{-1.176}$ in Figure 2.3. Here the dispersed concentration does indeed increase approximately linearly with increasing barrier height (i.e. decreasing M_W) for all molecular weights except the lowest two, where the concentration saturates. This explains the molecular weight dependence of the solubility and confirms that steric stabilization is at work in these systems.

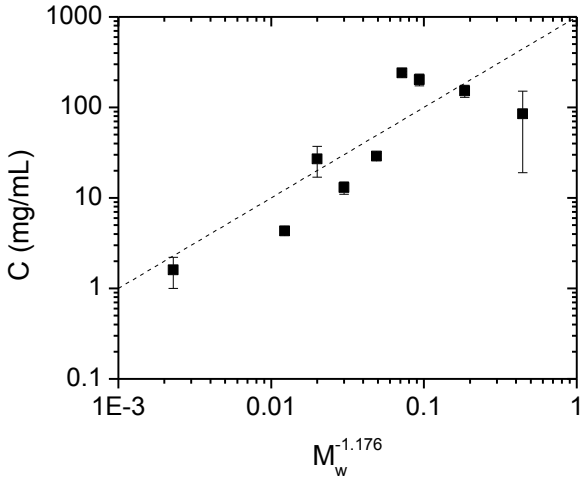

Figure 2.3: Dispersed concentration of PS-SWNTs plotted as a function of $M_W^{-1.176}$. This quantity is approximately proportional to the steric barrier height. The dashed line illustrates linearity.

2.2.4. Mechanical Properties of Solids

It might be expected that the graft density or molecular weight of grafted polymer will play an important role in the mechanical properties of any solids prepared from the functionalized nanotubes. To test this we prepared vacuum filtered films (Buckypaper) from nanotubes functionalized with a range of PS molecular weights. Stress-strain curves for a subset of the films are shown in Figure 2.4A. It is clear from this data that the mechanical properties tend to improve as the molecular weight is decreased. As shown in Figure 2.4A and B insets, the Young's modulus increases from ~0.3 GPa for the 47 kDa sample to ~2 GPa for the 7.5 kDa sample before falling off slightly. Similarly, the strength

increases from ~10 MPa for the highest molecular weight samples to ~85 MPa for the 7.5 kDa sample before falling off. It is worth noting that these mechanical properties are reasonably promising. Carbon nanotube Buckypaper tends to have moduli of ~1 GPa and strength of ~ 10 MPa.[36] In addition, the values found here are significantly above those found for nanotube Buckypaper infiltrated with non-covalently bound PS.[37]

These trends are contrary to our original expectations, as we assumed that polymer chains on adjacent nanotubes would entangle, with high molecular weight leading to greater entanglement.[29,30] Thus, we expected higher molecular weight to result in better mechanical properties. However, more careful analysis rules out polymer entanglement as a source of inter-tube interaction. The minimum molecular weight for which entanglement can occur for polystyrene at room temperature is ~35 kDa.[38,39] All of the samples tested mechanically except one have molecular weights below this critical value, which means that polymer chains attached to adjacent nanotubes cannot entangle.

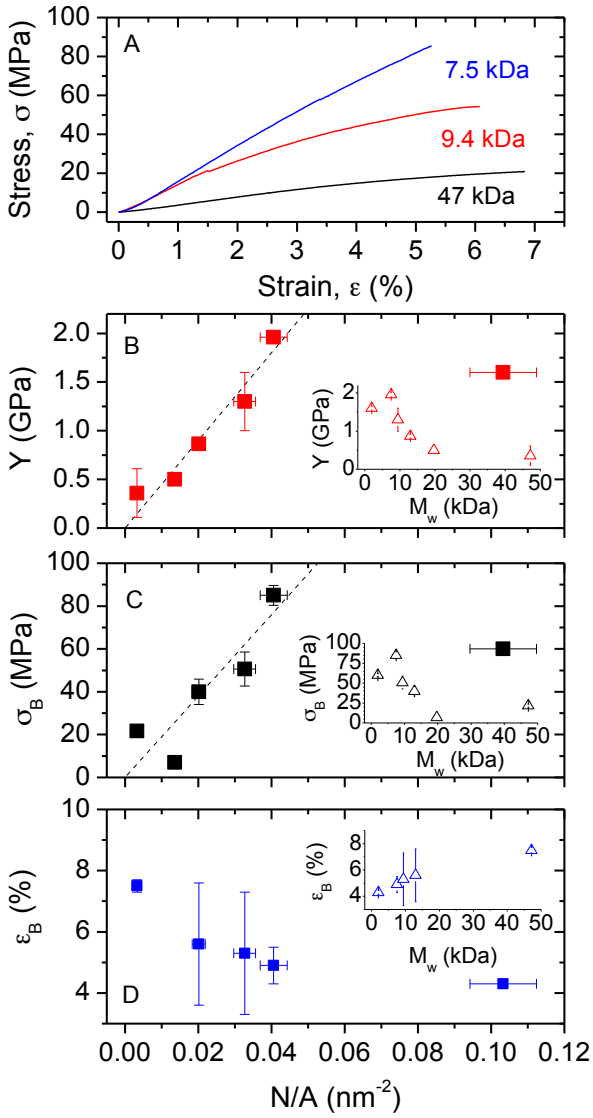

Figure 2.4: A) Representative stress strain curves for some of the Buckypapers studied in this work. B), C) and D) Young's modulus, strength, and strain at break for the Buckypapers plotted as a function of grafted chain density, N/A, respectively. Insets: Mechanical parameters plotted as a function of molecular weight.

This implies that the interactions between neighboring chains must be limited to van der Waals interactions. That all of the composites show greater modulus and tensile strength than unfunctionalized buckypapers provides compelling evidence that the inter-chain van der Waals interactions are the dominant interaction, rather than π-stacking amongst SWNTs.

In fact, that better results are obtained for lower molecular weights suggests that the grafting density is the primary variable. The fact that adjacent chains interpenetrate (k=0.75), coupled with equations 2-5, show that graft density increases as the molecular weight is reduced as: $N/A \propto M_w^{-2\nu}$. This implies that better mechanical properties are associated with higher graft density. Shown in Figure 2.4 B and C are the modulus and strength plotted versus *N/A*. Here we see both mechanical parameters increase linearly with graft density up to the point where the molecular weight is reduced to 7.5 kDa before falling off. The linearity of modulus and strength implies that the inter-tube stress transfer and inter-tube shear strength respectively are both controlled by the graft density. In addition, this data suggests all chains contribute equally to these parameters, irrespective of size. The fact that mechanical properties fall off for molecular weights below a threshold shows that a minimum chain length is required to give the interchain van der Waals interactions required to provide intertube stress transfer and interfacial strength. We can understand these systems crudely by treating the Buckypaper as a polymer-nanotube composite. Then, the fact that the strength is

controlled by interfacial properties suggests the nanotube aspect ratio to be below the critical length.[7,40] Under these circumstances, the strength is given by[40]

$$\sigma_B = \left[\tau \frac{l}{D} - \sigma_P\right] V_f + \sigma_P \quad (6)$$

where τ is the interfacial shear strength, l and D are the nanotube length and diameter respectively, V_f is the nanotube volume fraction and σ_P is the strength of the polymer matrix. Making the approximation that we can neglect the strength of the matrix, we get $\sigma_B = V_f \tau l / D$. We can write the interfacial strength as the product of the grafted chain density and the contribution per chain, τ_C:

$$\sigma_B = \frac{l}{D} V_f \tau_C \frac{N}{A} \quad (7)$$

By fitting the data in Figure 2.4C and approximating l~1000 nm, D~1 nm and taking V_f~0.3, [41] we find τ_C~6 pN per chain. This is of the correct order although perhaps somewhat small as Blighe *et al.*[36] found the average breaking force per junction in unfunctionalised nanotube Buckypaper to be ~110 pN/junction. However, we note that it would be unwise to extrapolate these results to gain insights into polymer-nanotube composites. Entanglements between functional groups and the matrix may behave in a manner considerably different to those between functional groups on adjacent nanotubes. Specifically, for interactions between functional groups and polymer matrices, the chemical structure of the matrix[42] as well as the molecular weight[43] of the functional group is very important.

It is worth noting that the strain at break falls with graft density (Figure 2.4D). However, it is probably more useful to think about strain at break as a function of molecular weight (Figure 2.4D inset). Here we see a gradual increase in strain at break with increasing molecular weight, reaching ~8% for the 47 kDa sample. This is probably a manifestation of the fact that the longer the chains are, the further adjacent nanotubes can move relative to each other before failure.

2.3. Conclusion

In this work we have measured the dependence of both graft density and solubility on the molecular weight of polystyrene chains grafted onto single walled nanotubes. We find the relationship between graft density and molecular weight to be consistent with the idea that the chains remain in a random walk configuration after attachment to the nanotube. The area of nanotube surface per chain is close to the square of the chain size, confirming that the chain packing is governed by steric hindrance. Once the footprint and extension of the grafted chains is known, we can estimate the relative size of the steric potential barrier preventing inter-tube aggregation. We find the dispersed concentration to scale well with the size of this barrier. We have prepared and mechanically characterized Buckypapers from functionalized nanotubes. We find the strength and modulus to scale linearly with the grafted chain density. This suggests that each chain contributes ~6 pN to the inter-tube shear strength.

These results imply that covalent attachment of polymer chains could dramatically increase the stiffness and strength of structures such as nanotube

fibers[44] or indeed Buckypaper made from graphene[45] or other two-dimensional materials. [46] However, correct choice of molecular weight will be crucial. In addition, it suggests that optimization of the molecular weight of grafted polymers will be important for the improvement of the mechanical properties of polymer-nanotube composites.

2.4. Experimental

2.4.1. General Experimental

***Materials**:* Styrene (Aldrich 98%) was passed through a column of basic alumina prior to use to remove inhibitor. Me_6TREN,[47] 4-TMS-alkynyl aniline,[26] and THPTA,[48] were synthesized according to established literature procedures. HiPco process single-walled carbon nanotubes, with a diameter range of 0.8-1.2 nm (avg. 1.1 nm) and length of ca. 1 μm, were purchased from Carbon Nanotechnologies Inc. (Houston, TX, purified grade, lot # P0347) and used as received. All other reagents were purchased from commercial suppliers and used as received.

Equipment: Laser Raman spectroscopy was performed on Renishaw inVia Raman spectrometer @ 514 and 785nm. NMR spectroscopy was performed on either a Bruker AV-200, or a Bruker AV-III 600 instrument in $CDCl_3$. Thermogravimetric analysis (TGA) was performed using a NETZSCG STA 409 PC instrument. All TGA was performed in an argon atmosphere. Molecular weights were estimated using gel permeation chromatography (GPC), on a Waters 2695 Separations Module, using Waters 2414 refractive index, and Waters 2996 photodiode array detectors. Separation was accomplished using three Polymer

Labs PLgel individual pore size columns, with polystyrene standards and THF as an eluent at a flow rate of 1.0 mL/min. Bath ultrasonication was performed in a Branson 2510 ultrasonicator bath.

UV-Vis Measurements. Concentrations of the soluble polymer-functionalized SWNTs were calculated by taking an air-dried sample with ~10 mg nanotube content and stirring in 10 mL THF overnight. The suspension was diluted to 40 mL and then bath ultrasonicated for 40 min in a polypropylene centrifuge tube. From this suspension, 8 mL was pipetted off and placed into a smaller centrifuge tube and centrifuged for 2 h at 2,487 g, after which 3 aliquots of dark brown supernatant were pipetted off with care to avoid disturbing the sediment. The aliquots were diluted with THF to an appropriate concentration to allow UV/vis absorption measurement. The specific extinction coefficient at 500 nm (0.0103 L mg-1 cm-1) was used to calculate the concentration with respect to the SWNTs.

2.4.2. Synthesis

General Synthesis. Polymerization of ω-bromopolystyrene (PS-Br) via ARGET-ATRP,[24] synthesis of ω-azidopolystyrene,[21] synthesis of p-TMS-alkynylaniline (**1**),[26] and preparation of 4-alkynylphenyl SWNTs (af-SWNTs)[27] were performed as per established literature procedures. Full experimental details follow:

p-TMS-alkynylaniline (2.1). A flask was charged with 4-iodoaniline (25.0 g, 0.114 mol), TMS-acetylene (25 mL, 0.175 mol), and triethylamine (150 mL).

The solution was deoxygenated with bubbling anhydrous N_2 gas. CuI (600 mg, 3 mmol) and tetrakis(triphenylphosphine) palladium(0) (800 mg, 0.75 mmol) were added. The mixture was stirred for 24 hours, the solids filtered and washed with ether. The organic phase was washed with 2M NH_4Cl (3 x 100 mL), NaCl brine (2 x 100 mL) and dried over $MgSO_4$. Dried under vacuum to yield light brown solid. Yield: 99%. ^{1}H NMR (600 MHz, $CDCl_3$): δ = 0.26 (s, 9H), 3.81 (br s, 2H), 6.60 (m, 2H) 7.29 (m, 2H).

TMS-alkyne functionalized SWNTs (af-SWNTs). In a 500 mL round bottom flask, 220 mg pristine HiPco SWNTs and 200 mL DMF were bath ultrasonicated for 30 minutes. p-TMS-alkynylaniline (7.0 g, 32 mmol) was added, and the mixture sonicated an additional 5 min. The solution was placed in an oil bath at 70° C and isoamyl nitrite (7.0 mL, 52 mmol) was added. The solutions were stirred vigourously for 12h, then filtered while warm through a 200 nm nylon membrane. The filter cake was washed with 20 mL fractions of DMF until the washings were clear, then re-suspended in 250 mL DMF by sonication (10 min). The solution was again filtered. This process was repeated a second time. The resulting washed af-SWNTs were stored damp under DMF until shortly before use. However, a fraction was removed for TGA and was dried under vacuum. It should be noted that experiments performed on fully dried af-SWNTs show that they are still fully reactive once reconstituted.

2.4.3. Polymerization of Styrene

ARGET polymerization of styrene. In a typical experiment, a dry Schlenk tube was charged with 20 mL of styrene (176 mmol), 50 mL anisole, and 4.0 mL of pre-prepared CuBr/Me_6Tren solution (0.01 M in anisole - 0.04 mmol). The solution was deoxygenated for 1 hour by bubbling with anhydrous N_2 gas. Next, 2 mL of a deoxygenated solution of tin(II) 2-ethylhexanoate/Me_6Tren in anisole (0.1 M – 0.2 mmol) was added by syringe. Finally, 1.0 mL of ethyl 2-bromoisobutyrate was added to initiate the reaction, and the reaction tube was placed in a 100° C oil bath for 8 hours. Progress was monitored by gel permeation chromatography, and the reaction stopped at the desired molecular weight – in this instance, ca. 2000 g/mol. The reaction mixture was twice precipitated into methanol (ca. 1.0 L) Conversion: 21 %), GPC: M_w = 2000, PDI (M_w/M_n) = 1.04. ^{1}H NMR (600 MHz, $CDCl_3$): δ = 0.80-1.04 (br), 1.20-2.30 (br), 3.66 (br), 4.40 (br), 6.38-7.36 (br). Polystyrene samples with molecular weight of 4.2, 7.5, 9.4, 13.0, 19.7, 27.8, 47.2, 176.0 kg/mol were synthesized in an identical fashion by adjusting the quantity of ethyl 2-bromoisobutyrate (conversion: 37-65%).

Preparation of azide-terminated polystyrene (PS-N_3). PS-Br (5.00 g, 1.00 mmol) was dissolved in 50 mL dimethyl formamide (DMF). Ten equivalents (0.65g, 0.01 mol), of sodium azide (NaN_3) was added. The reaction mixture was stirred overnight at 20° C. The polymer was precipitated in water, rinsed with ca. 1L water, re-dissolved in THF, and precipitated in methanol. The white powder

was dried *in vacuo*. ^{1}H-NMR (600 MHz, $CDCl_3$): δ = 0.80-1.04 (br), 1.20-2.30 (br), 3.66 (br), 3.95 (br), 6.30-7.36 (br).

2.4.4. Polystrene/SWNT Coupling

General procedure for the coupling of PS-N_3 to the af-SWNTs by azide/alkyne, Huisgen cycloaddition,[21,27,49] In a typical experiment, 50 mg af-SWNTs were sonicated in 60 mL anhydrous dimethylformamide using a bath sonicator for 30 min at 0°C, in a 100 mL flask. 100 uL 1M tetrabutylammonium fluoride (in THF) was added and the mixture was stirred 5 min at 0°C, then allowed to warm to room temperature and stirred one hour. During this time the mixture was deoxygenated using bubbling anhydrous N_2 gas. 25 mg THPTA, 50 mg $Cu(MeCN)_4PF_6$, 10 mg CuI, 500 uL 2,6-lutidine, and between 0.1 and 0.2 mmol of polystyrene were added. The mixture was stirred 48 hours at room temperature, then filtered through a 200 nm PTFE membrane and rinsed sequentially with 250 mL of tetrahydrofuran (three times), methanol, ammonia, water and again with THF. The filter cake was dried under vacuum overnight. The product's solubility was measured in THF. Thermogravimetric analysis was also performed.

2.4.5. SWNT Film Preparation and Characterization.

Nanotube films were prepared by filtering the PS-SWNT solutions through 200 nm Sartorius PTFE porous membranes using a glass-fritted vacuum filtration apparatus. The resulting films were washed with a sequence of 100 mL aliquots of solvent (THF, methanol, aqueous ammonium hydroxide, methanol, and finally THF). The films were then dried in a vacuum oven at ~ 1 torr and 40°C for 12 hours. The filter membranes were peeled from the Buckypaper films and these films, approximately 200 μm in thickness, were then cut into strips of dimensions 2.25 mm wide and 18 mm long using a die cutter. Mechanical testing was performed using a Zwick Roell tensile tester with 100 N load cell at a strain rate of 5 mm/min. Typically, five strips were tested per sample and the results averaged.

2.5. References

(1) Avouris, P. *Acc. Chem. Res.* **2002**, *35*, 1026–1034.
(2) Baughman, R. H.; Zakhidov, A. A.; de Heer, W. A. *Science* **2002**, *297*, 787–792.
(3) Endo, M.; Strano, M.; Ajayan, P. In *Topics in Applied Physics*; Springer Berlin Heidelberg, 2008; Vol. 111, pp. 13–62.
(4) Iijima, S. *Nature* **1991**, *354*, 56–58.
(5) Iijima, S.; Ichihashi, T. *Nature* **1993**, *363*, 603–605.
(6) Coleman, J. N.; Khan, U.; Gun'ko, Y. K. *Adv. Mater.* **2006**, *18*, 689–706.
(7) Coleman, J.; Khan, U.; Blau, W.; Gun ko, Y. *Carbon* **2006**, *44*, 1624–1652.
(8) Collins, P. G.; Avouris, P. *Scientific American* **2000**, *283*, 62–69.
(9) Li, C.; Thostenson, E. T.; Chou, T.-W. *Compos. Sci. Technol.* **2008**, *68*, 1227–1249.
(10) Baughman, R. H.; Cui, C.; Zakhidov, A. A.; Iqbal, Z.; Barisci, J. N.; Spinks, G. M.; Wallace, G. G.; Mazzoldi, A.; De Rossi, D.; Rinzler, A. G.; Jaschinski, O.; Roth, S.; Kertesz, M. *Science* **1999**, *284*, 1340–1344.
(11) Bianco, A.; Kostarelos, K.; Partidos, C. D.; Prato, M. *Chem. Commun.* **2005**, 571–577.
(12) Chen, Z.; Zhang, X.; Yang, R.; Zhu, Z.; Chen, Y.; Tan, W. *Nanoscale* **2011**, *3*, 1949–1956.
(13) Tasis, D.; Tagmatarchis, N.; Bianco, A.; Prato, M. *Chem. Rev.* **2006**, *106*, 1105–1136.
(14) Banerjee, S.; Hemraj-Benny, T.; Wong, S. S. *Adv. Mater.* **2005**, *17*, 17–29.
(15) Dyke, C. A.; Tour, J. M. *J. Phys. Chem. A* **2004**, *108*, 11151–11159.
(16) Holzinger, M.; Vostrowsky, O.; Hirsch, A.; Hennrich, F.; Kappes, M.; Weiss, R.; Jellen, F. *Angew. Chem. Int. Ed.* **2001**, *40*, 4002–4005.
(17) Hirsch, A. *Angew. Chem. Int. Ed.* **2002**, *41*, 1853–1859.
(18) Bahun, G. J.; Cheng, F.; Homenick, C. M.; Lawson, G.; Zhu, J.; Adronov, A. *Chemistry of Carbon Nanotubes*; American Scientific Publishers: Stevenson Ranch, 2008; Vol. 2.
(19) Liu, P. *Eur. Polym. J.* **2005**, *41*, 2693–2703.
(20) Kolb, H. C.; Finn, M. G.; Sharpless, K. B. *Angew. Chem. Int. Ed.* **2001**, *40*, 2004–2021.
(21) Li, H.; Cheng, F.; Duft, A. M.; Adronov, A. *J. Am. Chem. Soc.* **2005**, *127*, 14518–14524.
(22) Rana, S.; Cho, J.-W. *Nanoscale* **2010**, *2*, 2550.
(23) Homenick, C. M.; Sivasubramaniam, U.; Adronov, A. *Polym. Int.* **2008**, *57*, 1007–1011.
(24) Jakubowski, W.; Min, K.; Matyjaszewski, K. *Macromolecules* **2006**, *39*, 39–45.
(25) Campidelli, S. *Curr. Org. Chem.* **2011**, *15*, 1151–1159.

(26) Hwang, J. J.; Tour, J. M. *Tetrahedron* **2002**, *58*, 10387–10405.
(27) Palacin, T.; Khanh, H.; Jousselme, B.; Jegou, P.; Filoramo, A.; Ehli, C.; Guldi, D.; Campidelli, S. *J. Am. Chem. Soc.* **2009**, *131*, 15394–15402.
(28) Tan, W. T.; Radhi, M. M.; Rahman, M. Z. A.; Kassim, A. B. *J. of Applied Sciences* **2010**, *10*, 139–144.
(29) Jones, R. A. L. *Soft Condensed Matter*; Oxford University Press: Oxford, 2002.
(30) Rubinstein, M.; Colby, R. H. *Polymer Physics*; 1st ed.; Oxford University Press: Oxford, 2003.
(31) Brandrup, J.; Immergut, E. H.; Grulke, E. A.; Abe, A.; Bloch, D. R. *Polymer Handbook, 2005*; New York, 2005.
(32) Sun, Q.; Faller, R. *J. Phys. Chem. B* **2005**, *109*, 15714–15723.
(33) Tsimpris, C. W.; Suryanarayanan, B.; Mayhan, K. G. *J. Polym. Sci. A-2 Polym. Phys.* **1972**, *10*, 1837–1839.
(34) Israelachvili, J. N. *Intermolecular and Surface Forces: With Applications to Colloidal and Biological Systems (Colloid Science)*; 2nd ed.; Academic Press: London, 1992.
(35) Smith, R. J.; Lotya, M.; Coleman, J. N. *New J. Phys.* **2010**, *12*, 125008.
(36) Blighe, F. M.; Lyons, P. E.; De, S.; Blau, W. J.; Coleman, J. N. *Carbon* **2008**, *46*, 41–47.
(37) Coleman, J. N.; Blau, W. J.; Dalton, A. B.; Munoz, E.; Collins, S.; Kim, B. G.; Razal, J.; Selvidge, M.; Vieiro, G.; Baughman, R. H. *Appl. Phys. Lett.* **2003**, *82*, 1682–1684.
(38) Dobkowski, Z. *Rheol. Acta* **1995**, *34*, 578–585.
(39) Tead, S. F.; Kramer, E. J. *Macromolecules* **1988**, *21*, 1513–1517.
(40) Rosenthal, J. *Polym. Compos.* **1992**, *13*, 462–466.
(41) Lyons, P. E.; De, S.; Blighe, F.; Nicolosi, V.; Pereira, L. F. C.; Ferreira, M. S.; Coleman, J. N. *J. Appl. Phys.* **2008**, *104*, –.
(42) Akcora, P.; Kumar, S. K.; García Sakai, V.; Li, Y.; Benicewicz, B. C.; Schadler, L. S. *Macromolecules* **2010**, *43*, 8275–8281.
(43) Maillard, D.; Kumar, S. K.; Rungta, A.; Benicewicz, B. C.; Prud'homme, R. E. *Nano Lett.* **2011**, *11*, 4569–4573.
(44) Koziol, K.; Vilatela, J.; Moisala, A.; Motta, M.; Cunniff, P.; Sennett, M.; Windle, A. *Science* **2007**, *318*, 1892–1895.
(45) Dikin, D. A.; Stankovich, S.; Zimney, E. J.; Piner, R. D.; Dommett, G. H. B.; Evmenenko, G.; Nguyen, S. T.; Ruoff, R. S. *Nature* **2007**, *448*, 457–460.
(46) Coleman, J. N.; Lotya, M.; O'Neill, A.; Bergin, S. D.; King, P. J.; Khan, U.; Young, K.; Gaucher, A.; De, S.; Smith, R. J.; Shvets, I. V.; Arora, S. K.; Stanton, G.; Kim, H.-Y.; Lee, K.; Kim, G. T.; Duesberg, G. S.; Hallam, T.; Boland, J. J.; Wang, J. J.; Donegan, J. F.; Grunlan, J. C.; Moriarty, G.; Shmeliov, A.; Nicholls, R. J.; Perkins, J. M.; Grieveson, E. M.; Theuwissen, K.; McComb, D. W.; Nellist, P. D.; Nicolosi, V. *Science* **2011**, *331*, 568–571.

(47) Xia, J.; Gaynor, S.; Matyjaszewski, K. *Macromolecules* **1998**.
(48) Hong, V.; Presolski, S. I.; Ma, C.; Finn, M. G. *Angew. Chem. Int. Ed.* **2009**, *48*, 9879–9883.
(49) Campidelli, S.; Ballesteros, B.; Filoramo, A.; Díaz, D.; La Torre, de, G.; Torres, T.; Rahman, G.; Ehli, C.; Kiessling, D.; Werner, F.; Sgobba, V.; Guldi, D.; Cioffi, C.; Prato, M.; Bourgoin, J.-P. *J. Am. Chem. Soc.* **2008**, *130*, 11503–11509.

Chapter 3: Functionalization of Single-Walled Carbon Nanotubes via the Piers-Rubinsztajn Reaction

Ryan C. Chadwick, John B. Grande, Michael A. Brook, Alex Adronov*

Department of Chemistry and Chemical Biology,
McMaster University,
1280 Main St. W.,
Hamilton, Ontario, L8S 4M1 (Canada)

The work detailed in this chapter was carried out in collaboration with Dr. John Grande and Professor Michael Brook (Department of Chemistry, McMaster University). Ryan Chadwick performed the synthesis and characterization of all small molecules, polymers, and the functionalized carbon nanotubes. Ryan Chadwick and John Grande shared the planning for the study.

Graphical Abstract:

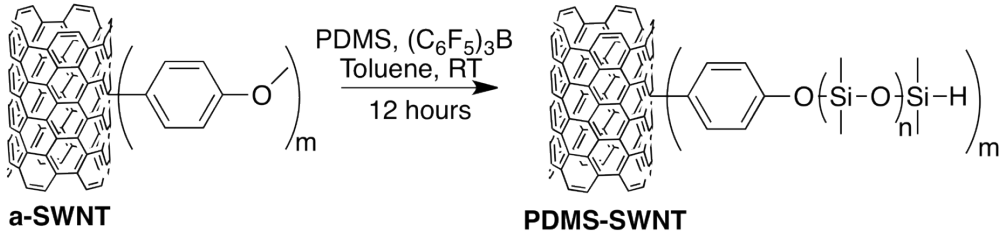

Abstract

We describe the modification of as-produced, HiPCO, single-walled carbon nanotubes with polydimethylsiloxane (PDMS). The single-walled carbon nanotubes were first functionalized with p-anisidine via diazonium radical chemistry, followed by reaction of the methoxy functionality with hydride-terminated PDMS using the Piers-Rubinsztajn reaction. PDMS samples with a range of molecular weights, from 1-28 kDa, were utilized. The reaction was rapid and efficient, resulting in highly-functionalized and well-dispersed carbon nanotubes. The resulting materials were found to be soluble in a wide range of organic solvents and to be suitable for suspension within PDMS elastomers produced by Piers-Rubinsztajn hydrosilylation.

3.1. Introduction

The silane and siloxane functionalization of carbon nanotubes has been widely investigated, and a number of silylation strategies have been employed.[1] These include the extensive use of halo- or alkoxysilanes to react with surface hydroxyls,[2-12] the use of polysilazanes,[13] direct hydrosilylation of the carbon nanotube surface,[14] silylesterification,[15] photochemical silylation,[16] and the formation of supramolecular complexes.[17] The interest in these conjugate materials stems from several potential applications including heat or charge dissipative elastomers,[2,18] bio-compatible and flexible electrodes or sensors,[19,20] Li-ion batteries,[21] robust elastomers,[22] capacitive energy harvesting,[23] artificial muscles,[24] skin-like stretch sensors,[25-27] and other electronics.[28]

However, despite this extensive research into the use of small-molecule silanes to decorate carbon nanotube side-walls, the functionalization of carbon nanotubes or graphene with polymeric silicones, such as PDMS, is still remarkably rare.[5,29] Likewise, there is little precedent for covalently anchoring single-walled carbon nanotube (SWNT) composites in a PDMS host material, despite having been shown to be an effective technique in this and similar elastomers.[30,31] The high solubility of silicone chains within a wide variety of common organic solvents makes them ideal solubilizing agents for insoluble materials, such as SWNTs, where they can operate as steric stabilizers. However, virtually all reports of PDMS-SWNT composites use slow-to-cure commercial silicone kits, leading to a high degree of nanotube flocculation or phase-

separation, processes that occur faster than the silicone chemistry.[2] This lack of activity in synthesizing PDMS-SWNT complexes is particularly surprising considering the interest in silicone composites for flexible electronics, such as artificial skin and other touch-based sensors,[32-34] where elastomer robustness is a key factor, but may have to do with the absence of facile processes for silicone-SWNT grafting.

The recently-developed Piers-Rubinsztajn (PR) reaction[35-37] is an efficient $(C_6F_5)_3B$-catalyzed hydrosilylative coupling between an alkoxy group (generally methoxy, ethoxy, and propoxy) and a hydrosilane (Si-H). This reaction has been used for the production of well-defined macromolecules, silicone elastomers, and silicone foams.[38-42] It is compatible with alkenes and alkyl halides, potentially enabling the sequential use of other common silicone chemistry.[43] However, to our knowledge, the Piers-Rubinsztajn reaction has not yet been explored for the modification of surfaces or graphitic materials. Here, we demonstrate the viability of the Piers-Rubinsztajn reaction for the functionalization of single-walled carbon nanotubes (SWNTs) by producing a series of PDMS-SWNT composites, and develop an easily dispersible silicone-nanotube composite that can participate in hydrosilylative cross-linking of bulk PDMS.

3.2. Results and Discussion

In order to test the efficiency of the Piers-Rubinsztajn reaction on the surface of nanotubes, anisole-grafted SWNTs (a-SWNTs) were synthesized via the Tour reaction, using *p*-anisidine and isoamyl nitrite (Scheme 3.1).[44,45] After removal of excess *p*-anisidine through extensive rinsing with DMF and toluene, the resulting a-SWNTs were re-dispersed in toluene and then treated with an excess of α,ω-dihydride terminated PDMS (PDMS-H_2) in the presence of $(C_6F_5)_3B$ as catalyst (Scheme 3.1). In each case, the addition of catalyst was followed by a short (ca. 15 s) induction period, and then by rapid gas evolution. In all, a series of 5 molecular weights of PDMS-H_2, ranging from 134 g/mol (tetramethyldisiloxane, TMDS) to 28 kDa were employed (Table 3.1). A control experiment was also performed, in which pristine carbon nanotubes were reacted directly with 1.1 kDa PDMS-H_2 at room temperature for 48 h. In general, we found the Piers-Rubinsztajn reaction was very effective for the functionalization of carbon nanotubes. If sufficiently thorough mixing was achieved, such as via light "milling" with glass beads, 2 to 12 h reaction times for each step of the reaction were sufficient to yield highly soluble materials (Table 3.1).

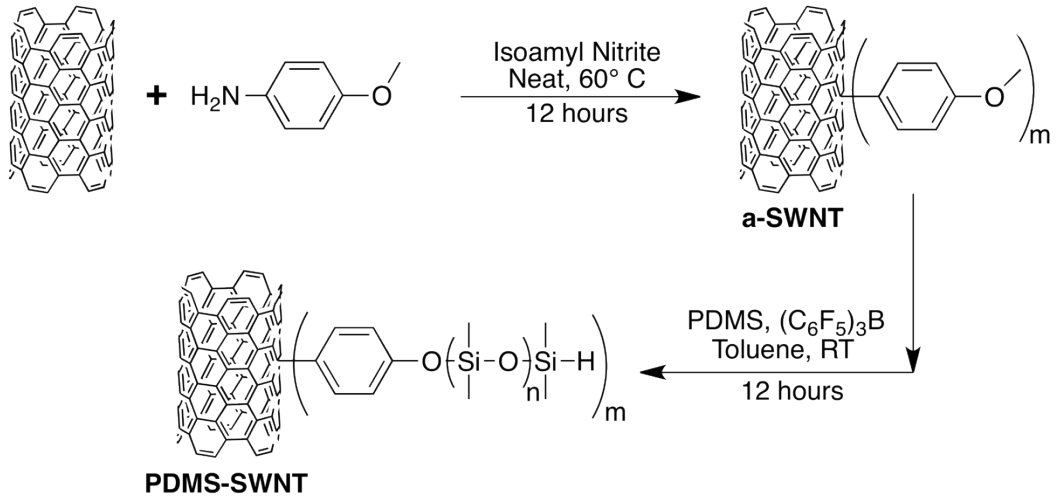

Scheme 3.1: Functionalization of single-walled carbon nanotubes via Tour reaction, followed by Piers-Rubinsztajn reaction.

Table 3.1: Solubility and graft weights for silicone carbon nanotube composites.

Graft	PDMS M_n (g mol^{-1})	PDMS Average DP	Solubility in THF (mg L^{-1})	Solubility in Toluene (mg L^{-1})	Total Mass Loss (%, TGA)	Mass PDMS (%)
Anisole	*108	N/A	0	0	17.4	0
TMDS	134	2	358 ± 20	8 ± 1	25.1	8.7
PDMS-1	1.1 k	14	335 ± 20	36 ± 2	31.5	14.1
PDMS-6	6.0 k	80	588 ± 30	7 ± 1	27.5	10.1
PDMS-17	17 k	230	730 ± 40	0	29.2	11.8
PDMS-28	28 k	380	540 ± 40	0	27.9	10.4
Control	1.1 k	14	< 20	0	6.7	6.7

* Molecular weight of Anisole. Error values represent relative standard deviation, calculated from a series of duplicate measurements.

Dispersibility in THF and toluene were measured for all samples using a modified literature method.[46] The materials functionalized using the Piers-Rubinsztajn reaction showed very high solubilities in THF (typically > 350 mg L^{-1}). In contrast to the SWNTs functionalized via the Piers-Rubinsztajn reaction, the control samples exhibited minimal solubility (< 20 mg/L, Table 1), consistent with the relatively low degrees of functionalization for the direct reaction, as observed in the literature.[14] Further characterization of the functionalized SWNTs was carried out using Raman spectroscopy (Figure 3.1). The introduction of anisole functionalities on the nanotube surface (a-SWNTs) was confirmed via the characteristic increase in the D-band (1300 cm^{-1}) relative to the G-Band (1590 cm^{-1}) when the sample was excited at either 514 or 785 nm.[47] The control sample exhibited no change in Raman spectrum after a reaction time of 48 hours.

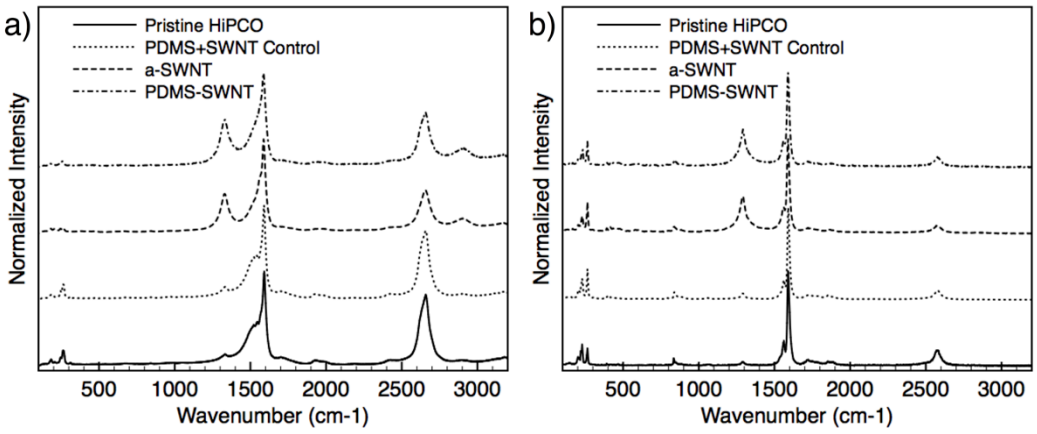

Figure 3.1: Raman spectra of functionalized HiPCO SWNTs with excitation at a) 514 nm, b) 785 nm.

The functionalized SWNTs were also characterized by thermogravimetric analysis (TGA). The samples were heated to 500 °C in an argon atmosphere and held until mass loss was complete (complete data provided in Appendix 2). Both anisole and PDMS are entirely lost at this temperature, allowing the calculation of their total graft mass. By subtracting the mass fraction of anisole, calculated from the TGA of a-SWNT samples, from the overall mass loss of the PDMS-SWNT samples, we were also able to determine the grafted mass fraction of PDMS (Table 3.1). Interestingly, the TGA curves all demonstrated approximately the same degree of mass-loss (except the TMDS-SWNTs). This was initially unexpected, as our previous studies suggest that graft masses generally increase with molecular weight to a maximum point, beyond which they gradually decline.[46] However, the commercial samples of PDMS used in this study are all produced by acid-equilibration polymerization of cyclic siloxanes, and thus exhibit broad polydispersity. We speculate that the presence of high and low molecular weight PDMS during the grafting reaction allows smaller silicones to fill in the gaps between higher molecular weight grafted chains, leading to an approximate equalization of the total grafted mass regardless of the average molecular weight of each sample, especially considering the large excess of PDMS used in these reactions. It should be noted that the bifunctional PDMS that we employed can potentially allow for intermolecular reactions and intramolecular looping of grafted chains, which prevents calculation of a precise graft density at each molecular weight. Despite the fact that the total grafted

silicone mass does not change with molecular weight, we can conclude from solubility figures that, to a point, grafting higher average molecular weight silicone chains results in greater stability of PDMS-SWNT dispersions.

The control sample exhibited a mass-loss of 6.7% after extensive washing to remove all physically-bound silicone chains. Although this suggests that silicones bind to the nanotube surface, we speculate that this results from non-covalent interactions between silicones and the SWNTs[48] Raman analysis of this control sample shows no increase in the disorder (D) band, which would be indicative of covalent functionalization. Additionally, UV-Vis-NIR spectra taken of the control and covalently modified dispersions in THF show fine structure reminiscent of un-modified suspended SWNTs, rather than the featureless curves of covalently modified products (see Appendix 2). Neither experiment is definitive, but both clearly demonstrate the control samples are lightly decorated, if at all.

The PDMS graft mass-fractions are lower than we have observed for some other systems, such as the Huisgen cycloaddition "click"-functionalization of polystyrene,[46,49] however, the solubilities are substantially greater. It is likely that the high solubility of the PDMS-SWNT structures results from the intrinsically high solubility of silicones in moderately polar organic solvents.

We were somewhat surprised by the vast disparity of solubilities of the SWNT complexes between THF and toluene, both of which are good solvents for PDMS. To further explore these effects, TMDS-SWNTs were suspended in a

variety of solvents, and were found to exhibit good solubility in a number of them (Table 3.2).

Table 3.2: Solubility of TMDS-SWNT in a variety of solvents.

Solvent	Solubility (mg/L)
THF	358
DMF	52
2-methyl-2-butanol	158
Toluene	8
Benzene	0
Acetone	0
1,2-Dichloroethane	273

It is worth noting that Rubinsztajn and colleagues have determined that $(C_6F_5)_3B$ catalyzes the oligomerization of TMDS.[50] Accordingly, it is possible that some oligomerization occurs on the surface of the TMDS-SWNT samples, producing longer than expected oligomeric chains, which explains the surprisingly high solubility of the TDMS functionalized material. However, the TMDS graft weight-fraction is much lower than that of the 1.1 kDa PDMS graft. This suggests that, regardless of any oligomerization, the species present on the surface of the carbon nanotube has a molecular weight of less than 1.1 kDa. This is consistent with the observation that this process produces only small oligomers.

Lastly, we attempted to assess the dispersion of the PDMS-SWNTs in PDMS elastomers. As these SWNT complexes form stable and very high concentration dispersions in a number of solvents, we expected them to form homogenous suspensions in silicone rubber. Our initial attempts focused on the

use of commercial silicone rubber kits, including Gelest OE41™ (unfilled) and Dow Corning Sylgard™ 184 (silica-filled). In each case, the 2-part silicone kit was mixed with half its volume of a nearly saturated solution (ca. 600 mg/L) of the 17 kDa PDMS-SWNT complex in THF. The resulting suspensions remained stable prior to cross-linking, however, some phase-separation and precipitation occurred during the cross-linking reaction (sample iii in Figures 3.2a and b). In addition, the maximum concentration of SWNTs that could be incorporated was relatively low (ca. 0.030%). To increase the concentration would require the use of additional saturated PDMS-SWNT suspension in THF; this was precluded by the platinum-cure rubber kits, which cured poorly if diluted in large amounts of THF.

In order to both accelerate silicone crosslinking and increase the SWNT loading, we again used the Piers-Rubinsztajn (PR) reaction, following previously published protocols.[38,39] PR-based crosslinking enables the rapid formation of both silicone rubbers and silicone foams. In general, silicon rubbers are produced when long chain PDMS dihydride (PDMS-H_2) fluids are crosslinked using a small amount of TEOS;[39] foams are produced when a shorter chain PDMS-H_2 and a correspondingly greater amount of TEOS is employed.[40] In the latter case, the large amount of ethane produced by the Piers-Rubinsztajn reaction acts as a blowing agent. Using these methods we were able to produce both rubbers and foams containing carbon nanotubes at loading levels of approximately 1 wt% (Figure 3.2a and b). In each case, the desired weight fraction of a-SWNTs was

rapidly shear-mixed with 2 g of the appropriate dihydride silicone fluid (PDMS-H_2). After initial mixing, TEOS and 2 mL of hexanes were added, and the mixture was aggressively mixed a second time before an aliquot of $(C_6F_5)_3B$ was added. The mixture was quickly poured (or extruded via syringe) into a PTFE mold. The addition of a small amount of heat initiated the crosslinking reaction (simply cupping the reaction flask in one's hand is sufficient). The foams formed within seconds, while the viscosity of the bulk rubber mixture required curing at 50 °C overnight.

A simple control experiment confirmed the ability of a-SWNTs to participate in the cross-linking reaction. If a-SWNTs were blended with a small amount of PDMS-H_2 in the absence of TEOS, the reaction still proceeded upon addition of catalyst (as evidenced by gas evolution), but the resulting materials were brittle and insoluble after rinsing away excess PDMS.

We observed that incorporation of carbon nanotubes decreased the rate of cross-linking reactions, requiring higher catalyst concentrations to achieve similar reaction times as with rubbers that did not contain nanotubes. This seems to stem from an increase in viscosity upon addition of nanotubes, which decreases mixing efficiency. The more viscous nanotube/PDMS-H_2 mixtures cured more slowly overall and rapid mixing was required to prevent inhomogeneous curing.

As the ability to produce high quality composites appears to be limited by the volume of the nanotubes within the solution and its viscosity, SWNT

loadings above 1% led to unsatisfactory results. At nanotube loadings of 2-5%, the mixtures were unacceptably dry and uniform catalyst mixing could not be achieved, resulting in inconsistent cross-linking. Homogeneous nanotube dispersion and uniform crosslinking could only be observed at loadings of 1% or lower, using the PR reaction protocol.

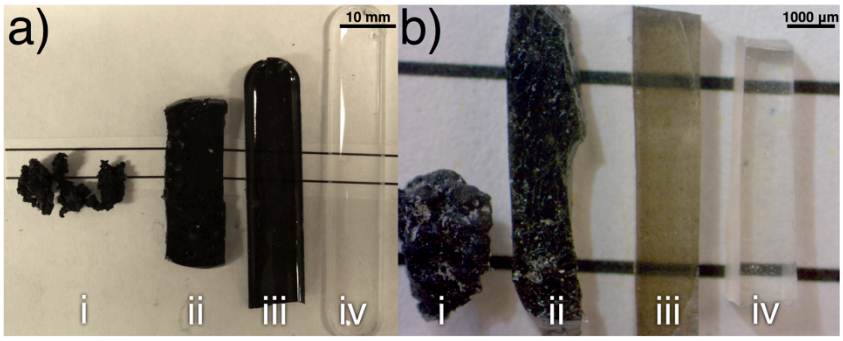

Figure 3.2: Photographs of SWNT/PDMS composites at a) 1× magnification (3 mm thick slice), and b) 10× magnification (1 mm thick slice). The different samples in each photograph correspond to the following: i) 1% SWNT foam (PR crosslinking); ii) 1% SWNT elastomer (PR crosslinking), iii) 0.030% SWNT elastomer (Dow Sylgard 184); iv) Pristine PDMS elastomer (Dow Sylgard 184).

3.3. Conclusion

In conclusion, the PR reaction allows for rapid and efficient functionalization of the carbon nanotube surface with silicones. The PDMS-functionalized materials have very high solubilities in a variety of polar organic solvents. Moreover, PR chemistry leads to materials that are potentially useful for

the incorporation of carbon nanotubes into bulk PDMS elastomers, including rubbers and foams. It is compatible with functional groups commonly present in commercial silicone elastomer kits, and alternative silicone cure chemistries. These materials allow for the rapid production of SWNT-PDMS composites and provide a convenient method to anchor them within the host material.

3.4. Experimental

3.4.1. General Experimental

Materials All experiments were performed on unpurified, as-produced HiPCO SWNTs, NanoIntegris Batch Number R1-901. SWNT masses were based on provided Wet SWNT content of 9.9%. Hydride terminated PDMS samples (PDMS-H_2) were all purchased from Gelest. PTFE filtration membranes (200 nm pore size) were purchased from Sartorius Stedim Biotech. All other reagents were purchased from fine chemical suppliers and used as received. Toluene was dried in a solvent purification system over alumina.

Equipment Laser Raman spectroscopy was performed on a Renishaw inVia Raman spectrometer at 514 and 785 nm. Thermogravimetric analysis (TGA) was performed using a TA-Q50 instrument and were performed under an argon atmosphere. Samples were held at 100 °C for 15 minutes, ramped to 500 °C at a rate of 20 °C/min, then held at 500 °C for 45 minutes. Ultrasonication was performed using a Branson 2510 ultrasonicator bath. UV-Vis-IR spectroscopy was performed on a Cary 5000 instrument.

Procedure for Nanotube Solubility Measurements 10 mg samples of functionalized SWNTs were sonicated in 10 mL of the desired solvent for 1 h. The suspensions were centrifuged for 1 h at 5000 g, then the supernatant was transferred via pipette, taking care to avoid disturbing any SWNT pellet present. The supernatant was then filtered through cotton and, if necessary, diluted to an appropriate concentration to allow UV-Vis spectroscopy. The specific extinction coefficient at 500 nm (0.0103 L mg^{-1} cm^{-1})[49] was used to calculate the SWNT concentration.

3.4.2. Synthesis

Procedure for the production of anisole functionalized SWNTs (a-SWNT)[45] A 25 mL round bottom flask was charged with a PTFE-coated magnetic stir bar, 6-12 glass beads (6 mm diameter), 20 mg (200 mg wet) of pristine HiPCO SWNTs, and 400 mg p-anisidine. Isoamyl nitrite (800 μL) was added by pipette and the mixture was stirred for 2 h at 60°C. The mixture was then diluted with DMF and filtered through a 200 nm PTFE membrane. The filter cake was then washed with DMF until the filtrate was colorless (ca. 100 mL) followed by secondary washing with toluene (100 mL). The filter cake was re-suspended by sonication in an additional 100 mL dry toluene, and again filtered to recover the functionalized a-SWNTs.

a-SWNT samples used for TMDS/PDMS functionalization were kept wet with toluene, and used directly. Samples for TGA were re-suspended in diethyl ether, filtered, and dried at 100 °C under vacuum overnight. a-SWNTs used in

PDMS rubber formation were re-suspended in hexanes and filtered once more before use.

General procedure for the silylation of a-SWNTs with PDMS-H_2 a-SWNT (10 mg nanotube basis), 400 μL PDMS-H_2 (or TMDS), and 10 mL of dry toluene were placed in a small round bottom flask equipped with a PTFE-coated magnetic stir bar and 6-12 glass beads (6 mm diameter). The mixture was purged with inert gas (N_2 or argon), while under bath sonication. After purging, 50 μL of 0.1 M $(C_6F_5)_3B$ solution was added. The mixture was stirred for 2 (TMDS) to 12 (PDMS) hours. After the reaction, the mixture was filtered through a 200 nm PTFE membrane. The filter cake was washed with toluene (100 mL), then air-dried.

If used for solution studies, the filter cake was also rinsed with the suspending solvent. Samples for TGA were re-suspended in diethyl ether, filtered, and dried at 100°C under vacuum overnight.

Note: Longer stirring times (> 2 h) did not increase graft mass in TDMS samples.

3.4.3. Production of Composite Materials

Procedure for the production of a-SWNT foam (1% CNT loading): 20 mg (SWNT basis) a-SWNT and 2 g of 1 kDa PDMS-H_2 were aggressively mixed for 2 min at 10 000 RPM using a variable speed rotary tool (Dremel) with a 1 cm stainless-steel brush attachment. An equal volume of hexanes was added and the suspension was mixed for an additional minute. 200 μL tetraethylorthosilicate (TEOS) was added and the suspension was mixed for 30 seconds. Then, the

mixture was cooled to 10°C, and 200 μL of 0.05 M $(C_6F_5)_3B$ (in toluene) was added, mixed for 15 seconds, and poured into a PTFE-lined mold. Gentle heating via cupping in hand or heat gun initiated the foam formation. The material was allowed to cure for 1 h at room temperature, then the hexanes was evaporated at 50 °C *in vacuo.*

Procedure for the production of a-SWNT rubber (1% CNT loading): 20 mg (SWNT basis) a-SWNT and 2 g of 17 kDa PDMS-H_2 were aggressively mixed for 2 min at 10 000 RPM using a variable speed rotary tool (Dremel) with a 1 cm stainless-steel brush attachment. An equal volume of hexanes was added and the suspension was mixed for an additional minute. 25 μL of TEOS was added and the suspension was mixed for 30 seconds. Then the mixture was cooled to 10 °C, 200 μL 0.05 M $(C_6F_5)_3B$ (in toluene) was added, mixed for 15 seconds, and poured into a PTFE-lined mold. The composite was heated for 24 h at 50 °C to cure and remove hexanes.

3.5. References:

(1) Velasco-Santos, C.; Martinez-Hernandez, A. L.; Castaño, V. M. In *Carbon Nanotubes - Polymer Nanocomposites*; InTech, 2011.

(2) Vast, L.; Mekhalif, Z.; Fonseca, A.; B Nagy, J.; Delhalle, J. *Compos. Sci. Technol.* **2007**, *67*, 880–889.

(3) Vast, L.; Philippin, G.; Destrée, A.; Moreau, N.; Fonseca, A.; Nagy, J. B.; Delhalle, J.; Mekhalif, Z. *Nanotechnology* **2004**, *15*, 781–785.

(4) Chua, T. P.; Mariatti, M.; Azizan, A.; Rashid, A. A. *Compos. Sci. Technol.* **2010**, *70*, 671–677.

(5) Vast, L.; Carpentier, L.; Lallemand, F.; Colomer, J. F. *J. Mater. Sci.* **2009**, *44*, 3476–3482.

(6) Ma, P.-C.; Kim, J.-K.; Tang, B.-Z. *Carbon* **2006**, *44*, 3232–3238.

(7) Velasco-Santos, C.; Martinez-Hernandez, A. L.; Alvarez-Castillo, A.; Castaño, V. M.; Lozada-Cassou, M. *Nanotechnology* **2002**, *13*, 495–498.

(8) Vennerberg, D.; Rueger, Z.; Kessler, M. R. *Polymer* **2014**, *55*, 1854–1865.

(9) Cheng, Y. Y.; Chou, S. C.; Huang, J. H. *J. Appl. Polym. Sci.* **2011**, *124*, 1137–1143.

(10) Aviles, F.; Sierra-Chi, C. A.; Nistal, A.; May-Pat, A.; Rubio, F.; Rubio, J. *Carbon* **2013**, *57*, 520–529.

(11) Lin, T.-W.; Shen, H.-H. *Nanotechnology* **2010**, *21*, 365604.

(12) Aizawa, M.; Shaffer, M. S. P. *Chem. Phys. Lett.* **2003**, *368*, 121–124.

(13) Li, Y.; Fernandez-Recio, L.; Gerstel, P.; Srot, V. *Chem. Mater.* **2008**, *20*, 5593–5599.

(14) Lee, Y.; Jeon, K.-S.; Lim, H.; Shin, H. S.; Jin, S. M.; Byon, H. R.; Suh, Y. D.; Choi, H. C. *Small* **2009**, *5*, 1398–1402.

(15) Seffer, J. F.; Detriche, S.; B Nagy, J.; Delhalle, J.; Mekhalif, Z. *Appl. Surf. Sci. 305*, 301–308.

(16) Hemraj-Benny, T.; Stanislaus S Wong. *Chem. Mater.* **2006**, *18*, 4827–4839.

(17) Ji, Y.; Huang, Y. Y.; Tajbakhsh, A. R.; Terentjev, E. M. *Langmuir* **2009**, *25*, 12325–12331.

(18) Sim, L. C.; Ramanan, S. R.; Ismail, H.; Seetharamu, K. N.; Goh, T. J. *Thermochim. Acta* **2005**, *430*, 155–165.

(19) Kim, T. A.; Kim, H. S.; Lee, S. S.; Park, M. *Carbon* **2012**, *50*, 444–449.

(20) Schwartz, G.; Tee, B. C.-K.; Mei, J.; Appleton, A. L.; Do Hwan Kim; Wang, H.; Bao, Z. *Nat. Comm.* **2013**, *4*, 1859.

(21) Huang, Z.-D.; Zhang, B.; He, Y.-B.; Oh, S.-W.; Yu, Y.; Kim, J.-K. *J. Electrochem. Soc.* **2012**, *159*, A2024–A2028.

(22) Tour, J.; Hudson, J.; Kirshnamoorti, R.; Yurekli, K.; Mitchell, C.; William Marsh Rice University; The University Of Houston. Elastomers Reinforced with Carbon Nanotubes. US 20070259994 A1, November 8, 2007.

(23) Brochu, P.; Stoyanov, H.; Chang, R.; Niu, X.; Hu, W.; Pei, Q. *Adv. Eng. Mater.* **2013**, *4*, 1300659.
(24) Brochu, P.; Pei, Q. *Macromol. Rapid Commun.* **2010**, *31*, 10–36.
(25) Lee, C.; Jug, L.; Meng, E. *Appl. Phys. Lett.* **2013**, *102*, 183511.
(26) Lipomi, D. J.; Vosgueritchian, M.; Tee, B. C.-K.; Hellstrom, S. L.; Lee, J. A.; Fox, C. H.; Bao, Z. *Nat. Nanotechnol.* **2011**, *6*, 788–792.
(27) Cai, L.; Song, L.; Luan, P.; Zhang, Q.; Zhang, N.; Gao, Q.; Zhao, D.; Zhang, X.; Tu, M.; Yang, F.; Zhou, W.; Fan, Q.; Luo, J.; Zhou, W.; Ajayan, P. M.; Xie, S. *Sci. Rep.* **2013**, *3*, 3048.
(28) Park, S.; Vosguerichian, M.; Bao, Z. *Nanoscale* **2013**, *5*, 1727–1752.
(29) Guimont, A.; Beyou, E.; Alcouffe, P.; Martin, G.; Sonntag, P.; Cassagnau, P. *Polymer* **2013**, *54*, 4830–4837.
(30) Sainsbury, T.; Erickson, K.; Okawa, D.; Zonte, C.; Fréchet, J.; Zettl, A. *Chem. Mater.* **2010**, *22*, 2164–2171.
(31) Velasco-Santos, C.; Martínez-Hernández, A. L.; Fisher, F. T.; Ruoff, R.; Castaño, V. M. *Chem. Mater.* **2003**, *15*, 4470–4475.
(32) Tok, J. B.-H.; Bao, Z. *Sci. China: Chem.* **2012**, *55*, 718–725.
(33) Benight, S. J.; Wang, C.; Tok, J. B.-H.; Bao, Z. *Prog. Polym. Sci.* **2013**, *38*, 1961–1977.
(34) In *Lecture Notes in Nanoscale Science and Technology*; Springer International Publishing: Cham, 2013; Vol. 19, pp. 225–244.
(35) Rubinsztajn, S.; Cella, J. A. *Macromolecules* **2005**, *38*, 1061–1063.
(36) Wakabayashi, R.; Kuroda, K. *ChemPlusChem* **2013**, *78*, 764–774.
(37) Brook, M. A.; Grande, J. B.; Ganachaud, F. In *Silicon Polymers*; Muzafarov, A. M., Ed.; Springer Berlin Heidelberg, 2011; Vol. 235, pp. 161–183.
(38) Grande, J. B.; Fawcett, A. S.; McLaughlin, A. J.; Gonzaga, F.; Bender, T. P.; Brook, M. A. *Polymer* **2012**, *53*, 3135–3142.
(39) Fawcett, A. S.; Grande, J. B.; Brook, M. A. *J. Polym. Sci. A Polym. Chem.* **2013**, *51*, 644–652.
(40) Gonzaga, F.; Grande, J. B.; Brook, M. A. *Chem. Eur. J.* **2011**, *18*, 1536–1541.
(41) Grande, J. B.; Gonzaga, F.; Brook, M. A. *Dalton Trans.* **2010**, *39*, 9369–9378.
(42) Thompson, D. B.; Brook, M. A. *J. Am. Chem. Soc.* **2008**, *130*, 32–33.
(43) Grande, J. B.; Thompson, D. B.; Gonzaga, F.; Brook, M. A. *Chem. Commun.* **2010**, *46*, 4988–4990.
(44) Bahr, J. L.; Tour, J. M. *Chem. Mater.* **2001**, *13*, 3823–3824.
(45) Dyke, C. A.; Tour, J. M. *J. Am. Chem. Soc.* **2003**, *125*, 1156–1157.
(46) Chadwick, R. C.; Khan, U.; Coleman, J. N.; Adronov, A. *Small* **2013**, *9*, 552–560.
(47) Dyke, C. A.; Tour, J. M. *J. Phys. Chem. A* **2004**, *108*, 11151–11159.

(48) Beigbeder, A.; Linares, M.; Devalckenaere, M.; Degée, P.; Degee, P.; Claes, M.; Beljonne, D.; Lazzaroni, R.; Dubois, P. *Adv. Mater.* **2008**, *20*, 1003–1007.
(49) Li, H.; Cheng, F.; Duft, A. M.; Adronov, A. *J. Am. Chem. Soc.* **2005**, *127*, 14518–14524.
(50) Chojnowski, J.; Fortuniak, W.; Kurjata, J.; Rubinsztajn, S.; Cella, J. A. *Macromolecules* **2006**, *39*, 3802–3807.

Chapter 4: Bulk Suspension of Single-Walled Carbon Nanotubes in Silicone Rubbers Using Diblock Copolymers

Ryan C. Chadwick, Darryl Fong, Nicole A. Rice, Michael A. Brook, and Alex Adronov*

Department of Chemistry and Chemical Biology,
McMaster University,
1280 Main St. W.,
Hamilton, Ontario, L8S 4M1 (Canada)

Reproduced with permission from The Journal of Polymer Science A: Polymer Chemistry, 2014. ASAP. DOI: 10.1002/pola.27313.

Ryan Chadwick performed the experimental planning and design for this chapter. Darryl Fong performed the synthesis of the polymers and materials. Darryl Fong performed the conductivity and UV-Vis measurements. Nicole Rice performed the photoluminescence mapping experiments.

Graphical Abstract:

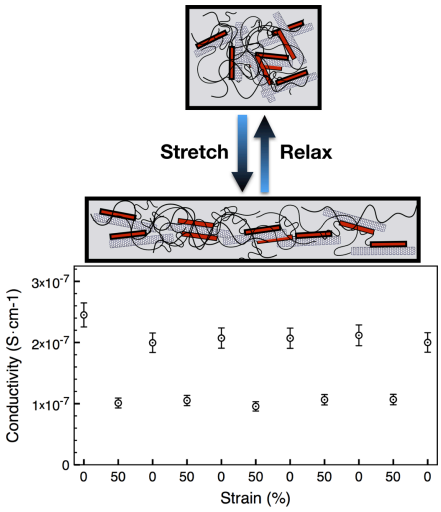

Abstract

The interactions of a series of poly(3-decylthiophene)-*block*-polydimethylsiloxanes (P3DT-*b*-PDMS) with single-walled carbon nanotubes were investigated. Allyl-terminated P3DT polymers (M_n = 4.6 – 17.3 kDa) with low PDI (ca. 1.2) were synthesized via Grignard metathesis (GRIM) polymerization. Monohydride-terminated PDMS (0.6 and 2.0 kDa) was coupled to the terminal allyl group of the P3DT via Pt-catalyzed hydrosilylation. In total, six diblock copolymers were synthesized, with three block lengths of P3DT (4.6, 9.8, and 17.3 kDa) and two lengths of PDMS (0.6 and 2.0 kDa). The formation of supramolecular complexes of P3DT-*b*-PDMS with single-walled carbon nanotubes (SWNTs) was studied in THF, toluene, xylenes, and $CHCl_3$, and the resulting complexes were characterized by UV-Vis-NIR absorption and fluorescence spectroscopy. The P3DT-*b*-PDMS-SWNT and P3DT-SWNT complexes were then integrated into a commercially available silicone rubber formulation. Percolation thresholds of < 0.02% (P3DT-*b*-PDMS-SWNT) and < 0.05% (P3DT-SWNT) were determined. The decrease in the observed percolation threshold when using the block copolymer for nanotube dispersion suggests that the presence of a covalently-linked PDMS block improves SWNT distribution in the silicone elastomer and allows for a percolation network to form at low SWNT loadings. In addition, it was found that entanglement of the silicone block of P3DT-PDMS with bulk silicones results in anchoring of the nanotubes within the composite, and leads to reversible conductivity changes upon repeated stretching and relaxation.

4.1. Introduction

Due to the high intrinsic conductivity and aspect ratio of carbon nanotubes, their incorporation into bulk materials including epoxy,[1-5] polystyrene (PS),[6-9] poly(methyl methacrylate) (PMMA),[10-13] polycarbonate (PC),[14-18] poly(vinyl chloride) (PVC),[19,20] poly(ethylene terephthalate) (PET),[21] and other bulk matrices[22-39] has attracted significant interest in recent years. Their ability to form electrical percolation networks at low filler loadings allows carbon nanotubes to impart electrical conductivity without perturbing intrinsic properties of the bulk material.[38] In particular, this is critical for creating electrically conductive elastomers, as too high a filler loading often results in compromised elasticity.[40] However, a major problem with carbon nanotubes is the strong inter-tube π-π interactions that lead to nanotube bundling.[41] This bundling results in low solubility in both aqueous and organic solvents, and thus makes it difficult to homogenously disperse pristine nanotubes into host materials. To improve nanotube solubility, covalent and noncovalent functionalization have been employed.[42-44] Noncovalent functionalization of carbon nanotubes using conjugated polymers is of particular interest, as it avoids introducing defects that disrupt the π-conjugation responsible for the advantageous electronic properties that nanotubes exhibit.[44] By tuning the solubility of the conjugated polymer, the solubility properties of carbon nanotubes can also be tuned.[43]

To our knowledge, there has been little exploration into the use of conjugated polymer-containing diblock copolymers to incorporate carbon

nanotubes into elastomeric materials. In work done by Zhai and co-workers, diblock copolymers containing blocks of the conjugated polymer poly(3-hexylthiophene) (P3HT) and the non-conjugated polymers PS, PMMA, poly(acrylic acid), or poly(ethylene glycol) were synthesized.[45-47] These diblock copolymers were used to disperse nanotubes into a bulk material identical to the non-conjugated block. It was observed that the P3HT block interacted with carbon nanotubes, while the non-conjugated block extended away from the nanotube surface and aided in forming homogenous composites. When a diblock copolymer with a mismatched non-conjugated block was used to disperse nanotubes into a bulk material, the percolation threshold was higher than when the non-conjugated block was matched to the bulk matrix.[47]

Recently, there has been growing interest in the use of carbon nanotubes as fillers in silicone elastomers.[48-50] These materials consist of high molecular weight cross-linked poly(dimethylsiloxane) (PDMS) chains, and are widely utilized because of its excellent thermal stability, elasticity, and biocompatibility.[51] Dubois has shown that incorporation of multi-walled carbon nanotubes (MWNTs) within silicone oil results in a dramatic increase in viscosity, and MWNT-filled crosslinked silicone can serve as a fire-resistant coating.[52] However, in subsequent work, crosslinked silicone elastomers containing small quantities of MWNTs did not show appreciable increases in tensile modulus, likely because compatibilizers between the nanotubes and silicone were not used. It was found that, at loadings above 0.1 wt%, the nanotubes tended to aggregate in

the crosslinked silicone, deteriorating any favourable properties.[52,53] Alternatively, Bao prepared electrically conductive crosslinked PDMS by spray-coating SWNTs onto the elastomer surface.[53] This material was investigated as a strain sensor, and was found to accommodate strains of up to 150%, while demonstrating conductivities as high as 2200 $S \cdot cm^{-1}$.[53] Furthermore, these materials could be stretched and relaxed many times within a specific length range without appreciable loss of conductivity. However, this approach again does not involve compatibilization between the nanotubes and silicone, precluding homogeneous incorporation of SWNTs throughout the bulk silicone material.

Considering the successful demonstration of block copolymers as compatibilizers between carbon nanotubes and bulk polymers,[45-47] we hypothesized that this strategy would enable homogeneous incorporation and anchoring of SWNTs within silicone elastomers. We therefore investigated the use of a diblock copolymer, poly(3-decylthiophene)-*block*-poly(dimethylsiloxane) (P3DT-*b*-PDMS), as a SWNT dispersant within crosslinked silicones. Here, we describe the preparation of homogeneous SWNT-silicone nanocomposites and contrast the ability of P3DT-*b*-PDMS with P3DT homopolymer, to suspend SWNTs within bulk PDMS. We demonstrate that the block copolymer is a superior compatibilizer for SWNTs relative to just the P3DT block, as it results in a decreased percolation threshold within composite elastomers and allows for restoration of bulk conductivity upon repeated stretching and relaxation of the elastomer, which was not observed with the homopolymer.

4.2. Results and Discussion

A systematic study of the effect of P3DT-*b*-PDMS block length on SWNT-silicone composite properties requires that the individual blocks be well defined and exhibit narrow polydispersity indices (PDIs). We therefore prepared well-defined P3DT via Grignard metathesis (GRIM) polymerization of 2,5-dibromo-3-decylthiophene (**2**), which was produced by Kumada coupling of commercially available 3-bromothiophene with decylmagnesium bromide followed by NBS bromination (Scheme 4.1). GRIM polymerization of **2** was initiated using Ni(dppp)(*o*-tolyl)Cl, which installs an *o*-tolyl group at the start of each polymer chain (Scheme 4.2).[54] The *o*-tolyl group provided a distinct ^{1}H NMR signal at 2.49 ppm corresponding to the Ar-CH_3 group, which could be compared to the thiophene proton resonance signal at 6.98 ppm to determine the number of repeat units and thus calculate the number average molecular weight, M_n (Figure 4.1). Introduction of a terminal allyl group at the chain end of each P3DT polymer was accomplished by quenching the polymerization with excess allyl magnesium bromide, as previously described.[55] Control over polymer molecular weight was achieved by varying the molar ratio of monomer to initiator, with the goal of preparing 5, 10, and 20 kDa chains. Monohydride-terminated PDMS with a molecular weight of 2.0 kDa was synthesized using anionic ring-opening polymerization following literature procedures,[56] while a lower molecular weight monohydride-terminated PDMS (M_n = 0.6 kDa) was commercially available. Monohydride-terminated PDMS with the two different

molecular weights (0.6 and 2 kDa) could then be coupled to the allyl-terminated P3DT using Pt-catalyzed hydrosilylation,[57] allowing for the synthesis of diblock copolymers containing different block ratios (Scheme 4.2). Overall, six different diblock copolymers **P1**-**P6** were investigated as part of this study (Table 4.1).

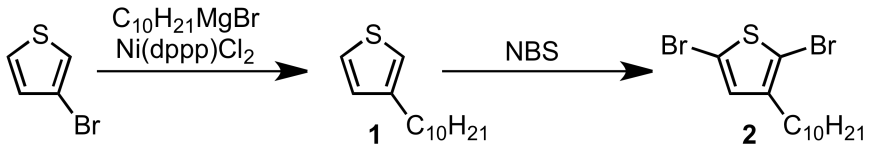

Scheme 4.1: Synthesis of 3-decyl-2,5-dibromothiophene

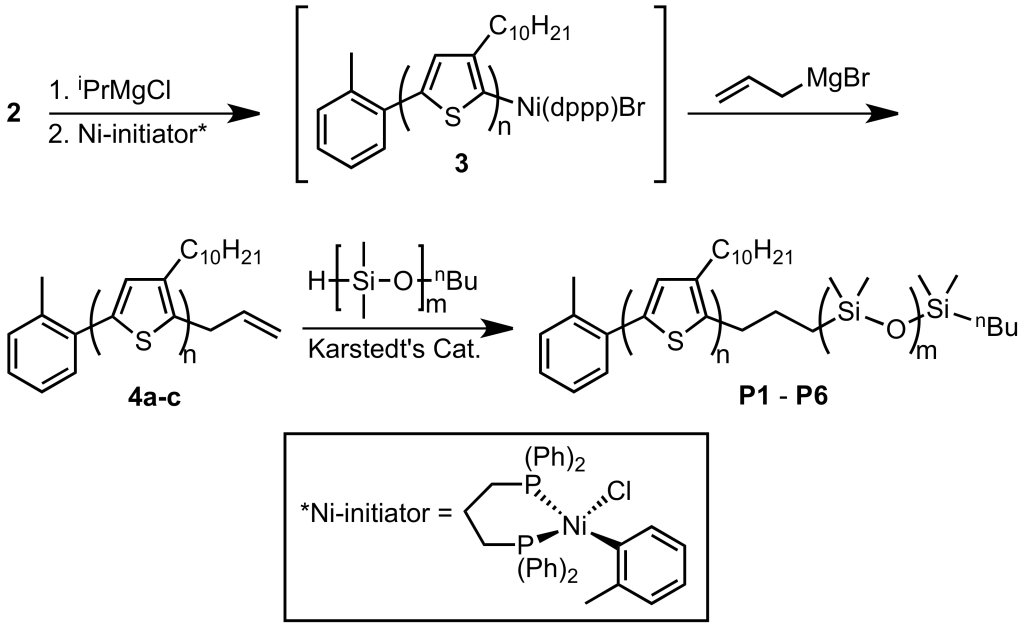

Scheme 4.2: Grignard metathesis polymerization of P3DT

Table 4.1: P3DT-*b*-PDMS properties: % mass of each block determined by TGA.

Polymer	M_n (P3DT:PDMS)	% Mass P3DT	% Mass PDMS
P1	4.6:0.6 kDa	79.4%	20.6%
P2	9.8:0.6 kDa	90.4%	9.6%
P3	17.3:0.6 kDa	97.2%	2.8%
P4	4.6:2.0 kDa	66.7%	33.3%
P5	9.8:2.0 kDa	82.6%	17.4%
P6	17.3:2.0 kDa	88.1%	11.9%

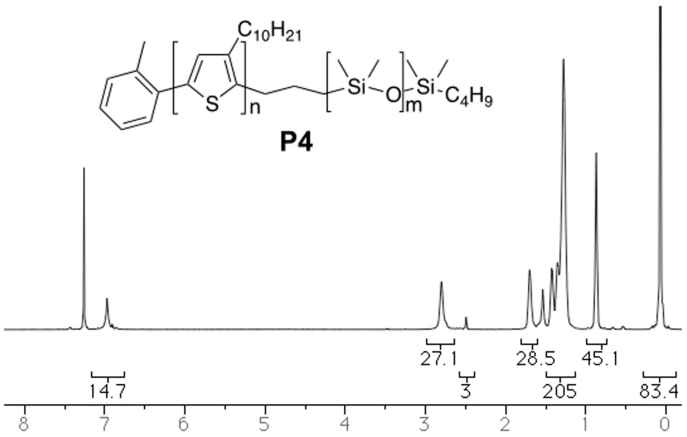

Figure 4.1: ^{1}H NMR spectrum of **P4** in $CDCl_3$.

Initial characterization of the polythiophenes **4a-c** was accomplished by NMR. Based on the NMR spectra, M_n values of 4.6, 9.8, and 17.3 kDa were calculated, corresponding to degrees of polymerization of 21, 44, and 78, for **4a-c**, respectively. These values for **4a-c** were also determined by gel permeation chromatography (GPC) relative to PS standards, with M_n = 6.7 – 25.6 kDa observed. All the polymers had narrow PDIs ranging from 1.13 to 1.21, which were in reasonable agreement with the NMR values. Hydrosilylation of **4a-c** with hydride-terminated silicones using Karstedt's catalyst proceeded smoothly despite the possibilty of catalyst complexation by the thiophene sulfur atoms,[58] which seemed to decrease the reaction rate but did not stop the reaction from occurring. The resulting block copolymers, P3DT-*b*-PDMS, **P1**-**P6**, were isolated by precipitation into methanol as purple solids in good yield (61-87%).

The thermal stability of P3DT-*b*-PDMS was characterized by thermogravimetric analysis (TGA) performed under Ar from 150 – 700 °C (Table

4.1). As a control, the thermal stability of **4b** and PDMS-2k was initially measured, and a total mass loss of 79% and 100% was observed, respectively, which was consistent with the literature (Figure 4.2).[59,60] Mass loss at 180 – 400°C corresponded to the PDMS block and mass loss at 400 – 550°C corresponded to the side-chains of the P3DT block. For each diblock copolymer, the mass % of each block determined by TGA was consistent with what was expected.

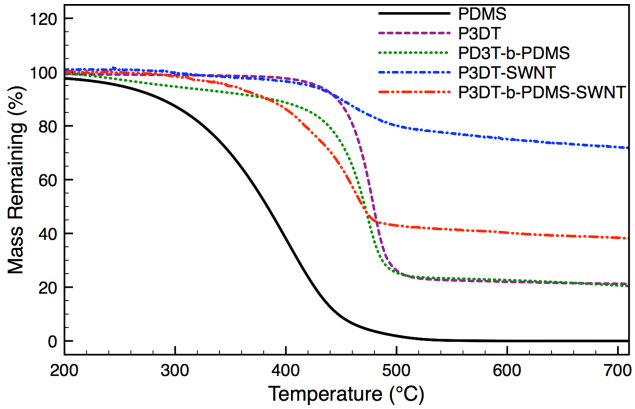

Figure 4.2: TGA data showing mass loss upon heating under an argon atmosphere for P3DT-9.8k (**4b**), PDMS-2k, P3DT-*b*-PDMS (**P5**), P3DT-SWNT and P3DT-*b*-PDMS-SWNT samples.

Supramolecular interactions between the diblock copolymers and SWNTs were investigated using UV-Vis-NIR absorption and fluorescence spectroscopy. The dispersions were prepared following previously published protocols with slight modifications.[61] Briefly, 2 mg of raw HiPCO SWNT powder was added to a solution containing 5 mg of polymer dissolved in 10 mL of solvent (THF, toluene, xylenes, or $CHCl_3$). Polymer-SWNT mixtures were sonicated for 1 h, diluted 1:5

in the same solvent, sonicated for an additional hour, and then centrifuged for 30 min at 5 000 *g*. The resulting supernatant was removed from the centrifuge tube to yield stable polymer-SWNT dispersions. The polymer-SWNT UV-Vis-NIR absorption spectra show absorbance peaks in both the visible and NIR regions, arising from the van Hove transitions of the various SWNT chiralities, as shown in Figure 4.3A for the polymer-SWNT complexes in THF. Figure 4.3B shows the UV-Vis-NIR absorption spectra for the **P3**-SWNT complexes in the four different solvents. The absorption spectra for the dispersions prepared in THF, toluene and xylenes all show well-defined peaks, indicative of debundled SWNTs. The absorbance spectrum for the $CHCl_3$ dispersion lacks the sharp features observed with the other three solvents, and there is significant broad exponential background absorbance, characteristic of bundled SWNTs. When comparing the absorbance intensities across the diblock copolymer series with the same PDMS block length, it was observed that diblock copolymers containing the 9.8 kDa P3DT block had the highest absorbance intensities, suggesting that this P3DT block length disperses and exfoliates SWNTs to the greatest extent. Very little difference in SWNT dispersion efficiency was observed between the short and long PDMS blocks, as can be seen by comparing the results with **P2** and **P5** (Figure 4.3a). For the SWNT-silicone composites, **P5** was chosen to suspend SWNTs because the difference in absorbance intensity in comparison to **P2** was small, but a larger PDMS block would be expected to interact more strongly with the surrounding bulk PDMS in the composite material.

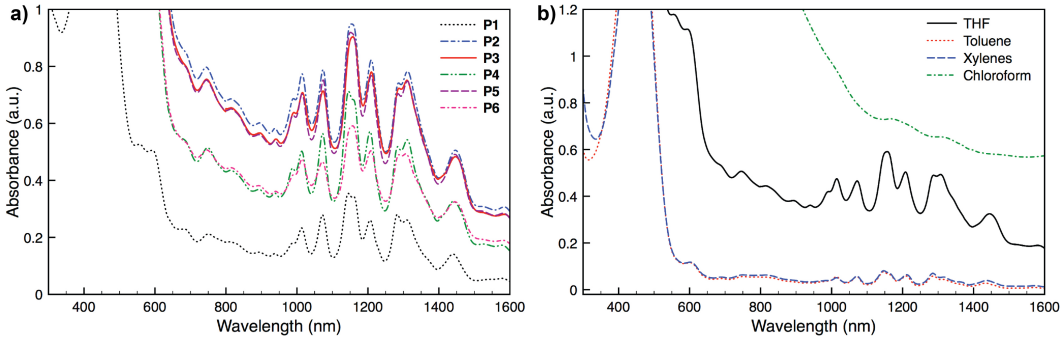

Figure 4.3: UV-Vis-NIR absorption data for polymer-SWNT dispersions (**P1**-**P6**) in THF (a); absorption spectra for **P6**-SWNT in THF, toluene, xylenes, and $CHCl_3$ (b).

Additional characterization of the polymer-SWNTs composites was carried out using photoluminescence (PL) mapping, which enables characterization of the semiconducting SWNT population in solution.[62,63] Figure 4.3 shows the PL maps obtained for **P4**-SWNT dispersions in THF, toluene, and xylenes. All three maps show strong SWNT fluorescence, again demonstrating that the diblock copolymers efficiently exfoliate SWNT bundles in these three solvents. Some solvent-dependent selectivity was observed upon comparison of the three maps, similar to what has been previously reported.[64] The (*6,5*) and (*7,5*) chiralities gave rise to the most intense PL peaks in THF, while the dispersions prepared in toluene and xylenes show more intense fluorescence from the (*8,4*) and (*9,2*) chiralities. A noticeable red shift in both the excitation and emission for the expected SWNT peak location was observed for all polymer-SWNT complexes, a phenomenon that has been previously observed for other polymer-SWNT dispersions. [64]

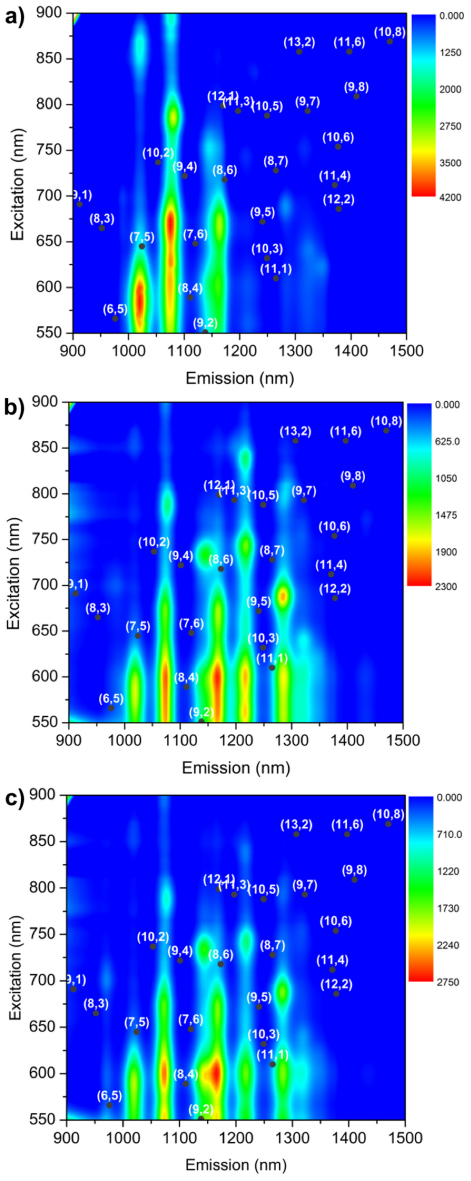

Figure 4.4. Photoluminescence maps of **P4**-SWNT samples in (a) THF (b) toluene and (c) xylenes.

Silicone composites were made using a commercially available two-component formulation (Gelest PP2-OE41). This formulation was selected because it did not contain any fillers, allowing the product silicone rubber to

stretch to a significant extent. In the first iteration, the base and cross-linker were mixed in a 1:1 ratio and an appropriate amount of polymer-SWNT dispersion made in THF or $CHCl_3$ was added to control SWNT loadings, followed by mixing of all the components and curing at 50°C. None of these samples were found to have measurably decreased bulk resistivity at 0.005 – 0.07% SWNT loadings (wt. %). Moreover, SWNT-silicone composite curing in the presence of solvent appeared to adversely affect the formation of a percolation network. If cured without mixing, we observed polymer-SWNT dispersions in both THF and $CHCl_3$ to form a distinct dark layer separate from that of the clear and colourless PDMS. Thus, the residual solvent caused phase separation and concentration of the functionalized SWNTs within solvent, preventing its homogeneous dispersion throughout the elastomer.

To avoid solvent, we attempted to directly add the solid polymer-SWNT complex and mechanically grind it into the PDMS matrix, but this did not produce satisfactory nanotube dispersions. We thus turned to evaporating the solvent prior to silicone curing. The polymer-SWNT complex dispersed in THF was isolated as a thin, purple film by vacuum filtration using a Teflon filtration membrane (200 nm pore diameter) and excess polymer was removed by washing with THF until the filtrate was no longer fluorescent when irradiated with UV light (365 nm). From TGA, the polymer-SWNT ratio was found to be 38:62 (**4b**:SWNT) and 75:25 (**P5**:SWNT). The polymer-SWNT complexes (11 mg of SWNTs) were individually sonicated for 1 h in 100 mL $CHCl_3$, resulting in homogeneous

dispersions, and aliquots were pipetted into separate glass vials immediately to avoid nanotube sedimentation. The separate aliquots were then mixed with 1 g of the silicone base and solvent was evaporated at elevated temperature. At low SWNT loadings (< 0.04 wt%) the SWNT-base composite was smooth and viscous, similar to pristine PDMS. At higher SWNT loadings (> 0.04 wt%), the SWNT-base composite was no longer smooth or completely self-levelling, and even more viscous. Once solvent was evaporated, 1 g of crosslinker was added and the SWNT-silicone composite was cured. To determine the percolation threshold, samples containing varying SWNT loadings were made using **4b** or **P5** to disperse the SWNTs. Sheet resistivity was measured using the 4-point probe method to account for contact resistance. When using **4b** and **P5** to suspend SWNTs into the silicone rubber matrix, the estimated percolation threshold values were < 0.02% and < 0.05%, respectively (Figure 4.5). However, in a control experiment without any SWNT noncovalent functionalization, samples below 0.1% SWNT loading were generally found to be non-conductive (occasionally, conductive spots within a sample could be found, but they were localized to a small area). Also, crosslinked silicones prepared with **P5** (at identical levels as for the polymer-SWNT complexes) but without any SWNTs produced samples with conductivities 5 orders of magnitude lower than those observed with SWNTs (data not shown). Thus, the percolation thresholds measured with **P5**-SWNTs were an order of magnitude lower than those reported by Zhai and co-workers.[47] Based on this data, we speculate that the percolation threshold is related to the

quality and homogeneity of the nanotube dispersion. When the SWNTs are functionalized with the P3DT-*b*-PDMS diblock copolymer, they are maximally exfoliated and homogeneously dispersed throughout the silicone, leading to the lowest percolation threshold. Removal of the PDMS block decreased the dispersion homogeneity, and thus increased the percolation threshold by a factor of ~2. With no polymer functionalization, the nanotubes are likely incorporated as aggregates and small bundles, and their presence in this state does not lead to appreciable bulk conductivity. The percolation threshold for the P3DT-SWNT-silicone composite falls within the lower range of reported values, while the percolation threshold for the P3DT-*b*-PDMS-SWNT-silicone composite is amongst the lowest reported.

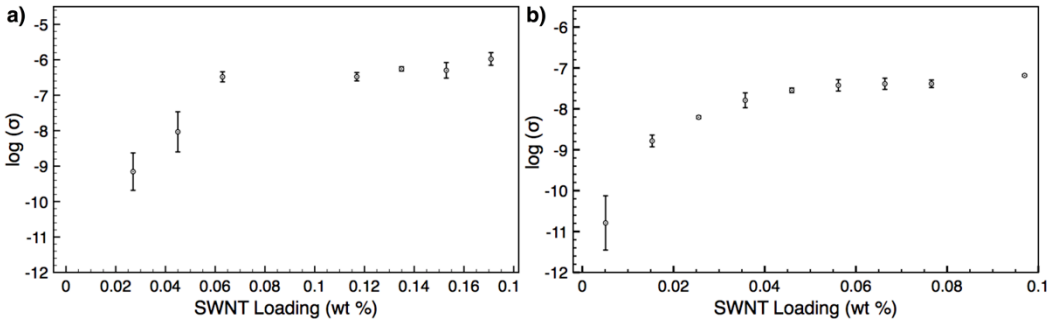

Figure 4.5. Conductivity, σ, as a function of SWNT wt %, when using (a) P3DT-*b*-PDMS (**P5**) or (b) P3DT (**4b**) to disperse SWNTs in crosslinked silicone. The error bars represent logarithmic relative error of triplicate measurements for each concentration.

Having achieved homogeneous SWNT dispersion using the diblock copolymer, we proceeded to test the responsiveness of the nanotube-loaded silicone elastomers to stretching. In a control experiment, we began with SWNTs that were functionalized with just the conjugated P3DT block. The nanotube dispersion was incorporated within the crosslinked silicone elastomer at a loading of 0.13 wt %. The rectangular sample was then subjected to five cycles of stretching to 50% elongation, and relaxation to the initial state. The conductivity of the silicone was measured in the elongated and relaxed states, and is plotted in Figure 6a. In the original unstretched state, the silicone conductivity was ca. 9×10^{-7} $S \cdot cm^{-1}$, and upon initial stretching to 50% elongation, the conductivity dropped approximately two-fold. Repeated stretching to 50% elongation always resulted in identical conductivity in the stretched state, but the conductivity upon relaxation rapidly degraded over the course of three stretching cycles to the point that it was identical to the conductivity in the stretched state. This indicates that the inter-nanotube junctions that impart conductivity to the overall material are irreversibly broken upon repeated stretching, likely resulting from reorganization of loosely held nanotubes within the bulk elastomer. Using a different sample (with 0.17 wt % SWNT loading) that was cut into two identical pieces, we compared the effect of repeated stretching with and without pre-stretching to 75% elongation (Figure 4.6b). In this case, overall conductivity of the original material was slightly higher than the sample in Figure 4.6a as the total nanotube loading was higher, but the behaviour of the material upon stretch cycling was identical,

even in the sample that was pre-stretched to 75% elongation. This sample also exhibited a decay in conductivity of the relaxed state after approximately three stretching/relaxation cycles. This data suggests that SWNTs that do not exhibit strong interactions with the silicone matrix are mobile, and can reorganize upon application of strain.

Conversely, when nanotubes functionalized with P3DT-*b*-PDMS were incorporated within crosslinked silicones, their reorganization behaviour upon repeated stretching was different (Figure 4.6c). At a loading of 0.077 wt %, the unstretched sample exhibited a conductivity of 5.5×10^{-8} S·cm^{-1}. When stretched to 50% elongation, the conductivity again dropped approximately two-fold. However, upon repeated stretching/relaxation cycles, the conductivity in the relaxed state always recovered to approximately the same level, which was only slightly lower than the original conductivity prior to initial stretching. The slight loss in conductivity upon the first stretch indicates that some strain-induced reorganization of SWNTs is still occurring, but the recovery upon subsequent stretch cycles demonstrates that the block copolymer architecture allows the nanotubes to more intimately interact with the silicone matrix, anchoring them in specific positions. This anchoring allows the nanotubes to re-form inter-nanotube junctions upon release of strain. We speculate that the 2 kDa PDMS blocks are capable of interacting or entangling with the bulk PDMS matrix, thus preventing slippage of the SWNTs with each strain cycle and preventing the loss of conductivity.

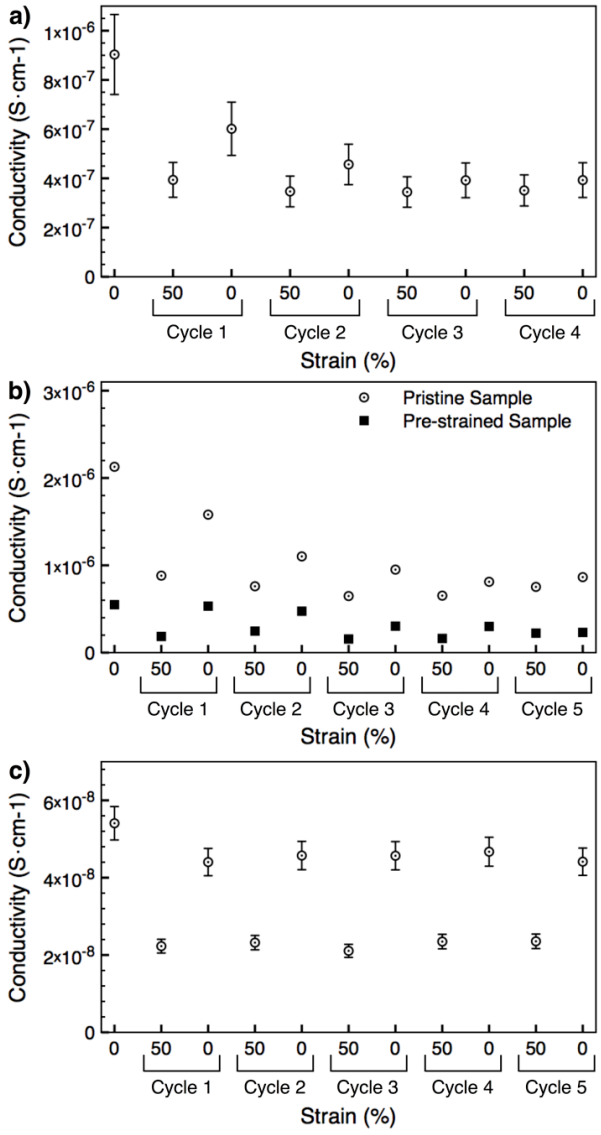

Figure 4.6: Conductivity as a function of strain for: a) P3DT coated SWNTs within bulk PDMS (0.13 wt % SWNT), b) Pristine and pre-stretched (ca. 75% elongation) P3DT coated SWNTs within bulk PDMS (0.17 wt % SWNT). c) P3DT-*b*-PDMS coated SWNTs within bulk PDMS (0.077 wt % SWNT). Error bars (a, c) represent relative standard error calculated from the full series of duplicate measurements; b) is a series of single measurements.

4.3. Conclusions

We successfully prepared a series of P3DT-*b*-PDMS using Pt-catalyzed hydrosilylation between well-defined allyl-terminated P3DT and monohydride-terminated PDMS. These diblock copolymers form strong supramolecular interactions with HiPCO SWNTs, and can successfully debundle SWNTs when polymer-SWNT dispersions are made in THF, toluene, and xylenes. Integration of non-covalently functionalized SWNTs into silicone rubbers was achieved by adding the polymer-SWNT dispersions in low-boiling solvent and evaporating solvent prior to curing the SWNT-silicone composite. When comparing SWNT-silicone composites prepared using the P3DT-*b*-PDMS block copolymer to composites prepared using the P3DT homopolymer, the percolation threshold was found to be lower by a factor of ~2 in the case of the block copolymer. Furthermore, repeated stretching to 50% elongation followed by relaxation resulted in reversible conductivity changes for SWNTs functionalized with the block copolymer, while irreversible degradation of conductivity was observed with control samples functionalized with just the P3DT homopolymer. This indicates that the block copolymer architecture enables the SWNTs to become anchored within the silicone matrix.

4.4. Experimental

4.4.1. General Experimental

Materials and Equipment: Raw HiPCO SWNTs were purchased from Carbon Nanotechnologies, Inc. (Houston, TX; lot #R6-503 for fluorescence and UV-Vis-NIR absorption spectroscopy, and lot #R1-901 for conductivity experiments) and used without further purification. All other reagents were purchased from commercial suppliers and used as received. NMR was performed on a Bruker Avance 600 MHz instrument and shift-referenced to the residual $CHCl_3$ resonance. Polymer molecular weights and polydispersity indices (relative to polystyrene standards) were analyzed via GPC using a Waters 2695 Separations Module equipped with a Waters 2414 refractive index detector, a Waters 2996 photodiode array detector, and three Jordi Fluorinated DVB mixed bed columns. THF was used as the eluent at a flow rate of 1.0 mL/min. UV-Vis-NIR spectra were recorded on a Cary 5000 spectrometer, while fluorescence spectra were measured on a Jobin-Yvon SPEX Fluorolog 3.22 equipped with a 450 W Xe arc lamp, digital photon counting photomultiplier and an InGaAs detector, and double excitation and emission monochromators. Slit widths for both excitation and emission were set to 10 nm band-pass, and correction factor files were applied to account to instrument variations. Photoluminescence maps were obtained at 25°C. Ultrasonication was performed in a Branson Ultrasonic B2510 bath sonicator. Filtration was done through a 200 nm-pore Teflon membrane (Sartorius). TGA was carried out on a TA Instruments Q50

thermogravimetric analyzer, and all measurements were done under an argon atmosphere, with sample masses ranging from 0.5 to 1.5 mg. Conductivity measurements were recorded using the Model 2450 Interactive Source Meter Instrument (Keithley) with Pt-wire probes. A Teflon mold was custom made with channel dimensions of 6 cm x 1 cm x 1 cm. Silicone/SWNT mixtures were homogenized using a FlackTek Inc. DAC 150 FVZ-K Speed Mixer.

4.4.2. Synthesis

3-decylthiophene and 2,5-dibromo-3-decylthiophene were synthesized according to literature procedures.[65,66]

Allylmagnesium bromide: An Ar-purged, 3-neck, round-bottom flask equipped with a stir bar was charged with Mg turnings (1g, 41 mmol) and Et_2O (12 mL). The suspension was cooled to 0 ºC, then a single crystal of I_2 was added. Allyl bromide (2 g, 16.5 mmol) was dissolved in Et_2O (1.5 mL) and added dropwise, while stirring, over 4 min via addition-funnel. The reaction mixture was stirred for 1 h at 0 ºC, then allowed to warm to room temperature and used directly for P3DT-polymerization quenching.

Representative P3DT synthesis (4a-c): **4a-c** were prepared using modified literature procedures.[54,67] Briefly, a flame-dried Schlenk tube under an Ar atmosphere was charged with Ni(dppp)Cl_2 (1 mmol). THF (20 mL) was added, and the solution was cooled to 0 ºC. *o*-Tolylmagnesium chloride (1.05 mmol) was added dropwise via syringe to produce the macro-initiator. In a separate flame-dried Schlenk tube under an Ar atmosphere, 2,5-dibromo-3-decylthiophene (**2)**

(500 mg, 1.31 mmol) was dissolved in THF (5 mL) and cooled to 0 ºC. Isopropylmagnesium chloride (1.37 mmol) was added dropwise at 0 ºC via syringe. Both mixtures were stirred at 0 ºC for 1 h. The monomer solution was allowed to warm to room temperature and an appropriate aliquot of macro-initiator solution was added rapidly. The polymerization mixture was stirred at RT for 10 min. The polymerization was quenched by adding an aliquot of allylmagnesium bromide solution (ca. 50-fold molar excess) followed by stirring an additional 30 min at RT. Then, $CHCl_3$ (50 mL) was added to the reaction mixture, and the resulting solution was washed with 1M HCl (2 × 25 mL). The $CHCl_3$ layer was concentrated under reduced pressure and precipitated into EtOH (200 mL). After filtration, the desired products **4a-c** were obtained as purple solids. Isolated yields ranged from 449 to 610 mg, 33 to 52%. ^{1}H NMR: ($CDCl_3$, 600 MHz): δ 6.97 (s), 5.99-5.89 (m), 5.24-5.09 (m), 3.55-3.49 (m), 2.80-2.79 (m), 2.49 (s), 1.76-1.63 (m), 1.28 (d, J = 5.3), 0.87 (t, J = 6.7).

Poly(dimethylsiloxane): PDMS was prepared according to literature procedures.[56] A flame-dried Schlenk tube equipped with a stir bar, under an Ar atmosphere, was charged with hexamethylcyclotrisiloxane (4.25 g, 19.1 mmol). Cyclohexane (12 mL) then *n*-BuLi (0.75 mL, 2.89 M, 2.2 mmol) were added via syringe and the reaction mixture was stirred for 2 h at RT. THF (1.2 mL) was then added and the reaction mixture was stirred for 48 h at 30 ºC. The reaction was quenched with chlorodimethylsilane (2.0 mmol) and then poured into MeOH (40 mL). The MeOH was decanted via pipette and residual solvent was evaporated

under reduced pressure to obtain a clear, colourless, viscous liquid (3.54 g, 83% yield). M_n (^{1}H-NMR) = 2.0 kDa, ^{1}H NMR: ($CDCl_3$, 600 MHz): δ 4.70 (s, 1H), 1.31 (dd, J = 6.9, 3.4, 4H), 0.88 (t, J = 6.9, 3H), 0.54 (dd, J = 9.4, 6.7, 2H), 0.07 (d, J = 12.5, 132H).

Representative P3DT-b-PDMS synthesis (P1-P6): An Ar-purged round bottom flask, equipped with a stir bar, was charged with allyl-terminated P3DT (**4a)** (50 mg, 10.9 μmol) and toluene (2 mL). Monohydride-terminated PDMS (32.6 μmol) and Karstedt's catalyst (2 wt% Pt, solution in xylenes) (54.5 nmol) were added quickly via syringe, and then the reaction mixture was heated to 60 ºC in an oil bath and stirred for 4 h. Longer reaction times (~1 day) were required with higher molecular weight PDMS. The reaction mixture was precipitated into MeOH (200 mL), filtered, and then washed with *n*-hexanes (25 mL). The desired product **P1** was obtained as a fine, purple powder. Isolated yields ranged from 34 to 60 mg, 61 to 87%. ^{1}H NMR: ($CDCl_3$, 600 MHz): 6.97 (d, J = 1.4), 2.80 (s), 2.49 (s), 1.70-1.69 (m), 1.28-1.27 (m), 0.87 (t, J = 6.6), 0.07 (d, J = 16.9).

4.4.3. Nanotube Dispersions

Raw HiPCO SWNT dispersions with P1-P6 To a solution of polymer (5 mg) in solvent (10 mL; THF, toluene, xylenes, or $CHCl_3$), raw HiPCO SWNTs (2 mg dry wt.) were added to make a stock solution and then the polymer-SWNT dispersion was sonicated for 1 h in a bath sonicator at 0 ºC. The stock solution was then diluted 1:5 (2 mL stock, 8 mL of the same solvent) and sonicated again for 1 h in a bath sonicator at 0 ºC. The resulting polymer-SWNT dispersion was

then centrifuged for 30 min at 5,000 *g*. The supernatant was transferred to a separate glass vial and investigated using fluorescence and UV-Vis-NIR absorption spectroscopy.

SWNT-silicone rubber composite: To a solution of polymer (70 mg) in THF (700 mL), raw HiPCO SWNTs (28 mg dry wt.) were added and the polymer-SWNT dispersion was sonicated for 1 h in a bath sonicator at 0 ºC. The resulting polymer-SWNT dispersion was vacuum filtered through a cotton plug to remove large particulate. The filtrate was vacuum filtered through a Teflon filtration membrane (0.2 μm pore diameter) to obtain a thin, purple film. Excess polymer was removed by washing with THF until the filtrate did not fluoresce when irradiated with UV light (365 nm). The recovered polymer was reused for additional cycles of SWNT suspension by repeating this process with the same reagent ratios. All solid polymer-SWNT extract complexes were combined in THF (100 mL) and sonicated for 30 min to homogenize the sample. The polymer-SWNT dispersion was then vacuum filtered, and a single thin, purple film was isolated. The polymer:SWNT ratio was determined by TGA, then the polymer-SWNT solid (11 mg of SWNTs) was dissolved in $CHCl_3$ (100 mL) to produce a stock solution. The appropriate volume of this stock solution was then added to 1 g of Gelest Optical Encapsulant Part A (PP2-OE41). The sample was mixed for 30 sec using a speed mixer (3,000 rpm) and then heated to 90 °C in an open vacuum oven to evaporate solvent. After solvent removal, the sample was re-mixed for 30 sec (3,000 rpm) and then heated to 80 ºC for 10 min before adding 1

g of Gelest Optical Encapsulant Part B (PP2-OE41). The SWNT-SR composite was then mixed using a speed mixer at 500 rpm (1 min) then 100 rpm (4 min) and transferred to a Teflon mold to be cured at 140 °C in air for 2 – 3 h.

4.4.4. Electrical Measurements

***Conductivity measurements*:** Measurements were taken using a modified van der Pauw method.[68] Liquid eutectic gallium-indium (eGaIn) was applied to each probe tip, and a series of measurements were taken at 1 V intervals ranging from 0 V – 40 V. For each potential applied to the sample the current was recorded. This procedure was repeated three additional times, each time rotating the sample by 90º. Voltage versus current was plotted between 13 and 40 V for each measurement and the line slopes calculated. The sheet resistivity R_s (Ω/sq) was calculated using the following formula where R is the mean of the line slopes.

$$R_s = R\frac{\pi}{\ln(2)}$$

Measurements were taken in triplicate per silicone rubber sample. Sheet resistivity was multiplied by the thickness (in cm) of the silicone rubber sample to obtain bulk resistivity (Ω·cm). Conductivity ($S \cdot cm^{-1}$) was taken as the inverse of bulk resistivity.

4.5. References

(1) Sumfleth, J.; Buschhorn, S. T.; Schulte, K. *J. Mater. Sci.* **2011**, *46*, 659–669.

(2) Du, F.; Guthy, C.; Kashiwagi, T.; Fischer, J. E.; Winey, K. I. *J. Polym. Sci., Part B: Polym. Phys.* **2006**, *44*, 1513–1519.

(3) Moisala, A.; Li, Q.; Kinloch, I. A.; Windle, A. H. *Compos. Sci. Technol.* **2006**, *66*, 1285–1288.

(4) Bryning, M. B.; Islam, M. F.; Kikkawa, J. M. *Adv. Mater.* **2005**, *17*, 1186–1191.

(5) Martin, C. A.; Sandler, J. K. W.; Shaffer, M. S. P.; Schwarz, M. K.; Bauhofer, W.; Schulte, K.; Windle, A. H. *Compos. Sci. Technol.* **2004**, *64*, 2309–2316.

(6) Antonucci, V.; Faiella, G.; Giordano, M.; Nicolais, L.; Pepe, G. *Macromol. Symp.* **2007**, *247*, 172–181.

(7) Poa, C. H.; Silva, S. R. P.; Watts, P. C. P.; Hsu, W. K.; Kroto, H. W.; Walton, D. R. M. *Appl. Phys. Lett.* **2002**, *80*, 3189–3191.

(8) Kim, S. T.; Choi, H.-J.; Hong, S. M. *Colloid Polym. Sci.* **2006**, *285*, 593–598.

(9) Chang, T. E.; Kisliuk, A.; Rhodes, S. M.; Brittain, W. J.; Sokolov, A. P. *Polymer* **2006**, *47*, 7740–7746.

(10) Skákalová, V.; Dettlaff-Weglikowska, U.; Roth, S. *Synth. Met.* **2005**, *152*, 349–352.

(11) Du, F.; Fischer, J. E.; Winey, K. I. *J. Polym. Sci., Part B: Polym. Phys.* **2003**, *41*, 3333–3338.

(12) Dai, J.; Wang, Q.; Li, W.; Wei, Z.; Xu, G. *Mater. Lett.* **2007**, *61*, 27–29.

(13) Kim, H.; Choi, M.-S.; Joo, J.; Cho, S.; Yoon, H. *Phys. Rev. B: Condens. Matter Mater. Phys.* **2006**, *74*, 054202.

(14) Hilarius, K.; Lellinger, D.; Alig, I.; Villmow, T.; Pegel, S.; Pötschke, P. *Polymer* **2013**, *54*, 5865–5874.

(15) Pegel, S.; P o tschke, P.; Petzold, G.; Alig, I.; Dudkin, S. M.; Lellinger, D. *Polymer* **2008**, *49*, 974–984.

(16) Hornbostel, B.; Pötschke, P.; Kotz, J. *Phys. Stat. Sol. (b)* **2006**, *243*, 3445–3451.

(17) Pötschke, P.; Dudkin, S. M.; Alig, I. *Polymer* **2003**, *44*, 5023–5030.

(18) Pötschke, P.; Abdel-Goad, M.; Alig, I.; Dudkin, S. *Polymer* **2004**, *45*, 8863–8870.

(19) Mamunya, Y.; Boudenne, A.; Lebovka, N.; Ibos, L.; Candau, Y.; Lisunova, M. *Compos. Sci. Technol.* **2008**, *68*, 1981–1988.

(20) Shaffer, M. S. P.; Windle, A. H. *Adv. Mater.* **1999**, *11*, 937–941.

(21) Hu, G.; Zhao, C.; Zhang, S.; Yang, M.; Wang, Z. *Polymer* **2006**, *47*, 480–488.

(22) Kyrylyuk, A. V.; Hermant, M.-C.; Schilling, T.; Klumperman, B.; Koning, C. E.; van der Schoot, P. *Nat. Nanotechnol.* **2011**, *6*, 364–369.

(23) Kodgire, P. V.; Bhattacharyya, A. R.; Bose, S.; Gupta, N.; Kulkarni, A. R.; Misra, A. *Chem. Phys. Lett.* **2006**, *432*, 480–485.
(24) Zhu, B.; Xie, S.; Xu, Z.; Xu, Y. *Compos. Sci. Technol.* **2006**, *66*, 548–554.
(25) Musumeci, A. W.; Silva, G. G.; Liu, J.-W.; Martens, W. N.; Waclawik, E. R. *Polymer* **2007**, *48*, 1667–1678.
(26) Awasthi, K.; Awasthi, S.; Srivastava, A.; Kamalakaran, R.; Talapatra, S.; Ajayan, P. M.; Srivastava, O. N. *Nanotechnology* **2006**, *17*, 5417–5422.
(27) McNally, T.; P o tschke, P.; Halley, P.; Murphy, M.; Martin, D.; Bell, S. E. J.; Brennan, G. P.; Bein, D.; Lemoine, P.; Quinn, J. P. *Polymer* **2005**, *46*, 8222–8232.
(28) Zhang, Q.; Rastogi, S.; Chen, D.; Lippits, D.; Lemstra, P. J. *Carbon* **2006**, *44*, 778–785.
(29) Lisunova, M. O.; Mamunya, Y. P.; Lebovka, N. I.; Melezhyk, A. V. *Eur. Polym. J.* **2007**, *43*, 949–958.
(30) Mierczynska, A.; Mayne-L'Hermite, M.; Boiteux, G.; Jeszka, J. K. *J. Appl. Polym. Sci.* **2007**, *105*, 158–168.
(31) Jiang, M.-J.; Dang, Z.-M.; Xu, H.-P. *Appl. Phys. Lett.* **2007**, *90*, 042914.
(32) Aarab, H.; Baïtoul, M.; Wéry, J.; Almairac, R.; Lefrant, S.; Faulques, E.; Duvail, J. L.; Hamedoun, M. *Synth. Met.* **2005**, *155*, 63–67.
(33) Tjong, S. C.; Liang, G. D.; Bao, S. P. *Scr. Mater.* **2007**, *57*, 461–464.
(34) Seo, M.-K.; Park, S.-J. *Chem. Phys. Lett.* **2004**, *395*, 44–48.
(35) Gryshchuk, O.; Karger-Kocsis, J.; Thomann, R.; K o nya, Z.; Kiricsi, I. *Compos. Part A: Appl. S.* **2006**, *37*, 1252–1259.
(36) Kim, Y. J.; An, K. J.; Suh, K. S.; Choi, H. D.; Kwon, J. H.; Chung, Y. C.; Kim, W. N.; Lee, A. K.; Choi, J. I.; Yoon, H. G. *IEEE Trans. Electromagn. Compat.* **2005**, *47*, 872–879.
(37) Engel, J.; Chen, N.; Pandya, S.; Liu, C. IEEE, 2006; pp. 246–249.
(38) Koerner, H.; Liu, W.; Alexander, M.; Mirau, P.; Dowty, H.; Vaia, R. A. *Polymer* **2005**, *46*, 4405–4420.
(39) Bian, C.; Xu, X.; Yang, G.; Zhao, Y.; Jin, S.; Wang, H. *Acat. Chim. Sinica.* **2007**, *65*, 525–531.
(40) Boonstra, B. B. *Polymer* **1979**, *20*, 691–704.
(41) Tasis, D.; Tagmatarchis, N.; Bianco, A.; Prato, M. *Chem. Rev.* **2006**, *106*, 1105–1136.
(42) Hirsch, A. *Angew. Chem. Int. Ed.* **2002**.
(43) Britz, D. A.; Khlobystov, A. N. *Chem. Soc. Rev.* **2006**, *35*, 637–659.
(44) Campidelli, S.; Klumpp, C.; Bianco, A.; Guldi, D. M.; Prato, M. *J. Phys. Org. Chem.* **2006**, *19*, 531–539.
(45) Zou, J.; Liu, L.; Chen, H.; Khondaker, S. I.; McCullough, R. D.; Huo, Q.; Zhai, L. *Adv. Mater.* **2008**, *20*, 2055–2060.
(46) Zou, J.; Chen, H.; Chunder, A.; Yu, Y.; Huo, Q.; Zhai, L. *Adv. Mater.* **2008**, *20*, 3337–3341.
(47) Zou, J.; Khondaker, S.; Huo, Q.; Zhai, L. **2009**, *19*, 479–483.

(48) Lahiff, E.; Ryu, C. Y.; Curran, S.; Minett, A. I.; Blau, W. J. *Nano Lett.* **2003**, *3*, 1333–1337.
(49) Dyke, C. A.; Tour, J. M. *J. Phys. Chem. A* **2004**, *108*, 11151–11159.
(50) Liu, C. H.; Fan, S. S. *Appl. Phys. Lett.* **2005**, *86*, 123106.
(51) Mata, A.; Fleischman, A. J.; Roy, S. *Biomed Microdevices* **2005**, *7*, 281–293.
(52) Beigbeder, A.; Linares, M.; Devalckenaere, M.; Degée, P.; Degee, P.; Claes, M.; Beljonne, D.; Lazzaroni, R.; Dubois, P. *Adv. Mater.* **2008**, *20*, 1003–1007.
(53) Lipomi, D. J.; Vosgueritchian, M.; Tee, B. C.-K.; Hellstrom, S. L.; Lee, J. A.; Fox, C. H.; Bao, Z. *Nat. Nanotechnol.* **2011**, *6*, 788–792.
(54) Senkovskyy, V.; Sommer, M.; Tkachov, R.; Komber, H.; Huck, W. T. S.; Kiriy, A. *Macromolecules* **2010**, *43*, 10157–10161.
(55) Jeffries-El, M.; Sauvé, G.; Mccullough, R. D. *Adv. Mater.* **2004**, *16*, 1017–1019.
(56) Peters, M. A.; Belu, A. M.; Linton, R. W.; Dupray, L. *J. Am. Chem. Soc.* **1995**, *117*, 3380–3388.
(57) Karstedt, B. Platinum complexes of unsaturated siloxanes and platinum containing organopolysiloxanes. US3775452 A, 11~27 1973.
(58) Liu, S.; Lucas, C. R.; Newlands, M. J.; Charland, J. P. *Inorg. Chem.* **1990**, *29*, 4380–4385.
(59) Camino, G.; Lomakin, S. M.; Lazzari, M. *Polymer* **2001**, *42*, 2395–2402.
(60) Boudouris, B. W.; Frisbie, C. D.; Hillmyer, M. A. *Macromolecules* **2008**, *41*, 67–75.
(61) Cheng, F.; Imin, P.; Maunders, C.; Botton, G.; Adronov, A. *Macromolecules* **2008**, *41*, 2304–2308.
(62) Bachilo, S. M.; Strano, M. S.; Kittrell, C.; Hauge, R. H.; Smalley, R. E.; Weisman, R. B. *Science* **2002**, *298*, 2361–2366.
(63) Weisman, R.; Bachilo, S. *Nano Lett.* **2003**, *3*, 1235–1238.
(64) Hwang, J.; Nish, A.; Doig, J.; Douven, S.; Chen, C.; Chen, L.; Nicholas, R. *J. Am. Chem. Soc.* **2008**, *130*, 3543–3553.
(65) Tamao, K.; Kodama, S.; Nakajima, I.; Kumada, M.; Minato, A. *Tetrahedron* **1982**, *38*, 3347–3354.
(66) Liu, B.; Yu, W.-L.; Lai, Y.-H.; Huang, W. *Macromolecules* **2000**, *33*, 8945–8952.
(67) Loewe, R. S.; Khersonsky, S. M. *Adv. Mater.* **1999**, *11*, 250–253.
(68) Chwang, R.; Smith, B. J.; Crowell, C. R. *Solid State Electron.* **1974**, *17*, 1217–1227.

Chapter 5: Synthesis of Conjugated Polymers Containing DIBAC-Derived Triazole Monomers

Ryan C. Chadwick, Vladimir Kardelis, Sophie Liogier, and Alex Adronov*

Department of Chemistry and Chemical Biology,
McMaster University,
1280 Main St. W.,
Hamilton, Ontario, L8S 4M1 (Canada)

This chapter has been adapted with permission from Macromolecules, 2013, 46, pp 9593-9598.

Ryan Chadwick performed the experimental planning and design. Ryan Chadwick, Vladimir Kardelis and Sophie Liogier performed the synthesis of the polymers and small molecules. Ryan Chadwick performed the characterization of all products.

Graphical Abstract:

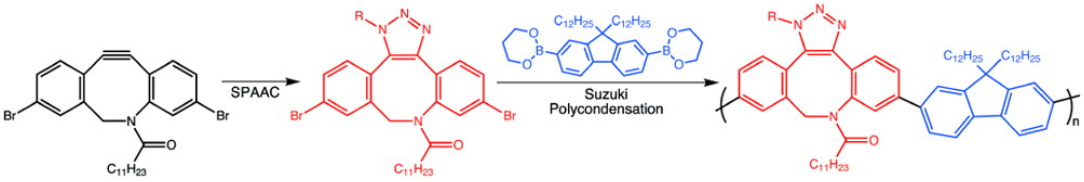

Abstract:

2,7-Dibromoazadibenzocyclooctyne (DIBAC-Br_2) was prepared as a pro-monomer unit that could be modified by the metal-free strain-promoted azide–alkyne cycloaddition (SPAAC). Click cyclization of DIBAC-Br_2 with five different benzyl azides produced a homologous series of monomers with different functionality on the resulting triazole ring, ranging from electron-withdrawing to electron-donating substituents. Using this series of monomers, in combination with 2,7-dialkylfluorene as a comonomer, five different conjugated polymers were prepared via Suzuki polycondensation, each having different electronic properties. The resulting copolymers exhibited M_w values ranging from 5 to 10 kDa and PDI values in the 1.5–2 range. These polymers were characterized by ^1H NMR spectroscopy, optical spectroscopy, and cyclic voltammetry. Finally, a coumarin-containing oligomer was synthesized and used to demonstrate a photo-cross-linking scheme via [2 + 2] cycloaddition.

5.1. Introduction:

The tunable electronic properties that conjugated polymers (CPs)[1-3] exhibit have made them extremely interesting for a variety of applications, including photovoltaics,[4,5] light-emitting diodes,[6] organic electronics,[7] field-effect transistors,[8] sensors,[9] and molecular switches.[10] Many classes of conjugated polymers with diverse structures have been studied, such as polyacetylenes,[11,12] poly(p-phenylenes),[13] poly(phenylenevinylenes),[14] polyanilines,[15,16] poly-fluorenes,[17] polythiophenes,[18-21] polycarbazoles,[22] and a large number of derivative structures (i.e., PEDOT).[1-3,10] In addition, recent work has demonstrated that CPs exhibit strong supramolecular interactions with carbon nanotubes[23-27] and that these interactions can be selective for specific types of single-walled carbon nanotubes (SWNTs), enabling the dispersion of certain SWNT chiralities.[28-31] Along these lines, it is becoming apparent that small changes in polymer structure and/or architecture can have large effects on the selectivity of the interactions with SWNTs.[29,32,33] Thus, in order to explore the selectivity of CP–SWNT interactions, it is imperative to prepare homologous series of CPs with systematic variation of their structural and electronic properties.

In general, control over structural and electronic properties of CPs, including variation of band gaps, redox potentials, optical properties, and conjugation lengths, has been achieved using different monomer structures and side chains. Extensive work into the preparation of conjugated copolymers has

also been performed, where variation of one comonomer allows extensive tuning of the overall polymer bandgap and can have a tremendous effect on polymer properties.[1,2] Furthermore, many conjugated polymers can be manipulated through doping, either via redox reactions or through acid/base chemistry.[34-39] However, systematic covalent alteration of the aromatic framework of conjugated monomers or polymer precursors, either pre- or post polymerization, has received relatively little attention. In particular, although the highly efficient Huisgen cycloaddition between an azide and an alkyne has been extensively used in the synthesis of well-defined macromolecules,[40] block copolymers,[41] cyclic polymers,[42] graft copolymers,[43] and other functional architectures,[44-46] the resulting aromatic triazole ring has received little attention as a structural unit within conjugated polymers or monomer units.

While Huisgen cycloaddition reactions are highly favorable,[47] they have high activation energies, requiring either high temperatures or a copper catalyst to achieve acceptable reaction rates.[48] Alternatively, several research groups have recently begun to explore "activated" alkynes through the use of electron-withdrawing groups or strain promotion to carry out bioconjugation as well as macromolecule synthesis.[49-54] In particular, strain-promoted alkyne-azide cycloaddition (SPAAC, Figure 5.1a), such as in the case of cyclooctyne derivatives, is extremely fast at room temperature, especially when aromatic rings flank the cyclooctyne structure (Figure 5.1b). Recently, Bertozzi and co-workers have shown that SPAAC with strained cyclooctynes is nonelectrophilic and bio-

orthogonal, while being exceedingly reactive toward a number of cycloaddition and cyclization processes.[55] However, because of the involved nature of their synthesis, strained alkynes have seen relatively little use outside of bioconjugation chemistry.

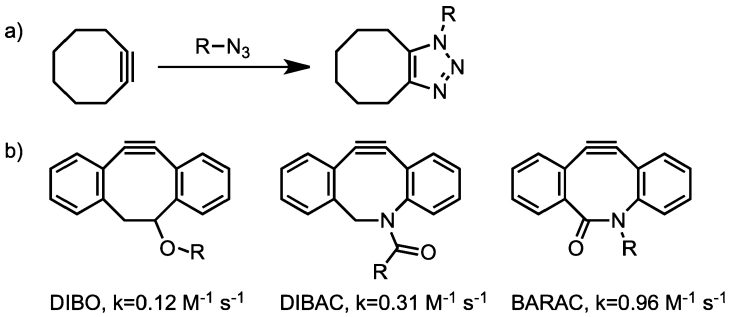

Figure 5.1: (a) Simplest conceptual strain promoted azide-alkyne cycloaddition (SPAAC) using cyclooctyne. (b) Previously reported conjugated dibenzocyclooctynes and their second-order rate constants in the reaction with benzyl azide.[56]

Noting both the structure and reactivity of conjugated dibenzocyclooctyne-type SPAAC reagents (Figure 5.1b),[56] we became interested in exploring these structures as backbone units within conjugated polymers. Creation of a monomer unit based on a biarylazacyclooctynone (DIBAC, Figure 5.1b), would allow the facile tuning of both monomer and polymer properties using SPAAC. Accordingly, we have synthesized a conjugated alkyne "pro-monomer" based on the DIBAC core structure and have investigated its cyclization and polymerization chemistry.

5.2. Results and Discussion

Preparation of our desired monomer was carried out through a modified Popik DIBAC synthesis to introduce aryl bromide groups para to the triple bond (Scheme 5.1).[57,58] This was accomplished by electrophilic aromatic substitution, following literature procedures.[59] Subsequent radical bromination, dehalogenation, oxime formation, and reduction/re-arrangement resulted in the cyclic secondary amine **6**. Amidation with lauroyl chloride ensures solubility in common organic processing solvents, followed by double benzylic bromination and elimination with KOtBu produced the desired dibromo-DIBAC derivative **9**, in eight steps (Scheme 5.1). Although lengthy, this synthesis was carried out on multigram scale, allowing the production of monomer **9** in gram quantities (6% overall yield). The presence of the aryl bromide groups in the 2- and 7-positions of **9** enable it to undergo palladium cross-coupling reactions, and the C-12 chain ensures solubility of the monomer and subsequent conjugated polymers.

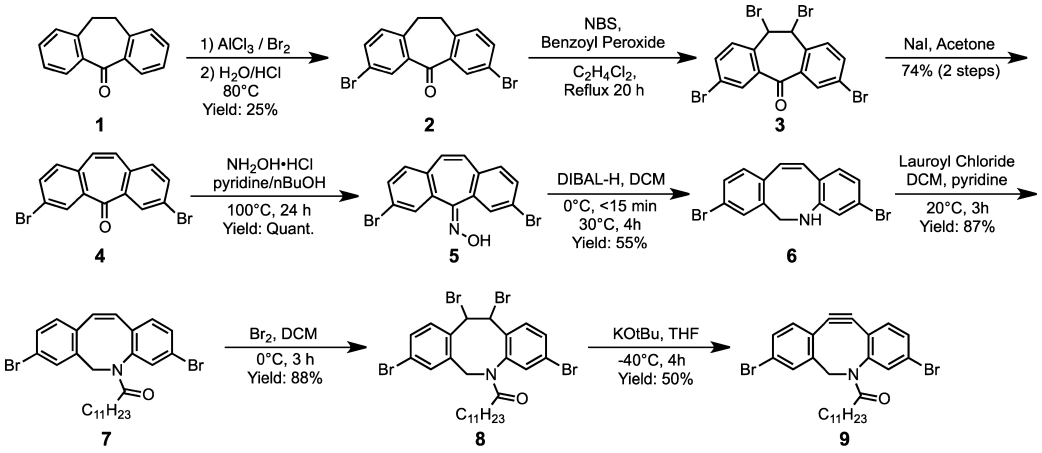

Scheme 5.1: Synthesis of the 2,7-Dibromobiarylazacyclooctynone pro-monomer **9.**

Attempts to copolymerize pro-monomer **9** with a diboronic ester derivative of fluorene under standard Suzuki polycondensation conditions resulted in rapid reaction between the strained alkyne and the Pd catalyst, likely forming a metallacyclopropene structure that may subsequently undergo further reactivity.[60] Although alkynes are generally stable to metal-catalyzed polycondensations,[61-63] the strained alkyne of **9** is clearly too reactive and successfully competes with oxidative insertion of the aryl bromide onto Pd. To avoid exposure of the alkyne to the metal during polymerization, SPAAC was carried out with a series of aryl azides prior to polymerization, as shown in Scheme 5.2. These specific aryl azides were chosen to incorporate electron-donating (methoxy, *tert*-butyl) and electron-withdrawing (nitro) groups in order to systematically vary the electronic properties of the resulting polymers. Each of the cycloaddition reactions was carried out in good yield, producing a homologous series of DIBAC-trizole monomers **10a**–**e** (Scheme 5.2a) that could subsequently be polymerized via Suzuki polyconensation. It should be noted that the triazole ring of these monomers was produced as a mixture of two regioisomers, and therefore, four stereoisomers were isolated for each of the final monomers.

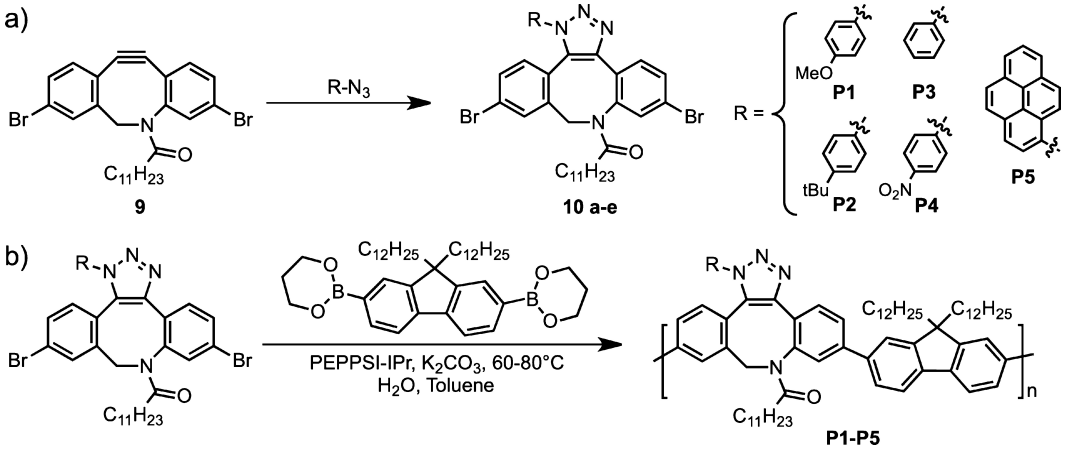

Scheme 5.2. (a) Synthesis of Monomers **10a**–**e**; (b) Synthesis of Conjugated Copolymers **P1–P5** via Suzuki Polycondensation with 9,9-Didodecylfluorene-2,7-diboronic Acid Bis(1,3-propanediol) Ester as the Comonomer.

Having produced monomers 10a–e, we performed their copolymerization with 9,9-didodecylfluorene-2,7-diboronic acid bis(1,3-propanediol) ester via Suzuki polycondensation. We chose this fluorene comonomer as it was expected to further enhance polymer solubility (via the alkyl chains) and because the properties of many polyfluorene copolymers have been established.[17] All the polymerizations occurred readily within 2–8 h at 60–80 °C under phase-transfer conditions (toluene/water) using the highly active *N*-heterocyclic carbene "PEPPSI-iPr" palladium(0) catalyst developed by Organ and co-workers.[64] All of the resulting polymers exhibited moderate molecular weights in the range of M_w = 5–10 kDa, with polydispersities between 1.5 and 2 (Table 5.1). We suspect that these molecular weights were limited by the purity of our commercial fluorene comonomer (Aldrich, 97%), which was found to be difficult to purify further. The

use of a higher purity comonomer, or a switch to aryl iodide monomers, is expected to result in higher molecular weight polymers. Solubility was not a limiting factor in the polymerization as all of the polymers, except the coumarin derivative (*vide infra*), showed excellent solubility. In all, five homologous polymers, P1–P5, were synthesized, containing anisole, 4-*tert*-butylphenyl, phenyl, 4-nitrophenyl, and pyrenyl groups conjugated to the triazole ring (Scheme 5.2b). The polymers generally formed translucent, brittle films with poor mechanical properties; however, thin films were found to be sufficiently robust for cyclic voltammetry and UV experiments.

The electronic properties of P1–P5 were investigated by UV–vis absorption spectroscopy, fluorescence spectroscopy, and cyclic voltammetry. Interestingly, the differences between the electron-rich derivatives (anisole, phenyl, 4-*tert*-butylphenyl, and pyrenyl) are subtle. Adjusting the side chain changes the fine structure and width of the absorption and fluorescence bands but has little effect on the λ_{max}, quantum yield, or extinction coefficient of the polymers. In all cases, absorption λ_{max} values were found to be approximately 350 nm (Figure 5.2a). This absorption profile is very similar to poly(phenylene-*co*-fluorene) (PPF) type copolymers and is blue-shifted as compared to a polyfluorene homopolymer or an alternating poly(fluorene-*co*-phenylenevinylene) polymer. This suggests the DIBAC triazole copolymers are unable to achieve extended conjugation as a result of steric hindrance at the fluorene-DIBAC bonds, which causes deviation from coplanarity between the comonomers and a decrease

in π-orbital overlap between them.[17,65] Additionally, the conjugation length may be further reduced by a lack of planarity in the DIBAC structure.

The torsion angle and energy of conjugated polymers can be difficult to precisely quantify via DFT—in polymers, these calculations are often combined with an NMR study to determine the angle in a specific solvent or concentration range.[66] However, a value of ca. 40° has been calculated for the fluorene dimer and 38° for biphenyl.[66] In our case, DFT geometry optimizations performed via GAMESS,[67] at the B3LYP[68,69] level of theory, using a 6-31G(d)[70] basis set, show a torsion angle of 38°, consistent with these results (see experimental and Appendix 3 for details). However, more striking is the lack of planarity within the DIBAC structure itself. Our DFT calculations and comparison to an analogous crystal structure (for a DIBAC–triazole Ru complex) confirm extensive deviations from planarity in the core DIBAC unit. Computational details and 3-D representations of these calculations can be found within Appendix 3.

Interestingly, the introduction of the strongly π-accepting nitro functionality has a profound effect on the polymer electronic properties. While the UV absorption maximum and extinction coefficient show very little change, the emission band becomes red-shifted by nearly 120 nm (Figure 5.2b). Furthermore, although the other derivatives exhibit quantum yields greater than 0.7 (similar to other fluorene containing polymers), the nitro derivative exhibits a quantum yield that is an order of magnitude lower (ΦF = 0.06, Table 5.1). Fluorescence quenching by nitro functionalities is well established in small molecules;[71]

however, this degree of quenching is not always observed in conjugated macromolecules.[72] In order to test whether this red-shift and quenching are due to intermolecular quenching or the presence of an additional intermediate excited energy state due to nitro derivatization, we performed a quenching experiment using nitrobenzene as the quencher with polymer P3 (see Appendix 3). The addition of nitrobenzene quenched the fluorescence; however, no emission red-shift was observed. These experiments suggest that a functional group introduced on the triazole ring experiences a high degree of conjugation and electronic communication with the polymer backbone.

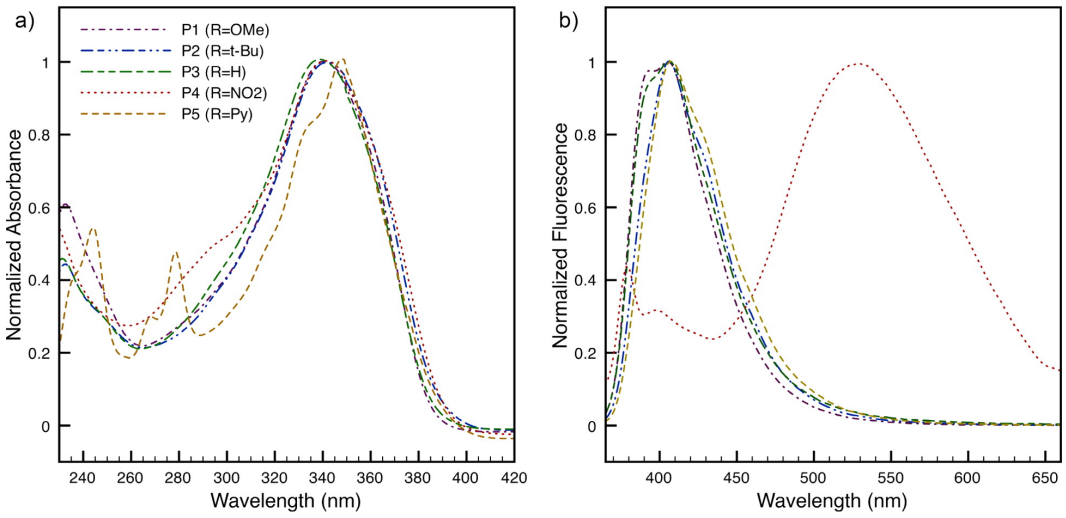

Figure 5.2: Normalized absorption (a) and emission (b) data for polymers **P1–P5**.

Cyclic voltammetry data for polymer thin films on a platinum electrode allowed calculation of the electrochemical bandgaps. The cyclic voltammograms were recorded at a scan rate of 200 mV/s using a silver wire quasi-reference electrode and were then calibrated to the ferrocene/ferrocenium (Fc/Fc^{+}) redox

couple using a saturated calomel electrode (SCE) reference. The resulting cyclic voltammograms (Fc/Fc^+ omitted) versus SCE are available within the Appendix 3 (Figure A3.3). The onset potentials for the oxidation and reduction peaks were calculated by determining the intersection of the tangents drawn at the rising oxidation or reduction current and the background current, and the HOMO and LUMO levels were calculated with respect to vacuum (−4.71 relative to SCE). The energy levels of the five polymers are very similar, and the electrochemical and optical bandgaps are in good agreement (Table 5.1). The HOMO and LUMO levels and bandgaps are similar to other polyfluorene copolymers.[73]Generally, both the oxidation and reduction waves were found to be irreversible. Even at high scan rates and with conservative voltages, virtually no reversibility was observed. Likewise, performing experiments in both THF and ACN yielded virtually identical results. As in the optical spectra, the pyrene derivative shows some additional features in the cyclic voltammogram, consisting of two or three closely spaced reduction waves. The HOMO and LUMO levels are slightly low compared to those of most other fluorene copolymers but are the same, to within a reasonable estimate of measurement error, as poly[2,7-(9,9-dialkylfluorenes)] or fluorene/phenyl-ene copolymers (HOMO = 5.9–6.0).[74] Again, it is likely that these properties arise from the inability of these polymers to adopt a completely planar conformation, due to either steric hindrance from the large side chains or the inherent twist in the DIBAC unit.

Table 5.1: The physical and electronic properties of the series of polymers.

Poly.	Eg, elec. (eV)	Eg, opt. (eV)	HOMO (eV)	LUMO (eV)	Φ em.	λmax, ab. (nm)	λmax, em. (nm)	Mn (kg/mol)	Mw (kg/mol)	PDI
P1	3.3	3.2	-6.2	-2.9	0.88	341	404	4.6	8.7	1.9
P2	3.4	3.2	-6.2	-2.8	0.74	341	406	4.9	8.3	1.9
P3	3.4	3.2	-6.2	-2.8	0.9	339	406	3.5	5.7	1.7
P4	3.2	3.1	-6.1	-2.9	0.06	341	528	4	7.8	2
P5	3.1	3.1	-6.1	-3	0.86	348	407	3.2	5	1.5

In addition to the ability to modify the electronic properties of these molecules, the strained alkyne moiety can be used as a functional handle to introduce reactive groups in the side chain. In order to further demonstrate the versatility and utility of this system, we have synthesized a coumarin-containing polymer, **P6**, via an azide-containing derivative of 7-hydroxycoumarin (Figure 5.3a). A full synthetic scheme can be found in Appendix 3.

Alkoxycoumarins have been demonstrated to photo-cross-link under UV (>350 nm) irradiation both in the solid state[75] and in solution (Figure 5.3b). Accordingly, we irradiated a thin film of polymer **P6** and monitored it by GPC and UV–vis spectroscopy. By using a low molecular weight polymer, we were able to successfully dissolve a portion of our partially cross-linked film after 1 h of UV irradiation (the undissolved gel was removed by filtration) and determined the molecular weight of this partially cross-linked material (Figure 5.3d). At $t > 1$ h, the film became increasingly insoluble, and monitoring by GPC proved fruitless. Interestingly, GPC also showed the appearance of a lower molecular weight peak, suggesting some decomposition. Following the progress of the cross-linking by measuring the absorbance of a drop-cast thin film over 2 h, we

can clearly see a decrease of the absorbance band at 340 nm and an increase in absorbance at *ca*. 270 nm. However, if we irradiate for long periods of time (16 h), we see the complete disappearance of the absorbance at 340 nm and a considerable reduction in intensity at lower wavelengths. We observe a similar effect upon irradiation at 254 nm, suggesting that long irradiation times or higher energy UV light are capable of degrading the polymer in some fashion. The polymers also changed in physical property upon cross-linking, from an amorphous film to one which is glassy, brittle, and translucent.

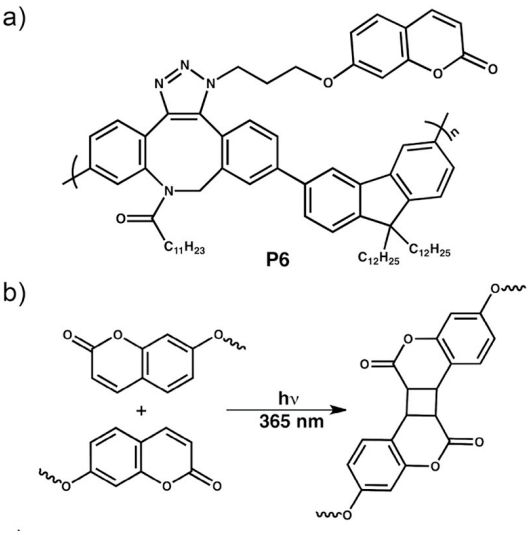

Figure 5.3: (a) Structure of coumarin-containing **P6**. (b) The coumarin photo-cross-linking reaction

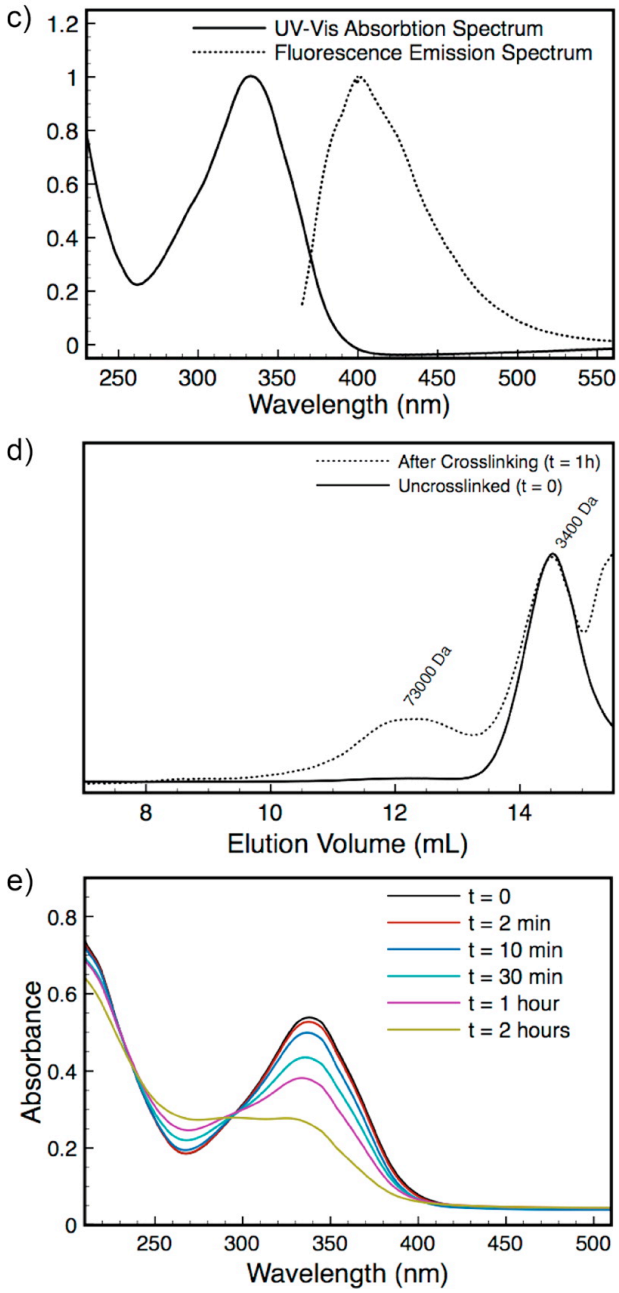

Figure 5.4. (c) UV–vis absorbance and emission spectra of **P6** in THF solution. (d) GPC data for the soluble fraction of **P6** before and after photo-cross-linking. (e) Time-resolved UV–vis absorbance study of cross-linking in a thin film of **P6**.

We attempted to suspend HiPCO single-walled carbon nanotubes with each of the produced polymers. However, none of the polymer/nanotube complexes were stable, even in the presence of a large excess of polymer. Generally, the nanotube complexes precipitated from solution over the course of several minutes to an hour. We speculate that there are two reasons for the lack of colloidal stability: 1) The polymers have a relatively low density of the alkyl chains necessary for SWNT suspension. 2) More importantly, the DFT calculations performed on these polymer structures suggests large backbone angles that may prevent efficient packing of these polymers on the nanotube surfaces.

5.3. Conclusion

In conclusion, we have synthesized a new conjugated monomer unit based on the triazole derivatives of the rigid, conjugated cyclooctyne, DIBAC. A series of monomers having different substituents on the triazole ring were copolymerized with a fluorene derivative to produce polymers with different electronic characteristics. These polymers were investigated to determine their optical and electrochemical properties. We found that the DIBAC–fluorene copolymers are similar to previously reported rigid copolymers of fluorene, such as fluorene-*co*-phenylene and fluorene-*co*-phenylenevinylene. While all of the polymers bearing electron-rich functional groups on the triazole show similar emission spectra, cyclic voltammetry shows that fine-tuning of the polymer redox potentials and band gaps is possible through triazole substitution. The use of a

strongly adsorbing (pyrene) side chain shows that the UV–vis absorption can also be modified. Furthermore, the presence of the strongly electron-withdrawing nitro group has a profound effect on the properties of the resulting polymer, exhibiting a highly quenched and red-shifted emission. Perhaps unsurprisingly, the properties of this polymer series generally appear to be dominated by the fluorene units and its apparent inability to form planar structures with a long conjugation length. Additionally, the versatility of the alkyne moiety allows the introduction of active or reactive functional groups, as demonstrated by the attachment of a photoactive coumarin unit. Further explorations of the DIBAC unit with other comonomers that allow for a greater degree of conformational flexibility, and show potentially less dominant absorption and electrochemical traits, will lead to more significant tuning of polymer properties by using the SPAAC reaction. In addition, exploration of other functional side chains can offer the potential for incorporation of SPAAC polymers within other materials.

5.4. Experimental

5.4.1. General Experimental

Reagents and Instrumentation: All chemical reagents were purchased from Aldrich Chemical Co. and Acros Organics. Peppsi-iPr was synthesized following a literature procedure.[64,76] Aryl azides were synthesized from aryl iodides by copper catalyzed substitution[59,77] or from aryl amines by Sandmeyer-type diazonium chemistry.[78,79] ^{1}H-NMR and ^{13}C-NMR spectra were recorded on a Bruker Avance 600 MHz spectrometer. High-resolution (HR) electrospray

ionization (ESI) mass spectrometry measurements were carried out on the Micromass Ultima Global instrument (quadrupole time-of-flight). Polymer molecular weights and polydispersity indices (PDI) were analyzed via gel permeation chromatography (GPC) using a Waters 2695 Separations Module, equipped with a Waters 2996 photodiode array detector, a Waters 2414 refractive-index detector, and three Jordi Fluorinated DVB mixed-bed columns. Polystyrene standards were used for calibration, with THF as the eluent at a flow rate of 1.0 mL/min. UV-Vis spectra were measured on a Cary 5000 spectrophotometer, while fluorescence spectra were measured on a Jobin-Yvon SPEX Fluorolog 3.22 equipped with a 450 W Xe lamp, double-excitation and double-emission monochromators, and a digital photon-counting photomultiplier. Ultrasonication was conducted in a Branson Ultrasonic B2500 bath sonicator. Cyclic voltammetry (CV) was conducted using a PAR (Princeton Applied Research) Model 283 potentiostat (using PAR PowerCV software) in conjunction with a three-electrode cell under an argon atmosphere. The auxiliary electrode was a platinum wire, the pseudo-reference electrode a silver wire, and the working electrode a platinum loop. The Pt loop was coated in a thin film of polymer (from a 3-10mg/mL solution in $CHCl_3$). 0.1 M $[N^nBu_4][ClO_4]$ in electrochemical grade (Aldrich) acetonitrile was used as the electrolyte solution. In all experiments, potentials were calibrated by addition of $[FeCp^*_2]$; the $E_{1/2}$value for $[FeCp^*_2]^{0/+1}$ is −0.37 V *vs.* the SCE in ACN.[76,78] All UV cross-linking experiments are performed in a

custom-assembled UV reactor containing 4x25 Watt (G25T8) "blacklight" fluorescent bulbs with a UV emission maximum of 365 nm.

Nitrobenzene Quenching Experiment: A four-sided cuvette was filled with 3.0 mL of a 0.004 mg/mL solution of coumarin polymer **P3** in uninhibited HPLC grade THF. Ten microliter aliquots of 1.0 M nitrobenzene were added by micropipette. After each addition the emission spectrum of the solution was measured. The results are plotted in Figure A3.4 (Appendix 3).

5.4.2. Coumarin Crosslinking Experiments

UV-Vis monitoring experiment: A thin film was cast from a 0.1 mg/mL solution of **P6** in 2-MeTHF on to a quartz slide. The slide was then irradiated under 365 nm light, and UV-Vis spectra taken periodically. These results are presented in Figure 5.3e.

GPC monitoring experiment: A moderate thickness film was cast from a 20 mg/mL solution of **P6** in 2-MeTHF on to a fluoro-polymer sheet. This film was then irradiated under 365 nm light for 1 hour. A GPC chromatogram was obtained before and after cross-linking. Experiments longer than 1 hour resulted in insoluble material.

5.4.3. Synthesis

3,7-Dibromo-10,11-dihydro-dibenzo[a,d]cyclohepten-5-one (2)[58,59] A 250 mL round-bottom flask was charged with $AlCl_3$ (23 g, 174 mmol) and heated to 80°C under a N_2 atmosphere. Aided by overhead mechanical stirring, dibenzosuberone (15 g, 72 mmol) was added via syringe over five minutes,

generating a thick brown paste. The mixture was allowed to stir for another 15 minutes before slowly adding Br_2 (7.9 mL, 153 mmol) via syringe pump over 20 minutes. The resultant mixture was allowed to stir for 1 hour. While molten, the mixture was added to 300 mL of a cold, stirred solution of 5% $HCl_{(aq),}$ then extracted with 3 x 150 mL of Et_2O. The combined organic layers were washed with Na_2SO_3 (2 x 100 mL), brine (1 x 150 mL), and dried over $MgSO_4$ then filtered and evaporated under reduced pressure. The crude material was purified via column chromatography using a 1:20 Et_2O/*n*-hexane eluent, followed by recrystallization in 1:1 toluene/*n*-heptane, yielding 6.59 g (25%) of crystalline product **(1)**. M.W.: 366.05 g/mol; ^{1}H-NMR (600 MHz; $CDCl_3$): δ 8.13 (d, J = 2.2, 2H), 7.55 (dd, J = 8.1, 2.2, 2H), 7.12 (d, J = 8.1, 2H), 3.15 (s, 4H); ^{13}C-NMR (151 MHz; $CDCl_3$): δ 196.4, 140.8, 139.6, 135.6, 133.6, 131.3, 120.9, 34.4.

3,7,10,11-Tetrabromo-10,11-dihydro-dibenzo[a,d]cyclohepten-5-one (3)[78,80] Into a 250 mL round-bottom flask, was placed a solution of **2** (3.660 g, 10 mmol), *N*-bromosuccinimide (4.270 g, 24 mmol), and benzoyl peroxide (150 mg) in 1,2-dichloroethane (100 mL). The mixture turned bright red and was refluxed for 20 hours in the dark. The warm solution was washed with warm H_2O (2 x 150 mL) and 3% $NaOH_{(aq)}$ (2 x 150 mL). The organic layer was separated and evaporated under reduced pressure to yield 5.231 (quant. recovery) of a highly insoluble off-white solid (**3**), which was moved onto the next reaction without purification. Monitoring the reaction by thin layer chromatography showed a single product at R_f = 0.3 (Et_2O/*n*-hexanes, 1:4).

3,7-Dibromo-dibenzo[a,d]cyclohepten-5-one (4)[57,78] Into a 250 mL round-bottom flask containing **3** (5.238 g, 10 mmol), was placed a solution of NaI (7.190 g, 24 mmol) and acetone (100 mL). The reaction immediately turned dark red, and was stirred at reflux for 30 minutes. The remaining acetone in the reaction vessel was evaporated under reduced pressure, leaving behind a crude green residue in the flask. The solid residue was partitioned with warm $CHCl_3$ (250 mL) and 5% $Na_2SO_{3(aq)}$ (200 mL)). The organic layer was washed with 5% $Na_2SO_{3(aq)}$ (1 x 200 mL), H_2O (2 x 200 mL), and brine (1 x 150 mL), then dried over $MgSO_4$, filtered, and evaporated under reduced pressure. The pale brown solid was purified via column chromatography on silica gel in 1:9 Et_2O/*n*-hexanes (R*f* = 0.2) to yield 3.701 g (74%) of pale yellow solid (**4**). ^{1}H-NMR (600 MHz; $CDCl_3$): δ 8.35 (d, J = 2.2, 2H), 7.75 (dd, J = 8.3, 2.2, 2H), 7.42 (d, J = 8.3, 2H), 7.02 (s, 2H); ^{13}C-NMR (151 MHz; $CDCl_3$): δ 189.9, 139.5, 135.4, 133.8, 133.2, 132.8, 131.3, 123.6.

3,7-dibromo-5H-dibenzo[a,d]cyclohepten-5-one oxime (5)[57,58] Compound **4** (1.500 g, 4.12 mmol) was added to a solution of $H_2NOH{\cdot}HCl$ (1.000 g, 14.4 mmol), pyridine (10 mL), and *i*PrOH (1 mL) in a 50 mL round bottom flask. The yellow reaction mixture was stirred at reflux for 24 h, at which point it was washed with 5% $HCl_{(aq)}$, then extracted with CH_2Cl_2 (2 x 100 mL). The combined organic layers were washed with brine (1 x 100 mL) and dried over $MgSO_4$, filtered, then evaporated under reduced pressure to yield 1.56 g (Quant.) of pale yellow solid (**5**). This mildly moisture sensitive product was used immediately in

the next reaction. ^{1}H NMR (600 MHz; $CDCl_3$): δ 7.79 (d, J = 2.0, 1H), 7.73 (d, J = 2.0, 1H), 7.54 (dd, J = 8.3, 2.1, 1H), 7.52 (dd, J = 8.4, 2.1, 1H), 7.30-7.29 (d, J = 8.3, 1H), 7.22 (d, J = 8.3, 1H), 6.85 (t, J = 5.0, 2H). HRMS (ESI+) (m/z) for $C_{15}H_{10}NOBr_2$ $[M + H]^+$ calculated: 377.9129, actual: 377.9134.

(Z)-3,8-dibromo-5,6-dihydrodibenzo[b,f]azocine (6)[80,81] Compound **5** (2.5 g, 6.60 mmol) was dissolved in dry CH_2Cl_2 (100 mL) in a 100 mL round bottom flask under N_2 atmosphere. At 0°C, a 1 M DIBAL-H solution in heptane (50 mL, 50 mmol) was added dropwise to the stirring reaction mixture via syringe. After finishing the addition of DIBAL-H, the reaction was slowly brought up to room temperature before heating it to 30°C. The reaction was stirred for 4 hours at which point it was quenched by slowly adding H_2O (4 mL) at 0°C, followed by potassium fluoride (18 g). The suspension was filtered, and the solvent was evaporated under reduced pressure and then purified via column chromatography in 1:19 EtOAC/*n*-hexanes to yield 1.31 g (55%) of yellow, crystalline product (**6**). M.W.: 365.06 g/mol; ^{1}H-NMR (600 MHz; DMSO-d6): δ 7.46 (dd, *J* = 8.1, 2.1 Hz, 1H), 7.45 (t, *J* = 2.9 Hz, 1H), 7.11 (d, *J* = 8.1 Hz, 1H), 6.81 (d, *J* = 8.4 Hz, 1H), 6.71 (d, *J* = 2.1 Hz, 1H), 6.58 (dd, *J* = 8.3, 2.1 Hz, 1H), 6.53 (t, *J* = 7.2 Hz, 1H), 6.47 (d, *J* = 13.1 Hz, 1H), 6.24 (d, *J* = 13.0 Hz, 1H), 4.47-4.44 (m, 2H); ^{13}C-NMR (600 MHz; DMSO-d6): δ 140.5, 138.2, 136.2, 132.7, 132.0, 131.9, 130.4, 128.4, 126.0, 120.8, 120.4, 119.4, 119.0, 118.5, 47.0. HRMS (ESI+) (m/z) for $C_{15}H_{12}NBr_2$ $[M + H]^+$ calculated: 363.9336, actual 363.9337.

(Z)-1-(3,8-dibromodibenzo[b,f]azocin-5(6H)-yl)dodecan-1-one (7)

Compound **6** (625 mg, 1.71 mmol) was dissolved in dry CH_2Cl_2 (20 mL) and pyridine (3 mL) in a 50 mL round bottom flask. At room temperature and under the flow of N_2, lauroyl chloride (750 mg, 3.42 mmol) was added dropwise to the reaction mixture, initiating the reaction immediately. The reaction was allowed to stir for 3 hours at 20°C before adding silica gel to stir as a slurry for 30 minutes. The slurry was filtered and rinsed with CH_2Cl_2 (80 mL), then washed with 5% $HCl_{(aq)}$ (2 x 100 mL) and brine (1 x 100 mL). The organic phase was dried over $MgSO_4$, filtered, and evaporated under reduced pressure and purified via column chromatography in 1:5 Et_2O/*n*-hexanes to yield 816 mg (87%) of amorphous white product (**7**). M.W.: 547.37 g/mol; ^{1}H NMR (600 MHz; DMSO-d6): δ 7.68 (d, J = 2.0, 1H), 7.56 (dd, J = 8.1, 1.9, 2H), 7.42-7.39 (m, J = 8.3, 1.9, 2H), 7.19 (d, J = 8.4, 1H), 6.74 (d, J = 13.7, 1H), 6.63 (d, J = 13.7, 1H), 5.25 (d, J = 15.3, 1H), 4.10 (d, J = 15.4, 1H), 1.99 (dt, J = 15.0, 7.4, 1H), 1.80 (dt, J = 15.1, 7.5, 1H), 1.32-1.16 (m, 10H), 1.15-1.11 (m, 2H), 1.11-1.06 (m, 2H), 1.04-0.98 (m, 2H), 0.97-0.92 (m, 2H), 0.85 (t, J = 7.2, 3H).

1-(3,8,11,12-tetrabromo-11,12-dihydrodibenzo[b,f]azocin-5(6H)-yl)dodecan-1-one (8)[57,82] Into a screw cap vial, was placed a solution of **7** (670 mg, 1.22 mmol) in CH_2Cl_2 (10 mL). In the dark, 2.06 mL of a 10% w/v solution of Br_2 in CH_2Cl_2 (0.206 g, 1.34 mmol) was added over 5 minutes via syringe. The reaction was stirred for 3 hours at 0°C before diluting with CH_2Cl_2 and washing it with Na_2SO_3 (2 x 50 mL) and brine (1 x 50 mL). The organic layer was dried over

$MgSO_4$, filtered, and evaporated under reduced pressure to yield 760 mg (88%) of solid, white product (**8**), which was immediately moved into the next reaction. Monitoring the reaction by TLC showed the product as two regioisomers R_f = 0.30, 0.35 (CH_2Cl_2/*n*-hexanes, 7:3).

(Z)-1-(3,8-dibromo-11,12-didehydrodibenzo[b,f]azocin-5(6H)-yl)dodecan-1-one (DIBAC-Br$_2$) (9)[57,83] Into an oven dried 50 mL round bottom flask, was placed a solution of **8** (1.94 g, 2.75 mmol) in dry THF (100 mL). At -40°C, 1 M KO^{t}Bu in THF (6 mL, 6 mmol) was added to the reaction dropwise, via syringe. After stirring for 2 hour, another aliquot of 1 M KO^{t}Bu in THF (2.0 mL, 2.0 mmol) was added, turning the reaction mixture dark brown. The reaction was stirred for an additional hour whereupon the reaction mixture was quenched with H_2O (50 mL), then extracted with CH_2Cl_2 (3 x 80 mL). The combined organic layers were washed with H_2O (2 x 100 mL) and brine (1 x 100 mL), then dried over $MgSO_4$, filtered, and purified via column chromatography in 7:3 CH_2Cl_2/*n*-hexanes to yield 760 mg (50%) of slow to solidify, off-white product (**9**). ^{1}H NMR (600 MHz; $CDCl_3$): δ 7.84 (d, J = 1.7, 1H), 7.53 (dd, J = 8.2, 1.9, 1H), 7.49 (d, J = 1.9, 1H), 7.44 (dd, J = 8.1, 1.8, 1H), 7.26 (d, J = 8.1, 1H), 7.09 (d, J = 8.1, 1H), 5.06 (d, J = 13.9, 1H), 3.56 (d, J = 13.9, 1H), 2.18 (dt, J = 15.0, 7.5, 1H), 1.94 (dt, J = 15.2, 7.5, 1H), 1.43-1.36 (m, 2H), 1.31-1.07 (m, 16H), 1.03 (dt, J = 13.3, 6.8, 2H), 0.89-0.86 (t, J = 7.2, 3H); ^{13}C NMR (151 MHz; $CDCl_3$): δ 173.5, 152.8, 149.6, 135.6, 132.3, 131.28, 131.20, 127.9, 126.6, 121.9, 121.5, 115.5, 108.1, 54.8, 34.9, 32.1, 29.72, 29.65, 29.52, 29.46, 29.27, 29.0, 25.4, 22.8,

14.3. HRMS (ESI+) (m/z) calculated for $C_{27}H_{32}NOBr_2$ $[M + H]^+$ 544.0851, measured 544.0841.

2,2'-(9,9-didodecyl-9H-fluorene-2,7-diyl)-bis-(1,3,2-dioxaborinane)[79,81]

9,9-didodecylfluorene-2,7-diboronic acid (415 mg, 0.703 mmol) was purified prior to reaction by sonication in *n*-hexanes for 30 minutes followed by filtering. The purified material was dried under vacuum, then dissolved in benzene (30 mL) and placed into a 50 mL round bottom flask. A solution of 1,3-propanediol in benzene (267 mg, 3.51 mmol) was added dropwise to the reaction mixture. The reaction was stirred at reflux for 3 hours, cooled, and then washed with H_2O (2 x 50 mL) and brine (1 x 50 mL). The organic layer was dried over $MgSO_4$, filtered, and evaporated under reduced pressure to yield 435 mg (92%) of a thick colorless oil. ^{1}H NMR (600 MHz; $CDCl_3$): δ 7.66-7.65 (m, 1H), 7.64 (d, J = 0.8, 1H), 7.62-7.61 (m, 2H), 7.59 (d, J = 0.2, 1H), 7.57 (d, J = 0.4, 1H), 4.10 (t, J = 5.4, 8H), 2.01-1.97 (m, 4H), 1.87 (dt, J = 8.0, 4.1, 4H), 1.18-1.15 (m, 4H), 1.12-0.99 (m, 23H), 0.96-0.92 (m, 4H), 0.92-0.87 (m, 9H), 0.76 (t, J = 7.1, 7H).

WARNING: Nitro and amino derivatives (and their minor side products) of PAH compounds are generally strong carcinogens, and pyrene derivatives are known to be particularly potent. Use proper safety precautions.

1-Nitropyrene[77,82] Pyrene (1.5 g, 7.5 mmol) was dissolved in a mixture of 15 mL ethyl acetate and 2 mL acetic anhydride. Copper (II) nitrate hydrate, $Cu(NO_3)_2 \bullet 2H_2O$ (2.5 g, 10.5 mmol) was added. Within 20 min, a large amount of

yellow precipitate was formed. At 30 min, TLC (1:2, DCM:Hexanes) showed no starting material (product Rf = 0.35). Product was filtered via vacuum filtration, washed with water (3x50 mL) and methanol (1 x 50 mL), and then purified by filtration through a silica plug using 1:2 DCM:Hexanes to yield: 1.4 g (76%) yellow crystalline powder. ^{1}H-NMR (600 MHz; $CDCl_3$): δ 8.99 (d, 1H), 8.74 (d, 1H), 8.41-8.39 (m, 3H), 8.32 (d, 1H), 8.25 (d, 1H), 8.18 (m, 2H).

1-Aminopyrene[83,84] Nitropyrene (1.4 g, 5.6 mmol), was dissolved in a ternary mixture of 10 mL THF, 20 mL ethyl acetate, and 2 mL acetic acid. 500 mg of 10% Pd/C (wet Degussa E101) was added. The mixture was placed under a hydrogen atmosphere (1 ATM) and heated to 30°C for 1.5 hours until TLC (1:1, DCM:hexane) showed complete disappearance of starting material. The product was purified by silica gel flash chromatography (1:3, DCM:hexanes). Yield: 0.90 g (73%).^{1}H-NMR (600 MHz; $CDCl_3$): δ 8.15-7.81 (m, 8H), 7.43 (m, 1H).

WARNING: While aryl azides are generally adequately stable, there is some concern of rapid or explosive decomposition. Accordingly, a prudent precaution is to generally work on small scale, and avoid isolating pure material. Generally, we added a small amount of toluene prior to rotary evaporation to prevent evaporation to dryness. Alternatively, the material can be used as a crude product after extraction. Aryl azides are generally not bench stable, and decompose on the order of weeks, even at freezer temperatures. As with all azides, it is generally a wise precaution to avoid metal particles or metallic tools as decomposition can be

catalytic. It is imperative that sodium azide, NaN_3, does not come into contact with halogenated solvents, as azidomethanes and azidoethanes are highly dangerous.

General procedure for the synthesis of aryl azides from aryl amines[67,79]

The appropriate aryl amine (2 mmol) was suspended in 6 mL water. An equal volume (6 mL) hydrochloric acid (conc. 34%) was added drop-wise by pipette. If required for solubility, ethanol was added (to a maximum of 24 mL) and the mixture was gently warmed until the amine was sufficiently dissolved. The solution/suspension was cooled to 0°C, and then 2 equivalents (4 mmol) of sodium nitrite, $NaNO_2$ was added, portion-wise, over 2-10 min. The mixure was stirred for 0.5 hours, then NaN_3 was added slowly over 10 min (portion-wise, or in H_2O solution). WARNING: some evolution of HN_3 is possible. Use an efficient fumehood, add NaN_3 slowly. If needed, additional ethanol was added to maintain stirring. The mixture was stirred for 1 hour, then extracted with ether (3 x 30 mL) and washed with saturated sodium bicarbonate (2x) and Brine (2x). A small amount of toluene (~1 mL) was added and the ether was evaporated under a gentle stream of N_2 gas. If purification was desired a short column of silica gel (eluent, DCM:hexanes) was sufficient to produce pure material.

1-Azidopyrene. Product is unstable – decomposes during silica gel purification. Used as crude product in solution of toluene after ether evaporation.

p-(t-Bu)-phenyl azide. 4 mmol scale: Yield: 235 mg (35%).^{1}H-NMR (600 MHz; $CDCl_3$): δ 7.40 (d, J = 8.7 Hz, 2H), 7.00 (d, J = 8.7 Hz, 2H), 1.34 (s, 9H).

p-Nitrophenyl azide. Yield: ~360 mg (> 90%). Fluffy yellow powder when dried. ^{1}H-NMR (600 MHz; $CDCl_3$): δ 8.28 (m, 2H), 7.18 (m, 2H).

General procedure for the synthesis of aryl azides from aryl iodides.[77,85] In a 20 mL screw cap vial: Aryl iodide (2 mmol), sodium azide (2.4 mmol), copper (I) iodide (0.2 mmol), L-proline (0.4 mmol), and sodium hydroxide (0.4 mmol) were flushed with argon. DMSO (4 mL) was added and the vial was capped and mixed at 60°C for 5 h. The mixture was partitioned between ethyl acetate and water. The ethyl acetate layer was dried over $MgSO_4$, toluene (500 uL) was added, and the ethyl acetate evaporated. If desired, the product was purified by column chromatography (DCM:hexanes).

Phenyl azide. Product is marginally stable – some decomposition during silica gel purification. Used as crude product (~80% purity) in solution of toluene after silica gel filtration. Yield: ~50%. ^{1}H NMR ($CDCl_3$, 500 MHz) δ 7.03 (m, 2H), 7.15 (t, J = 7.5 Hz, 1H), 7.36 (m, 2H);

p-Methoxyphenyl azide. Solidifies at ca. -10°C. ^{1}H-NMR (500 MHz; $CDCl_3$): δ 6.99 (m, 2H), 6.92 (m, 2H), 3.82 (s, 3H).

7-(3-bromopropyloxy)coumarin.[84] Potassium carbonate (10 g, 72 mmol) and 1,3-dibromopropane (10 g, 50 mmol) was suspended/dissolved in 50 mL acetone in a 200 mL round-bottom flask and the mixture brought to reflux. To this solution, 7-hydroxycoumarin (810 mg, 5 mmol) was added drop-wise over 30 min. The mixture was refluxed for an additional 2 hours. After the reaction was complete, the acetone was evaporated and the mixture partitioned between 100

mL DCM and water. The DCM layer was collected, the water extracted 2 x with 100 mL DCM and the combined organic layers dried over $MgSO_4$. After drying the product was purified by flash chromatography on silica gel (Gradient 100% hexanes to 100% DCM) to yield 1.20 g (4.2 mmol, 84% yield) of the title compound. ^{1}H-NMR (500 MHz; CDCl3): δ 7.64 (d, J = 9.5 Hz, 1H), 7.38 (d, J = 8.4 Hz, 1H), 6.86-6.83 (m, 2H), 6.26 (d, J = 9.5 Hz, 1H), 4.18 (t, J = 5.8 Hz, 2H), 3.61 (t, J = 6.4 Hz, 2H), 2.38-2.33 (m, 2H).

7-(3-azidopropyloxy)coumarin. To a solution of 1.2 g (4.2 mmol) of 7-(3-bromopropyloxy)coumarin in 30 mL DMF was added 1.0 g (15 mmol) of sodium azide. The mixture was stirred at 60°C for 1 hour, at which time TLC showed complete conversion (TLC in 100% DCM). The reaction mixture was diluted in diethyl ether (50 mL) and washed with 3x50 mL 5% aqueous lithium chloride. The ether layer was dried over $MgSO_4$ and evaporated to yield 1.04 g (4.2 mmol, quant.) of faintly yellow solid. 1H-NMR (500 MHz; CDCl3): δ 7.63 (d, J = 9.4 Hz, 1H), 7.37 (dd, J = 8.6, 3.3 Hz, 1H), 6.85-6.81 (m, 2H), 6.25 (dd, J = 9.5, 2.8 Hz, 1H), 4.11 (t, J = 5.9 Hz, 2H), 3.54 (t, J = 6.6 Hz, 2H), 2.09 (quintet, J = 6.2 Hz, 2H). ^{13}C-NMR (151 MHz, CDCl3): δ 161.85, 161.14, 155.87, 143.36, 128.84, 113.30, 112.77, 101.51, 65.14, 48.05, 28.57. HRMS (ESI+) (m/z) for $C_{12}H_{11}N_3O_3$ $[M + H]^+$ calculated: 246.0879, actual 246.0870.

General procedure for the SPAAC synthesis of triazole monomers. A solution of (~10 wt %) aryl azide in toluene (1.1-3.0 equiv.) was added drop-wise to a solution of DIBAC-Br_2 pro-monomer in toluene (10-20 mM). The mixture

was heated to 60°C (5 min – 2 h) and monitored by TLC (Hexanes:EtOAc). When the reaction was complete, the product was concentrated and then purified by column chromatography over a short plug of silica gel (Hexanes:EtOAc). NOTE 1: Unpurified aryl azides or aryl azide reaction mixtures can be used with equal efficacy and give equally high-yield reactions, however purification of the final monomer is slightly more demanding when using impure starting materials. NOTE 2: In all cases, two regiosomers were produced, but showed identical mass spectra if separated by thin layer chromatography. No effort was made to purify on a bulk scale, ratio of products appears to be roughly 2:1 in all cases except **P6** (1:4).

1-(6,11-dibromo-1-(4-methoxyphenyl)-1H-dibenzo[b,f]-[1,2,3]triazolo[4,5-d]azocin-8(9H)-yl)dodecan-1-one(DIBAC-Br$_2$ Methoxyphenyltriazole) (10a). A 10 % w/w solution of pure 1-methoxy-phenyl azide in toluene (2 mL, ~1 mmol) was placed in a screw cap vial containing a solution of compound **9** (300 mg, 0.550 mmol) in toluene (5 mL). The reaction was stirred at 60°C for 30 min, whereupon the mixture was evaporated under reduced pressure and purified via column chromatography in 1:6 EtOAc/*n*-hexanes to yield 350 mg (91%) of pure product (**10a**). M.W.: 720.58 g/mol. ^{1}H-NMR indicated the production of a ~2:1 mixture of regioisomers. Thin layer chromatography (DCM) shows two products. ^{1}H-NMR (Two Regioisomers, 600 MHz; $CDCl_3$): δ 7.70 (m), 7.65 (m), 7.56 (m), 7.48-7.30 (m), 7.10 (dd), 6.95-6.92 (m), 6.73 (d), 6.52 (d), 6.23 (d), 5.97-5.94 (m), 5.54-5.50 (m,), 4.95-4.92 (m,),

4.37 (d, J = 17.3 Hz, 1H), 3.86 (s), 2.39 (s), 2.21 (s,), 1.82-1.78 (m), 1.41-1.00 (m, 21H), 0.86 (t, 3H). ^{13}CNMR (Two Regioisomers, 151 MHz, $CDCl_3$): δ 173.58, 160.32, 160.26, 143.66, 143.04, 142.17, 142.04, 137.81, 135.48, 134.36, 132.81, 132.09, 131.52, 131.29, 131.14, 131.06, 130.94, 130.80, 130.52, 130.26, 129.53, 129.17, 128.36, 126.73, 126.51, 126.34, 124.55, 123.90, 123.48, 123.40, 122.82, 114.92, 114.66, 55.69, 55.65, 54.98, 51.75, 33.99, 33.29, 32.04, 29.72, 29.67, 29.52, 29.44, 29.38, 29.19, 29.13, 24.91, 24.70, 22.82, 14.27.HRMS (ESI+) (m/z) for $C_{34}H_{39}N_4O_2Br_2$ $[M + H]^+$ calculated: 693.1440, actual: 693.1456.

1-(6,11-dibromo-1-(4-(tert-butyl)phenyl)-1H-dibenzo[b,f]-[1,2,3]triazolo[4,5-d]azocin-8(9H)-yl)dodecan-1-one (DIBAC-Br$_2$ (t-Bu)phenyltriazole) (10b). A 10 % w/w solution of pure 4-(*t*-bu)-phenyl azide in toluene (1.1 mL, ~0.60 mmol) was placed in a screw cap vial containing a solution of compound **9** (295 mg, 0.541 mmol) in toluene (5 mL). The reaction was stirred at 60°C for 2 hours, whereupon the mixture was evaporated under reduced pressure and purified via column chromatography in 1:6 EtOAc/*n*-hexanes to yield 362 mg (93%) of product (**10b**). M.W.: 720.58 g/mol; ^{1}H-NMR indicated the production of a ~2:1 mixture of regioisomers. Thin layer chromatography (DCM:Hexanes, 1:1) shows two products. ^{1}H-NMR (Two Regioisomers, 600 MHz; $CDCl_3$): δ 7.70 (d), 7.69 (d), 7.66 (d), 7.65 (d), 7.58-7.55 (m), 7.49-7.31 (m), 7.11 (dd), 6.89 (d), 6.77 (d), 6.55 (d), 6.25 (d), 5.98-5.89 (m), 5.57-5.48 (m), 4.98-4.88 (m) 4.40-4.31 (m), 2.40 (s), 2.22 (s), 1.83-1.77 (m), 1.60-1.56 (m), 1.35-0.96 (m), 0.90-0.82 (t). ^{13}C-NMR (Two Regioisomers, 151 MHz; CDCl3): δ 173.48, 173.43, 152.73,

152.67, 143.6, 143.2, 142.3, 142.0, 137.7, 135.4, 134.9, 134.37, 134.23, 133.9, 133.6, 132.94, 132.76, 132.5, 132.19, 132.11, 131.99, 131.7, 131.48, 131.29, 131.11, 131.07, 130.88, 130.84, 130.74, 130.5, 130.3, 129.1, 128.3, 127.5, 126.94, 126.88, 126.62, 126.46, 125.4, 124.6, 124.2, 123.9, 123.54, 123.46, 122.8, 54.9, 53.0, 51.7, 34.9, 34.7, 34.0, 33.3, 32.0, 31.3, 29.68, 29.62, 29.48, 29.39, 29.33, 29.15, 29.09, 25.2, 24.86, 24.66, 22.8, 14.2 HRMS (ESI+) (m/z) for $C_{37}H_{45}N_4OBr_2$ $[M + H]^+$ calculated: 719.1960, actual: 719.1958.

1-(6,11-dibromo-1-(phenyl)-1H-dibenzo[b,f][1,2,3]triazolo[4,5-d]azocin-8(9H)-yl)dodecan-e-one (DIBAC-Br$_2$ phenyltriazole) (10c). A 10 % w/w solution of phenyl azide (~80% purity) in toluene (2 mL, ~1 mmol) was placed in a screw cap vial containing a solution of compound **9** (185 mg, 0.340 mmol) in toluene (5 mL). The reaction was stirred at 60°C for 1 h, whereupon the mixture was evaporated under reduced pressure and purified via column chromatography in 1:6 EtOAc/Hexanes to yield 174 mg (77%) of pure product (**10c**). M.W.: 662.13 g/mol; ^{1}H-NMR indicated the production of a ~2:1 mixture of regioisomers. Thin layer chromatography (DCM) shows two products. ^{1}H-NMR (Two Regioisomers, 600 MHz; $CDCl_3$): δ 7.72-7.70 (d), 7.67-7.65 (m), 7.59-7.57 (m), 7.50-7.29 (m), 7.19-7.03 (m), 6.72-6.71 (d), 6.52-6.50 (m), 6.26 (dd), 5.95 (d), 5.56-5.51 (m), 4.95 (d), 4.45-4.42 (d), 4.39 (d), 2.41 (m), 2.22 (m), 1.89-1.79 (m), 1.72 (m), 1.56 (m), 1.41 (m), 1.34-0.97 (m), 0.90-0.84 (m). ^{13}C NMR (Two Regioisomers, 151 MHz; $CDCl_3$): δ 173.49, 173.42, 143.5, 143.1, 142.3, 141.9, 137.7, 136.4, 136.1, 135.4, 134.8, 134.25, 134.13, 133.0, 132.7, 132.5, 132.05,

131.93, 131.55, 131.38, 131.24, 131.04, 130.97, 130.83, 130.67, 130.4, 130.1, 129.80, 129.70, 129.65, 129.46, 129.41, 129.36, 129.0, 128.2, 127.2, 126.7, 125.19, 125.02, 124.96, 124.6, 123.9, 123.5, 123.2, 122.8, 54.9, 52.9, 51.6, 33.9, 33.2, 31.9, 29.72, 29.57, 29.53, 29.46, 29.38, 29.30, 29.25, 29.22, 29.06, 28.99, 25.1, 24.8, 24.6, 22.7, 14.1 HRMS (ESI+) (m/z) for $C_{33}H_{37}N_4OBr_2$ $[M + H]^+$ calculated: 663.1334, actual: 663.1333.

1-(6,11-dibromo-1-(4-nitrophenyl)-1H-dibenzo[b,f][1,2,3]triazolo[4,5-d]azocin-8(9H)-yl)dodecan-e-one (DIBAC-Br$_2$ Nitrophenyltriazole) (10d). A 10 % w/w solution of 1-azido-4-nitrobenzene in toluene (903 mg, 0.501 mmol) was placed in a screw cap vial containing a solution of compound **9** (200 mg, 0.367 mmol) in toluene (5 mL). The reaction was stirred at 60°C for 1 hour, whereupon the mixture was evaporated under reduced pressure and purified via column chromatography in 1:49 EtOAc/CH_2Cl_2 to yield 205 mg (79%) of pure product (**10d**). M.W.: 709.47 da; ^{1}H-NMR indicated the production of a ~2:1 mixture of regioisomers. Thin layer chromatography (DCM) shows two products. ^{1}H-NMR (Two Regioisomers, 600 MHz; $CDCl_3$): δ 8.36-8.34 (m), 7.95-7.94 (m), 7.75-7.64 (m), 7.54-7.52 (m), 7.50 (d), 7.40-7.38 (m), 7.17-7.16 (m), 6.74 (d), 6.48 (d), 6.26 (d), 5.59-5.56 (m), 5.01-4.97 (m), 4.44 (d), 4.15 (d), 2.47-2.42 (m), 2.25-2.20 (m), 1.87-1.81 (m), 1.60-1.57 (m), 1.43-1.00 (m), 0.88 (t). ^{13}C-NMR (Two Regioisomers, 151 MHz; $CDCl_3$): δ 173.7, 147.88, 147.74, 143.9, 143.6, 142.9, 142.1, 141.1, 140.8, 138.0, 135.4, 135.0, 134.2, 133.4, 133.0, 132.5, 131.8, 131.6, 131.22, 131.14, 131.07, 130.70, 130.61, 130.44, 129.8, 126.6, 126.1, 125.76,

125.57, 125.36, 125.33, 125.27, 125.1, 124.5, 124.3, 123.3, 122.4, 54.9, 51.7, 34.0, 33.2, 32.0, 29.67, 29.64, 29.59, 29.57, 29.46, 29.38, 29.34, 29.29, 29.13, 29.06, 24.8, 24.6, 22.8, 14.2 HRMS (ESI+) (m/z) for $C_{33}H_{36}N_5O_3Br_2$ $[M + H]^+$ calculated: 708.1185, actual: 708.1210.

1-(6,11-dibromo-1-(pyrenyl)-1H-dibenzo[b,f][1,2,3]triazolo[4,5-d]azocin-8(9H)-yl)dodecan-e-one (DIBAC-Br$_2$ pyrenyltriazole) (10e). A 10 % w/w solution of 1-azido-pyrene in toluene (0.6 mL, 0.300 mmol) was placed in a 100 mL round bottom flask containing a solution of compound **9** (65 mg, 0.120 mmol) in toluene (50 mL). The reaction was stirred at 60°C for 30 min, whereupon the mixture was evaporated under reduced pressure and purified via column chromatography in 1:4 EtOAc/hexanes to yield 60 mg (64%) of pure product **(10e)**. ^{1}H-NMR indicated the production of a ~2:1 mixture of regioisomers. Thin layer chromatography (DCM) shows two products. (Two Regioisomers, 600 MHz; $CDCl_3$): δ 8.37-8.09 (m), 7.96 (dd), 7.84-7.83 (m), 7.79-7.74 (m), 7.67 (d), 7.59-7.55 (m), 7.48-7.45 (m), 7.40 (s), 7.33-7.31 (s), 7.07 (d), 6.94 (dd), 6.74 (d), 6.50-6.47 (s), 6.39 (d), 5.98 (d), 5.60 (d), 5.01 (d), 4.50 (d), 4.43 (d), 2.56-2.49 (s), 2.35-2.29 (s), 1.95 (m), 1.89-1.75 (m), 1.55 (m), 1.47 (m), 1.26-1.13 (m), 0.85-0.81 (t) HRMS (ESI+) (m/z) for $C_{43}H_{40}N_4OBr_2$ $[M + H]^+$ calculated: 787.1647, actual: 787.1649.

1-(6,11-dibromo-3-(7-propyloxycoumarin)-1*H*-dibenzo[*b,f*][1,2,3]-triazolo[4,5-*d*]azocin-8(9*H*)-yl)dodecan-e-one (DIBAC-Br$_2$ 7-propyloxy-coumarin triazole) (10f) 7-(3-azidopropyloxy)coumarin (300 mg, 1.2 mmol) in

toluene (10 mL) was placed in a 100 mL round bottom flask. Compound **9** (550 mg, 1 mmol) was added. The reaction was stirred at 60°C for 30 min, whereupon the mixture was evaporated under reduced pressure and purified via column chromatography in 1:2 EtOAc/hexanes to yield 620 mg (80%) of pure product **(10e)**. ^{1}H-NMR indicated the production of a ~4:1 mixture of regioisomers. Thin layer chromatography (1:2 EtOAc:Hexanes) shows two products. ^{1}H-NMR (Two Regioisomers, 600 MHz; $CDCl_3$): δ 7.65-7.27 (m), 7.03 (d), 6.87 (d), 6.72-6.70 (m), 6.26 (q), 6.12 (d, 1H), 6.02 (d), 5.45 (d), 4.66 (m,), 4.45 (m), 4.33 (m), 4.17-4.05 (m), 3.98-3.84 (m), 2.72 (m), 2.58 (m), 2.48 (m), 2.26 (m), 2.08 (s,), 1.74 (m), 1.56 (m Hz, 1H), 1.44-1.00 (m), 0.89-0.83 (m).^{13}C NMR (Two Regioisomers, 151 MHz; $CDCl_3$): δ 173.3, 161.43, 161.26, 155.9, 155.7, 143.45, 143.29, 142.1, 141.7, 137.9, 135.2, 134.8, 134.3, 133.7, 132.80, 132.70, 132.3, 131.9, 131.6, 131.07, 130.90, 130.82, 130.60, 130.46, 129.7, 129.1, 128.89, 128.73, 127.5, 126.6, 125.1, 124.04, 123.85, 122.84, 122.76, 113.8, 113.45, 113.37, 112.89, 112.74, 112.4, 112.0, 102.03, 101.85, 65.5, 65.1, 63.8, 55.0, 52.5, 51.1, 45.7, 45.28, 45.13, 34.17, 34.00, 33.1, 32.0, 30.2, 29.82, 29.71, 29.56, 29.52, 29.46, 29.40, 29.21, 29.16, 28.8, 25.02, 24.97, 24.6, 22.8, 14.2 HRMS (ESI+) (m/z) for $C_{39}H_{42}N_4O_4Br_2$ $[M + H]^+$ calculated: 789.1651, actual: 789.1664.

5.4.4. Polymerization Procedure (Compounds P1-P6)

Respective 10 % w/w solutions of **10a-10e** in toluene (0.1 mmol) were combined with a 10 % w/w solution of 2,2'-(9,9-didodecyl-9*H*-fluorene-2,7-diyl)-bis-(1,3,2-dioxaborinane) in toluene (0.102 mmol) in a Schlenk tube, along with

K_2CO_3 (56 mg), Aliquat 336 (scant drop), and H_2O (2.5 mL). Toluene (1 mL) was used to rinse the sides of the Schlenk tube before degassing the mixture via bubbling argon under sonication for 15 min. PEPPSI™-IPr (2-4 mg) was added to the degassed mixture, whereupon it was stirred at 60°C under an Ar atmosphere for 2-8 hours, monitoring by GPC. The organic layer was extracted from the Schlenk tube via pasteur pipet, and precipitated into cold methanol (200 mL). The precipitate was filtered with a 200 nm Teflon membrane and rinsed with cold methanol, followed by cold ethanol. The polymer was dried under reduced pressure.

alt-polydidodecylfluorene-co-DIBAC methoxyphenyltriazole (P1) Yield: 97 mg (80%), gray powder. M_w:8.3 kDa (GPC): ^{1}H-NMR spectrum in Appendix 3.

alt-polydidodecylfluorene-co-DIBAC methoxyphenyltriazole (P2) Yield: 60 mg (60%) of grey product (**P2b**) M_w: 8.3 kDa (GPC), ^{1}H-NMR spectrum in Appendix 3.

alt-polydidodecylfluorene-co-DIBAC phenyltriazole (P3) Yield: 80 mg (60%) light brown solid (**P3**). M_w: 5.7 kDa (GPC). ^{1}H-NMR spectrum in Appendix 3.

alt-polydidodecylfluorene-co-DIBAC nitrophenyltriazole (P4) Yield: 123 mg (83%) of off white product **(P4)**. M_w: 7.4 kDa (GPC). ^{1}H-NMR spectrum in Appendix 3.

alt-polydidodecylfluorene-co-DIBAC pyrenyltriazole (P5) Yield: 60 mg (82%), light brown product (**P5**). M_w: 5.0 kDa (GPC). ^{1}H- spectrum in Appendix 3.

alt-polydidodecylfluorene-co-DIBAC (7-propyloxycoumarin)triazole (P6) Yield: 145 mg (55%), light brown product (**P5**). M_w: 4.1kDa (GPC). ^{1}H-NMR spectrum below.

5.4.5. Computational Methods

All calculations were performed using Gamess[67] (1 May 2013 – R1, 64-bit Linux), run in Mac OSX 10.8 on a desktop computer equipped with an Intel i5-3570k processor. The B3LYP density functional and 6-31G(d) basis set were used all DFT calculations. For more complicated structures the semi-empirical Parametric Method 3 (PM3)[85] was used.

Primarily, geometry optimizations were performed on a repeat unit consisting of a methyl amide analog of the DIBAC-phenyltriazole and dimethyl fluorene co-monomer (Appendix: Figures A3.19, A3.20). Calculation of the full Hessian (and thereby vibrational frequencies) proved too computationally demanding for the dimeric unit using the B3LYP functional, thus the structure was re-optimized and frequencies computed with PM3 to confirm the presence of a minimum.

In order to confirm this geometry, a model monomer was constructed with a methyl substituted DIBAC-triazole and both geometry optimization and the

calculation of the full Hessian were performed using DFT/B3LYP with the 6-31G(d) basis set, confirming the structure as a minimum.

Finally, PM3 geometry/frequency calculations were used to determine the general structure for a tetrameric unit.

Result of Computations: Starting from 2 different geometries, a common stationary point was located by iterative 20-step optimizations (2-5 iterations were required). As computing the harmonic vibrational frequencies using B3LYP proved too computationally demanding, the geometry was re-optimized with PM3 from this minimum, and the vibrational frequencies calculated. Both structures are displayed in Appendix 3 (Figure A3.20 (a, b)).

Using both methods, the fluorene unit and DIBAC-triazole units have significant torsional angles, as expected. The B3LYP geometry shows a dihedral angle of 38 degrees, PM3 calculates 49 degrees – even though PM3 is known to over-estimate π-delocalization energies and favor planar structures. [86] In general, the exact angle should be regarded with a degree of skepticism, as dimers in vacuum are unlikely to represent a "true" conformation of the molecules. Nonetheless, these results are highly suggestive of a non-planar geometry akin to polyfluorene, or poly(fluorene-co-phenylene). The fluorene unit has a planar geometry

When the fluorene and phenyl groups were removed and the geometry/frequencies recalculated using the B3LYP functional, the general shape of the DIBAC-triazole remained (Appendix 3, Figure A3.20c), thus helping us

corroborate the shape of the DIBAC unit, and to confirm it as a minimum by computing the full Hessian and confirming that no imaginary frequencies were present.

Moreover, the located minimum was compared to the crystal structure of a known analog.[87] The structures of the DIBAC triazole portions are closely matched – suggesting the located structure is akin to the global minimum. (Appendix 3, Figure A3.19d,e). The 2D representations of the optimized structures are shown in Appendix 3 (Figure A3.19).

Finally, a tetramer (2-repeat units) was optimized with PM3. The structure is interesting, showing a very non-linear structure that likely has several possible conformations. (Appendix 3, Figure A3.18) Detailed log files are also available in Appendix 3.

5.5. References

(1) Leclerc, M.; Morin, J.-F. *Design and Synthesis of Conjugated Polymers*; John Wiley & Sons, 2010.
(2) *Conjugated Polymers: Theory, Synthesis, Properties, and Characterization*; Skotheim, T. A.; Reynolds, J., Eds.; 3rd ed.; CRC Press: Boca Raton, 2007.
(3) Skotheim, T. A.; Reynolds, J. *Conjugated Polymers: Processing and Applications*; 3rd ed.; Taylor & Francis: Boca Raton, 2006.
(4) Heeger, A. J. *Chem. Soc. Rev.* **2010**, *39*, 2354.
(5) Li, J.; Grimsdale, A. C. *Chem. Soc. Rev.* **2010**, *39*, 2399.
(6) Donat-Bouillud, A.; Lévesque, I.; Tao, Y.; D'Iorio, M.; Beaupré, S.; Blondin, P.; Ranger, M.; Bouchard, J.; Leclerc, M. *Chem. Mater.* **2000**, *12*, 1931–1936.
(7) Facchetti, A. *Chem. Mater.* **2011**, *23*, 733–758.
(8) Sirringhaus, H. *Science* **1998**, *280*, 1741–1744.
(9) McQuade, D. T.; Pullen, A. E.; Swager, T. M. *Chem. Rev.* **2000**, *100*, 2537–2574.
(10) Beaujuge, P. M.; Reynolds, J. R. *Chem. Rev.* **2010**, *110*, 268–320.
(11) Chiang, C.; Fincher, C.; Park, Y.; Heeger, A.; Shirakawa, H.; Louis, E.; Gau, S.; Macdiarmid, A. *Phys. Rev. Lett.* **1977**, *39*, 1098–1101.
(12) Moore, J. S.; Gorman, C. B.; Grubbs, R. H. *J. Am. Chem. Soc.* **1991**, *113*, 1704–1712.
(13) Rehahn, M.; Schlüter, A.-D.; Wegner, G.; Feast, W. J. *Polymer* **1989**, *30*, 1060–1062.
(14) Burroughes, J. H.; Bradley, D. D. C.; Brown, A. R.; Marks, R. N.; Mackay, K.; Friend, R. H.; Burns, P. L.; Holmes, A. B. *Nature* **1990**, *347*, 539–541.
(15) D'Aprano, G.; Leclerc, M.; Zotti, G.; Schiavon, G. *Chem. Mater.* **2002**, *7*, 33–42.
(16) D'Aprano, G.; Leclerc, M.; Zotti, G. *Macromolecules* **1992**, *25*, 2145–2150.
(17) Leclerc, M. *J. Polym. Sci. A Polym. Chem.* **2001**, *39*, 2867–2873.
(18) Leclerc, M. *Adv. Mater.* **1999**, *11*, 1491–1498.
(19) Leclerc, M.; Faid, K. *Adv. Mater.* **1997**, *9*, 1087–1094.
(20) McCullough, R. D. *Adv. Mater.* **1998**, *10*, 93–116.
(21) Osaka, I.; McCullough, R. D. *Acc. Chem. Res.* **2008**, *41*, 1202–1214.
(22) Morin, J.-F.; Leclerc, M.; Adès, D.; Siove, A. *Macromol. Rapid Commun.* **2005**, *26*, 761–778.
(23) Hirsch, A. *Angew. Chem. Int. Ed.* **2002**, *41*, 1853–1859.
(24) Star, A.; Liu, Y.; Grant, K.; Ridvan, L.; Stoddart, J. F.; Steuerman, D. W.; Diehl, M. R.; Boukai, A.; Heath, J. R. *Macromolecules* **2003**, *36*, 553–560.

(25) Rice, N. A.; Soper, K.; Zhou, N.; Merschrod, E.; Zhao, Y. *Chem. Commun.* **2006**, 4937.
(26) Cheng, F.; Adronov, A. *Chem. Eur. J.* **2006**, *12*, 5053–5059.
(27) Cheng, F.; Imin, P.; Maunders, C.; Botton, G.; Adronov, A. *Macromolecules* **2008**, *41*, 2304–2308.
(28) Nish, A.; Hwang, J.-Y.; Doig, J.; Nicholas, R. J. *Nat. Nanotechnol.* **2007**, *2*, 640–646.
(29) Hwang, J.-Y.; Nish, A.; Doig, J.; Douven, S.; Chen, C.-W.; Chen, L.-C.; Nicholas, R. J. *J. Am. Chem. Soc.* **2008**, *130*, 3543–3553.
(30) Lee, H. W.; Yoon, Y.; Park, S.; Oh, J. H.; Hong, S.; Liyanage, L. S.; Wang, H.; Morishita, S.; Patil, N.; Park, Y. J.; Park, J. J.; Spakowitz, A.; Galli, G.; Gygi, F.; Wong, P. H. S.; Tok, J. B.-H.; Kim, J. M.; Bao, Z. *Nat. Comm.* **2011**, *2*, 541.
(31) Lemasson, F. A.; Strunk, T.; Gerstel, P.; Hennrich, F.; Lebedkin, S.; Barner-Kowollik, C.; Wenzel, W.; Kappes, M. M.; Mayor, M. *J. Am. Chem. Soc.* **2011**, *133*, 652–655.
(32) Imin, P.; Imit, M.; Adronov, A. *Macromolecules* **2012**, *45*, 5045–5050.
(33) Lemasson, F.; Berton, N.; Tittmann, J.; Hennrich, F.; Kappes, M. M.; Mayor, M. *Macromolecules* **2012**, *45*, 713–722.
(34) van Haare, J. A. E. H.; Havinga, E. E.; van Dongen, J. L. J.; Janssen, R. A. J.; Cornil, J.; Brédas, J. L. *Chem. Eur. J.* **1998**, *4*, 1509–1522.
(35) Sirringhaus, H.; Brown, P. J.; Friend, R. H.; Nielsen, M. M.; Bechgaard, K.; Langeveld-Voss, B. M. W.; Spiering, A. J. H.; Janssen, R. A. J.; Meijer, E. W.; Herwig, P.; de Leeuw, D. M. *Nature* **1999**, *401*, 685–688.
(36) Welch, G. C.; Bazan, G. C. *J. Am. Chem. Soc.* **2011**, *133*, 4632–4644.
(37) Welch, G. C.; Coffin, R.; Peet, J.; Bazan, G. C. *J. Am. Chem. Soc.* **2009**, *131*, 10802–10803.
(38) Zalar, P.; Kuik, M.; Henson, Z. B.; Woellner, C.; Zhang, Y.; Sharenko, A.; Bazan, G. C.; Nguyen, T.-Q. *Adv. Mater.* **2013**, *26*, 724–727.
(39) Zalar, P.; Henson, Z. B.; Welch, G. C.; Bazan, G. C.; Nguyen, T.-Q. *Angew. Chem. Int. Ed.* **2012**, *51*, 7495–7498.
(40) Wu, P.; Feldman, A. K.; Nugent, A. K.; Hawker, C. J.; Scheel, A.; Voit, B.; Pyun, J.; Frechet, J. M. J.; Sharpless, K. B.; Fokin, V. V. *Angew. Chem. Int. Ed.* **2004**, *43*, 3928–3932.
(41) Quémener, D.; Davis, T. P.; Barner-Kowollik, C.; Stenzel, M. H. *Chem. Commun.* **2006**, 5051.
(42) Laurent, B. A.; Grayson, S. M. *J. Am. Chem. Soc.* **2006**, *128*, 4238–4239.
(43) Tsarevsky, N. V.; Bencherif, S. A.; Matyjaszewski, K. *Macromolecules* **2007**, *40*, 4439–4445.
(44) Golas, P. L.; Matyjaszewski, K. *Chem. Soc. Rev.* **2010**, *39*, 1338.
(45) Iha, R. K.; Wooley, K. L.; Nyström, A. M.; Burke, D. J.; Kade, M. J.; Hawker, C. J. *Chem. Rev.* **2009**, *109*, 5620–5686.
(46) Sumerlin, B. S.; Vogt, A. P. *Macromolecules* **2010**, *43*, 1–13.
(47) Huisgen, R. *Angew. Chem. Int. Ed.* **1963**, *2*, 565–598.

(48) Rostovtsev, V.; Green, L.; Fokin, V.; Sharpless, K. *Angew. Chem. Int. Ed.* **2002**, *41*, 2596.
(49) Baskin, J. M.; Prescher, J. A.; Laughlin, S. T.; Agard, N. J.; Chang, P. V.; Miller, I. A.; Lo, A.; Codelli, J. A.; Bertozzi, C. R. *Proc. Natl. Acad. Sci. U. S. A.* **2007**, *104*, 16793–16797.
(50) Becer, C. R.; Hoogenboom, R.; Schubert, U. S. *Angew. Chem. Int. Ed.* **2009**, *48*, 4900–4908.
(51) van Berkel, S. S.; Dirks, A. T. J.; Meeuwissen, S. A.; Pingen, D. L. L.; Boerman, O. C.; Laverman, P.; van Delft, F. L.; Cornelissen, J. J. L. M.; Rutjes, F. P. J. T. *ChemBioChem* **2008**, *9*, 1805–1815.
(52) Gonzaga, F.; Sadowski, L. P.; Rambarran, T.; Grande, J.; Adronov, A.; Brook, M. A. *J. Polym. Sci. A Polym. Chem.* **2013**, *51*, 1272–1277.
(53) Gonzaga, F.; Yu, G.; Brook, M. A. *Chem. Commun.* **2009**, 1730.
(54) Sletten, E. M.; Bertozzi, C. R. *Angew. Chem. Int. Ed.* **2009**, *48*, 6974–6998.
(55) Sletten, E. M.; Bertozzi, C. R. *Acc. Chem. Res.* **2011**, *44*, 666–676.
(56) Debets, M. F.; van Berkel, S. S.; Dommerholt, J.; Dirks, A. T. J.; Rutjes, F. P. J. T.; van Delft, F. L. *Acc. Chem. Res.* **2011**, *44*, 805–815.
(57) Debets, M. F.; van Berkel, S. S.; Schoffelen, S.; Rutjes, F. P. J. T.; van Hest, J. C. M.; van Delft, F. L. *Chem. Commun.* **2010**, *46*, 97.
(58) Kuzmin, A.; Poloukhtine, A.; Wolfert, M. A.; Popik, V. V. *Bioconj. Chem.* **2010**, *21*, 2076–2085.
(59) Wei, Y.; Chen, C.-T. *J. Am. Chem. Soc.* **2007**, *129*, 7478–7479.
(60) Wittig, G.; Fischer, S. *Chem. Ber.* **1972**, *105*, 3542–3552.
(61) Devadoss, C.; Bharathi, P.; Moore, J. S. *J. Am. Chem. Soc.* **1996**, *118*, 9635–9644.
(62) Haussler, M.; Zheng, R.; Lam, J. W. Y.; Tong, H.; Dong, H.; Tang, B.-Z. *J. Phys. Chem. B* **2004**, *108*, 10645–10650.
(63) Suzuki, A. *Proc. Jpn. Acad., Ser. B* **2004**, *80*, 359–371.
(64) Organ, M. G.; Avola, S.; Dubovyk, I.; Hadei, N.; Kantchev, E. A. B.; O'Brien, C. J.; Valente, C. *Chem. Eur. J.* **2006**, *12*, 4749–4755.
(65) Ranger, M.; Leclerc, M. *Can. J. Chem.* **1998**, *76*, 1571–1577.
(66) Knaapila, M.; Almásy, L.; Garamus, V. M.; Ramos, M. L.; Justino, L. L. G.; Galbrecht, F.; Preis, E.; Scherf, U.; Burrows, H. D.; Monkman, A. P. *Polymer* **2008**, *49*, 2033–2038.
(67) Schmidt, M. W.; Baldridge, K. K.; Boatz, J. A.; Elbert, S. T.; Gordon, M. S.; Jensen, J. H.; Koseki, S.; Matsunaga, N.; Nguyen, K. A.; Su, S.; Windus, T. L.; Dupuis, M.; Montgomery, J. A. *J Comput Chem* **1993**, *14*, 1347–1363.
(68) Becke, A. D. *J. Chem. Phys.* **1993**, *98*, 5648–5652.
(69) Lee, C.; Yang, W.; Parr, R. G. *Phys. Rev. B* **1988**, *37*, 785–789.
(70) Hehre, W. J. *J. Chem. Phys.* **1972**, *56*, 2257.
(71) Williams, R. T.; Bridges, J. W. *J. Clin. Pathol.* **1964**, *17*, 371–394.

(72) Hou, J.; Huo, L.; He, C.; Yang, C.; Li, Y. *Macromolecules* **2006**, *39*, 594–603.
(73) Scherf, U.; Neher, D. *Polyfluorenes*; Springer: Berlin, 2008; Vol. 212.
(74) Scherf, U.; Gutacker, A.; Koenen, N. *Acc. Chem. Res.* **2008**, *41*, 1086–1097.
(75) Gnanaguru, K.; Ramasubbu, N.; Venkatesan, K.; Ramamurthy, V. *J. Org. Chem* **1985**, *50*, 2337–2346.
(76) Wijsboom, Y. H.; Sheynin, Y.; Patra, A.; Zamoshchik, N.; Vardimon, R.; Leitus, G.; Bendikov, M. *J. Mater. Chem.* **2011**, *21*, 1368–1372.
(77) Zhu, W.; Ma, D. *Chem. Commun.* **2004**, 888–889.
(78) Thompson, W. J.; Anderson, P. S.; Britcher, S. F.; Lyle, T. A.; Thies, J. E.; Magill, C. A.; Varga, S. L.; Schwering, J. E.; Lyle, P. A.; Christy, M. E. *J. Med. Chem.* **1990**, *33*, 789–808.
(79) Wilkening, I.; del Signore, G.; Hackenberger, C. P. R. *Chem. Commun.* **2011**, *47*, 349–351.
(80) Liu, C.; Li, T.; Rosi, N. L. *J. Am. Chem. Soc.* **2012**, *134*, 18886–18888.
(81) Becerril, H. A.; Miyaki, N.; Tang, M. L.; Mondal, R.; Sun, Y.-S.; Mayer, A. C.; Parmer, J. E.; McGehee, M. D.; Bao, Z. *J. Mater. Chem.* **2009**, *19*, 591–593.
(82) Lee, J.; Hwang, E.; Lee, E.; Seo, S.; Lee, H. *Chem. Eur. J.* **2012**, *18*, 5155–5159.
(83) Babu, P.; Sangeetha, N. M.; Vijaykumar, P.; Maitra, U.; Rissanen, K.; Raju, A. R. *Chem. Eur. J.* **2003**, *9*, 1922–1932.
(84) Xie, S.-S.; Wang, X.-B.; Li, J.-Y.; Yang, L.; Kong, L.-Y. *Eur. J. Med. Chem.* **2013**, *64*, 540–553.
(85) Stewart, J. J. P. *J. Comput. Chem.* **1989**, *10*, 209–220.
(86) Dávila, L. Y. A.; Caldas, M. J. *J. Comput. Chem.* **2002**, *23*, 1135–1142.
(87) Cruchter, T.; Harms, K.; Meggers, E. *Chem. Eur. J.* **2013**, 19, 16682-16689.

Chapter 6: Metal-Free Reduction of Secondary and Tertiary N-Phenyl Amides by Tris(pentafluorophenyl)boron Catalyzed Hydrosilylation

Ryan C. Chadwick, Vladimir Kardelis, Philip Lim, Alex Adronov*

Department of Chemistry and Chemical Biology,
McMaster University,
1280 Main St. W.,
Hamilton, Ontario, L8S 4M1 (Canada)

Reproduced with permission from The Journal of Organic Chemistry, 2014, 79, 7728-7733. DOI: 10.1021/jo501299j

The experimental planning and design was performed by Ryan Chadwick. The synthesis was performed primarily by Vladimer Kardelis with contributions from Ryan Chadwick and Phillip Lim. The characterization was performed by Vladimir Kardelis and Ryan Chadwick

Graphical Abstract:

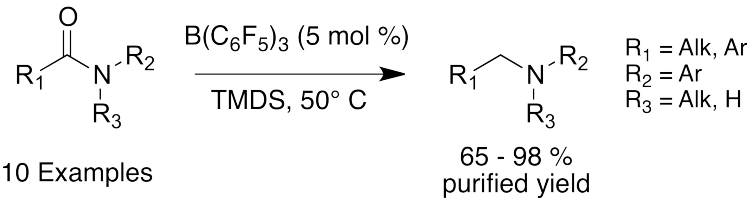

Abstract:

Tris(pentafluorophenyl)boron $B(C_6F_5)_3$ is an effective catalyst for the hydrosilylative reduction of tertiary and N-phenyl secondary amides. It allows for the mild reduction of a variety of these amides in near quantitative yield, with minimal purification, at low temperatures, and with short reaction times. This reduction shows functional group tolerance for alkenes, nitro groups and aryl halides including aryl iodides.

6.1. Introduction

Mild reduction of the amide functionality to the corresponding amine is a valuable transformation in organic synthesis. Traditionally, the most common procedures for the transformation of amides to amines have involved the use of metal hydride reagents in stoichiometric amounts.[1] These reagents are not generally selective and result in by-product mixtures that are difficult to purify. More recently, catalytic reductions of amides have received significant attention. Although ideal, reports of direct catalytic hydrogenation of amides to amines are quite rare, and limited in scope and versatility. Most early reports utilized very harsh conditions and were substrate specific.[2] A 2007 report by Núñez Magro *et al*. utilized a ruthenium-triphos catalyst to achieve a general reduction of amides, but the reaction required high temperatures (164°C) and moderately high pressures (40 bar H_2).[3] More recently, a lower pressure (10 mbar), but higher temperature (200°C) optimized protocol that is effective for reducing secondary and aryl amides has been reported.[4] Burch *et. al*. succeeded in developing a reduction that operated at lower temperatures and pressures (120°C, 20 bar, H_2), but the substrate scope was not widely explored.[5] Most recently, Stein et. al. developed a Pt/Re system that is general and high yielding, but still requires moderately high temperatures (160°C, 30 bar H_2).[2] In addition, these reductions generally exhibit poor functional group tolerance, precluding the presence of alkenes and other easily hydrogenated functionalities. It should also be noted that

mild methods are available to reduce amides to other functionalities such as alcohols[6] and aldehydes.[7]

In contrast, catalytic hydrosilylation as a methodology for amide reduction has received significant recent attention, and a number of reports utilizing transition metal catalysts (Rh,[8] Mn,[9] Ru,[9-11] Os,[9] Ir, [9,12] Pt,[9,13] Pd,[9] Re,[9] Fe,[14-16] In[17]) have appeared. However, many of these catalysts are expensive, and reaction conditions involve high temperatures that decrease compatibility with thermally-sensitive functional groups. More recently, Beller and co-workers have developed amide reduction methods using Cu,[18] Fe,[15] and Zn[19,20] containing Lewis acids that overcome most of the limitations of previous methods. For example, the reduction of a wide variety of secondary and tertiary amides was demonstrated with remarkable substrate scope and functional group tolerance using $Zn(OTf)_2$.[19]

Alternatively, the state-of-the-art "metal-free" method relies on the use of triflic anhydride and "Hantzsch" ester to facilitate the reduction.[21] This method is remarkable, resulting in high yields of amine without the need for column chromatography. Charette and co-workers demonstrated the utility of this approach with both tertiary[21] and secondary[22] amides, which allowed formation of imines, amines, or aldehydes through control of the workup procedure following formation of the intermediate iminium triflate ion.[22] While synthetically ideal from a control and tolerance perspective, this procedure requires expensive

cofactors, highly reactive and expensive triflic anhydride, and cryogenic temperatures, making it somewhat onerous.

Recently, we attempted to reduce the secondary amides **1** and **2** (Scheme 6.1) by a number of conventional methods. However, the combination of functional groups within these structures made it difficult to achieve high-yielding reduction.[23] In our attempts, $LiAlH_4$ rapidly dehalogenated the aryl halide groups, while DIBAL-H allowed the reduction of the dibromide in modest yield (ca. 50%), but also dehalogenated the diiodide. Surprisingly, *in situ* generated alane (AlH_3) reduced the double bond. Attempts to use borohydrides or boranes failed, either due to insufficient reactivity or to reduction of the alkene functionality. We thus turned to the use of $Zn(OTf)_2$ and tetramethyldisiloxane (TMDS) in toluene, as developed by Beller and co-workers.[19] These conditions were effective for the reduction of both **1** and **2**, but required unusually high temperatures. No reduction was observed at 110°C (over 3 days), and even at elevated temperatures of 130°C, reaction times were long (48 h) and the use of a high-pressure vessel was required. Attempts to reduce the reaction time by heating to 150°C drastically reduced the yield. Additionally, we hypothesize that catalyst decomposition occurred during the course of the reaction (some black precipitate was produced at high temperature), resulting in partial dehalogenation of the substrate and, although yields were acceptable (ca. 80%), purification from these dehalogenated side products was generally difficult.

To circumvent these issues, we turned our attention to other, more powerful Lewis acids for this hydrosilylative reduction. Tris(pentaflurophenyl)boron ($B(C_6F_5)_3$) is a powerful Lewis acid, having activity intermediate to BCl_3 and BF_3, yet is relatively water stable.[24-27] Piers and colleagues have described the use of this catalyst for the hydrosilylation of many functional groups, including alcohols and ethers,[28] carbonyl groups,[29-31] as well as imines and nitriles.[27,32,33] In addition, it has been shown to be particularly effective for the silylation of various alcohols,[34] as well as the condensation of hydrosilanes and alkoxysilanes to produce branched and linear silicones with well-defined structures (Piers-Rubinsztajn reaction).[35-39] It is also capable of a rapid cross-linking reaction as an alternative room-temperature vulcanization method for making silicone rubbers and silicone foams.[40] However, to the best of our knowledge, only one report exists in the literature detailing the use of $B(C_6F_5)_3$ for the hydrosilylative reduction of amides.[41] This report utilized diphenylsilane as the reducing agent with amides derived from phenyl acetic acid. Considering the vast literature on the reduction of imines, nitriles and carbonyl groups with $B(C_6F_5)_3$, including in-depth discussions of the reduction mechanism,[27,29,32,33] we found it surprising that the scope of the corresponding amide reduction has not been explored, nor was the reaction protocol optimized.[41]

6.2. Results and Discussion

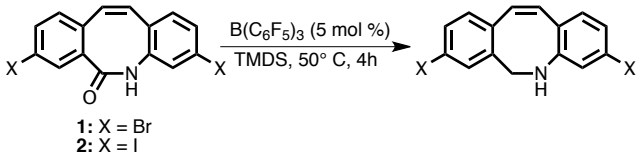

Scheme 6.1: The reduction of model amides **1**, and **2**.

In our experiments, we rapidly discovered that the use of 5 mol % $B(C_6F_5)_3$ as a substitute for $Zn(OTf)_2$ in the reduction of **1** and **2** to the corresponding amines proceeded in near quantitative yield at mild temperatures (50 °C, Table 6.1). The use of less catalyst (1-2 mol %), prevented complete reaction in a reasonable amount of time, while the addition of more catalyst (10 mol %) decreased the reaction time markedly, to less than 1 hour (though 5 % was always enough to ensure complete conversion). It is known that $B(C_6F_5)_3$ forms complexes with imine and amine reagents, and we expect the product poisons the catalyst to some degree, dramatically slowing the reaction when low catalyst loading is used.[42] Most notably, when sufficient catalyst quantities are present, no side-products appear to be produced, and purification requires only standard flash chromatographic purification to remove excess silane, spent siloxane, and the residual boron catalyst.

As this method was mild, rapid, and capable of cleanly reducing amides **1** and **2**, we set out to investigate its scope. The functional group tolerance of $B(C_6F_5)_3$ is well established,[29,30,34,42] so our primary aim was to determine the structural variability of amides that could be reduced by this methodology. The

structures of the different amides that were attempted, along with the corresponding amines, are presented in Table 6.1.

Generally, this method was capable of reducing N-phenyl amides in excellent yield (Table 6.1, entries 1-7), and was also effective at reducing tertiary benzyl amides (Table 6.1, entry 8). These substrates were all reduced in high yield in 4 hours or less. The reaction rate for these substrates appeared to be primarily controlled by their solubility. Entries 1 and 6 involved amide structures that were poorly soluble in toluene, and therefore required a 4-hour reaction time to reach completion. The other N-phenyl amides in the first 7 entries of Table 6.1 required 1.5 h or less at 50 °C. The presence of halogens, or electron withdrawing substituents did not substantially affect the reaction rate or yield. Entry 5 was significantly faster than the other N-phenyl amides, only requiring 2 h at room temperature. This increased reaction rate may result from the extra coordination to boron afforded by the furan oxygen.[32] Heptane was also a suitable solvent for these reductions, but all reactions were found to be slower, again due to the reduced solubility in this solvent. It should be noted that, despite longer reaction times for the less soluble structures, product yields were generally high.

Table 6.1: Amines from the Hydrosilylation of Amides [a]

Entry	Amide	Amine	Conditions	Yield (%)
1	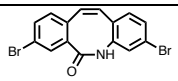	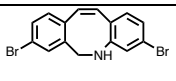	50 °C, 4 h	92
2	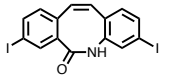	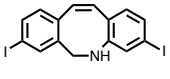	50 °C, 1.5 h	86
3	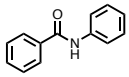	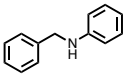	50 °C, 1 h	96
4	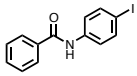	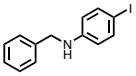	50 °C, 1.5 h	>98
5	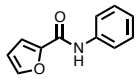	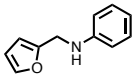	r.t., 2 h	91
6	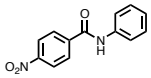	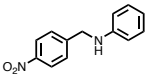	50 °C, 4 h	92
7	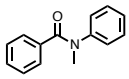	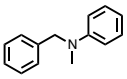	r.t., 1.5 h	>98
8	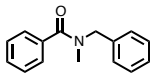	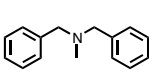	50 °C, 1 h	>98
9	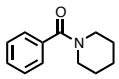	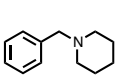	50 °C, 1 h	97
10	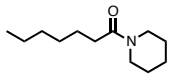	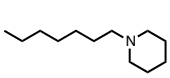	130 °C, 1d	65
11	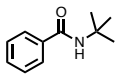	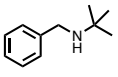	110 °C, 1d	0[b]
12	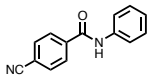	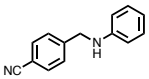	50 °C, 1 h	0[c]
13	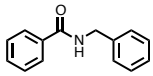	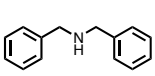	130 °C, 1d	0[b]
14	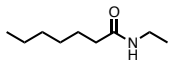	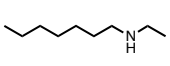	130 °C, 1d	0[b]
15	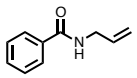	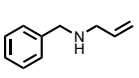	130 °C, 1d	0[b]
16	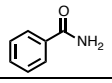	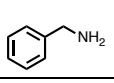	130 °C, 1d	0[b]

[a] Conditions: Amide (1 mmol), TDMS (4 mmol, 8 eqv. Si-H), $B(C_6F_5)_3$ (0.05 mmol as 0.05 M solution in toluene), toluene (3 mL), $Ar_{(g)}$.

[b] Only starting materials were isolated; [c] Multiple Products

As noted in the previous report,[41] reduction of aliphatic tertiary amides with aromatic substituents on the carbonyl carbon proceeded smoothly (Table 6.1, entry 9). However, in the case where aliphatic substituents were present on both sides of the amide, the reductions were more difficult and yields suffered accordingly (Table 6.1, entry 10). Interestingly, this method appears to be unable to reduce primary amides or secondary N-alkyl, N-benzyl, or N-allyl amides, though it appears that it is not essential that the system be conjugated through the carbonyl side (Table 6.1, entries 11, 13-16).[41] Furthermore, while nitro groups were well tolerated (Table 6.1, entry 6), it was found that nitriles underwent reduction, leading to multiple products (Table 6.1, entry 12). In the cases where reduction was not observed, isolation of the starting material allowed for approximately 95% recovery. We speculate the mechanism of reaction follows a similar pathway as the reduction of esters.[42] This differs from the mechanism of $B(C_6F_5)_3$ reduction of imines in that no Si-N bond is formed. Accordingly, we were unable to reduce secondary *tert*-butyl amides, in contrast to results by Blackwell *et al*. with tert-butyl imines.[42]

In order to determine the mechanism of inhibition for secondary N-alkyl amides we attempted a reduction of N-benzylbenzamide using 25% loading of $B(C_6F_5)_3$. We were able to obtain ca. 70% recovery of our starting material, however we also observed a highly polar product by TLC (R_f = 0.2, 1:9 MeOH:EtOAc). When isolated via chromatography (ca. 15% yield), the solid product produced a ^{1}H-NMR spectrum consistent with dibenzylamine. This is

consistent with the production of a strong $B(C_6F_5)_3$ adduct. In fact, literature confirms that the adducts of $B(C_6F_5)_3$ are especially strong due to a bifurcated F-H-F hydrogen bond between the amine proton and two of the ring fluorine atoms.[43-45] Based on this evidence, we hypothesize the variation in rate across amide types is primarily dependent on the strength of the amine-$B(C_6F_5)_3$ complex. N-phenyl amines are considerably less basic than aliphatic amines, and would be expected to form a much weaker complex. Tertiary amines are more basic, but lack the presence of an amine N-hydrogen to form additional hydrogen bonds. Secondary N-alkyl amines form strong bifurcated H-bonds with the $B(C_6F_5)_3$ ring fluorides,[43] and we speculate that this H-bonded complex is too strong to permit catalyst turnover, thus poisoning the catalyst after a single cycle.

Lastly, reductions of N-phenylamide with silanes other than TMDS were also successful. The use of diphenylsilane (DPS), diphenylmethylsilane (DPMS) and polymethylhydrosiloxane (PMHS, Gelest; M_n: *ca.* 2 kDa) were equally efficient for these reductions (Table 6.2). However, in each case purification was less facile. The phenyl silanes had similar R_f values to the product amines, due to their more polar nature. While ideal from a cost standpoint and its status as an industrial byproduct, the use of PMHS as a reducing agent produces a cross-linked gel that makes product isolation tedious.

Table 6.2: Product yield from hydrosilylative reduction using different silanes[a]

Silane	Yield %
TMDS	96
DPS	95
DPMS	95
PMHS	80

[a] Conditions: Amide (1 mmol), silane (4 mmol), $B(C_6F_5)_3$ (0.05 mmol as 0.05 M solution in toluene), toluene (3 mL), $Ar_{(g)}$.

6.3. Conclusion

In conclusion, the use of $B(C_6F_5)_3$ leads to efficient, mild, and selective reduction of both secondary and tertiary N-phenyl amides, as well as conjugated tertiary amides. The scope and limitations for the reductions of amides appears to mirror that which is found in the literature for imines.[42] In particular, we have found this to be very useful in the reduction of amides in the presence of alkenes and aryl iodides.

6.4. Experimental

6.4.1. General Experimental

All reactions were run under an argon atmosphere. The toluene used for the reductions was dried via alumina column in a solvent purification system (MBraun). All amides, except for entries **1** and **2** were synthesized from their respective amines and acyl chlorides using a modified literature method.[19] Amide **1** was synthesized via a previously reported procedure.[23] An analogous synthesis of amide **2**, following modified literature procedures is reported below. All yields are isolated yields. Solutions were deoxygenated by sparging with argon whilst sonicating using a Branon Ultrasonic Cleaner Model 2510. NMR spectra were measured on Bruker Avance 600 and 700 MHz spectrometers. All chemical shifts (δ) are reported in ppm and coupling constants (*J*) in Hz. High resolution ES-MS measurements were performed on a Micromass Ultima Global instrument (quadrupole time-of-flight).

6.4.2. Synthesis

General Procedure for the Reduction of Amides A dry 50 mL schlenk tube, or round bottom flask was charged with the amide (1 mmol) and dry toluene (3 mL). The mixture was degassed with argon in an ultrasonicator for 15 minutes before adding TMDS (537 mg, 4 mmol). While stirring at 50 °C, a 0.05 M degassed solution of $B(C_6F_5)_3$ in dry toluene (1 mL, 0.05 mmol) was added in two aliquots, over 30 minutes, resulting in gas evolution. The reaction was monitored

by thin layer chromatography. Upon completion, the remaining toluene was evaporated under reduced pressure leaving behind a crude mixture that was purified via a short basic alumina column eluting with hexanes to remove silyl compounds followed by CH_2Cl_2 to elute product.

Procedure for the Reduction of 1-(piperidin-1-yl)heptan-1-one A dry pressure vessel of appropriate size was charged with 1-(piperidin-1-yl)heptan-1-one (197 mg, 1 mmol), $B(C_6F_5)_3$ (25.6 mg, 0.05 mmol), and toluene (4 mL). The mixture was degassed with argon in an ultrasonicator for 15 minutes before adding TMDS (537 mg, 4 mmol). The pressure vessel was sealed with a stir bar and submerged in an oil bath at 130 °C for 24 hours. The vessel was removed from the oil bath and allowed to cool to room temperature before being opened. After evaporating the remaining toluene under reduced pressure, the oily residue was purified via column chromatography using silica gel passivated with Et_3N in EtOAc/*n*-hexanes 1:4.

6.4.2. Synthesis of 3,8-Difluorodibenzo[b,f]azocin-6(5H)-one[23]

3,7-Diiodo-10,11-dihydro-dibenzo[a,d]cycloheptен-5-one[46] Dibenzosuberone (10.50 g, 50 mmol), I_2 (16.50 g, 65 mmol) and acetic acid (100 mL) were added to a 500 mL 2-N round bottom flask equipped with a condenser and addition funnel, forming a red-violet mixture. A mixture of HNO_3 (4 mL) and H_2SO_4 (10 mL) was then added dropwise to the stirring reaction, followed by CCl_4 (5 mL). The reaction was heated and stirred at reflux for 5 h, then partitioned between water (500 mL) and chloroform (500 mL) while molten. The aqueous

phase was further extracted with chloroform (3 x 100 mL). The organic phases were combined and washed with 2 M $NaSO_3$ (4 x 150 mL), 5% $NaHCO_3$ (3 x 150 mL), and brine (1 x 150 mL). The organic phase was dried over magnesium sulfate, then filtered and evaporated under reduced pressure to yield a crude reddish solid. The crude material was passed through a silica plug and purified via recrystallization from 1:8 1,4-dioxane/EtOH to yield 6.44 g, 14.0 mmol (28%) of an off-white crystalline solid. ^{1}H-NMR (700 MHz; $CDCl_3$): δ 8.29 (d, J = 1.6, 2H), 7.74 (dd, J = 8.0, 1.7, 2H), 6.97 (d, J = 8.0, 2H), 3.12 (s, 4H). ^{13}C-NMR (176 MHz; $CDCl_3$): δ 192.5, 141.42, 141.37, 139.7, 139.4, 131.4, 91.8, 34.4. HRMS (ESI+) (m/z) calculated for $C_{15}H_{11}OI_2$ $[M + H]^+$ 460.8899, measured 460.8919.

3,7-diiodo-5H-dibenzo[a,d][7]annulen-5-one[47] A mixture of 3,7-Diiodo-10,11-dihydro-dibenzo[a,d]cyclohepten-5-one (2.00 g, 4.35 mmol), *N*-bromo-succinimide (1.01 g, 5.65 mmol), benzoyl peroxide (42 mg, 0.17 mmol), and 1,2-dichloromethane (30 mL) was added to a 100 mL round bottom flask equipped with a reflux condenser. The light brown mixture was stirred at reflux for 4 h then slowly cooled to room temperature. The precipitate was dissolved in dichloromethane before washing with 5% NaOH (3 x 75 mL), water (1 x 75 mL), and brine (1 x 75 mL). The organic phase was dried over $MgSO_4$ and evaporated under reduced pressure to yield 2.34 g (quant. recovery) of tan powder that was moved on to the next reaction without purification. Monitoring the reaction by thin layer chromatography showed the product at R_f = 0.35 (Et_2O/n-hexanes, 1:4).

The crude 10-bromo-3,7-diiodo-10,11-dihydro-5H-dibenzo[a,d][7]annulen-5-one (2.34 g, 4.35 mmol), Et_3N (12 mL) and benzene (25 mL) were added to a 100 mL round bottom flask equipped with a reflux condenser. The light brown mixture was stirred at reflux for 7 h, then slowly cooled to 0 °C and filtered. The light yellow filtered solid was stirred in 1 M HCl (50 mL), filtered and washed again with water (50 mL) followed by MeOH (20 mL). The crude solid was purified via recrystallization from toluene to yield 1.39 g, 3.00 mmol (70%) of a light yellow crystalline solid. ^{1}H-NMR (700 MHz; DMSO): δ 8.36 (s, 2H), 8.11 (d, J = 8.0, 2H), 7.56 (d, J = 6.8, 2H), 7.23 (s, 2H). ^{13}C-NMR (176 MHz; DMSO): δ 189.0, 141.1, 138.7, 138.0, 133.9, 133.2, 131.5, 95.8. HRMS (ESI+) (m/z) calculated for $C_{15}H_9OI_2$ $[M + H]^+$ 458.8743, measured 458.8728.

(Z)-3,8-diiododibenzo[b,f]azocin-6(5H)-one[48,49] 3,7-diiodo-5H-dibenzo[a,d][7]annulen-5-one (1.39 g, 3.03 mmol) was added to a mixture of $H_2NOH{\cdot}HCl$ (1.05 g, 15.2 mmol) and pyridine (10 mL) in a 25 mL round bottom flask equipped with a reflux condenser. The yellow reaction mixture was stirred while refluxing for 4 h then diluted with CH_2Cl_2 (200 mL). The solution was washed with 5% $HCl_{(aq)}$ (2 x 100 mL) and brine (1 x 100 mL), then dried over $MgSO_4$ and evaporated under reduced pressure to yield 1.43 g (quant. recovery) of pale yellow powder. The mildly moisture sensitive compound was used immediately. Monitoring the reaction by thin layer chromatography showed a single product at R_f = 0.15 (Et_2O/n-hexanes, 1:4).

Eaton's reagent (10 mL) was added to a dry 50 mL round bottom flask containing the crude 3,7-diiodo-5H-dibenzo[a,d][7]annulen-5-one oxime (1.43 g, 3.03 mmol). The brown reaction mixture was stirred at 100 °C for 30 minutes before being slowly cooled to room temperature and quenching via dropwise addition of water (30 mL) over an ice bath. The resulting precipitate was filtered and rinsed with 5% $NaHCO_{3(aq)}$ (2 x 30 mL) followed by MeOH (10 mL). The tan solid was dried under vacuum to a yield of 1.29 g, 2.73 mmol (90%). An analytically pure product can be obtained by recrystallizing from $CHCl_3$. ^{1}H NMR (700 MHz; $CDCl_3$): δ 7.79 (s, 1H), 7.64 (d, J = 8.0, 1H), 7.53 (d, J = 8.9, 2H), 7.46 (s, 1H), 6.86 (m, 2H), 6.77 (t, J = 11.3, 2H). ^{13}C NMR (176 MHz; $CDCl_3$): δ 171.4, 138.9, 137.1, 136.5, 136.2, 136.1, 135.3, 134.6, 133.3, 132.9, 130.7, 129.9, 129.5, 93.2, 93.0. HRMS (ESI+) (m/z) calculated for $C_{15}H_{10}NOI_2$ $[M + H]^+$ 473.8852, measured 473.8842.

6.4.3. Characterization of Amines

(Z)-3,8-dibromo-5,6-dihydrodibenzo[b,f]azocine, (1) Yield: 336 mg, 0.92 mmol (92%), bright yellow crystalline solid. Oxidizes readily to a light orange solid. ^{1}H-NMR (700 MHz; $CDCl_3$): δ 7.58 (dd, J = 8.1, 1.7, 1H), 7.56 (s, 1H), 6.98-6.96 (m, 2H), 6.87 (d, J = 8.0, 1H), 6.65 (d, J = 8.2, 1H), 6.50 (d, J = 12.9, 1H), 6.34 (d, J = 12.9, 1H), 5.79 (s, 1H), 4.51 (s, 2H). ^{13}C-NMR (176 MHz; $CDCl_3$): δ 146.2, 138.8, 138.6, 138.1, 137.1, 135.4, 132.4, 131.7, 128.22, 128.10, 127.1, 122.5, 93.6, 92.5, 49.1. HRMS (ESI+) (m/z) calculated for $C_{15}H_{12}NBr_2$ $[M + H]^+$ 363.9336, measured 363.9337.

(Z)-3,8-diiodo-5,6-dihydrodibenzo[b,f]azocine, (2) Yield: 394 mg, 0.86 mmol (86%), bright yellow crystalline solid. Oxidizes readily to a dark orange solid. ^{1}H-NMR (700 MHz; $CDCl_3$): δ 7.58 (dd, J = 8.0, 1.7, 1H), 7.55 (s, 1H), 6.91 (dd, J = 8.2, 1.5, 1H), 6.88 (d, J = 8.1, 1H), 6.85 (s, 1H), 6.63 (d, J = 8.2, 1H), 6.46 (d, J = 13.0, 1H), 6.27 (d, J = 13.0, 1H), 4.60 (s, 1H), 4.49 (s, 2H). ^{13}C-NMR (176 MHz; $CDCl_3$): δ 147.5, 139.7, 138.7, 138.0, 137.0, 135.8, 132.7, 131.8, 127.5, 127.2, 126.5, 121.5, 93.6, 92.4, 48.8. HRMS (ESI+) (m/z) calculated for $C_{15}H_{12}NI_2$ $[M + H]^+$ 459.9059, measured 459.9072.

N-benzylaniline, (3) Yield: 176 mg, 0.96 mmol (96%), clear, colourless liquid. ^{1}H-NMR (700 MHz; $CDCl_3$): δ 7.40 (d, J = 7.5, 2H), 7.37 (t, J = 7.5, 2H), 7.30 (t, J = 7.2, 1H), 7.21-7.19 (m, 2H), 6.75 (t, J = 7.3, 1H), 6.67-6.66 (m, 2H), 4.35 (s, 2H), 4.09 (s, 1H). ^{13}C-NMR (176 MHz; $CDCl_3$): δ 148.2, 139.5, 129.4, 128.8, 127.6, 127.4, 117.7, 113.0, 48.5. HRMS (ESI+) (m/z) calculated for $C_{13}H_{14}N$ $[M + H]^+$ 184.1126, measured 184.1132.

***N*-benzyl-4-iodoaniline, (4)** Yield: 303 mg, 0.98 mmol (98%), white crystalline solid. Oxidizes readily to a green solid. ^{1}H-NMR (700 MHz; $CDCl_3$): δ 7.41 (d, J = 8.8, 2H), 7.35-7.34 (m, 4H), 7.28 (m, 1H), 6.42 (d, J = 8.8, 2H), 4.30 (s, 2H), 4.20 (s, 1H). ^{13}C-NMR (176 MHz; $CDCl_3$): δ 147.7, 138.9, 137.9, 128.9, 127.5, 115.3, 78.4, 48.3. HRMS (ESI+) (m/z) calculated for $C_{13}H_{13}NI$ $[M + H]^+$ 310.0093, measured 310.0099.

N-(furan-2-ylmethyl)aniline, (5) Yield: 157 mg, 0.91 mmol (91%), clear, colourless liquid. ^{1}H-NMR (700 MHz; $CDCl_3$): δ 7.40 (s, 1H), 7.23 (t, J = 7.9,

2H), 6.79 (t, J = 7.3, 1H), 6.71 (d, J = 7.7, 2H), 6.36 (s, 1H), 6.27 (s, 1H), 4.35 (s, 2H), 4.04 (s, 1H). ^{13}C-NMR (176 MHz; $CDCl_3$): δ 152.8, 147.7, 142.0, 129.3, 118.1, 113.2, 110.4, 107.1, 41.5. HRMS (ESI+) (m/z) calculated for $C_{11}H_{12}NO$ $[M + H]^+$ 174.0919, measured 174.0912.

N-(4-nitrobenzyl)aniline, (6) Yield: 210 mg, 0.92 mmol (92%), bright yellow liquid. Oxidizes readily to a dark brown liquid. ^{1}H-NMR (700 MHz; $CDCl_3$): δ 8.17 (d, J = 8.6, 2H), 7.51 (d, J = 8.3, 2H), 7.15 (t, J = 8.0, 2H), 6.73 (t, J = 7.3, 1H), 6.57 (d, J = 7.7, 2H), 4.46 (s, 2H), 4.28 (s, 1H). ^{13}C-NMR (176 MHz; $CDCl_3$): δ 147.58, 147.39, 147.31, 129.5, 127.8, 124.0, 118.4, 113.1, 47.8. HRMS (ESI+) (m/z) calculated for $C_{13}H_{13}N_2O_2$ $[M + H]^+$ 229.0977, measured 229.0969.

N-benzyl-N-methylaniline, (7) Yield: 193 mg, 0.98 mmol (98%), clear, colourless liquid. ^{1}H-NMR (700 MHz; $CDCl_3$): δ 7.35 (t, J = 7.5, 2H), 7.28-7.25 (m, 5H), 6.80 (d, J = 7.8, 2H), 6.75 (t, J = 6.9, 1H), 4.57 (s, 2H), 3.05 (s, 3H). ^{13}C-NMR (176 MHz; $CDCl_3$): δ 149.9, 139.1, 129.3, 128.7, 126.99, 126.87, 116.7, 112.5, 56.8, 38.6. HRMS (ESI+) (m/z) calculated for $C_{14}H_{16}N$ $[M + H]^+$ 198.1283, measured 198.1273.

N-benzyl-N-methyl-1-phenylmethanamine, (8) Yield: 207 mg, 0.98 mmol (98%), clear, colourless liquid. ^{1}H-NMR (700 MHz; $CDCl_3$): δ 7.37 (d, J = 7.5, 4H), 7.33 (t, J = 7.5, 4H), 7.26-7.24 (m, 2H), 3.53 (s, 4H), 2.20 (s, 3H). ^{13}C-NMR (176 MHz; $CDCl_3$): δ 139.5, 129.1, 128.4, 127.1, 62.0, 42.4. HRMS (ESI+) (m/z) calculated for $C_{15}H_{18}N$ $[M + H]^+$ 212.1439, measured 212.1433.

1-benzylpiperidine, (9) Yield: 170 mg, 0.97 mmol (97%), clear, colourless liquid. ^{1}H-NMR (700 MHz; $CDCl_3$): δ 7.32-7.30 (m, 4H), 7.25-7.23 (m, 1H), 3.48 (s, 2H), 2.38 (s, 4H), 1.58 (quintet, J = 5.5, 4H), 1.43 (s, 2H). ^{13}C-NMR (176 MHz; $CDCl_3$): δ 138.8, 129.4, 128.2, 126.9, 64.0, 54.6, 26.1, 24.5. HRMS (ESI+) (m/z) calculated for $C_{12}H_{18}N$ $[M + H]^+$ 176.1439, measured 176.1438.

1-heptylpiperidine, (10) Yield: 119 mg, 0.65 mmol 65%, clear, colourless liquid. ^{1}H-NMR (600 MHz; $CDCl_3$): δ 2.35 (m, 4H), 2.25 (dd, J = 9.2, 6.7, 2H), 1.57 (quintet, J = 5.7, 4H), 1.48-1.46 (m, 2H), 1.41 (m, 2H), 1.29-1.24 (m, 8H), 0.86 (t, J = 7.0, 3H). ^{13}C-NMR (176 MHz; $CDCl_3$): δ 59.9, 54.8, 32.0, 29.4, 27.9, 27.1, 26.1, 24.7, 22.8, 14.2. HRMS (ESI+) (m/z) calculated for $C_{12}H_{26}N$ $[M + H]^+$ 184.2065, measured 184.2069.

6.5. References

(1) Seyden-Penne, J. *Reductions by the Alumino and Borohydrides in Organic Synthesis, 1991*; Wiley-VCH: New York, 1997.
(2) Stein, M.; Breit, B. *Angew. Chem. Int. Ed. Engl.* **2013**, *52*, 2231–2234.
(3) Núñez Magro, A. A.; Eastham, G. R.; Cole-Hamilton, D. J. *Chem. Commun.* **2007**, 3154–3156.
(4) Coetzee, J.; Dodds, D. L.; Klankermayer, J.; Brosinski, S.; Leitner, W.; Slawin, A. M. Z.; Cole-Hamilton, D. J. *Chem. Eur. J.* **2013**, *19*, 11039–11050.
(5) Burch, R.; Paun, C.; Cao, X. M.; Crawford, P.; Goodrich, P.; Hardacre, C.; Hu, P.; McLaughlin, L.; Sá, J.; Thompson, J. M. *J. Catal.* **2011**, *283*, 89–97.
(6) Szostak, M.; Spain, M.; Eberhart, A. J.; Procter, D. J. *J. Am. Chem. Soc.* **2014**, *136*, 2268–2271.
(7) Spletstoser, J. T.; White, J. M.; Tunoori, A. R.; Georg, G. I. *J. Am. Chem. Soc.* **2007**, *129*, 3408–3419.
(8) Kuwano, R.; Takahashi, M.; Ito, Y. *Tett. Lett.* **1998**, *39*, 1017–1020.
(9) Igarashi, M.; Fuchikami, T. *Tett. Lett.* **2001**, *42*, 1945–1947.
(10) Matsubara, K.; Iura, T.; Maki, T.; Nagashima, H. *J. Org. Chem* **2002**, *67*, 4985–4988.
(11) Motoyama, Y.; Mitsui, K.; Ishida, T.; Nagashima, H. *J. Am. Chem. Soc.* **2005**, *127*, 13150–13151.
(12) Cheng, C.; Brookhart, M. *J. Am. Chem. Soc.* **2012**, *134*, 11304–11307.
(13) Hanada, S.; Tsutsumi, E.; Motoyama, Y.; Nagashima, H. *J. Am. Chem. Soc.* **2009**, *131*, 15032–15040.
(14) Sunada, Y.; Kawakami, H.; Imaoka, T.; Motoyama, Y.; Nagashima, H. *Angew. Chem. Int. Ed. Engl.* **2009**, *48*, 9511–9514.
(15) Zhou, S.; Junge, K.; Addis, D.; Das, S.; Beller, M. *Angew. Chem. Int. Ed.* **2009**, *48*, 9507–9510.
(16) Das, S.; Wendt, B.; Möller, K.; Junge, K.; Beller, M. *Angew. Chem. Int. Ed. Engl.* **2012**, *51*, 1662–1666.
(17) Sakai, N.; Fujii, K.; Konakahara, T. *Tett. Lett.* **2008**, *49*, 6873–6875.
(18) Das, S.; Join, B. I. T.; Junge, K.; Beller, M. *Chem. Commun.* **2012**, *48*, 2683–2685.
(19) Das, S.; Addis, D.; Junge, K.; Beller, M. *Chem. Eur. J.* **2011**, *17*, 12186–12192.
(20) Das, S.; Addis, D.; Zhou, S.; Junge, K.; Beller, M. *J. Am. Chem. Soc.* **2010**, *132*, 1770–1771.
(21) Barbe, G.; Charette, A. B. *J. Am. Chem. Soc.* **2008**, *130*, 18–19.
(22) Pelletier, G.; Bechara, W. S.; Charette, A. B. *J. Am. Chem. Soc.* **2010**, *132*, 12817–12819.
(23) Chadwick, R. C.; Kardelis, V.; Liogier, S.; Adronov, A. *Macromolecules* **2013**, *46*, 9593–9598.

(24) Jacobsen, H.; Berke, H.; Döring, S.; Kehr, G.; Erker, G.; Fröhlich, R.; Meyer, O. *Organometallics* **1999**, *18*, 1724–1735.
(25) Massey, A. G.; Park, A. J. *J. Organomet. Chem.* **1964**, *2*, 245–250.
(26) Erker, G. *Dalton Trans.* **2005**, 1883–1890.
(27) Piers, W. E.; Chivers, T. *Chem. Soc. Rev.* **1997**, *26*, 345–354.
(28) Gevorgyan, V.; Rubin, M.; Benson, S.; Liu, J. X. *J. Org. Chem.* **2000**, *65*, 6179–6186.
(29) Parks, D. J.; Piers, W. E. *J. Am. Chem. Soc.* **1996**, *118*, 9440–9441.
(30) Parks, D. J.; Blackwell, J. M.; Piers, W. E. *J. Org. Chem* **2000**, *65*, 3090–3098.
(31) Gevorgyan, V.; Rubin, M.; Liu, J. X. *J. Org. Chem.* **2001**.
(32) Piers, W. E.; Marwitz, A. J. V.; Mercier, L. G. *Inorg. Chem.* **2011**, *50*, 12252–12262.
(33) Hog, D. T.; Oestreich, M. *Liebigs Ann. Chem.* **2009**, *2009*, 5047–5056.
(34) Blackwell, J. M.; Foster, K. L.; Beck, V. H.; Piers, W. E. *J. Org. Chem.* **1999**, *64*, 4887–4892.
(35) Thompson, D. B.; Brook, M. A. *J. Am. Chem. Soc.* **2008**, *130*, 32–33.
(36) Grande, J. B.; Thompson, D. B.; Gonzaga, F.; Brook, M. A. *Chem. Commun.* **2010**, *46*, 4988–4990.
(37) Grande, J. B.; Fawcett, A. S.; McLaughlin, A. J.; Gonzaga, F.; Bender, T. P.; Brook, M. A. *Polymer* **2012**, *53*, 3135–3142.
(38) Kamino, B. A.; Mills, B.; Reali, C.; Gretton, M. J.; Brook, M. A.; Bender, T. P. *J. Org. Chem* **2012**, *77*, 1663–1674.
(39) Kamino, B. A.; Grande, J. B.; Brook, M. A.; Bender, T. P. *Org. Lett.* **2011**, *13*, 154–157.
(40) Fawcett, A. S.; Grande, J. B.; Brook, M. A. *J. Polym. Sci. A Polym. Chem.* **2013**, *51*, 644–652.
(41) Tan, M.; Zhang, Y. *Tett. Lett.* **2009**, *50*, 4912–4915.
(42) Blackwell, J. M.; Sonmor, E. R.; Scoccitti, T.; Piers, W. E. *Org. Lett.* **2000**, *2*, 3921–3923.
(43) Mountford, A. J.; Lancaster, S. J.; Coles, S. J.; Horton, P. N.; Hughes, D. L.; Hursthouse, M. B.; Light, M. E. *Inorg. Chem.* **2005**, *44*, 5921–5933.
(44) Mountford, A. J.; Hughes, D. L.; Lancaster, S. J. *Chem. Commun.* **2003**, 2148–2149.
(45) Focante, F.; Mercandelli, P.; Sironi, A.; Resconi, L. *Coord. Chem. Rev.* **2006**, *250*, 170–188.
(46) Lešetický, L.; Smrček, S.; Sváta, V.; Podlahová, J.; Podlaha, J.; Císařová, I. *Collect. Czech. Chem. Commun.* **1990**, *55*, 2677–2684.
(47) Evans, B. E. *US Patent 4,235,820* **1980**.
(48) Kuzmin, A.; Poloukhtine, A.; Wolfert, M. A.; Popik, V. V. *Bioconj. Chem.* **2010**, *21*, 2076–2085.
(49) Chadwick, R. C.; Van Gyzen, S.; Liogier, S.; Adronov, A. *Synthesis 46*, 669–677.

Chapter 7: Thesis Conclusions and Recommendations for Future Work

7.1. Summary and General Conclusions

Carbon nanotubes represent one of the most promising materials available for both mechanical reinforcement of bulk polymers and the creation of electrical percolation networks in bulk polymers.

In Chapter 2 of this thesis, we explored the suspension of single-walled carbon nanotubes in bulk polystyrene using polystyrene grafts. A series of polystyrene grafters were synthesized by atom transfer radial polymerization and attached to the SWNTs using 1,3-Huisgen cycloaddition ("click") chemistry. We determined that the graft density is directly controlled by steric factors and that it was possible to calculate a radius in which the polystyrene chain excluded other chains. Comparison to previous results demonstrated that this is common behavior when a "grafting-to" approach is used. While polymer coating has been previously utilized to suspend carbon nanotubes in bulk matrices of the same material, we found that the graft densities we achieved were insufficient to provide the necessary stabilization and achieve high-quality dispersion in bulk material. However, mechanical testing on films made by intercalation demonstrated that polystyrene coating substantially improved the quality of nanotube/matrix interaction producing stronger composites than polystrene or SWNTs alone.

In Chapter 3, we adapted the newly-developed Piers-Rubinsztajn reaction for use on single-walled carbon nanotubes. We first functionalized the surface of

SWNTs with methoxyphenyl groups using Tour diazonium chemistry, and then we reacted the functionalized SWNTs with a series of hydride-terminated polydimethylsiloxanes (silicones). In this fashion, we were able to produce highly dispersible, silconized carbon nanotubes in a facile manner. We demonstrated that the siliconized carbon nanotubes could be dispersed in various organic solvents and silicon rubbers. Finally, we demonstrated the ability to crosslink the dispersed SWNTs within bulk silicone elastomers by both commercial Pt-cured silicon rubber kits and by using recently developed Piers-Rubinsztajn crosslinking methods.

In Chapter 4 we synthesized a series of diblock co-polymers containing a polydimethylsiloxane (silicone) block and a poly-3-hexylthiophene (conjugated polymer) block. Both polymers were produced with low polydispersity indices: Poly-3-hexylthiophene via Grignard metathesis and polydimethylsiloxane via living anionic polymerization. The blocks were coupled using Pt-catalyzed hydrosilylation. We demonstrated that these diblock polymers were able to form complexes with carbon nanotubes and that these complexes showed high solubility in organic solvents. Using the supramolecular complex with the greatest solubility, we produced a series of composites, dispersing the SWNT-complex in commercially available Pt-cured silicone elastomers. The composites had a very low percolation threshold (*ca.* 0.01% wt.%), indicative of a high quality of dispersion. Moreover, when stretched, the composites demonstrated a reversible change in conductivity proportional to the degree of stretching. This was starkly

contrasted by a series of control composites made from a SWNT-P3HT complex. Without the silicone block, the conductivity change was partially irreversible on stretching and the composites conductivity degraded over *ca.* five cycles, until conductivity in the stretched form was indistinguishable from the relaxed form.

In Chapter 5 we performed the initial studies on conjugated polymers derived from a dibenzocyclooctyne repeat unit with the intention of developing a "universal" polymer for the solubilization of carbon nanotubes. The objective was to create a backbone that would interact strongly with carbon nanotubes yet could be rapidly modified post-polymerization via reactions with 1,3-dipoles such as azides or with dienes. Unfortunately, dibenzooctyne structures proved to be reactive toward the transition metal catalysts used in poly-cross-coupling polymerizations, including Ni, Cu, and Pd. Accordingly, we then functionalized the core DIBAC monomer unit using a series of azides, and co-polymerized with a diethynyl fluorene, post derivatization. The copolymers were able to produce only metastable suspensions of SWNTs; density functional theory calculations suggested that the DIBAC units introduce a large bend into the polymer backbone. We speculate that this prevents the formation of stable SWNT complexes. Nonetheless, we were able to demonstrate the fundamental concept of a "universal" conjugated polymer and were able to manipulate the polymers' electronic properties via functionalization with the series of aryl azides. Finally, we synthesized a coumarin-containing derivative that was able to undergo

photocrosslinking reactions, as demonstration of the adaptability of the cycloaddition chemistry.

Chapter 6 discusses the development of a protocol for reducing amides to amines using $(C_6F_5)_3B$ catalyzed hydrosilylation. We found that this is an especially effective and mild method of reducing N-phenyl amides, and was ideal for the reduction of the DIBAC amide precursor containing aryl bromide or aryl iodide units. This chapter outlines our studies of the scope of this reduction and the optimization of conditions.

In summary, the most significant contribution of this thesis arises from the investigation of various methods for suspending carbon nanotubes within bulk materials. Studies with both covalent and supramolecular approaches suggest that supramolecular approaches are more effective and should be the focus of any future work in nanotube/polymer suspensions.

7.2. Recommendations for Future Work

The work performed in this thesis leads to two major avenues of future work based on the goals outlined in Section 1.9 of the introduction.

1) The development of a "universal" polymer for the suspension of carbon nanotubes.
2) The improvement of suspension "quality" with the intention of producing SWNT-polymer complexes with greater conductivity.

The first goal can be approached by two methods: The adaptation of polymerization methods that do not rely on metal catalysts to produce

cyclooctyne-containing polymers; and the utilization of modular diblock co-polymer synthesis such that the non-conjugated block can be used to provide strong interactions with the host polymer.

The diblock approach is particularity promising as we have shown that diblock functionalized SWNTs have excellent adherence and good dispersion within bulk polymers (PDMS). This method of suspension can be adapted to many areas of carbon nanotube science, including the suspension of carbon nanotubes in bulk materials and the separation of carbon nanotubes by chirality, by modifying the structure of the two polymer blocks. In particular, future work should focus on using a selective conjugated block in order to suspend specific types, diameters, or chiralities of carbon nanotube for use in bulk materials.

Achieving the second goal is more complex. Future work should focus on improving the junction quality, as this is the single largest factor affecting the conductivity of carbon nanotube composites. There are several potential strategies such as using purely metallic carbon nanotubes, utilizing electron-accepting dopants, by exploring strategies to reduce the tube-tube distance within composites, and/or bridging the junctions between nanotubes with a smaller conductive macromolecule.

Appendix I: Supporting Information for: ***Polymer Grafting to Single-Walled Carbon Nanotubes: Effect of Chain Length on Solubility, Graft Density and Mechanical Properties of Macroscopic Structures***

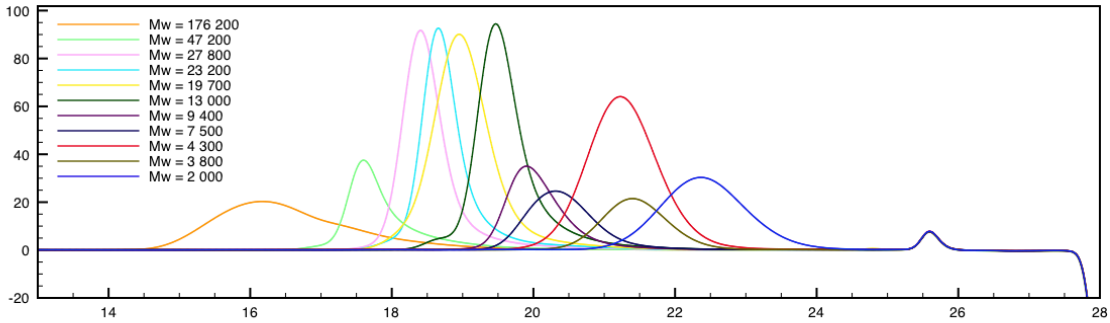

Figure A1.1. GPC Overlay plotted from raw data of ten runs. There are no peaks with retention times <14 min. Solvent front is at 28 min.

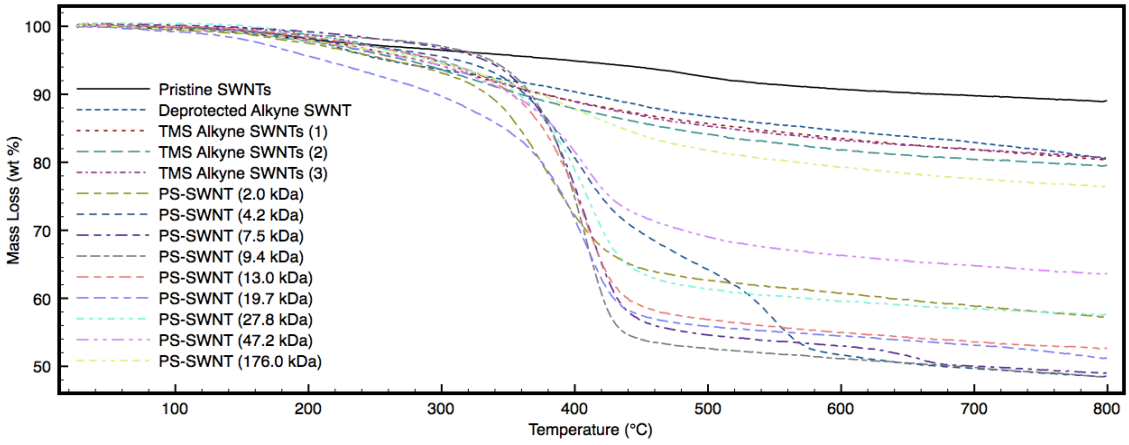

Figure A1.2. Thermogravimetric analysis of pristine SWNTs and SWNT conjugates, before and after reaction with N_3-PS.

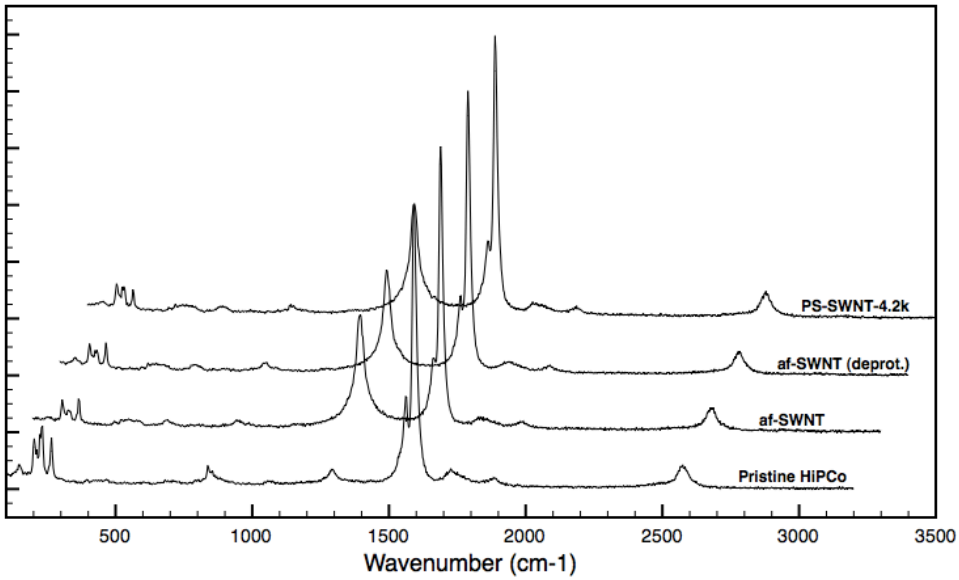

Figure A1.3: Raman spectra of pristine and functionalized SWNTs. The sharp increase in the D-band (~1300 cm^{-1}) indicates successful covalent functionalization.

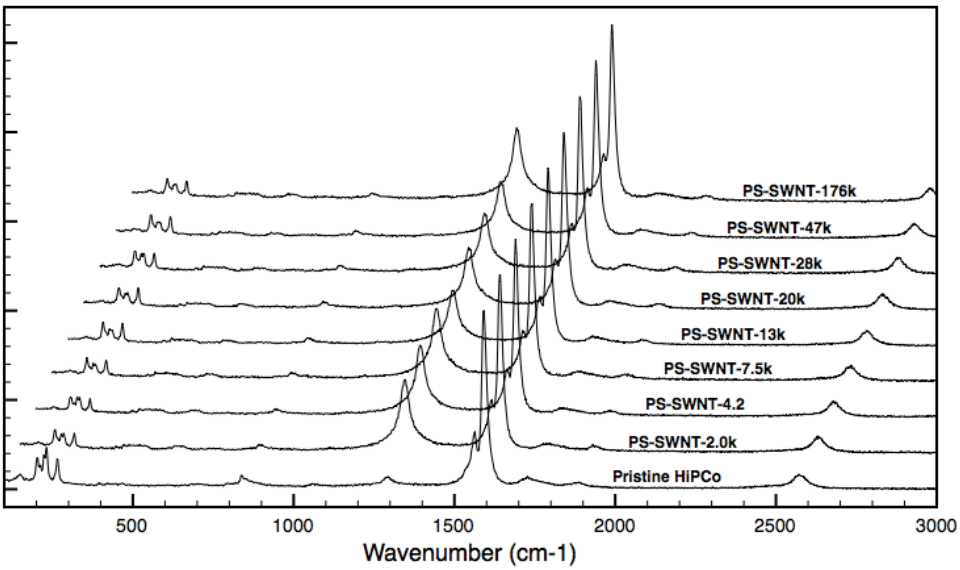

Figure A1.4: Overlay of Raman spectra of PS-SWNTs. No appreciable difference is noted between grafts.

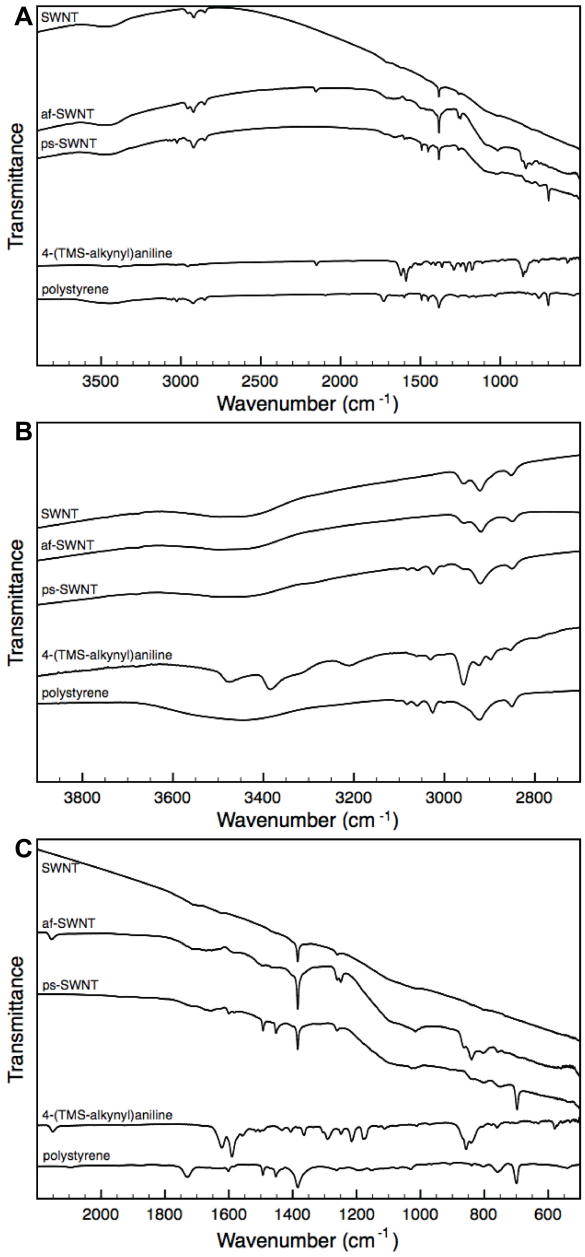

Figure A1.5: IR spectra for SWNTs, SWNT derivatives, and precursor molecules. (A) full spectra; (B) Upper region of the IR spectra; (C) Fingerprint region of the IR spectra.

Appendix II: Supporting Information for: *Functionalization of Single-Walled Carbon Nanotubes via the Piers-Rubinsztajn Reaction*

Thermogravimetric Analysis Traces:

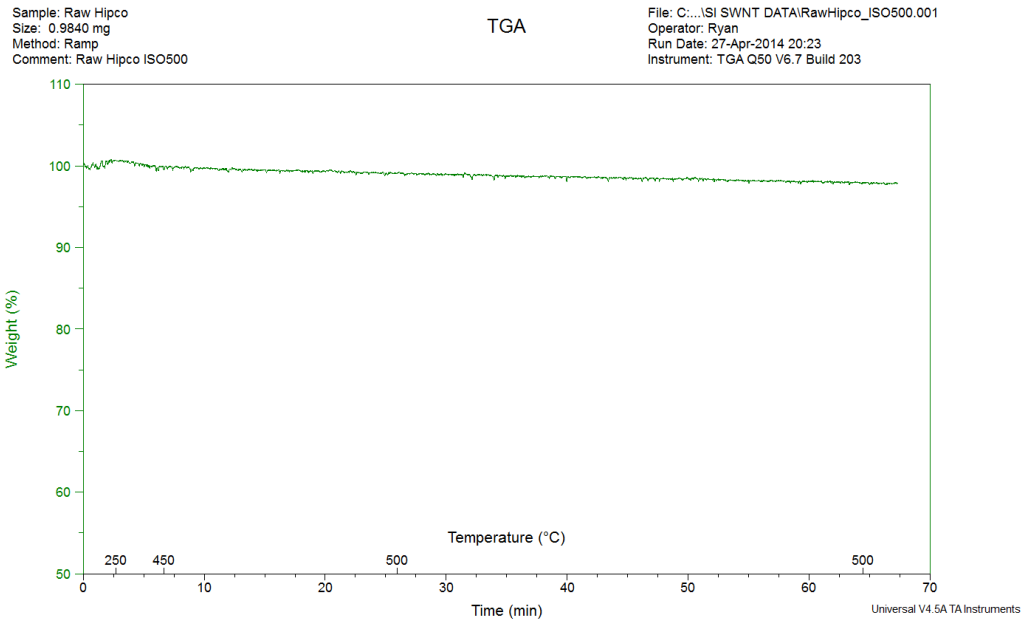

Figure A2.1: TGA of Raw HiPCO SWNT

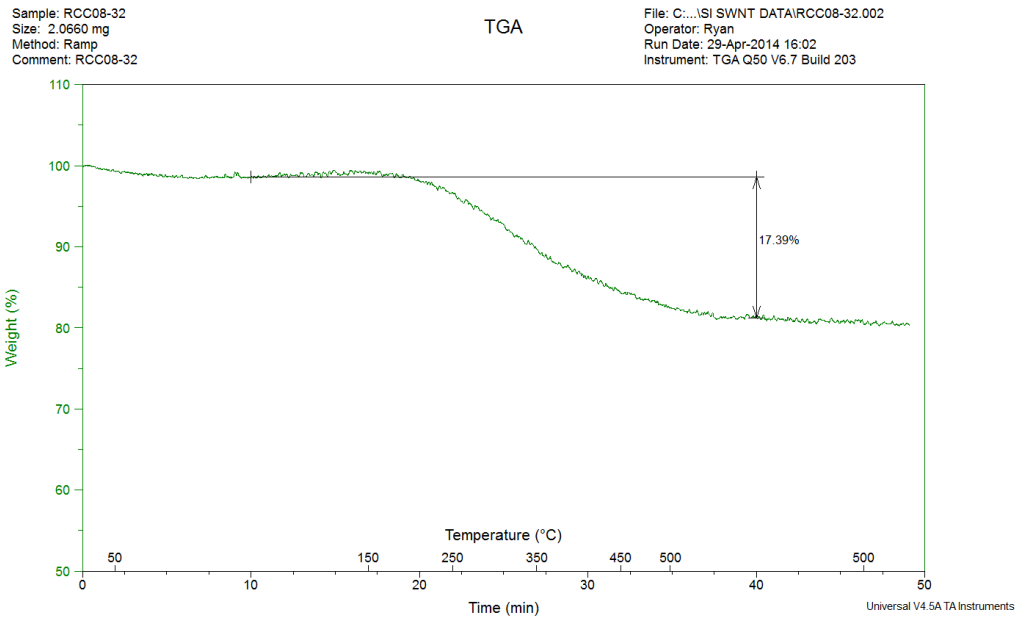

Figure A2.2: TGA of a-SWNT

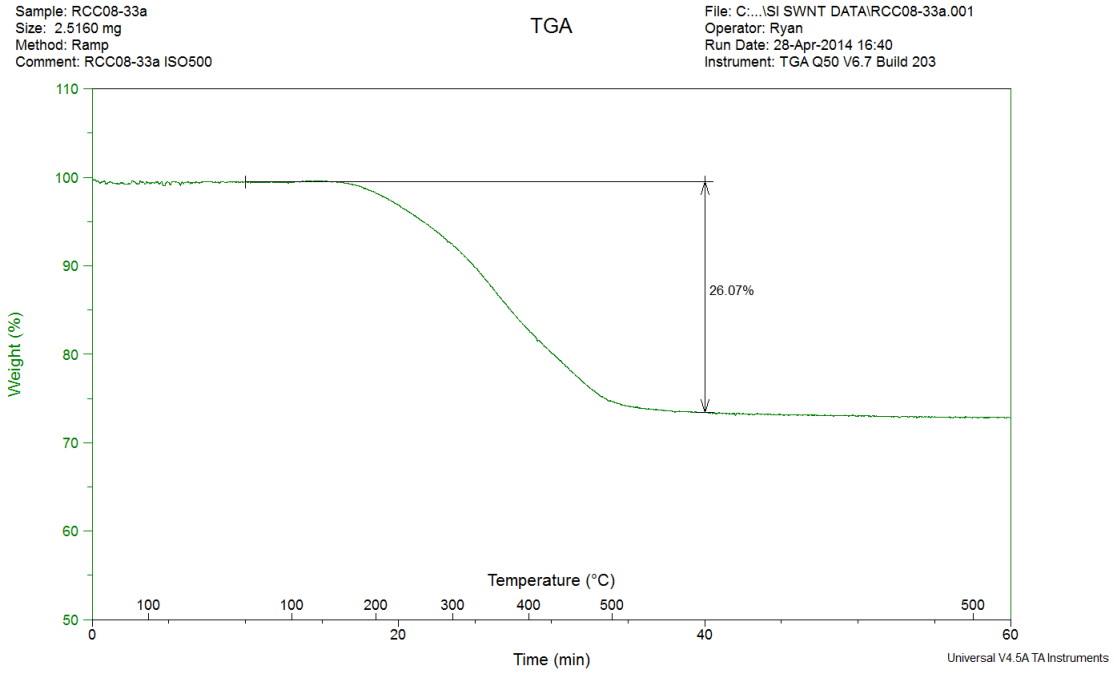

Figure A2.3: TGA of TMDS-SWNT

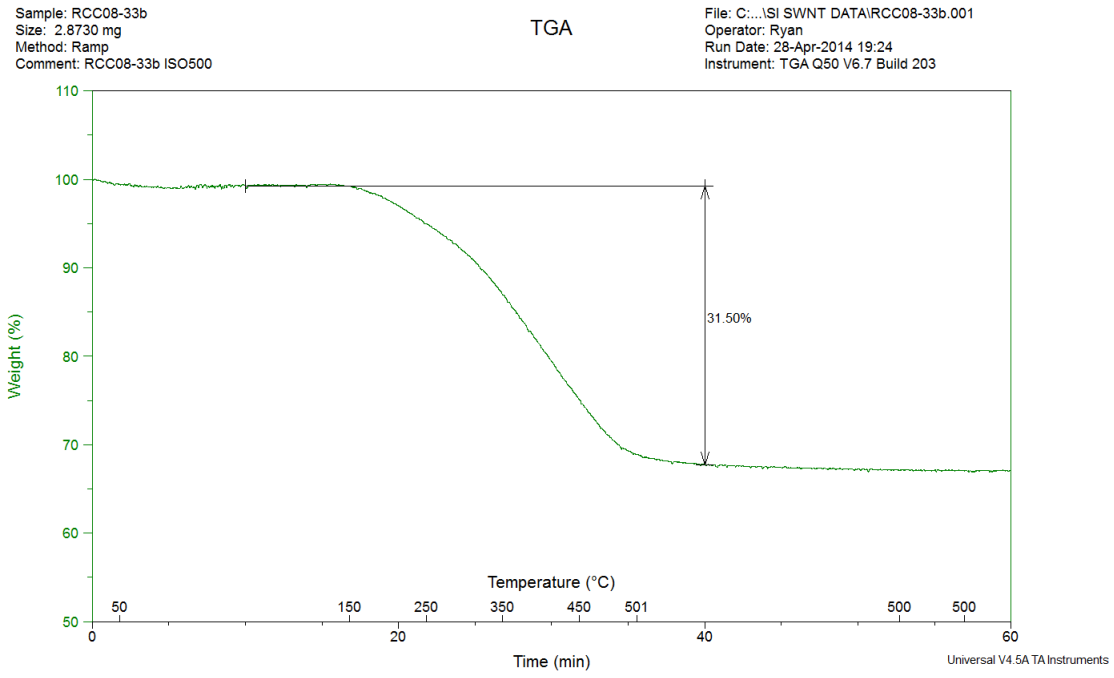

Figure A2.4: TGA of PDMS-SWNT-1k

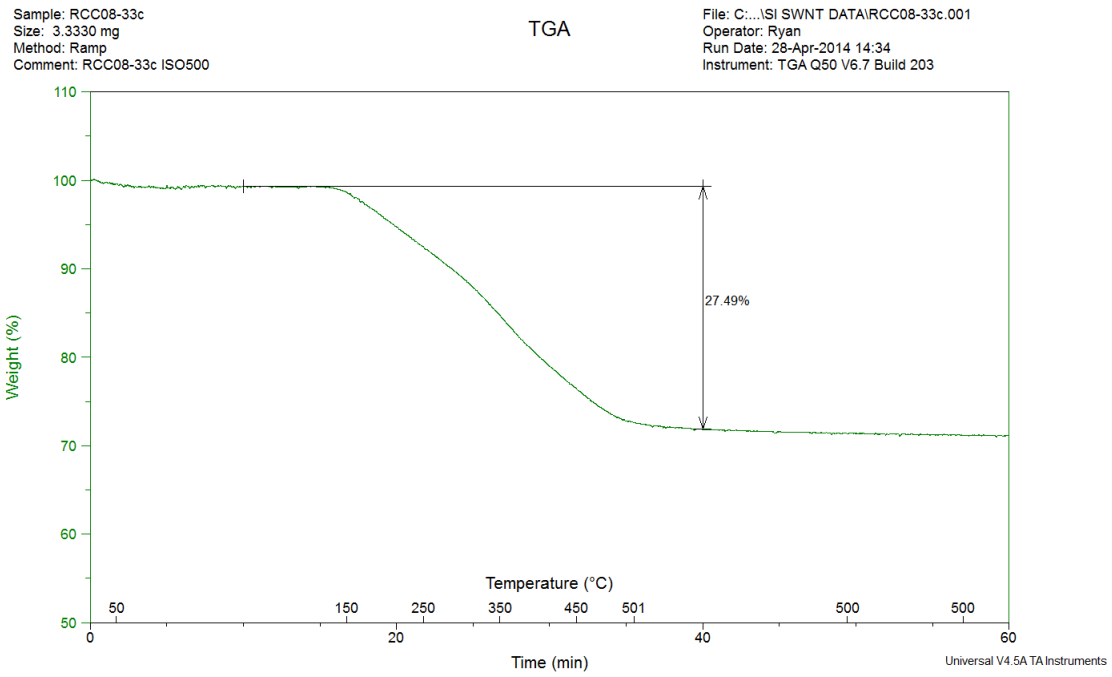

Figure A2.5: TGA of PDMS-SWNT-6k

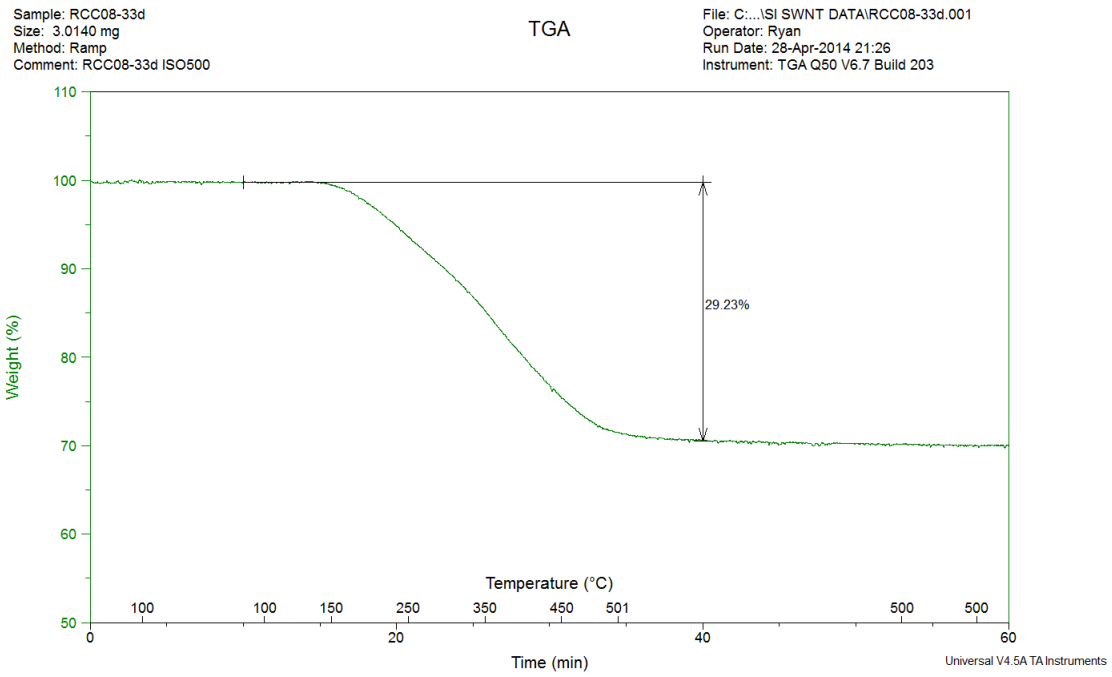

Figure A2.6: TGA of PDMS-SWNT-17k

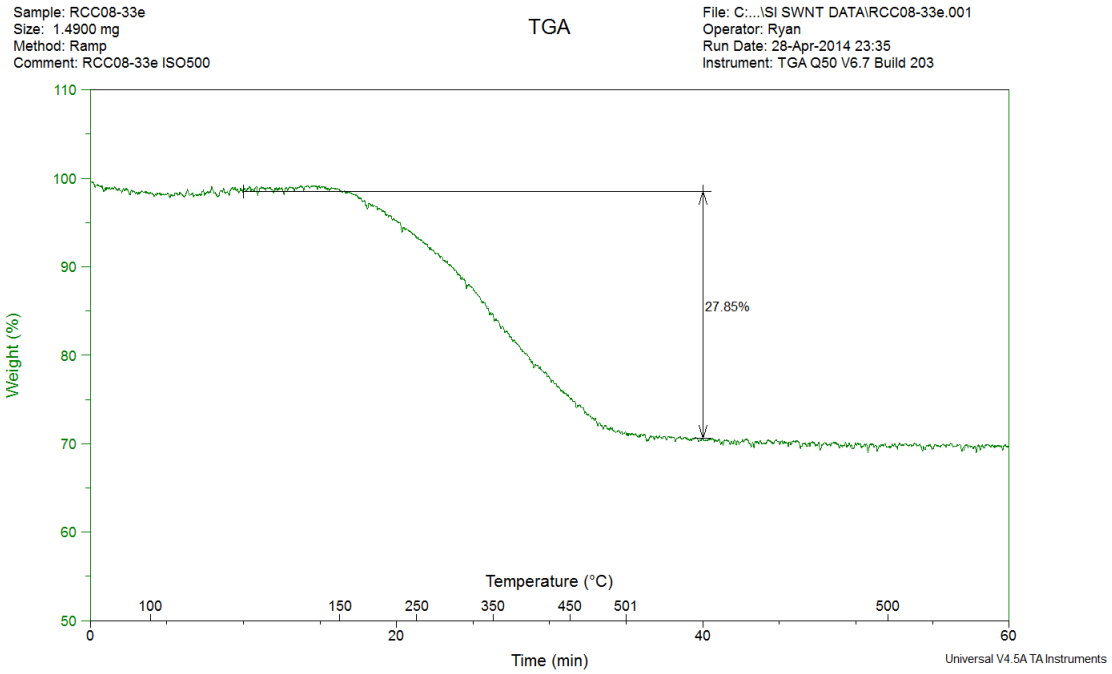

Figure A2.7: TGA of PDMS-SWNT-28k:

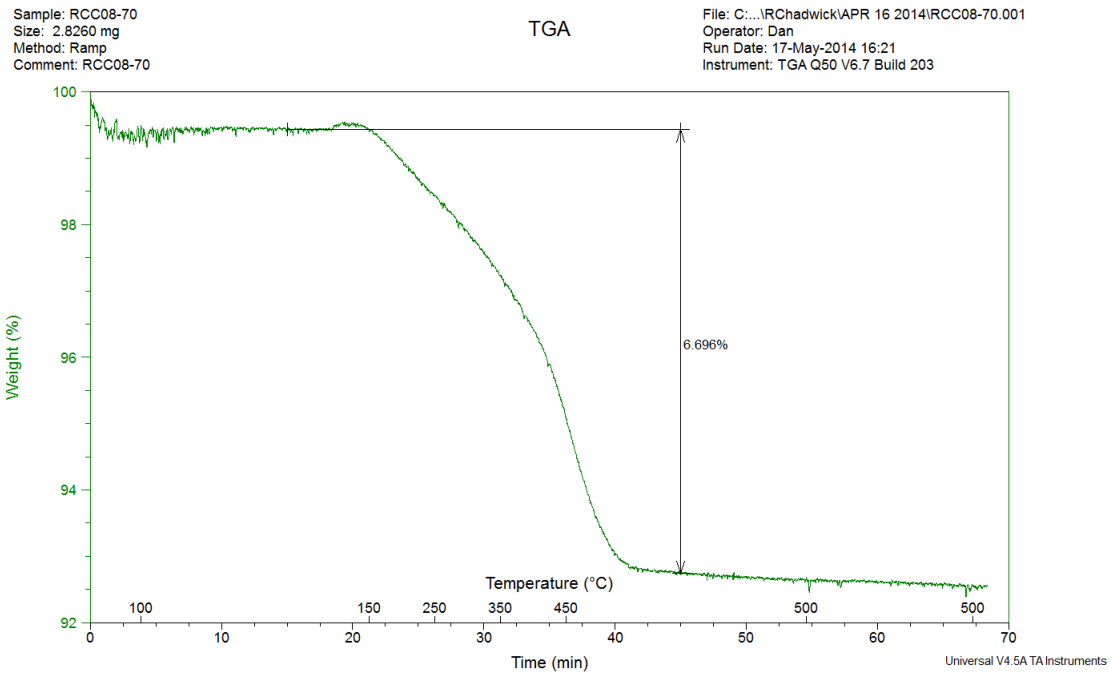

Figure A.2.8: TGA of PDMS+SWNT Control

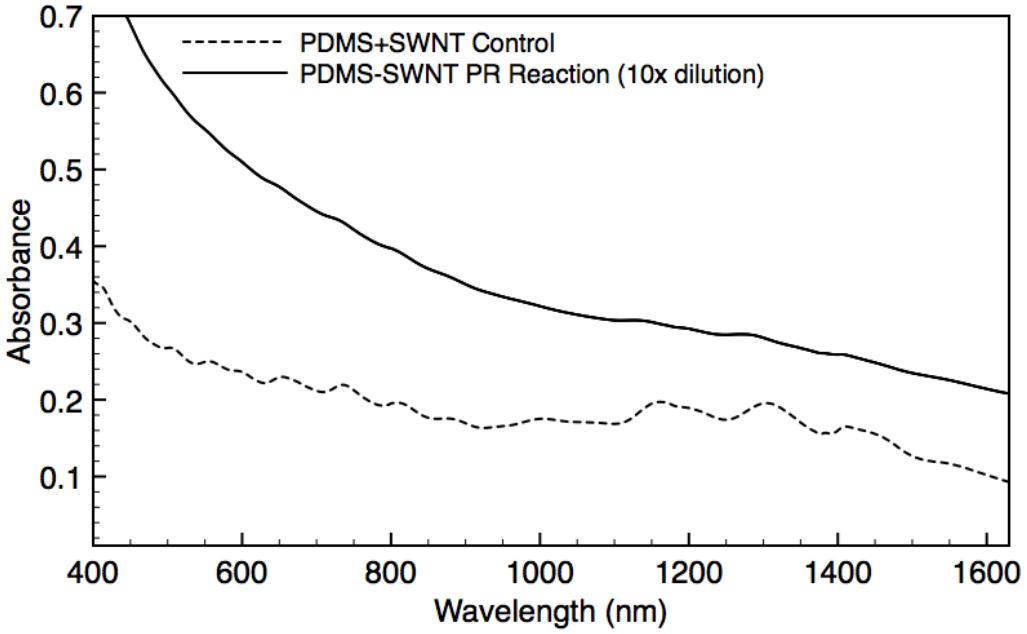

Figure A2.9: Representative UV-Vis-NIR Spectra

Appendix III: *Supporting Information for Synthesis of Conjugated Polymers Containing DIBAC-Derived Triazole Monomers*

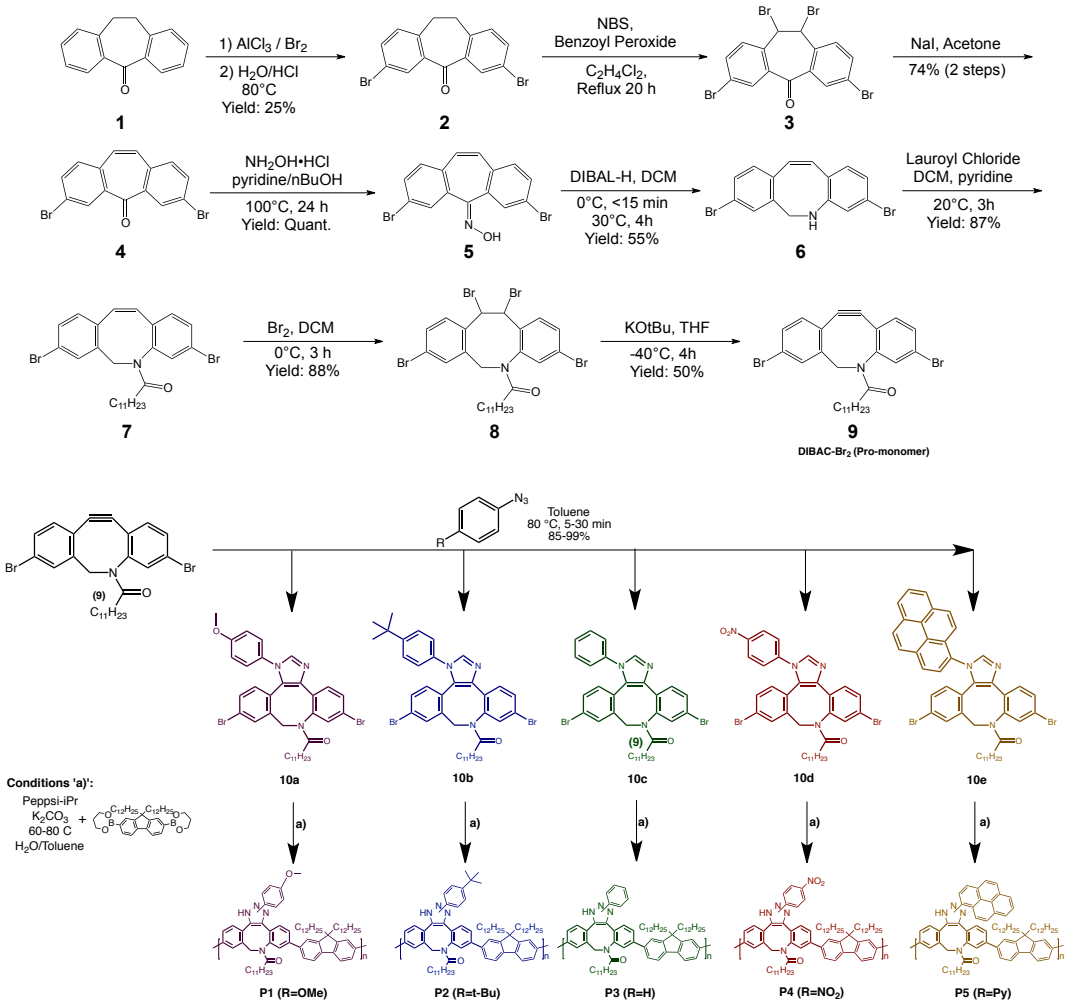

Figure A3.1: Full polymer synthetic scheme for reference.

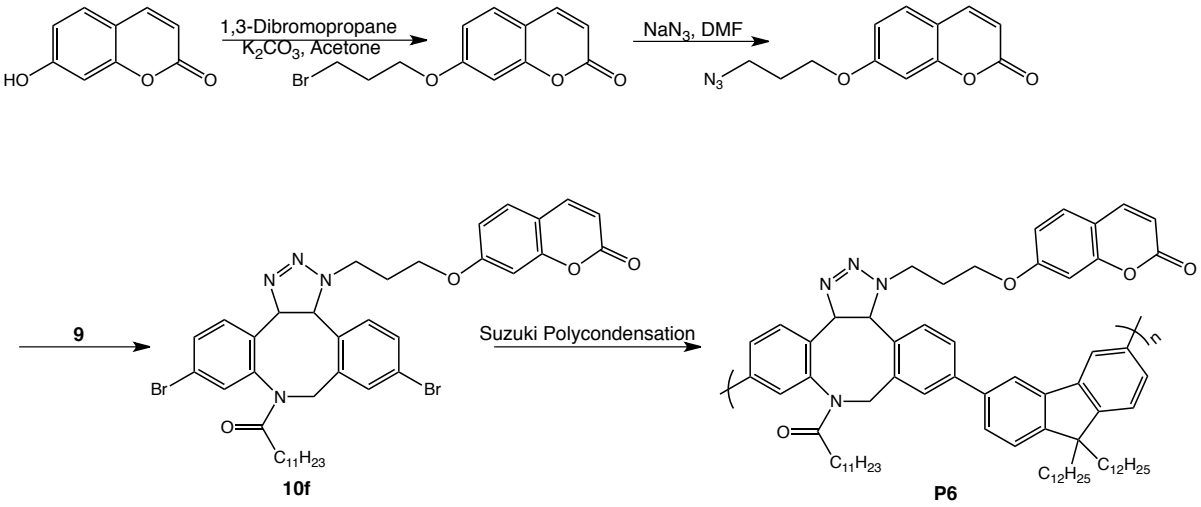

Figure A3.2: Synthesis Scheme for coumarin polymer **P6.**

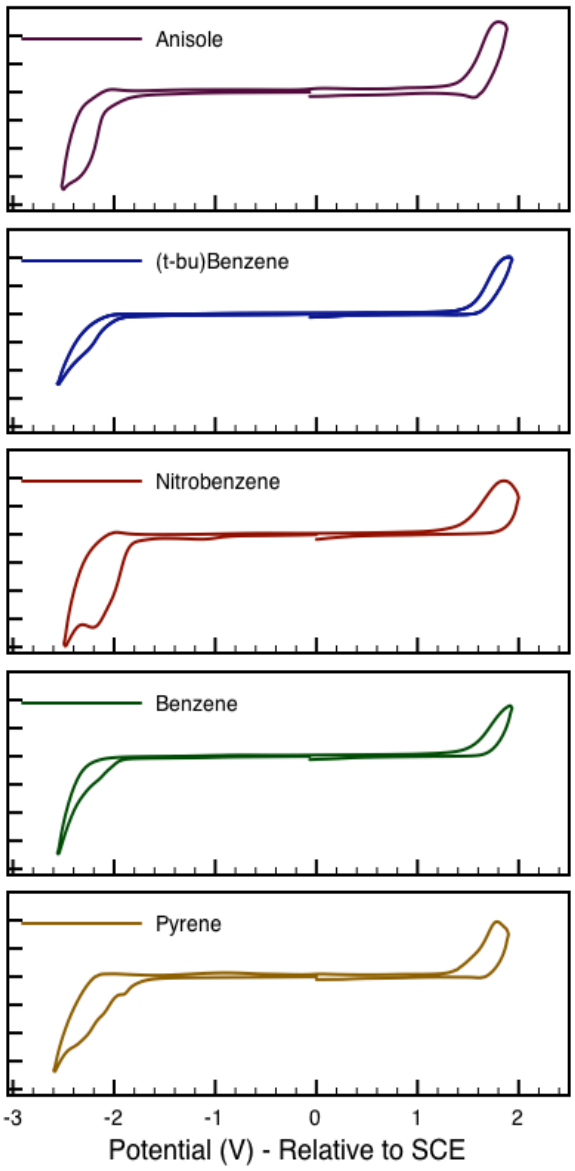

Figure A3.3: Cyclic Voltammograms **P1-P5**

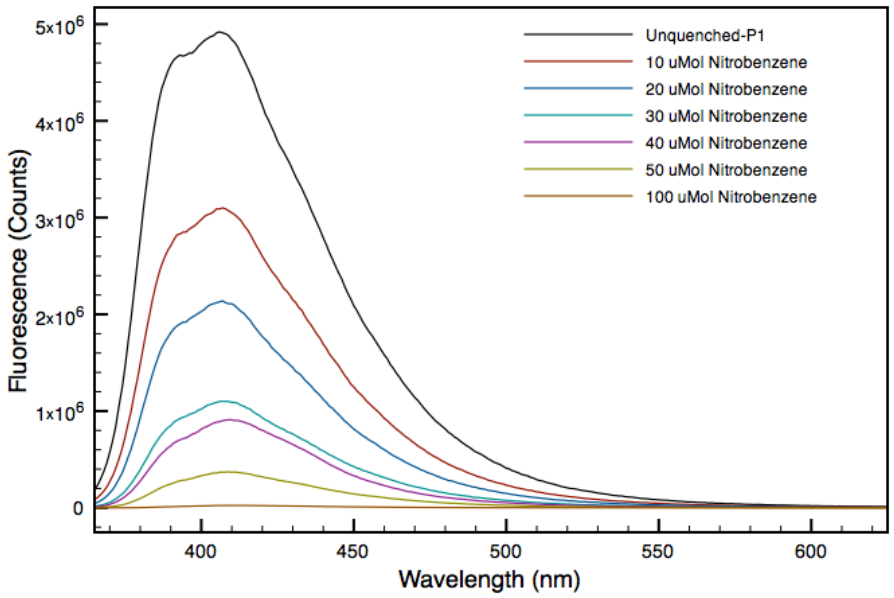

Figure A3.4: Emission spectra during the quenching of **P3** (0.004 mg/mL in THF) with nitrobenzene (1.0 M in THF).

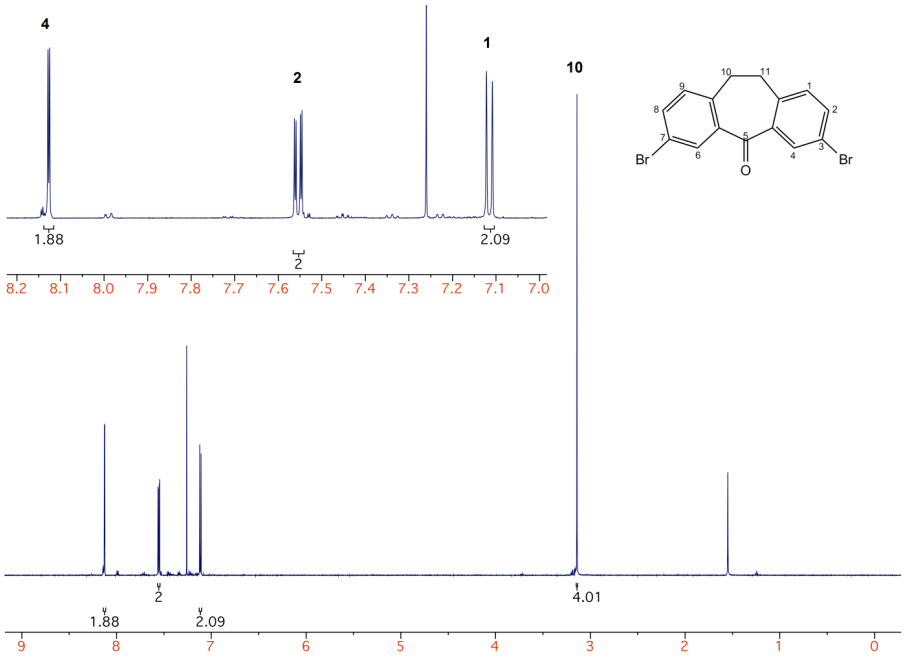

Figure A3.5: ^{1}H-NMR spectrum of **2** in $CDCl_3$

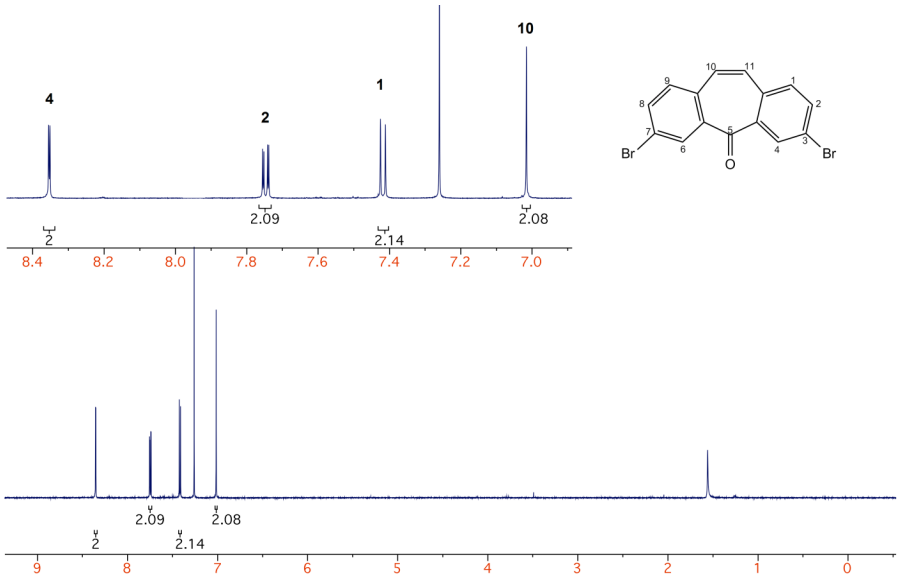

Figure A3.6: ^{1}H-NMR spectrum of **4** in $CDCl_3$

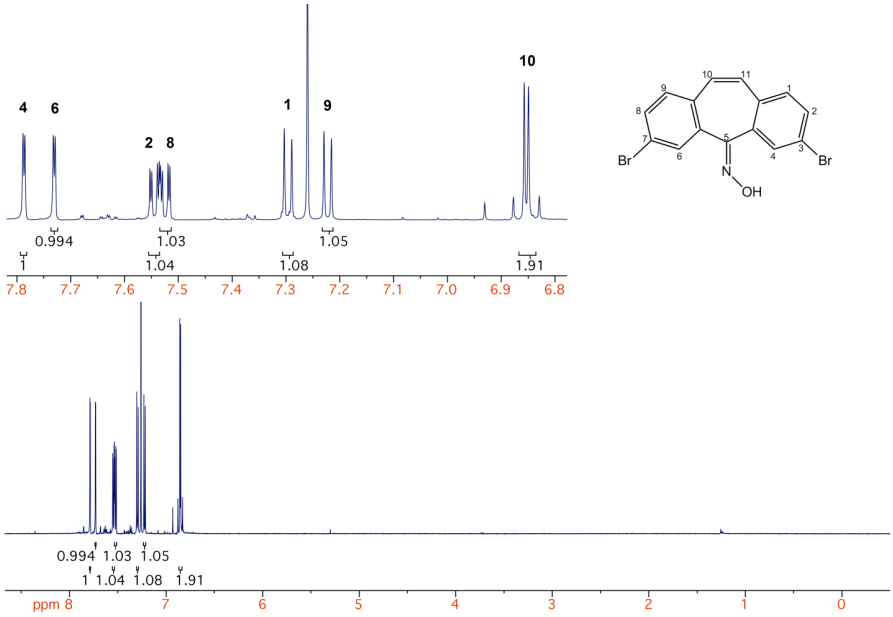

Figure A3.7: ^{1}H-NMR spectrum of **5** in $CDCl_3$

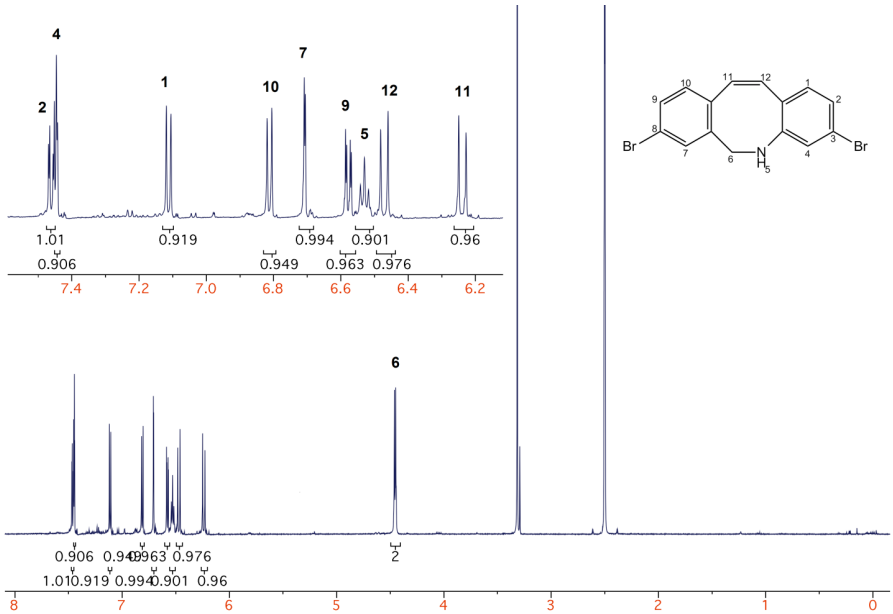

Figure A3.8: ^{1}H-NMR spectrum of **6** in DMSO-d6

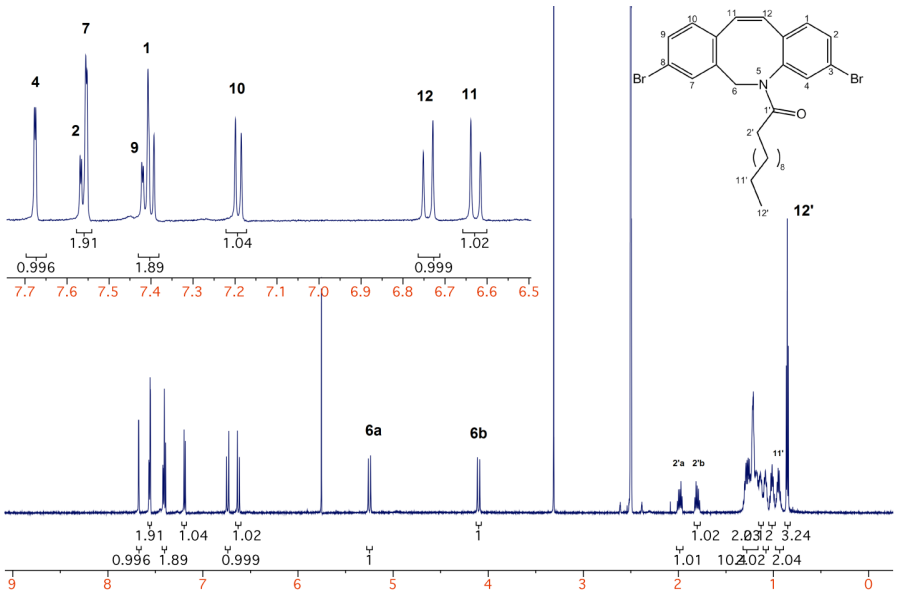

Figure A3.9: ^{1}H-NMR spectrum of **6** in DMSO-d6

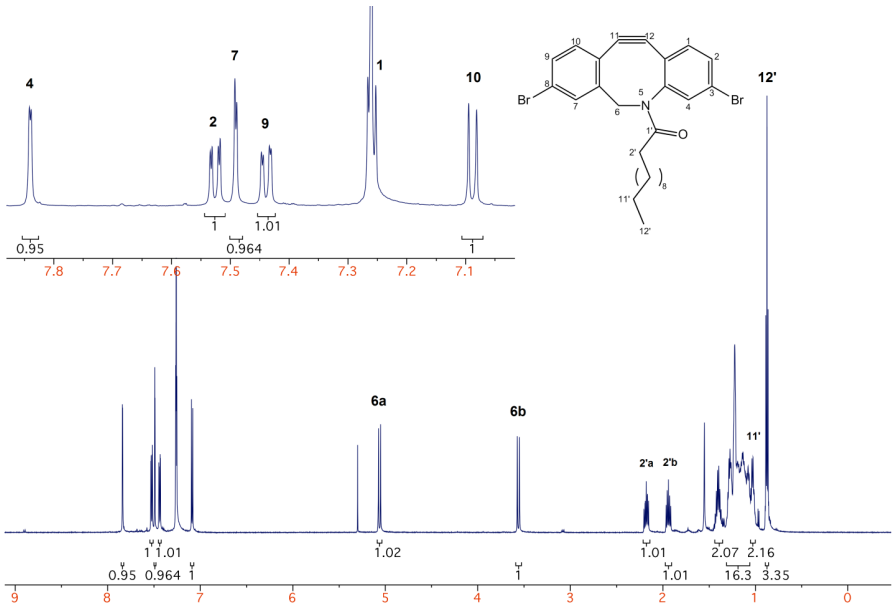

Figure A3.10: ^{1}H-NMR spectrum of **9** in $CDCl_3$

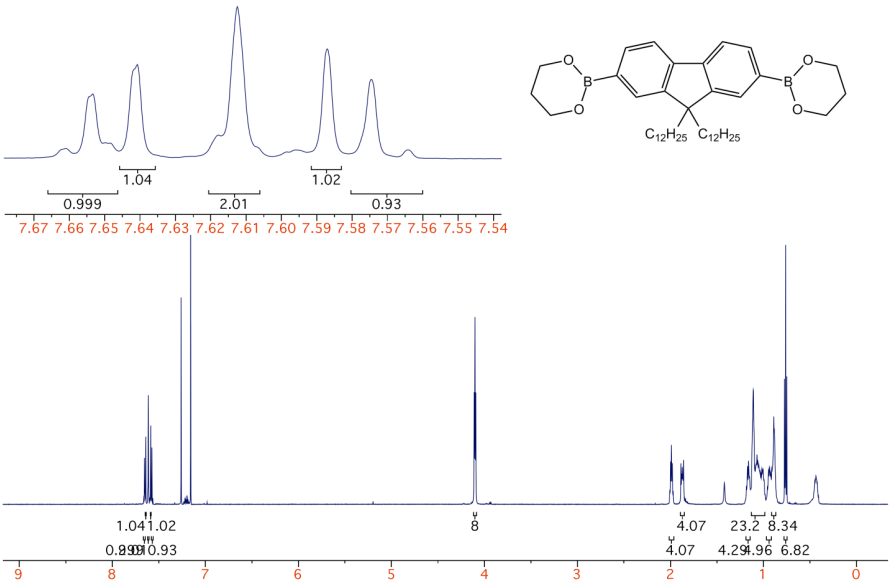

Figure A3.11: ^{1}H-NMR spectrum of fluorene boronic ester in $CDCl_3$

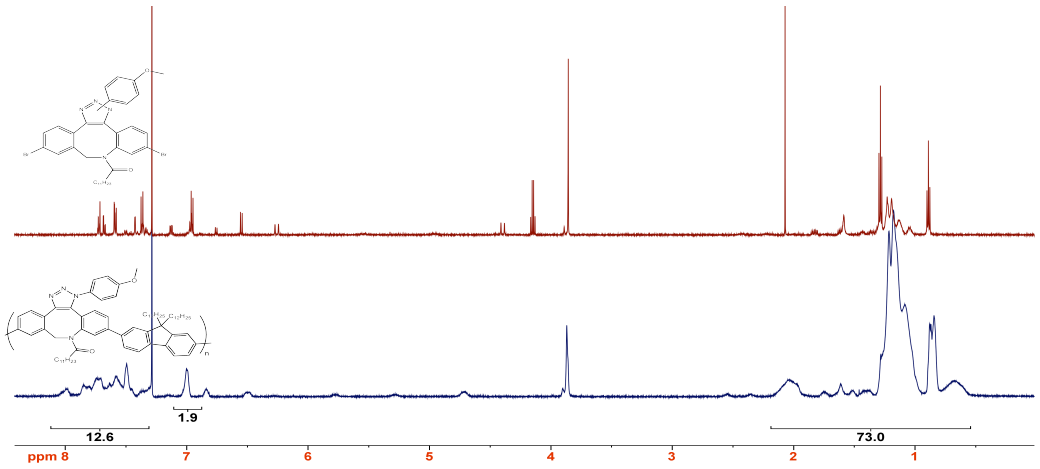

Figure A3.12: ^{1}H-NMR spectra of **10a** and **P1** (anisole derivative)

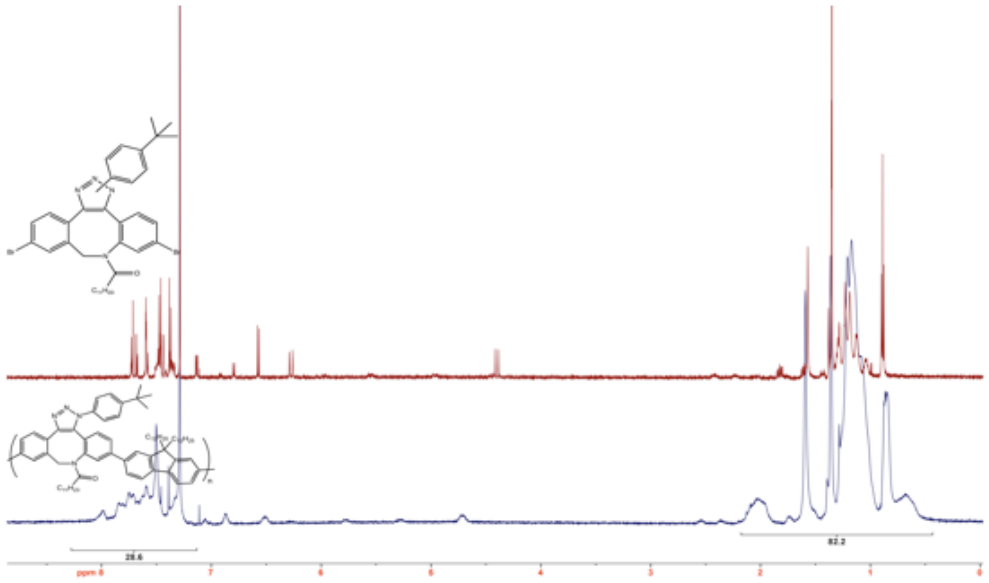

Figure A3.13: ^{1}H-NMR spectra of **10b** and **P2** (t-Bu derivative)

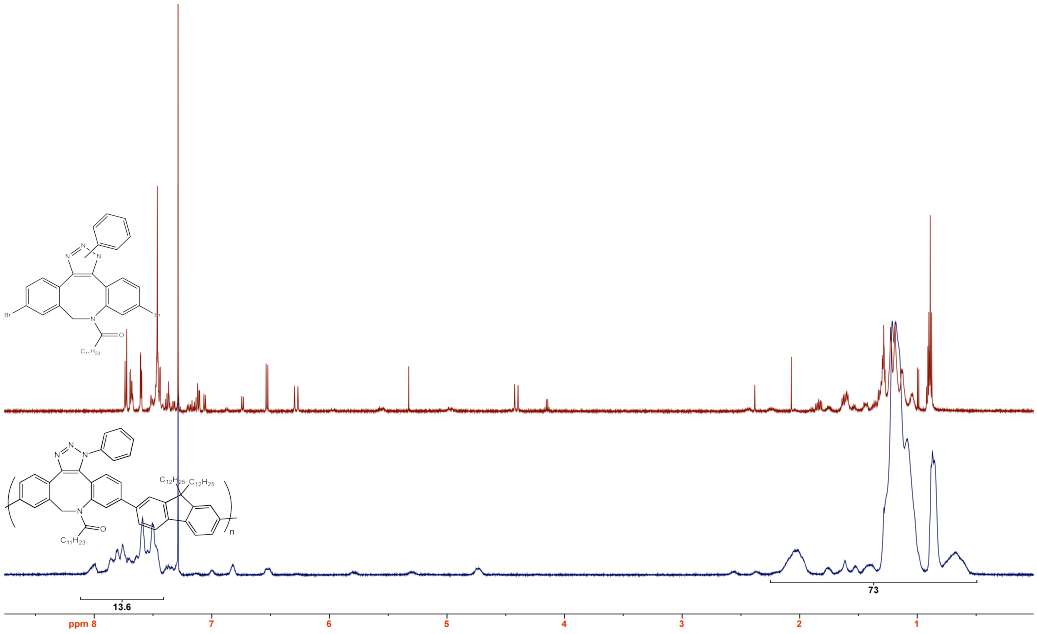

Figure A3.14: ^{1}H-NMR spectra of **10c** and **P3** (phenyl derivative)

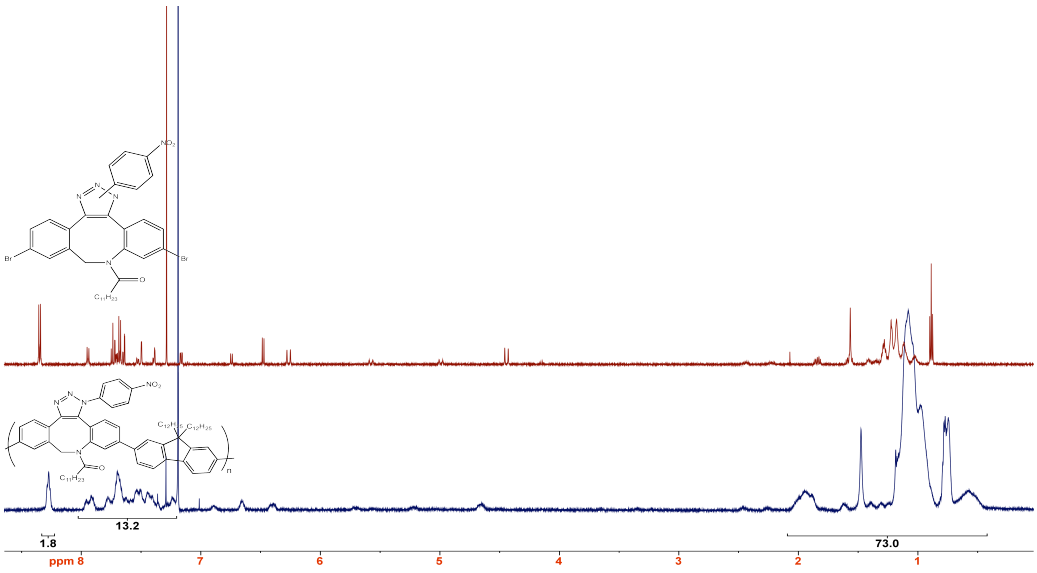

Figure A3.15: ^{1}H-NMR spectra of **10d** and **P4** (Nitro derivative)

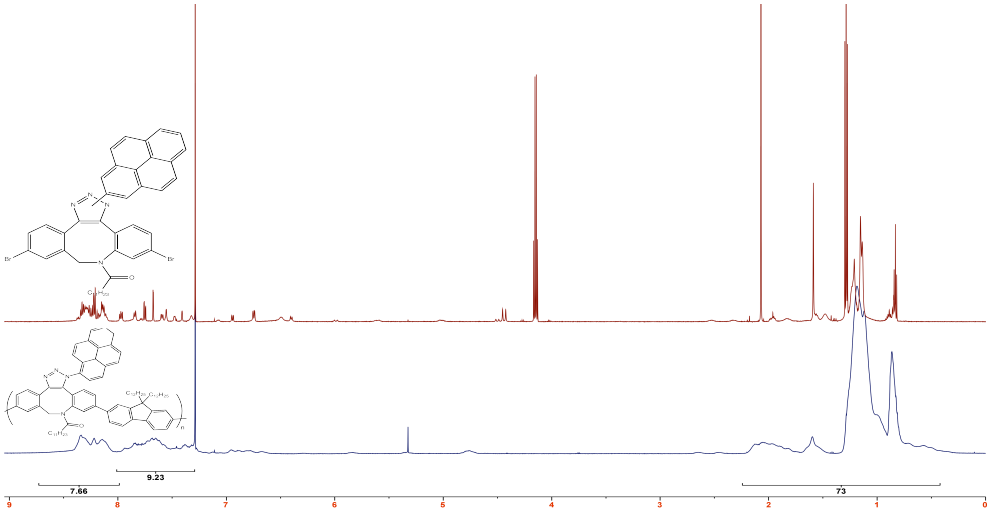

Figure A3.16: ^{1}H-NMR spectra of **10e** and **P5** (Pyrene derivative)

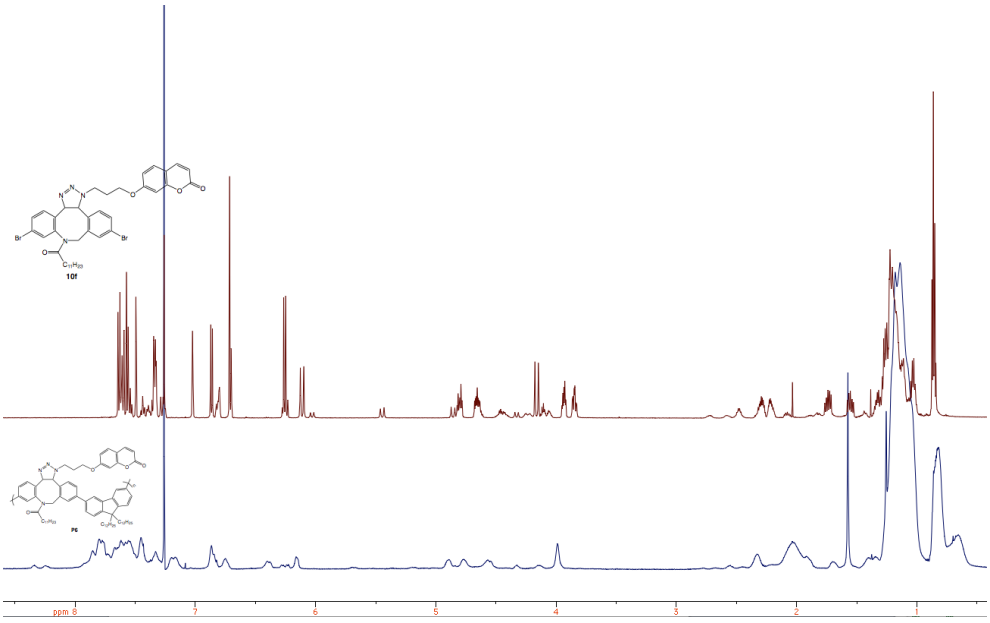

Figure A3.17: ^{1}H-NMR spectra of **10f** and **P6** (Coumarin derivative)

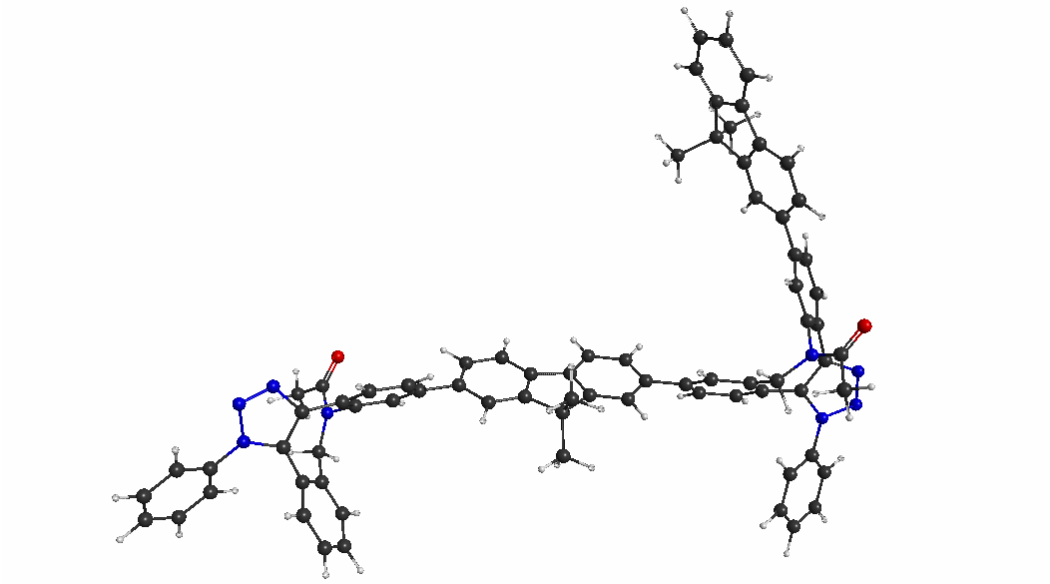

Figure A3.18: Tetramer of Model DIBAC Polymer (PM3)

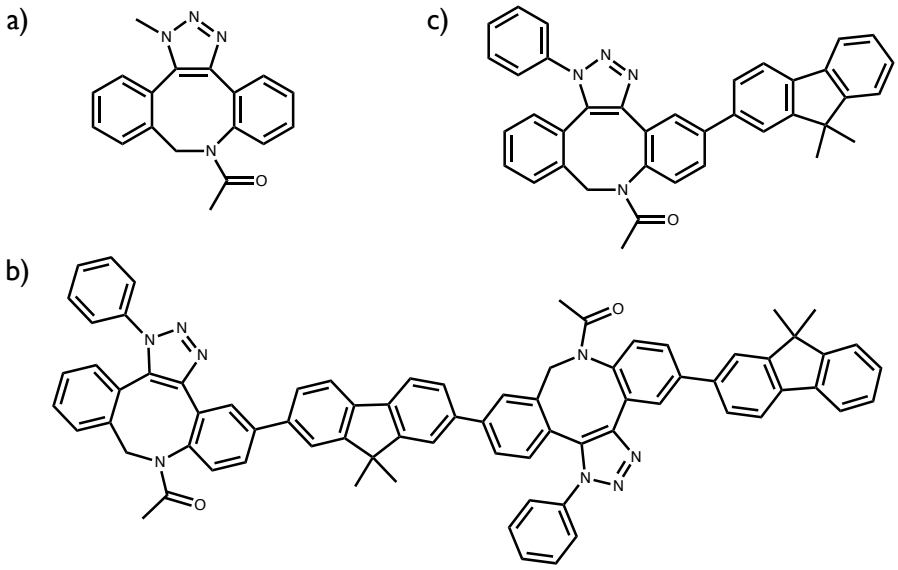

Figure A3.19: Optimized Structures, a) Model Monomer, b) Model Dimer, c) Model Tetramer

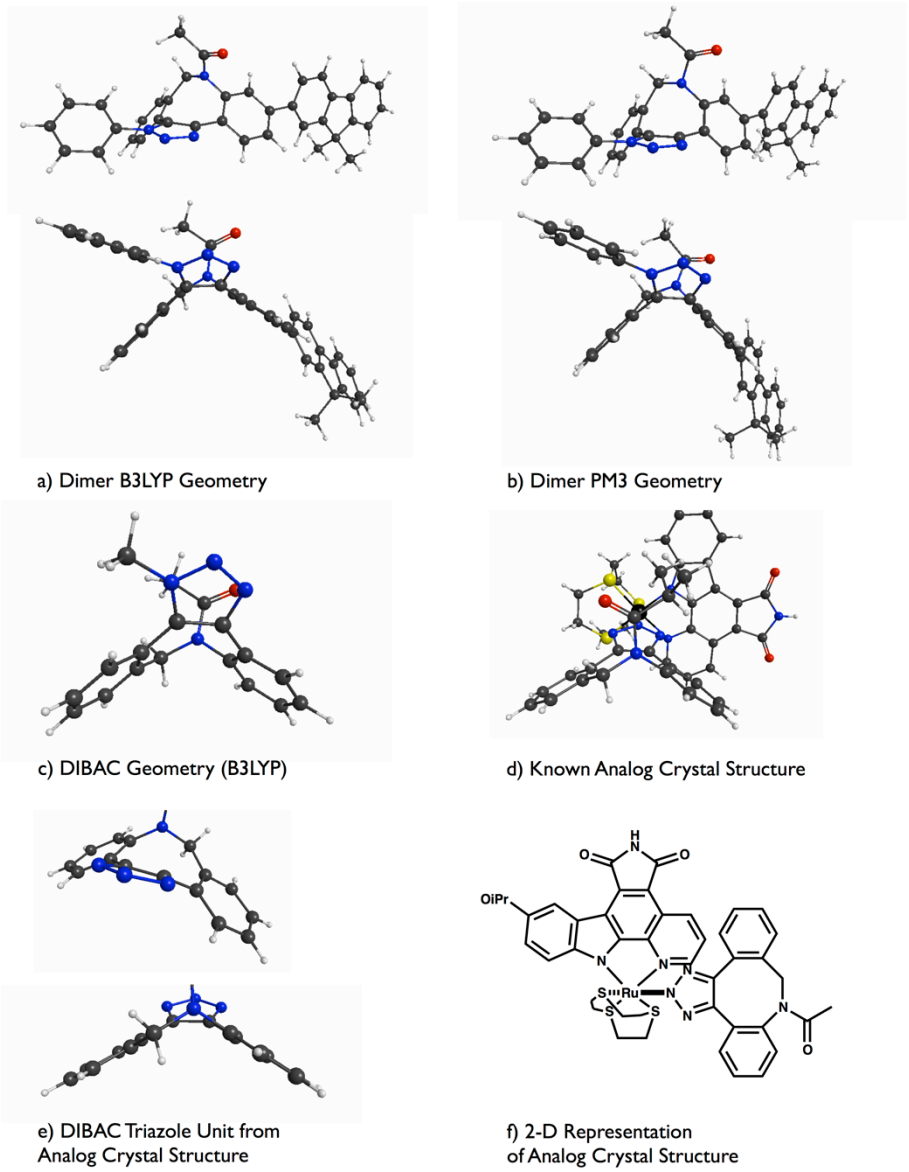

Figure A3.20 a) Calculated dimer stationary point (B3LYP), b) Calculated dimer stationary point (PM3), c) Simplified DIBAC geometry, d) Crystal structure of known analog,[17] e) Crystal structure of (c), with extraneous structure removed (from CCDC database – YIKGOQ00). f) 2D-structure of DIBAC containing analog

Coordinates of B3YLP/6-31G(d) stationary points:

Monomer

ATOM	CHARGE	X	Y	Z
C	6.0	-5.9825071182	-1.5759315337	2.9380556810
C	6.0	-5.4154435512	-2.8505267576	2.9651184550
C	6.0	-4.6503104334	-3.2733380105	1.8845586645
C	6.0	-4.4400243041	-2.4755519581	0.7480440922
C	6.0	-5.0246597940	-1.1897136405	0.7100541537
C	6.0	-5.7764733055	-0.7655612320	1.8292834466
C	6.0	-3.6171896343	-3.1597263890	-0.3474893049
N	7.0	-3.0690612958	-2.3481185181	-1.4190864215
C	6.0	-2.0203448023	-1.4202432575	-1.0861121964
C	6.0	-2.3431671710	-0.0671558474	-0.8850998485
C	6.0	-3.7418133059	0.3659009751	-0.9761038883
C	6.0	-4.8652960243	-0.2015240841	-0.3790693801
C	6.0	-0.6970439633	-1.8518047666	-0.9981595602
C	6.0	0.3192984133	-0.9371914592	-0.7194457989
C	6.0	0.0108616508	0.4148074424	-0.5501816958
C	6.0	-1.3111525321	0.8467535289	-0.6361334921
N	7.0	-4.1339199874	1.4351765505	-1.7267790226
N	7.0	-5.4292082041	1.5561427540	-1.6580575852
N	7.0	-5.8920290940	0.5793336258	-0.8431376380
C	6.0	-3.4676184946	-2.4201699034	-2.7502421202
O	8.0	-2.9091232972	-1.7630277820	-3.6128456239
C	6.0	-4.6302255239	-3.3469621598	-3.0920259885
H	1.0	-6.1777049764	0.2431942088	1.8312742707
H	1.0	-6.5639532144	-1.2082678192	3.7791018679
H	1.0	-5.5527547352	-3.5016890004	3.8242388967
H	1.0	-4.1942995967	-4.2616586809	1.9146245296
H	1.0	-4.8745386541	-3.1749325268	-4.1411911180
H	1.0	-4.3603848478	-4.4027368845	-2.9668119816
H	1.0	-5.5172017460	-3.1496081549	-2.4796567354
H	1.0	-4.2296348445	-3.9471203589	-0.7945815948
H	1.0	-2.7873233970	-3.6788056727	0.1520300806
H	1.0	-1.5605023862	1.8959340330	-0.5089151264
H	1.0	-0.4664089149	-2.8994228046	-1.1735122483
H	1.0	0.8015172584	1.1331451359	-0.3501130615
H	1.0	1.3497212905	-1.2759968299	-0.6531199070
C	6.0	-7.3304062444	0.4630265137	-0.6532193368
H	1.0	-7.8091848964	0.8443975182	-1.5564169630
H	1.0	-7.6693817109	1.0509896844	0.2056453631
H	1.0	-7.5992028516	-0.5838110763	-0.5000660223

ENERGY: -989.1661063203

Dimer

ATOM	CHARGE	X	Y	Z
C	6.0	-5.9072177114	-1.5666264309	2.9797701924
C	6.0	-5.3155096717	-2.8306037973	3.0107954087
C	6.0	-4.5793303016	-3.2609380950	1.9138504681
C	6.0	-4.4206968261	-2.4777997228	0.7581923379
C	6.0	-5.0241428532	-1.2020115421	0.7215949038
C	6.0	-5.7520371871	-0.7703856380	1.8535306576
C	6.0	-3.6359475942	-3.1666459517	-0.3608467155
N	7.0	-3.0907993685	-2.3481489696	-1.4297124256
C	6.0	-2.0453505202	-1.4187319946	-1.0902930005
C	6.0	-2.3704681467	-0.0714215745	-0.8632667579
C	6.0	-3.7659441340	0.3665107802	-0.9483329614
C	6.0	-4.8921108288	-0.2199958256	-0.3788634376
C	6.0	-0.7251883459	-1.8533500119	-1.0151354193
C	6.0	0.3193531634	-0.9605170988	-0.7266391609
C	6.0	-0.0112208912	0.3926425977	-0.5282915932
C	6.0	-1.3295871535	0.8288353875	-0.5988490983
N	7.0	-4.1497633234	1.4709320451	-1.6551975541
N	7.0	-5.4393864136	1.5999517487	-1.5907583628
N	7.0	-5.9205073906	0.5841585140	-0.8161730599
C	6.0	-7.3327865244	0.4628768696	-0.6555048253
C	6.0	-8.0931168302	1.6241056885	-0.4830159279
C	6.0	-9.4776339916	1.5226279163	-0.3550938589
C	6.0	-10.1015253315	0.2733704684	-0.3873357781
C	6.0	-9.3335962875	-0.8799461440	-0.5616060210
C	6.0	-7.9496548958	-0.7908619453	-0.7047611589
C	6.0	1.7237298758	-1.4341111628	-0.6486434285
C	6.0	-3.4400468060	-2.4546949811	-2.7719216716
O	8.0	-2.8648134529	-1.8002289039	-3.6262097833
C	6.0	-4.5706135622	-3.4106077663	-3.1389299481
C	6.0	2.1918289571	-2.4359722176	-1.5216494954
C	6.0	3.5020625575	-2.9066566405	-1.4544342597
C	6.0	4.3701800438	-2.3686927216	-0.5020281066
C	6.0	3.9204652204	-1.3604920505	0.3736095869
C	6.0	2.6139695032	-0.8979578743	0.3035848750
C	6.0	5.7749794738	-2.6625528272	-0.1965653049
C	6.0	6.1828671267	-1.8325940814	0.8675684399
C	6.0	5.0368483808	-0.9296844932	1.3265826805
C	6.0	6.6663768505	-3.5720536017	-0.7709447208
C	6.0	7.9695961296	-3.6453341694	-0.2735299468
C	6.0	8.3759001020	-2.8212478011	0.7819981789
C	6.0	7.4819437533	-1.9098641581	1.3573709784
C	6.0	5.3894326766	0.5640870870	1.1430807507
C	6.0	4.6574283609	-1.2039822049	2.7997330304
H	1.0	-7.5946636639	2.5868230512	-0.4635664586
H	1.0	-10.0688797122	2.4248362978	-0.2240581419
H	1.0	-11.1801573881	0.1990299110	-0.2801729631
H	1.0	-9.8120569748	-1.8548434687	-0.5980563362
H	1.0	-7.3523384855	-1.6832607200	-0.8580080995

H	**1.0**	**-6.1889077649**	**0.2230299257**	**1.8406685264**
H	**1.0**	**-6.4713422895**	**-1.1975111857**	**3.8318368815**
H	**1.0**	**-5.4146475845**	**-3.4680401442**	**3.8854177960**
H	**1.0**	**-4.1066526491**	**-4.2412319774**	**1.9440415785**
H	**1.0**	**-4.7715600541**	**-3.2699899212**	**-4.2018058117**
H	**1.0**	**-4.2908576804**	**-4.4579695125**	**-2.9722611113**
H	**1.0**	**-5.4874560697**	**-3.2116724554**	**-2.5725928919**
H	**1.0**	**-4.2762320879**	**-3.9313216426**	**-0.8084695831**
H	**1.0**	**-2.8102094801**	**-3.7144205880**	**0.1151818926**
H	**1.0**	**-1.5690315589**	**1.8786410184**	**-0.4579440273**
H	**1.0**	**-0.5100682886**	**-2.9046169340**	**-1.1847677204**
H	**1.0**	**2.2582129438**	**-0.1403977753**	**0.9979243204**
H	**1.0**	**1.5216093572**	**-2.8292685623**	**-2.2807543179**
H	**1.0**	**3.8389167613**	**-3.6767943444**	**-2.1441444048**
H	**1.0**	**6.3548051055**	**-4.2137317949**	**-1.5916897373**
H	**1.0**	**8.6750603007**	**-4.3476854862**	**-0.7102743152**
H	**1.0**	**9.3935018092**	**-2.8893234029**	**1.1582430700**
H	**1.0**	**7.8074522690**	**-1.2738806571**	**2.1778725988**
H	**1.0**	**4.5439383445**	**1.2005703750**	**1.4305318862**
H	**1.0**	**5.6450961032**	**0.7847334017**	**0.1014900079**
H	**1.0**	**6.2446081662**	**0.8390292468**	**1.7718034871**
H	**1.0**	**5.4871685318**	**-0.9455064796**	**3.4683941592**
H	**1.0**	**3.7903936979**	**-0.6004486835**	**3.0933229897**
H	**1.0**	**4.4086737110**	**-2.2591318770**	**2.9535345424**
H	**1.0**	**0.7798725888**	**1.1130144100**	**-0.3399796535**

ENERGY = -1759.2694350154

Coordinates of PM3 stationary points:

Dimer

ATOM	CHARGE	X	Y	Z
C	6.0	-6.4373529754	-2.4988890862	1.8869346619
C	6.0	-6.0130795157	-3.6089236921	1.1630862206
C	6.0	-5.2348760857	-3.4410119145	0.0245990489
C	6.0	-4.8795218611	-2.1625984361	-0.4087442919
C	6.0	-5.3520755991	-1.0475506530	0.2941111783
C	6.0	-6.1122852458	-1.2193419145	1.4539948027
C	6.0	-3.9731191251	-1.9882166878	-1.5932950208
N	7.0	-2.5382953059	-1.9741584502	-1.2167394021
C	6.0	-1.8636329518	-0.7457743680	-0.8287562979
C	6.0	-2.4445156427	0.4903941453	-0.4886549976
C	6.0	-3.8520111926	0.8694909995	-0.5885908242
C	6.0	-5.0585593518	0.2801021478	-0.2196831322
C	6.0	-0.4584925244	-0.8443470790	-0.8744652966
C	6.0	0.3632099065	0.2085851240	-0.4913112781
C	6.0	-0.2184238373	1.4007278163	-0.0542185421
C	6.0	-1.5945855537	1.5330051179	-0.0718540182
N	7.0	-4.1802952565	2.1486493430	-1.0975651547
N	7.0	-5.4331192875	2.3556128532	-1.0595551501
N	7.0	-6.0373511959	1.2508590219	-0.5261231803
C	6.0	-7.4790562285	1.1428446844	-0.4186567831
C	6.0	-8.2010717201	2.1635076717	0.2086598557
C	6.0	-9.5862646852	2.0666153828	0.2861790227
C	6.0	-10.2467993753	0.9681295725	-0.2534433854
C	6.0	-9.5231659443	-0.0425939377	-0.8785752942
C	6.0	-8.1388528353	0.0385450842	-0.9685569220
C	6.0	1.8250078664	0.0673675236	-0.5387976462
C	6.0	-2.0814887150	-3.2185776192	-0.5815312748
O	8.0	-1.5268578051	-3.1937555542	0.4996937845
C	6.0	-2.3085680923	-4.4937778895	-1.3571079109
C	6.0	2.4401387591	-0.4342934665	-1.6873216612
C	6.0	3.8270874631	-0.5721804509	-1.7572570798
C	6.0	4.5823895191	-0.2047064475	-0.6571106128
C	6.0	3.9647510844	0.3011062024	0.5098507882
C	6.0	2.5927480219	0.4422396505	0.5757368303
C	6.0	6.0267886282	-0.2392894912	-0.4402919538
C	6.0	6.2968901303	0.2439631988	0.8610269181
C	6.0	5.0066530596	0.6251022403	1.5685934650
C	6.0	7.0530386662	-0.6478858573	-1.2746093956
C	6.0	8.3635988708	-0.5706360735	-0.7976180234
C	6.0	8.6309102661	-0.0962253180	0.4808883399
C	6.0	7.5964103908	0.3171303901	1.3254708365
C	6.0	4.9911360504	2.1079819550	1.9143909198
C	6.0	4.7974923610	-0.2217073111	2.8167769551
H	1.0	-7.6941226463	3.0421446286	0.6265922330
H	1.0	-10.1579725372	2.8637543477	0.7737370401
H	1.0	-11.3379613826	0.8995414686	-0.1889088691
H	1.0	-10.0445301362	-0.9057449430	-1.3060818190

H	**1.0**	**-7.5749666012**	**-0.7647323465**	**-1.4592313499**
H	**1.0**	**-6.4538468983**	**-0.3464180410**	**2.0214623875**
H	**1.0**	**-7.0296353645**	**-2.6324566175**	**2.7983960938**
H	**1.0**	**-6.2809267159**	**-4.6166248725**	**1.4979053857**
H	**1.0**	**-4.8711672961**	**-4.3208333854**	**-0.5304401874**
H	**1.0**	**-1.6359800036**	**-5.2919049880**	**-1.0158441299**
H	**1.0**	**-3.3439397252**	**-4.8487664222**	**-1.2103797915**
H	**1.0**	**-2.1460905611**	**-4.3576244666**	**-2.4341275194**
H	**1.0**	**-4.1148065928**	**-2.8198469857**	**-2.3153008225**
H	**1.0**	**-4.1986879861**	**-1.0572842001**	**-2.1508844258**
H	**1.0**	**-2.0262455129**	**2.4934614243**	**0.2375766140**
H	**1.0**	**0.0217605660**	**-1.7783563208**	**-1.1991849079**
H	**1.0**	**2.1123736161**	**0.8346258846**	**1.4799221594**
H	**1.0**	**1.8244776595**	**-0.7212860070**	**-2.5477039047**
H	**1.0**	**4.3081675271**	**-0.9615182951**	**-2.6603131430**
H	**1.0**	**6.8398566105**	**-1.0211096078**	**-2.2813884682**
H	**1.0**	**9.1898013495**	**-0.8887604912**	**-1.4418718212**
H	**1.0**	**9.6657510939**	**-0.0442149338**	**0.8348198568**
H	**1.0**	**7.8075572300**	**0.6909328542**	**2.3330044405**
H	**1.0**	**4.0319030653**	**2.3954613948**	**2.3651083666**
H	**1.0**	**5.1409358371**	**2.7301133859**	**1.0232539328**
H	**1.0**	**5.7874636718**	**2.3521914030**	**2.6299868452**
H	**1.0**	**5.5888055087**	**-0.0346557337**	**3.5547910160**
H	**1.0**	**3.8331312607**	**0.0078625043**	**3.2892635422**
H	**1.0**	**4.8068144725**	**-1.2932510774**	**2.5815295905**
H	**1.0**	**0.4137109526**	**2.2305933319**	**0.2812712569**

ENERGY = -216.9402798122

Tetramer

ATOM	CHARGE	X	Y	Z
C	6.0	-3.0204167297	-2.6596726724	4.4697085984
C	6.0	-2.2724640860	-3.8113772296	4.2439763441
C	6.0	-2.0049287870	-4.2131417821	2.9455034355
C	6.0	-2.4743598626	-3.4875443595	1.8387504748
C	6.0	-3.2257786938	-2.3285977709	2.0721299227
C	6.0	-3.4866219848	-1.9249952483	3.3918263644
C	6.0	-2.1503385552	-4.1071256960	0.5081952922
N	7.0	-2.0339056088	-3.1920793787	-0.6544402907
C	6.0	-1.0373108882	-2.1302987487	-0.5136308655
C	6.0	-1.5151982603	-0.8526027103	-0.1729677290
C	6.0	-2.9343738407	-0.7028744773	0.1074462851
C	6.0	-3.6940591055	-1.4306942050	1.0218213519
C	6.0	0.3245315853	-2.3394771277	-0.7244215733
C	6.0	1.2118199785	-1.2648200031	-0.6157560075
C	6.0	0.7313820537	0.0085009785	-0.3018037462
C	6.0	-0.6257338972	0.2162121089	-0.0822526089
N	7.0	-3.8090969422	0.1496980734	-0.5816265511
N	7.0	-5.0052421184	-0.0178407470	-0.1755088378
N	7.0	-5.0104934465	-0.9765744277	0.8096506101
C	6.0	-6.2333884459	-1.4487507389	1.4209732173
C	6.0	-7.2806766305	-0.5523402070	1.6634010711
C	6.0	-8.4593599711	-1.0214528417	2.2328401010
C	6.0	-8.5986177186	-2.3657090345	2.5607274722
C	6.0	-7.5551019841	-3.2529574450	2.3166880022
C	6.0	-6.3716592834	-2.8035663663	1.7445689767
C	6.0	2.6480513644	-1.4754206293	-0.8449305549
C	6.0	-2.2551605721	-3.7484375577	-1.9704218170
O	8.0	-1.5937597132	-3.3289947049	-2.9043418604
C	6.0	-3.3715211669	-4.7471709060	-2.1492852410
C	6.0	3.0767068535	-2.1686418857	-1.9787622781
C	6.0	4.4351335015	-2.3782532732	-2.2201689097
C	6.0	5.3509410189	-1.8859799803	-1.3062754754
C	6.0	4.9225275320	-1.1833589317	-0.1565491234
C	6.0	3.5783809415	-0.9728042220	0.0791484378
C	6.0	6.8098819619	-1.9531425493	-1.2918927208
C	6.0	7.2790290444	-1.2913216082	-0.1335367852
C	6.0	6.1149617779	-0.7499012435	0.6810285131
C	6.0	7.6943125410	-2.5297224794	-2.1871288220
C	6.0	9.0610647325	-2.4462578403	-1.9179310230
C	6.0	9.5301555063	-1.7925132918	-0.7770353190
C	6.0	8.6318303819	-1.2047672069	0.1285624035
C	6.0	6.1832610578	0.7675333790	0.7890725924
C	6.0	6.0727531945	-1.3872520296	2.0633102436
H	1.0	-7.1918122821	0.5093050733	1.3994744512
H	1.0	-9.2830386238	-0.3242788722	2.4213828794
H	1.0	-9.5302915006	-2.7267502421	3.0089928528
H	1.0	-7.6649988998	-4.3119822840	2.5732684303
H	1.0	-5.5501910749	-3.5087331657	1.5608434822
H	1.0	-4.0615544474	-1.0097320353	3.5759639427

H	**1.0**	**-3.2331690604**	**-2.3317010376**	**5.4925329547**
H	**1.0**	**-1.8934037937**	**-4.3955332011**	**5.0891105722**
H	**1.0**	**-1.4093010744**	**-5.1202927591**	**2.7814017817**
H	**1.0**	**-3.2077981793**	**-5.3717227384**	**-3.0372936255**
H	**1.0**	**-3.4885676724**	**-5.4179499492**	**-1.2836279563**
H	**1.0**	**-4.3237120872**	**-4.2172833439**	**-2.2896321189**
H	**1.0**	**-2.9545167491**	**-4.8455788077**	**0.2819552377**
H	**1.0**	**-1.2055723313**	**-4.6890721226**	**0.6024220700**
H	**1.0**	**-0.9967494176**	**1.2185943434**	**0.1580814466**
H	**1.0**	**0.7054130222**	**-3.3320324480**	**-0.9954664648**
H	**1.0**	**3.2445096713**	**-0.4254242893**	**0.9685234215**
H	**1.0**	**2.3345563395**	**-2.5480731819**	**-2.6918973236**
H	**1.0**	**4.7698912659**	**-2.9180929650**	**-3.1119848358**
H	**1.0**	**7.3283694746**	**-3.0386237731**	**-3.0849127472**
H	**1.0**	**9.7766748358**	**-2.8982468073**	**-2.6143784885**
H	**1.0**	**8.9966744386**	**-0.6906781181**	**1.0257422615**
H	**1.0**	**5.3064232658**	**1.1624640879**	**1.3192602965**
H	**1.0**	**6.2155987871**	**1.2400512661**	**-0.2005396190**
H	**1.0**	**7.0803160851**	**1.0818212620**	**1.3390018982**
H	**1.0**	**6.9678722143**	**-1.1260343369**	**2.6433503743**
H	**1.0**	**5.1937233214**	**-1.0453799136**	**2.6257272848**
H	**1.0**	**6.0236760150**	**-2.4814272141**	**2.0001229817**
H	**1.0**	**1.4305754075**	**0.8498566006**	**-0.2317455823**
C	**6.0**	**11.5634274100**	**-0.4968266792**	**-0.1653401764**
C	**6.0**	**10.9738950772**	**-1.7146606958**	**-0.5167238532**
C	**6.0**	**11.7697469630**	**-2.8522659328**	**-0.6126912595**
C	**6.0**	**13.1506187667**	**-2.8099636170**	**-0.3685243871**
C	**6.0**	**13.7316284468**	**-1.5844616037**	**-0.0182956160**
C	**6.0**	**12.9240796094**	**-0.4400006069**	**0.0817382371**
C	**6.0**	**13.8569647784**	**-4.1192000959**	**-0.5860162557**
N	**7.0**	**15.0957184714**	**-4.3580842268**	**0.1955801689**
C	**6.0**	**14.9413237122**	**-4.2781217500**	**1.6482473777**
C	**6.0**	**15.3624544917**	**-3.0875516863**	**2.2663218925**
C	**6.0**	**15.8183060274**	**-1.9978032480**	**1.4179263958**
C	**6.0**	**15.1325519606**	**-1.4172562322**	**0.3521490313**
C	**6.0**	**14.4273128862**	**-5.3244831762**	**2.4122581904**
C	**6.0**	**14.3529349833**	**-5.1915837286**	**3.8018163091**
C	**6.0**	**14.7972620074**	**-4.0182773958**	**4.4156276399**
C	**6.0**	**15.3010914690**	**-2.9702432965**	**3.6534721986**
N	**7.0**	**17.0878432203**	**-1.4047562237**	**1.4739326660**
N	**7.0**	**17.2204729150**	**-0.5486281775**	**0.5392698278**
N	**7.0**	**16.0573702602**	**-0.5046816439**	**-0.1919589900**
C	**6.0**	**15.9160370914**	**0.3226394976**	**-1.3699695734**
C	**6.0**	**16.5126442837**	**1.5882420416**	**-1.4067488676**
C	**6.0**	**16.3869685808**	**2.3663058265**	**-2.5523733402**
C	**6.0**	**15.6755004949**	**1.8956645936**	**-3.6506609635**
C	**6.0**	**15.0854268880**	**0.6363596967**	**-3.6096234359**
C	**6.0**	**15.2038643684**	**-0.1570338629**	**-2.4754545332**
C	**6.0**	**13.8175366243**	**-6.2924447960**	**4.6148746841**
C	**6.0**	**16.0523490012**	**-5.3026053381**	**-0.3364442997**
O	**8.0**	**16.6727243476**	**-6.0104242577**	**0.4379765446**
C	**6.0**	**16.3194451382**	**-5.2955328941**	**-1.8212317605**
C	**6.0**	**14.2795963648**	**-7.5944999541**	**4.4132482434**

C	**6.0**	**13.7884573509**	**-8.6557620767**	**5.1750348411**
C	**6.0**	**12.8271868723**	**-8.3895820658**	**6.1347585380**
C	**6.0**	**12.3555225783**	**-7.0729995735**	**6.3428663859**
C	**6.0**	**12.8456541010**	**-6.0229667333**	**5.5920901815**
C	**6.0**	**12.1384085702**	**-9.2818188673**	**7.0643144383**
C	**6.0**	**11.2427065529**	**-8.5135164675**	**7.8435864309**
C	**6.0**	**11.3102688738**	**-7.0477934436**	**7.4465837755**
C	**6.0**	**12.2508564103**	**-10.6489185462**	**7.2504253533**
C	**6.0**	**11.4556515790**	**-11.2506700509**	**8.2285035897**
C	**6.0**	**10.5746913776**	**-10.4973291188**	**8.9950093038**
C	**6.0**	**10.4594173332**	**-9.1165412276**	**8.8092873260**
C	**6.0**	**11.7706980922**	**-6.1866072404**	**8.6150173110**
C	**6.0**	**9.9676707217**	**-6.5630458538**	**6.9163385850**
H	**1.0**	**17.0878928094**	**1.9696432889**	**-0.5534043895**
H	**1.0**	**16.8546957282**	**3.3562736241**	**-2.5870307290**
H	**1.0**	**15.5810275812**	**2.5151224679**	**-4.5487996842**
H	**1.0**	**14.5259317050**	**0.2649768438**	**-4.4747866589**
H	**1.0**	**14.7295320880**	**-1.1469983098**	**-2.4479413183**
H	**1.0**	**13.3739011818**	**0.5181571418**	**0.3680034460**
H	**1.0**	**10.9479195923**	**0.4064638318**	**-0.0822119764**
H	**1.0**	**11.2967940673**	**-3.8066582196**	**-0.8829229655**
H	**1.0**	**16.7131699044**	**-6.2633353508**	**-2.1586258944**
H	**1.0**	**15.4211045957**	**-5.0724430381**	**-2.4179933084**
H	**1.0**	**17.0734221851**	**-4.5322620388**	**-2.0579712374**
H	**1.0**	**14.1202148498**	**-4.1771212746**	**-1.6678915881**
H	**1.0**	**13.1433252056**	**-4.9512935774**	**-0.3899404403**
H	**1.0**	**15.6525216923**	**-2.0546949797**	**4.1416974795**
H	**1.0**	**14.1000193547**	**-6.2584477603**	**1.9386451316**
H	**1.0**	**12.4836509019**	**-5.0010058745**	**5.7548392111**
H	**1.0**	**15.0436187549**	**-7.7837911765**	**3.6493116306**
H	**1.0**	**14.1554162596**	**-9.6754991281**	**5.0192303848**
H	**1.0**	**12.9463407432**	**-11.2399735730**	**6.6459003200**
H	**1.0**	**11.5297653762**	**-12.3308227560**	**8.3919855817**
H	**1.0**	**9.9610888145**	**-10.9894696617**	**9.7566972728**
H	**1.0**	**9.7655574869**	**-8.5232197398**	**9.4141895581**
H	**1.0**	**11.8838489262**	**-5.1381063864**	**8.3088462597**
H	**1.0**	**12.7374040484**	**-6.5257503563**	**9.0075899886**
H	**1.0**	**11.0448887424**	**-6.2219159310**	**9.4383076831**
H	**1.0**	**9.1978202967**	**-6.6079764468**	**7.6981117170**
H	**1.0**	**10.0356405844**	**-5.5238339538**	**6.5680514461**
H	**1.0**	**9.6236737517**	**-7.1755191841**	**6.0736462170**
H	**1.0**	**14.7503388341**	**-3.9261846599**	**5.5069465925**

ENERGY = -432.7587148125

Gamess File Headers:

B3LYP

Dimer:

$BASIS GBASIS=N31 NGAUSS=6 NDFUNC=1 $END
$CONTRL SCFTYP=RHF RUNTYP=OPTIMIZE DFTTYP=B3LYP $END
$STATPT OPTTOL=0.0005 NSTEP=20 $END
$contrl nzvar=1 $end
$zmat dlc=.t. auto=.t. $end
$SYSTEM mwords=100 $END
$scf dirscf =.t. $end

Monomer

$BASIS GBASIS=N31 NGAUSS=6 NDFUNC=1 $END
$CONTRL SCFTYP=RHF RUNTYP=OPTIMIZE DFTTYP=B3LYP $END
$STATPT OPTTOL=0.0001 NSTEP=200 HSSEND=.TRUE. $END
$contrl nzvar=1 $end
$zmat dlc=.t. auto=.t. $end
$SYSTEM mwords=100 $END
$scf dirscf =.t. $end

PM3

$BASIS GBASIS=PM3 $END
$CONTRL SCFTYP=RHF RUNTYP=OPTIMIZE $END
$STATPT OPTTOL=0.0001 NSTEP=100 HSSEND=.TRUE. $END
$contrl nzvar=1 $end
$zmat dlc=.t. auto=.t. $end
$SYSTEM mwords=100 $END
$scf dirscf =.t. $end